DENSE-PHASE PNEUMATIC TRANSPORT OF COHESIONLESS SOLIDS

by

Thomas S. Totah

Thesis submitted to the Faculty of the

Virginia Polytechnic Institute and State University

in partial fulfillment of the requirements for the degree of

MASTER OF SCIENCE

in

Chemical Engineering

APPROVED:

Dr. Kenneth Konrad, Chairman

Dr. Arthur M. Squires

Dr. John C. Parker

July, 1987

Blacksburg, Virginia

DENSE-PHASE PNEUMATIC TRANSPORT OF COHESIONLESS SOLIDS

by

Thomas S. Totah

Committee Chairman: Dr. Kenneth Konrad
Department of Chemical Engineering

(ABSTRACT)

An experimental program has been undertaken to gain a more fundamental understanding of dense-phase pneumatic transport of cohesionless solids. A 50.8 mm internal diameter circulating unit with both horizontal and vertical sections has been constructed. The pipe material is transparent lexan which allows for visual observation of the flow pattern. The particles used were a mixture of 95% white and 5% black polyethylene granules (particle diameter approximately 3 mm). The black particles were used to aid the visual observation of the flow pattern. The flow patterns ranged from dilute-phase flow to dense-phase plug flow. High-speed photographic techniques have been used to document the flow patterns in both the horizontal and vertical sections. Pressure drop measurements across a 70 cm test section have been coordinated with the film work.

At the higher superficial air velocities (approximately 15 m/sec), the particles flow in a dilute suspension within the air stream. The pressure drop across the 70 cm section fluctuates very rapidly. For the horizontal

dilute-phase flow, the mean pressure drop is approximately 0.12 kPa with fluctuations ranging from 0 to 0.3 kPa. For the vertical dilute-phase flow, the mean pressure drop is approximately 0.25 kPa with fluctuations ranging from 0 to 0.5 kPa. Upon reducing the superficial air velocity to 6.8 m/sec, the flow pattern in the horizontal section changes to a type of strand flow. The particles are conveyed in a dilute phase above a stationary layer. Large peaks in the pressure drop data (approximately 1 to 2 kPa) correspond to increases in the dilute-phase solids concentration.

At the lower superficial air velocities (below 5 m/sec), the solids flow pattern changes to dense-phase flow. The particles move in the form of plugs that occupy the entire pipe cross-section. For the horizontal flow, the plug length ranged from 0.17 to 0.60 m and the pressure drop across the plugs ranged from 1 to 5.2 kPa. The pressure gradient range can be predicted from the equations of Konrad et al. (1980). The analysis of the vertical dense-phase flow films is not as straightforward as the horizontal films. However, the flow pattern resembles that described by Konrad (1987) and there is qualitative agreement with the concepts outlined by Konrad (1987).

Acknowledgments

The list of people who have supported me as I worked toward the completion of this thesis is very long indeed. First of all I thank my advisor, Dr. Kenneth Konrad, for his guidance and assistance in all aspects of this work. I would also like to thank Dr. A.M. Squires and Dr. J.C. Parker for serving on my graduate advisory committee.

I am grateful to the National Science Foundation for their financial support and to the Phillips 66 Company for supplying the polyethylene granules used in the experiments.

The staff at Virginia Tech and many of my colleagues deserve recognition for their contributions, especially:

Riley Chan for his many helpful suggestions and for his electronic wizardry.

Billy Williams and Wendell Brown for fabricating numerous items of equipment.

Mark Mason and Vance Bergeron for their assistance in assembling the circulating unit.

The Virginia Tech film unit for their advice and the use of equipment.

Benku Thomas, Renato Sprung, and C.W. Cheah for many rewarding discussions.

My fellow graduate students Greg Benge, Danny Thompson, Carl Reed, Jeff Smith, Paul Hathaway, and Alma Rodarte (among many others) for their continuous encouragement.

Finally, I thank my family for their unending love and support.

Table of Contents

List of Figures

List of Tables

List of Symbols

A	Pipe cross-sectional area
A_{St}	Settled Streamer cross-sectional area
B_c	Ratio of compressive stresses in the plug (close to one for ideal plugs)
c	Plug speed
c	Interparticle cohesion
c_w	Particle/wall cohesion
D	Pipe diameter
d_p	Particle diameter
F	Stress on plug front
Fr_c	Froude number
g	Acceleration due to gravity
K_w	Coefficient of internal friction at the wall
ℓ_p	Plug length
R	Radial distance from center of shear cell
R_i	Inner radius of shear cell
R_o	Outer radius of shear cell
S_c	Force due to collection of streamer
T	Total shear torque
u_s	Particle velocity within a plug
W	An indicator of the fractional change in fluid pressure gradient with respect to the logarithm of the particulate normal stress
W_F	Wave front velocity

Greek Symbols

ΔP	Pressure drop across the plug
θ	Angle of pipe inclination
Λ	Dimensionless measure of the plug length
λ	Ratio of radial to axial compressive stress
μ	Coefficient of internal friction
μ_w	Coefficient of wall friction
ρ_b	Solids bulk density
$\rho_{b,St}$	Solids bulk density in the settled streamer
σ	Normal stress
σ_w	Normal stress for wall friction
τ	Shear stress
τ_w	Wall shear stress
ϕ	Angle of internal friction
ϕ_w	Angle of wall friction
χ	Wedge number
ψ_χ	Angle of wall friction

$$\omega = \sin^{-1}\left[\frac{\sin\phi_w}{\sin\phi}\right]$$

(Note: strictly this is for cohesionless materials, but is a good approximation for cohesive materials).

1.0 INTRODUCTION

Many processes require the conveyance of bulk solids from one point to another within the plant site. There are a variety of methods for moving solids which can be divided into two broad categories: (1) mechanical conveying and (2) pneumatic conveying (refer to Figure 1.1). Since solid properties (bulk density, particle size and shape, etc.) vary greatly, each operation is unique. Therefore, a transport system must be designed to meet a particular need, taking into account such factors as the particle properties, conveying rates, conveying distance and path, and the operating environment (Reece, 1985).

There are many different types of mechanical conveyors and elevators (Colijn, 1981). The movement in mechanical conveyors is horizontal or on an incline from the horizontal (~10-15°), whereas that in elevators is vertical or on an incline from the vertical (~15°). The most common types of conveyors are belt, screw, chain and vibratory, and the most common elevators are bucket, screw and vibratory. Basically, all of these devices utilize some kind of mechanical motion (the movement of a belt, turning of a screw, raising of buckets, etc.) to transport the solids from one location to another.

Pneumatic conveying of solids, on the other hand, can be described as the use of the energy of flowing air to move solids through a pipeline. The first conveying line was set up in 1887 to transport agricultural products (Rizk, 1986). Since that time, pneumatic conveying has found applications in a wide range of industries (cement, baking, plastics, pulp and paper, and synthetic

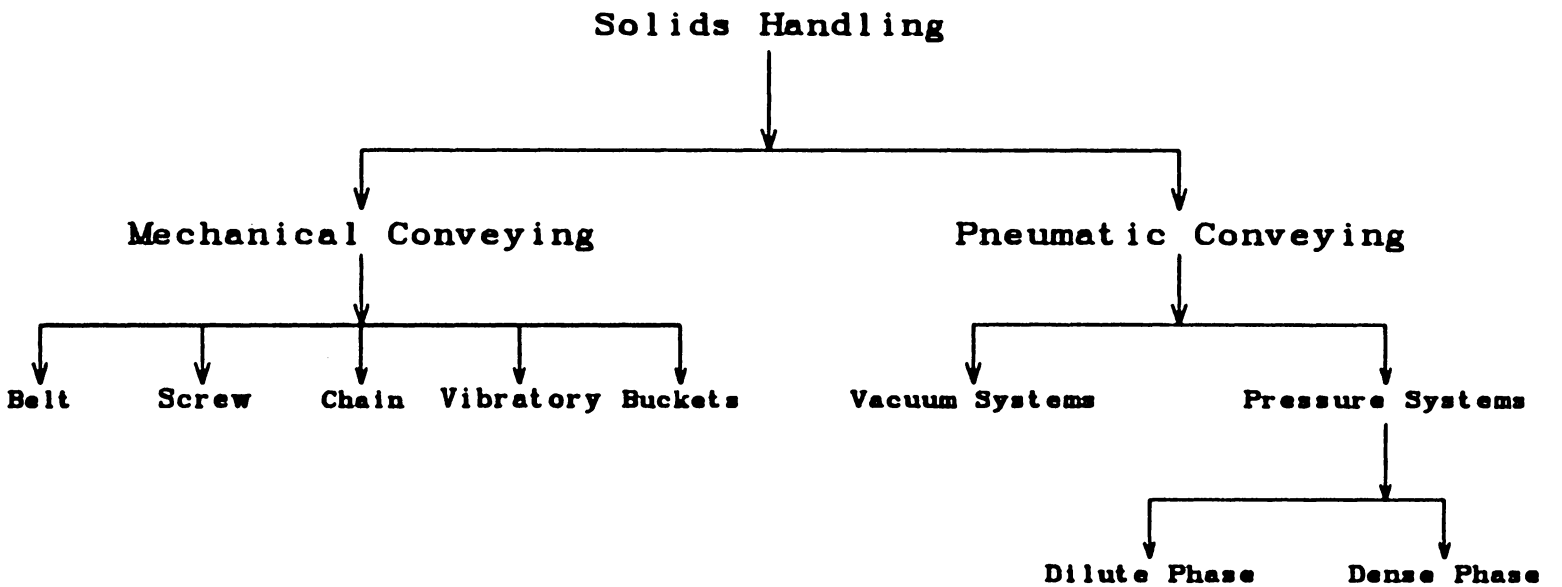

Figure 1.1 Solids Handling Options Within a Plant Site

fuels to name a few). Pneumatic conveyors offer some advantages over mechanical conveyors (Stoess, 1983). First, the straightline conveying of mechanical conveyors is eliminated. Mechanical conveyors require transfer points for changes in direction, therefore a series of conveyors may be required which can add to the cost and to control problems. In pneumatic conveying, short and long radius bends are utilized to change direction and to bypass obstructions. Also, space and accesses needed for maintenance purposes are minimized. A second advantage of pipeline conveying is cleanliness. The solids transported by mechanical conveyors are open to the atmosphere which can cause significant dust problems, especially at transfer points. Since the solids are enclosed in a pipe in pneumatic conveying, the dust problem is virtually eliminated. Also, there is little chance for contamination of the solid product in a pneumatic conveying system. This is important in the transport of foodstuffs, pharmaceuticals, or even plastics where one different-colored part in 80,000 may cause an off-color condition to the final product (Stoess, 1983). A third advantage of pneumatic conveyors is greater safety over their mechanical counterparts. Fire and explosion hazards are reduced. There is less risk of injury while conveying hazardous materials. This enhanced safety factor can result in lower insurance rates for industries that utilize pneumatic conveyors.

One of the prime disadvantages of pneumatic conveyors is that, even to this day, the design of these systems is more of an art than a science. Each year, researchers are learning more about the two-phase gas-solid flows thereby improving the reliability, but the final design is primarily based on

experimental correlations, tests with the actual material to be conveyed and past experience. Another disadvantage of pneumatic conveyors is the higher power costs compared to other conveyors. Recent research has been aimed at lowering this cost. A third disadvantage is the higher initial capital investment, but this can be offset by the labor-saving quality and possible reduction in insurance rates. A minor disadvantage is the ability of this conveyor to convey in one direction only. There are some limitations to the selection of pneumatic conveyors. These limiting factors are primarily based on the characteristics of the material and the conveying distance. Reece (1985) provides some general guidelines for deciding which type of system might be best suited for a particular application.

Pneumatic conveyors can be divided into two main categories: (1) vacuum and (2) pressure systems. For vacuum systems, the fan or blower is located at the discharge end of the pipe. The solids move under the influence of negative air pressure (i.e., less than 14.7 psia). This is especially useful when material from several different feed points must be transported to a single discharge point. With pressure systems, the fan or blower is located at the feed point, and the solids move under the influence of positive air pressure. The selection of the system depends on the particular conveying requirements. Several references describe the selection criteria between the different systems (see for example Stoess, 1983 or Krauss, 1986).

Depending on the flow conditions within the pipe, the pressure systems can be further classified into two categories: (1) dilute phase and (2) dense phase. Consider the flow patterns found in horizontal pneumatic conveying

(Figure 1.2). At high air velocities, the particles are suspended in the air stream and the solids loading is low. This is generally accepted as true dilute-phase flow. Upon reducing the air velocity, some particles begin to settle out of the suspension. The solids flow in strands sliding along the bottom of the pipe and in suspended flow above the strands. Further reduction of air velocity causes dunes or heaps of material to be formed within the pipe. These dunes are pushed down the pipe by impinging particles. At even lower velocities, a stationary layer is formed along the bottom of the pipe and the solids are transported in suspended flow in the upper portion. Further reduction of air velocity leads to plugs of solid material that completely fill the pipe cross-section separated by air slugs. In the final flow condition, particles completely fill the entire pipe and are extruded en masse through the pipe. Generally, some type of restriction is required at the discharge end to ensure that the entire pipe is filled.

Similar flow patterns exist in vertical pneumatic conveying. At high air velocities, the particles are transported in a dilute suspension in the pipe. Upon reducing the air velocity, the particle concentration increases across the pipe cross-section. Clusters are seen to form. Further reduction of air velocity leads to the formation of discrete plugs. Particles are seen to drop from the back-end of one plug and "rain" down on the front of the next plug of material.

Many definitions of dense-phase pneumatic conveying have been proposed. Konrad (1981) has reviewed several of these definitions and has analyzed the strengths and limitations of each. He has defined dense-phase transport as the

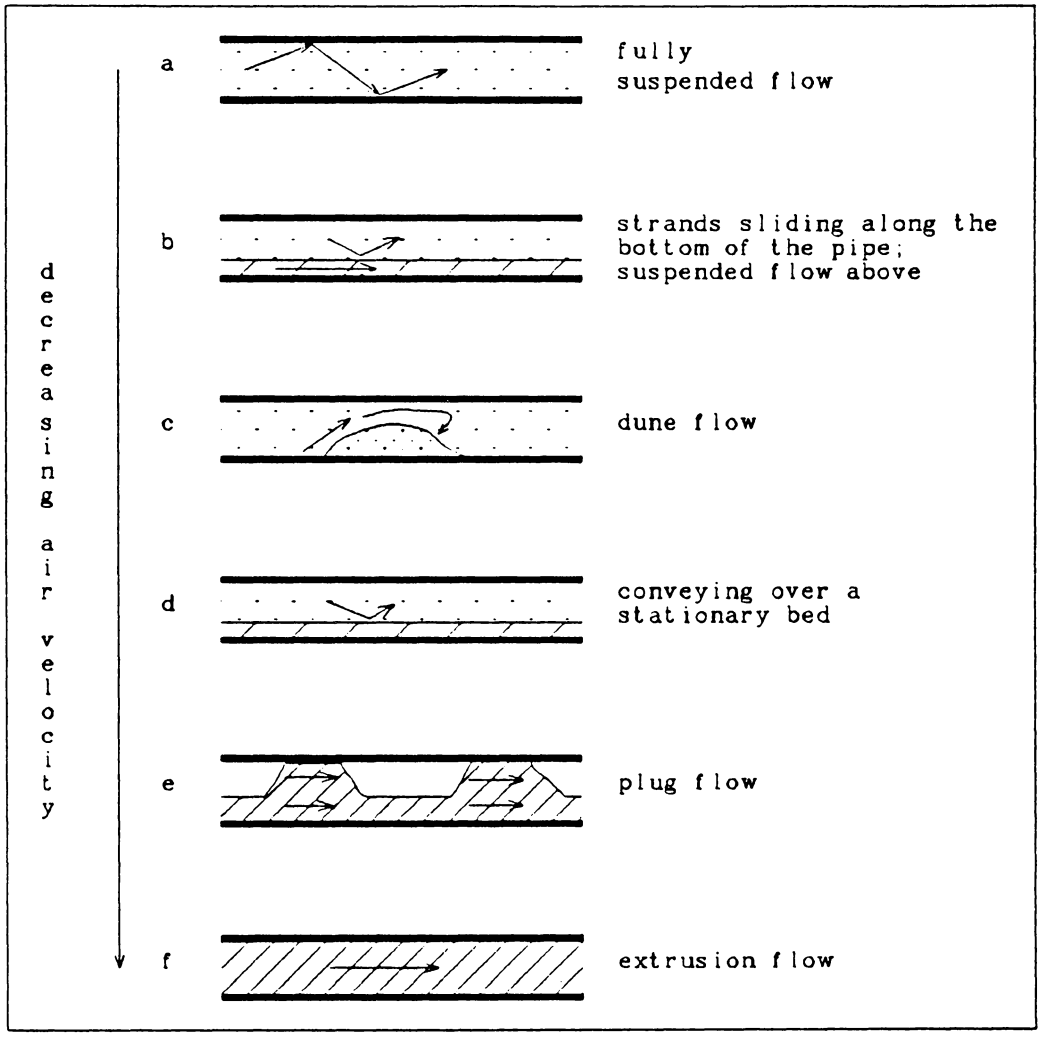

Figure 1.2 Flow Patterns in Horizontal Pneumatic Conveying (a through e according to Wirth and Molerus, 1984)

conveying of solids by air along a pipe that is filled with bulk solids at one or more cross-sections. This definition has been adopted for use in this thesis.

Until comparatively recently, all pneumatic conveying was done in the dilute phase. The early systems were designed to ensure that no pipe blockages occurred. Therefore, these systems used very high air velocities and volumetric flow rates. Consequently, these systems were not very efficient. Within the last 30 years, considerable research has been performed on dense-phase flow. Since the 1960's, several commercial systems have been successfully developed, and there is growing acceptance of this form of conveying within industry today.

Dense-phase conveying offers several advantages over dilute phase. The lower air velocities and subsequently lower particle velocities result in less pipe wear and particle attrition. The volume of gas is lowered which can be important when feeding coal to a gasification reactor or solids to a fluidized-bed reactor. The lower volume of gas is also important if an expensive gas such as nitrogen must be used to prevent an explosive mixture of the solids with air. Dense-phase conveying also helps in retaining the flavor of foodstuffs such as instant coffee.

Another advantage of dense-phase over dilute-phase transport is that the air-solids separation at the end of the pipeline is much easier. In dense phase, the solids are not in suspension so they merely fall out the pipe end into a storage vessel. For coarse particles, only an air filter is usually required. Finer particles require a cyclone and filter, but these are much smaller than would be necessary for dilute-phase conveying.

Some workers have claimed that dense-phase systems have a lower specific power consumption. Using the values of Lippert (1966), Konrad (1981, 1986) has shown a 40% lower specific energy consumption for dense-phase compared to dilute-phase conveying. Therefore, this claim seems reasonable though there could be cases where this is not so.

The primary disadvantage of dense-phase conveying compared to dilute phase is that the hydrodynamic transport mechanism is still not very well understood. Recently, there have been numerous studies (both experimental and theoretical) analyzing plug conveying. However, some quarters within industry are apprehensive of dense-phase transport believing that these systems are on the verge of a total pipe blockage. Dilute-phase conveying has been successful for many years and they see no need to change at this point even if dense phase can be demonstrated as less costly. The results of this research project should help alleviate some of these fears and provide a better basis for design.

An experimental program has been undertaken to gain a more fundamental understanding of the dense-phase transport of cohesionless solids. High-speed photography has been used to document the flow patterns of polyethylene granules in both the vertical and horizontal sections of a 50.80 mm diameter circulating unit. Pressure drop measurements across a 70 cm length in both the horizontal and vertical sections have been coordinated with the film work. The results of these experiments are compared with a theoretical model developed by Konrad et al. (1980).

In the next chapter, the pertinent literature concerning dense-phase

conveying is reviewed. A vast amount of literature has appeared over the past few years. With the increasing number of research efforts, there has been a proliferation of nomenclature and terminology thereby confusing an already complicated subject. Marcus (1986) has called for some international uniformity in the literature so that all workers can communicate effectively with one another. To illustrate this point, consider the flow pattern of Figure 1.2f. I have called this extrusion flow, but it has also been called thrust conveying, solid dense phase, full bore, mass flow and moving bed. Some researchers consider the latter definition to be the flow pattern of Figure 1.2b. This may seem trivial, but there are many even more confusing examples. With this in mind, let us delve further into the realm of dense-phase pneumatic transport of solids.

2.0 LITERATURE REVIEW

There are many texts, handbooks and conference proceedings concerning gas-solids handling. Most of these deal extensively with dilute-phase flow; describing the flow pattern, analyzing the equations which govern the gas-solids interaction and providing correlations and design techniques. The treatment of dense-phase flow in these works is cursory at best. A general review of some of the previous research is usually given with a description of the flow pattern. Then, it is usually stated that the hydrodynamics of these two-phase flow systems are quite complex and not very well understood.

Gradually, with the recent emphasis on dense-phase pneumatic transport, a theoretical description is beginning to evolve. Recently there have been a few reviews concerning only dense-phase conveying (see Konrad, 1986 or Klintworth and Marcus, 1986). This chapter is divided into four sections: (1) Horizontal Conveying, (2) Vertical Conveying, (3) Theory of Konrad et al. (1980), and (4) Stresses Within a Particulate Mass of Solids: Application of Soil Mechanics.

2.1 Horizontal Conveying

Albright et al. (1951), using a fluidized-bed feeder, transported coal through horizontal copper tubes to a gasifier. The objective of their experimental program was to measure the pressure drop as a function of tube

diameter, coal flow rates and coal/air ratio. Two different experimental rigs were used: (1) a small scale model 12 feet long and 3/16-inch diameter tube and (2) a larger unit 58 feet long and tube diameters of 5/16-, 3/8-, and 1/2-inch. They presented the data in tabular form and provide an empirical equation relating the pressure drop, average density of coal/air mixture and tube diameter. They conclude that the tube diameter has a definite effect on the pressure drop. For a particular mass velocity of the coal/air mixture, the pressure drop is greater in the smaller tubes. Unfortunately, since copper tubes were used, no description of the flow pattern was given. The authors admit that the measured pressure drop data for the three larger tubes includes any acceleration effects of the particles.

Wen and Simons (1959) conveyed various sizes of coal and glass beads through glass and steel pipes. Data were collected for approximately 200 runs with glass beads of 0.011-, 0.0058-, 0.0028-in. diameter and coal powder of 0.0297-, 0.0197-, and 0.0044-in. diameter flowing through 0.5-, 0.75-, and 1.0-in. I.D. glass pipe and 1/4-in. steel pipe (0.364-in. I.D.). Four diagrams based on visual observation of the flow pattern were provided. They describe the transition from suspended flow to dune flow. In dune flow, the solids flow took place by moving from one dune to the next, undergoing deceleration and acceleration alternatively. At higher solids loadings, small ripples appeared on top of a thick solid layer which was practically stationary. They also describe the intermittent flow of gas and solids in alternate slugs. Considerable pressure drop fluctuation was observed for slug flow.

Based on their data, Wen and Simons (1959) present both a correlation

and a design method. The correlation is for the pipeline pressure gradient in terms of the pipe and particle properties together with the mass flow rate of solids and air. Konrad (1981) has analyzed the correlation and design method. He concludes that the correlation is probably only valid at air pressures close to ambient and that the design method is not to be recommended.

Lippert (1966) recognized the economic attractiveness of dense-phase conveying, and was one of the first workers to study all aspects of plug flow. He made measurements of plug length, pressure drop and velocity of the solids at various air flow rates for both horizontal and vertical conveying of alumina. He found that the pressure required to move a plug rose progressively with the plug length. In order to break up excessively long plugs, Lippert introduced a by-pass pipe. In this design, an auxiliary line is connected with the main pipe at several intervals. If a plug becomes too long (and therefore, according to Lippert, the pressure drop becomes too large), or if the plug becomes stationary, the air will enter the by-pass pipe and re-enter the main pipe at such a point where the pressure required to move the plug in the main pipe is equal to or less than the pressure in the auxiliary line. This will cause the long plug to separate into two smaller plugs. Lippert claims that the total pressure loss required to move the two smaller plugs will be less than the pressure drop required to move the initially long plug. This design has become the basis of several commercial systems.

The main purpose of the work presented in the P.E.C. Report (1966) was to obtain data for gas-solid flows in larger pipes and over longer distances

than had been done previously. Also, clear plastic pipe was used in the investigation in order to visually document the flow pattern. Unfortunately, the report is poorly written; containing many errors and inconsistencies. However, the report contains a vast amount of data on the transport of sand/air mixtures. Three different sand sizes (0.034, 0.094, and 0.143 inch average particle diameter) were transported in 1-, 2-, and 3-inch diameter transparent plastic tubes over distances ranging from 75 feet to 550 feet. Solid-to-air mass flow ratios ranging from about 5 to 290 were used. Pressure taps were installed at several locations along the pipe length.

On the basis of visual observation, the authors of the report describe several different flow patterns in various sections of the pipe. In the early sections of the pipe, the solids move in the form of shifting dunes above a layer of stationary solids. Further down the pipe, the thickness of the dunes increases and hence the depth of the stationary mass decreases. There is a velocity gradient of solids across the pipe cross-section, the bottom layers moving slower than the top ones. In the final region, the solids move in a similar fashion to plug flow without any solid velocity gradients in the cross-section. Another mode of transport was observed for the finer sized sand in the early section of the pipe. The particles were compacted and moved as a piston pushing the solids in front of it. In all cases, as a solid slug passed a pressure tap, the indication of the pressure gauge showed considerable fluctuation.

Some of the results presented in the P.E.C. Report were published in a paper by Ramachandran et al. (1970). They analyze the data assuming that

the expansion of the air along the pipe length is adiabatic and reversible. However, Konrad (1981) has shown that the expansion is isothermal, and therefore concludes that the calculations of Ramachandran et al. (1970) are not directly relevant.

Dickson et al. (1978) conveyed single plugs of solids in horizontal pipes by applying air pressure, mechanical force and a combination of the two. The solids were loosely confined at the ends by porous fiber slugs backed with expanded metal discs. The discs were connected together by a length of string passing through the plug. The solids investigated were glass beads (1.5 mm and 0.07 mm diameter) and bentonite (mean particle size about 0.03 mm). Both transparent perspex and galvanized iron pipes (44 mm I.D. and 4 m long) were used in the experiments. A plug of the desired length was formed by turning the pipe vertically, inserting one plug end, loading the particles and then attaching the second plug end.

For the pneumatic propulsion experiments, air was supplied to the pipe through a regulator. The air flow was increased until a slow, continuous motion of the plug was observed. The corresponding air pressure was recorded. The data show that in all cases the pressure drop increased linearly with the plug length up to the maximum plug length of 1600 mm. However, there was more scatter for the smaller glass particles. These results conflict with Lippert's (1966) data that showed a square law relationship for Alumina 66.

For the mechanical propulsion experiments, the string connecting the plug ends was continued through the pipe and over a pulley at the downstream end. A force could be applied to the plug by adding weights to a bucket attached to

the string. The force required to maintain a slow, continuous motion of the plug was recorded for various plug lengths. A plot of the applied force versus the plug length shows an exponentially increasing dependence of the force on the plug length for 1.5 mm glass beads in the perspex pipe. They developed a theoretical relationship that predicted the exponential dependence and represented the data quite satisfactorily (approximately ±10%).

Cardoso (1978) used the same apparatus (with slight modifications) to convey 1.4 mm diameter glass beads in perspex and galvanized pipe. He provided a more detailed description of the system and operating procedures. He found similar results to those reported earlier by Dickson et al. (1978). Cardoso also describes some of the experimental difficulties. The plug ends were susceptible to tilting and wedging in the pipe, especially for the rougher galvinized pipe. He recommends a better design for the plug end system and a transport pipe with a better surface finish and roundness.

Konrad et al. (1980) developed a method to predict the overall pipeline pressure drop in horizontal dense-phase transport. Since one goal of the present work is to test the method and theory of Konrad et al. (1980), a more detailed description is given in Section 3 of this chapter. Only a brief description will be given here.

Konrad observed the flow pattern of cohesionless polyethylene granules. He concluded that the solids are conveyed in plugs of material (at about their maximum packing density) and in the regions just in front of and behind the plugs. A stationary layer of material rests at the bottom of the pipe between the plugs. As a plug moves down the pipe, the stationary material in front of

the plug is "swept" up and becomes part of the moving plug. Simultaneously, solids are dropped from the back of the plug, reforming the stationary layer. Sweeping up the stationary solids generates a stress on the front end of the plug. This stress is transmitted through the plug by intergranular forces to the tube wall where it generates a shear stress in addition to that due to the weight of the particles. From these observations, Konrad developed an equation for the pressure drop over a single plug based on a Janssen (1895) style analysis for stresses within a granular media. A packed-bed model was used to relate the overall pressure drop to the slip between the gas and the solids. Konrad et al. (1980) also recognized the similarity between this dense solid-gas flow and horizontal gas-liquid slug flow. Applying the gas/liquid analogy allows a method to predict the velocity of the interface at the back of the plug. Combining these three developments leads to a method to calculate the overall pressure drop in a horizontal pipe.

Legel and Schwedes (1984) present the results of a study on plug flow conveying of cohesionless solids in horizontal pipes. A theoretical equation for the pressure drop is derived based on a force balance over a single plug of solids. Experimental results were used in conjunction with the theoretical equation to develop semi-empirical relationships for the pressure drop over a single plug and for the total pipeline pressure drop.

Legel and Schwedes describe the flow pattern of cohesionless solids in a horizontal pipe. Their description and subsequent analysis is very similar to that presented by Konrad et al. (1980). As a plug is transported through a horizontal pipe, solids are continuously lost from the back which settles as a

streamer along the bottom of the pipe. The front of the plug collects a streamer of bulk solids which has been lost from the preceding plug. An equilibrium exists between the driving force originating from the gas and the reaction forces between the plug and its bounds. The energy of the conveying gas is divided into the pressure force acting on the solid particles and the flow resistance through the channels of the packed bed of solids. The weight of the particles, when multiplied by the coefficient of wall friction, gives the frictional force in the lower half of the pipe. When the plug collects a settled streamer, a pushing force acts on the plug front. The external forces in the conveying direction tend to compress the particles in the axial direction resulting in an axial compressive stress. This leads to a radial compressive stress perpendicular to the pipe wall. Therefore an additional friction force between the particles and the pipe wall acts along the entire circumference of the pipe. Combining these into the force balance leads to an expression for the pressure drop over a plug of particles:

$$\frac{\Delta P}{\ell_p \rho_b g} - \tan \psi_x = (\chi)(Fr_c) \qquad (2.1)$$

where ΔP is the pressure drop over a plug

ℓ_p is the plug length

ρ_b is the bulk density of the solids

g is the acceleration due to gravity

ψ_x is the angle of wall friction

χ is the wedge number

$$= \frac{\rho_{b,St}}{\rho_b} \frac{A_{St}}{A} \; 4 \lambda \, (\tan\psi_\chi) \, B_c$$

Fr_c is the Froude number

$$= \frac{c^2}{D\,g}$$

$\rho_{b,St}$ is the solids bulk density in the settled streamer

A_{St} is the settled streamer cross-sectional area

A is the pipe cross-sectional area

λ is the ratio of radial to axial compressive stress

B_c is the ratio of compressive stresses in the plug (close to one for ideal plugs)

c is the plug speed

D is the pipe diameter

A test facility was constructed to collect data for horizontal conveying of a variety of materials. The solids were fed into a 22 m long pipe through a pressure vessel. Steel pipes with internal diameters of 40 mm and 65 mm and acrylic glass pipe with an internal diameter of 40 mm were used. The test materials included three different sized silica sand (mean sizes 0.51 mm, 1.68 mm, amd 2.83 mm), polyethylene granules (3.19 mm) and blue bitter lupines (5.63 mm).

The plugs were generated by two methods: (1) a pulse of air was injected into the conveying line to separate the solids into individual plugs, and (2) over a small range of pressure in the feed vessel, plug flow established itself.

The majority of the experiments were conducted using the first method. The mass flow rate of solids, the volumetric air flow and the overall pipeline pressure drop were measured. A measuring pipe was inserted halfway down the pipe to determine the conveying state of individual plugs. The friction force between the plug and pipe wall was measured by a load cell. The pressure drop over a single plug was determined by the difference between two pressure gauges. The bulk density of the conveyed plugs was measured by a gamma-ray density gauge. Two light barriers, with 8 photo-transistors on the circumference, were fitted around the pipe in order to determine the plug speed, plug length and settled streamer height.

Legel and Schwedes present fitted curves from the experimental data for the plug speed as a function of the superficial air velocity, the ratio of the streamer cross-sectional area to the pipe cross-sectional area as a function of the Froude number, the drag coefficient as a function of Reynolds number and the wedge number as a function of the Froude number. They found that a minimum gas velocity (which is on the order of the minimum fluidization velocity) was required to initiate the motion of a plug of solids. Also, a higher gas velocity was necessary to reach the same plug velocity with increasing size of the three silica sands. The streamer cross-sectional area decreases much more rapidly for the coarser and lighter solids (polyethylene granules and blue bitter lupines) than for the heavier silica sands. The density measurements indicated that the solids bulk density is nearly equal to that of loosely packed solids at the onset of fluidization. In general, the drag coefficients for pneumatically conveyed plugs were larger than the drag coefficients determined from

fluidization experiments. The wedge number was plotted as a function of the Froude number. From the data, average values of the fitted parameters were used to derive a semi-empirical relationship of the pressure drop over a single plug of solids:

$$\Delta P = (1 + 2.6 Fr_c^{0.2}) (\tan \psi_x) \rho_b g \ell_p \qquad (2.2).$$

A few comments should be made about the work of Legel and Schwedes (1984). First, the theoretical equation predicts a linear dependence of the pressure drop on the plug length. This is in agreement with the theoretical work of Konrad et al. (1980) and the experimental work of Dickson et al. (1978), but contradicts the work of Lippert (1966). It should be noted that Lippert's work was for fine, cohesive material whereas the other workers were dealing with cohesionless particles. Second, Legel and Schwedes calculated the slip velocity as the difference between the gas superficial velocity and the plug speed. However, Konrad et al. (1980) have shown that the true slip velocity for plug flow conveying is the gas superficial velocity plus the solids superficial velocity minus the mean particle velocity. Third, the force due to the collection of a streamer according to the momentum balance of Legel and Schwedes is:

$$S_c = c^2 \rho_{b,St} A_{St} \qquad (2.3).$$

However, Konrad et al. (1980) give the momentum balance for the force as:

$$S_c = \frac{c^2 \rho_b A_{St}}{1 - \frac{A_{St}}{A}} \qquad (2.4).$$

Note that Konrad assumes the bulk density of the settled stationary material is

the same as the bulk density in the moving plug. Other than these couple of discrepancies, the theoretical work of Legel and Schwedes is very good and the experimental technique was excellent.

In order to reconcile the differences between the experiments that show a linear relationship for the pressure drop as a function of the plug length and those that show a progressively increasing variation, Wilson (1986) has proposed a generalized formulation that yields both cases as particular solutions. The analysis takes into account the variation of stress along the plug, and the effects of interstitial fluid flow through the particulate mass. He has shown that the effects of plug length, pipe radius, and particle and fluid properties can be characterized by two independent dimensionless groups:

(1) Λ - a dimensionless measure of the plug length,

(2) W - an indicator of the fractional change in fluid pressure gradient with respect to the logarithm of the particulate normal stress.

For an incompressible material (i.e. the bulk density does not vary with applied stress), W equals zero and the analysis leads to a linear solution. For positive values of W, the linear case remains as a possible solution, but non-linear solutions are also possible. In practice, the non-linear case leads to a blockage in the pipeline, whereas during successful plug conveyance, the pressure drop is linearly proportional to plug length.

Tomita et al. (1981) studied the dense-phase flow of polyethylene pellets in a horizontal pipe. The granular solids were fed from a blow tank into the transport pipe by compressed air introduced at the upper part of the tank. A

transparent plastic pipe 11.8 m long with an internal diameter of 42 mm was used for the experiments. Four photocells were spaced at 2 m intervals in order to detect the flow of individual solid plugs. The pressure in the feed tank and at two points along the transport line were measured. The air and solid mass flow rates were also measured. The polyethylene pellets used in the experiments had a mean diameter of 3.09 mm, a particle density of 920 kg/m^3 and a bulk density of 589 kg/m^3.

The description of the flow pattern given by Tomita et al. (1981) is similar to that of Konrad et al. (1980) and Legel and Schwedes (1984). The bottom section of the pipe was initially lined with a stationary layer of particles. Once this layer was formed, the net transport of solids began. As one plug exited the pipe, a new plug formed at the entrance. The particles in the stationary layer are accelerated by an oncoming plug and transported over a certain distance. By observing successive photographs of a moving plug, the authors infer that the particles moving in the upper part is faster than those moving in the lower part. However, Konrad et al. (1980) found through high-speed cinematography that the entire plug moves as a packed bed at a constant velocity (except for the particles just in front or behind the plug which are either being accelerated or decelerated).

Tomita et al. (1981) plot their experimental data in a variety of ways. The solids mass flow rate was uniquely determined by the inlet superficial air velocity for the blow tank design used in the experimental work. A minimum air velocity of about 1 m/s was required before solids transport began. The solids flow increased in proportion to the air velocity. The solids loading increased

with the air velocity, reached a maximum, then tailed off at an inlet superficial air velocity greater than about 6 m/s. The experimental results also showed that the height of the settled layer decreased with increasing air velocity, and that the plug speed increased in proportion to the air velocity. A plot of the pressure drop over a plug versus the superficial air velocity shows that for a velocity less than 6 m/s, the pressure drop varies proportionately. The pressure drop goes through a maximum, then tails off at a higher velocity. For a certain range of plug flow, the total pressure drop is given by the pressure drop over a single plug multiplied by the total number of plugs in the pipe. At larger values of the superficial air velocity, this underestimates the total pressure drop which suggests that the pressure drop due to air flow between the plugs cannot be neglected. The authors plot the pressure gradient versus the slip velocity (superficial air velocity minus average particle velocity). Also shown on the plot are curves calculated from the Ergun (1952) equation for two different porosity values. The authors conclude that the plug pressure drop can be estimated by the Ergun equation although there is considerable spread in the data. However (as noted previously), Konrad et al. (1980) have shown that the slip velocity in plug flow conveying is the superficial air velocity plus the superficial solids velocity minus the average particle velocity. This may account for some of the spread in the data. Finally, a plot of the plug length versus the pressure drop over a plug is provided. The authors draw a curve through the data that shows a progressively increasing pressure drop with increasing plug length similar to that of Lippert (1966). It should be noted that the authors did not always

observe true plug flow conveying. The wavelike slug flow sometimes occurred without completely filling the pipe cross-section at larger values of the superficial air velocity.

Tsuji and Morikawa (1982a, 1982b, 1982c) have extensively studied the horizontal plug flow of solids. Tsuji and Morikawa (1982a, 1982c) present the experimental results of dense-phase conveying with secondary air injection through a sub-pipe inserted along the bottom of the main pipe. The internal diameter of the transparent acrylic main pipe was 50 mm and the length was about 6.2 m. The sub-pipe was vinyl with a 10 mm outer and 8 mm inner diameters. Solids were fed into the main pipe through two electromagnetic feeders. Measured quantities included the air flow rates in the main and sub-pipes, particle flow rate, passing period of plugs and the pressure drop across a plug. Four pressure taps connected to three differential pressure transducers were placed along the length of the pipe. Four photo-detectors to measure the plug passage were located at the pressure taps. Tsuji and Morikawa (1982a) established the experimental technique for one particle type (polyethylene spheres; d_p = 1.1 mm) and for one sub-pipe configuration (six secondary air injection holes; 4 mm diameter). Visual observation of the plug motion and the effects of the main and sub-pipes air flow rates were documented. Tsuji and Morikawa (1982c) extended the technique to include a variety of particle sizes (polystyrene spheres; d_p = 0.4, 1.1, and 3.0 mm) and three different sub-pipe configurations (1, 6, and 15 secondary air injection holes).

The flow pattern description based on visual observation is slightly

different than given previously. The authors indicate that a stationary layer is always present in the pipe and that the plug of solids moves on this layer in a wavy motion. The effect of the sub-pipe is unknown, but this may account for the difference in the observed flow pattern.

As a plug passes a pressure tap, the pressure increases linearly, reaches a maximum when the plug is between the two taps, then decreases linearly as the plug passes the downstream tap. Tsuji and Morikawa (1982a) found that the pressure drop over a plug depended on the air flow rate in the sub-pipe and not in the main pipe. The authors found that the pressure gradient in the moving plugs was significantly lower than that in a packed bed. They concluded that a relation such as the Ergun (1952) equation cannot be applied to a moving plug with secondary air injection from a sub-pipe located at the bottom of the main pipe. Tsuji and Morikawa (1982c) compared the pressure drop from the experimental plug flow data to the Ergun equation for flow through a packed bed by plotting the pressure gradient versus the superficial air velocity. However, the slip velocity for plug flow conveying given by Konrad et al. (1980) should have been used in the calculation. This might explain the observed deviation.

Tsuji and Morikawa (1982b) investigated the relation between the pressure fluctuations and the flow patterns for horizontal air-solid two-phase flow. Solid particles were supplied by an electro-magnetic feeder to a transparent acrylic pipe (40 mm I.D.; 14 m long). Two pressure transducers and photo detectors were placed 1.4 m apart along the pipe. Two sizes (0.19 and 2.8 mm mean diameter) of spherical plastic pellets (ρ_p = 1000 kg/m^3) were used

in the experiments.

The flow patterns were classified into five major types ranging from dilute-phase flow to dense-phase plug flow. For the smaller particles, plug flow was not steady and led immediately to a blockage. For the larger particles, the authors did not observe either dune flow or suspended flow over a stationary layer. The pressure signal for dilute-phase flow showed very small fluctuations. For dune flow of smaller particles, the pressure fluctuation had a long period component. For plug flow of large particles, large fluctuations corresponded to a plug passing the pressure tap. The frequency power spectrum of the pressure fluctuation was generated by the Fast Fourier Transform (FFT) technique. For the small pressure fluctuations of dilute-phase flow, the higher frequency components were dominant. For the more dense-phase flow (dune or plug), the lower frequency components were dominant which corresponds to the longer period of the pressure fluctuations.

Kano et al. (1984) derived a theoretical expression for the pressure required to move a plug of particles in a pipe inclined at an angle θ from the horizontal. The equation, based on a force balance, predicts an exponential dependence of the pressure on the plug length. However, the analysis appears to be flawed. For minimum fluidization in a vertical tube, the pressure drop through the bed equals the weight of the particles. Applying this condition to their equation (6) would lead to a pressure drop across the bed equal to zero. Clearly, this is incorrect. In a subsequent paper, Kano (1986) modified the analysis. He considered the inclined pipe case where a plug slides on a stagnant layer of solids. The equation given for the pressure loss over a plug

shows a linear dependence on the plug length.

Kano et al. (1984) measured the air pressure required to move a single plug of calcium carbonate packed into a transparent acrylic pipe. The pipes were either 10 m long horizontal or 8 m long vertical with internal diameters of 66, 78, and 98 mm. The length of the packed plug varied between 0.2 and 0.8 m. The air pressure required to move the plug, the air flow rate and the plug velocity were measured. The pressure required to move the plug and the volumetric air flow were plotted versus the plug length. For the horizontal case, the data show a progressively increasing pressure with increasing plug length. From their experimental data, the authors conclude that the larger the pipe diameter, the lower the power required to convey a unit mass of material, and the shorter the plug length the greater the efficiency of transport.

Kano (1986) suggests that vibrating the pipe in plug conveying should reduce the wall friction and therefore lower the power consumption in dense-phase conveying. Preliminary experiments with calcium carbonate packed to a plug length of 300 mm in 25 mm acrylic pipes 1 m long (both horizontal and vertical) indicate that the air pressure required to move a plug decreases with an increasing vibration frequency. Millet was conveyed in a 5 m long horizontal pipe vibrated at different positions and in different directions. The power requirement was reduced by about 20% with vibration applied to the pipeline centerpoint.

Chan et al. (1982) have proposed a theoretical model of plug flow pneumatic conveying. The model takes into account the pressure and stress distributions through a plug. The model is used to predict the time average

pressure distribution in a pipe of multiple plugs. A non-linear differential equation governing the pressure gradient through a single plug as a function of time was derived and solved numerically. A linearized version of the differential equation was solved analytically. The authors considered the case of a single plug of uniform initial pressure accelerating at a constant rate in a pipeline with a linear pressure gradient. A constant pressure difference between the upstream and downstream faces of the plug for all times greater than zero was also assumed.

The solution was provided for conditions typical of those reported in the PEC Report (1966) for coarse and fine particles. The graphical presentation of the pressure distribution shows that the pressure goes through a maximum at the center of the plug. This effect is more pronounced for the smaller particles and for longer time values (i.e. the plug further down the pipe). For the fine particles at time equals 18 seconds, the pressure in the center is approximately double the pressure at either end. The authors rationalize this by claiming that the fluid is retained inside the plug to an extent dependent upon the permeability and therefore the particle size. The only support for this conclusion is based on the observations in the PEC Report that the pressure gauges became unstable as a plug passed; the pressure increasing by 21-55 kPa and then decreasing.

The pressure distributions were then used to compute the interparticle stresses using the expression of Dickson et al. (1978) for the wall frictional force due to the radial transmission of the axial stress. With a pressure drop over the plug of 18 kPa and a zero stress on the front of the plug, the stress

distribution lies almost entirely in the tensile region. The authors therefore conclude that only cohesive plugs can be sustained with a zero frontal stress. Cohesionless materials require a positive frontal stress which is caused by accelerating the stationary layer to the plug velocity. Stress distributions through a plug with an arbitrary frontal stress of 14 kPa and various pressure drops over the plug are presented graphically. For certain pressure drops, the axial stress lies entirely in the compressive region. There is a particular pressure drop such that the axial stress goes through zero and into the tensile region. The authors conclude that for cohesionless particles, the negative stress region corresponds to a situation where the plug is collapsing.

For multiple plugs in a pipeline, the pressure drop in the interplug space is minimal. Therefore, the total pipeline pressure drop is the sum of the pressure drops over each individual plug. Chan et al. (1982) develop a relationship for the time average pressure distribution in a pipeline. Their results compared favorably to one set of flow conditions provided in the PEC Report. Since all of the relevant parameters were not given in the PEC Report, some of the values had to be estimated. The authors extended the relationship by correlating a vast amount of data found in the PEC Report. The authors caution that the proposed method could lead to inaccuracies if extrapolated beyond the conditions considered in its formulation.

While Chan et al. make several valid conclusions, there are some curious results presented in the paper. The most striking is the assertion that the pressure within the plug reaches a maximum in the middle. For fine particles, this maximum can be significantly greater than the pressure at either end. This

scenario does not seem plausible and is not supported by any experimental work. In discussing multiple plugs in a pipeline, the authors correctly note that the pressure drop in the interplug space is negligible. The time average pressure gradient in the pipeline is approximately linear. However, this would not be the case for a single plug as was assumed in solving the differential equation for the pressure distribution in a plug. Also, the final analytical solution to the linearized differential equation is not dimensionally consistent. In solving the equation in their Appendix A, the authors assumed that the equation was cast in dimensionless form. Therefore, a transformation of variables has probably been made which has not been reflected back into the final solution in the main body of the text. The authors do not state the value of all parameters used in the solution, so it is difficult to determine if the solution is correct.

Some of the conclusions that are made are worth noting. Chan et al. point out the importance of the stationary layer for plug conveying of cohesionless solids. Accelerating the particles in the stationary layer just ahead of the plug causes a frontal stress which helps maintain the plug stability. In future experiments, measurements of the porosity, friction coefficient, stress ratio, plug length and stationary particle depth should be made.

Lilly (1984) performed similar experiments to those of Dickson et al. (1978). He measured the pressure drop and air flow rate required to move a plug of cohesionless solids in horizontal pipes. The results were compared to the theoretical model of Konrad et al. (1980). The solids were confined to a specified length by a plug-end conveying system. Two steel rings, with wire

mesh welded to it, were connected together by two radio antennae. The plug length was changed by adjusting set-screws in the antennae. The frontal stress could be adjusted by adding weights to a basket on the front plug end. The solids were loaded through a hole drilled in the pipe by placing the pipe on a 45° from the horizontal. Two sizes of polyethylene granules (4.4 mm and 3.2 mm diameter) and spherical alumina (1.0 mm diameter) were used in the experiments. The pipes were clear lexan (internal diameters of 25.4, 50.8, and 95.25 mm). The particle shear properties (particle/particle and particle/wall) were measured with an annular ring shear cell.

The plug lengths ranged from 368.3 to 952.5 mm. Lilly's results show a linear dependence of the pressure drop as a function of the plug length. Also a larger frontal stress causes a higher pressure drop required to move a plug. While the results were in qualitative agreement with the theory of Konrad et al. (1980), the quantitative agreement was not so good.

2.2 Vertical Conveying

Lippert (1966) conveyed alumina through a 12.5 m long, 40 mm diameter, vertical pipe. Unfortunately the flow pattern was not fully described or discussed even though transparent pipes were used. The pressure drop versus average air velocity was plotted on a phase diagram. The by-pass pipe arrangement was used for the experiments. It is difficult to assess the impact that this arrangement had on the flow pattern or required pressure drop.

The PEC Report (1966) contains data for the vertical transport of sand in

pipes 10 and 15 feet in length, 2- and 3-inch in diameter. No description of the flow pattern is given. The time and quantity of air required to completely transport a given amount of sand to the receiver vessel as well as the pressure at specified intervals along the pipe were recorded. The air and solids flow rate versus the feed tank pressure are presented graphically. Data for the pressure along the pipe, air and solids flow rate, and time required to transport the sand are presented in tabular form.

Sandy et al. (1970) transported several types of particles with a variety of gases (a total of 13 gas-solid systems) in upward moving bed flow through stainless steel tube. However, only data for the fused alumina (70-80 U.S. mesh)/air system is presented in the paper. The experimental apparatus consisted of three sections increasing in cross-sectional area in the flow direction (12 ft. of 1/2-in., 8 ft. of 5/8-in., and 4 ft. of 3/4-in. 20 BWG stainless steel tubing). Pressure taps were located at several locations along the pipe. The solids flow rate was regulated so that the bulk density in the lift-line was maintained near the bulk density of the static bed. Since the tubing was not transparent, the authors could not be totally certain of the flow pattern. The solids and gas flow rates were measured for each run.

Sandy et al. attempted to correlate the data with a theoretical equation they developed for the pressure drop. However, Konrad (1981) has pointed out three errors that they made in the theoretical development.

(1) They add the pressure drop due to the gas-solids friction to that due to the work done by the gas in moving the solids whereas these terms should be equal.

(2) They incorrectly calculate the pressure drop due to the work done in moving the solids through a specified height.

(3) They ignore the effect of wall friction. Since the pressure gradient is always greater than that required to overcome the weight of the solids, it follows that there must be some wall friction.

In view of these errors, the procedure outlined by Sandy et al. to calculate the pressure drop is not recommended.

Tomita et al. (1980) transported cement vertically through PVC pipes of about 24 m length and inside diameters of 41.0 and 66.8 mm. The solids and air mass flow rate and the pressure at several points along the pipe were recorded with time. The authors did not describe the flow pattern, therefore the PVC pipes were probably not transparent. The graph of pressure versus time shows considerable pressure fluctuations typical of plug flow conveying.

Kano et al. (1984) transported discrete plugs of calcium carbonate vertically through 8 m long, transparent acrylic pipes with internal diameters of 66, 78, and 99 mm. The air flow was gradually increased until the plug began to move. The pressure and air velocity required to move the plug were recorded. The data show an approximately linear dependence of the pressure on the plug length. Kano (1986) also measured the effect of vibration on the pressure drop required to move a plug. He found that the air pressure required to move the plug decreases with an increasing vibration frequency.

In vertical pneumatic transport of solids, the transition from dilute-phase to dense-phase flow is usually called choking. There have been several studies analyzing this phenomenon. However, the definition of the choking point is not precise and there is much confusion over the use of this term. Leung (1980)

described two distinct transitions from dilute-phase to dense-phase flow. In the first type, a sharp transition point occurs from the uniform suspension of dilute-phase flow to dense-phase plug (slugging) flow. In general, coarse particles in small tubes exhibit this behavior. Leung has defined the sharp transition as the choking type system. In the second type, a fuzzy transition occurs as the gas velocity is gradually reduced at a fixed solid rate. Clusters and streams of particles appear and solids are then conveyed upwards with considerable internal solid recirculation. Upon further reduction of air velocity, the flow pattern changes to slugging dense-phase flow. This second type of system is defined by Leung as the non-choking type. In general, fine particles in large tubes tend to exhibit this behavior. Leung has reviewed several analyses from the literature for predicting whether a particular system may be classified as the choking or non-choking type system. He has proposed a quantitative flow regime diagram which can be used to determine the flow pattern for a particular gas-solid system.

Satija et al. (1985) studied the pressure fluctuations in vertical transport of fine particles. They developed a criterion based on the power spectral density function and the standard deviation of the pressure fluctuations to determine the choking transition. Four different types of fine particles were transported through a plexiglass tube (0.107 m I.D., 6.46 m long). The air velocity and solids flow rate were measured. The average pressure in the bed was determined from several manometers. A differential pressure transducer was used to obtain the pressure fluctuations.

Satija et al. found that coarse sand, fine sand, and spent FCC particles

exhibited the choking-type behavior whereas glass beads showed the non-choking type behavior. For dilute-phase flow, the pressure fluctuations were found to be extremely small. Transforming the data to the frequency domain by the Fast Fourier Transform technique, some spikes in the power density spectral function (PDSF) are observed at almost zero frequency. Upon reducing the air velocity, the pressure fluctuations become more pronounced for the choking systems. Higher frequencies are found to exist in the PDSF and an average dominant frequency can be determined. There is a particular air velocity at which the dominant frequency abruptly drops and then remains constant with decreasing air velocity. This velocity corresponds to the choking velocity, and is confirmed by visual observation and hold-up measurements of the fine particles. Also, the standard deviation of the pressure fluctuation signal increases sharply at the choking point upon reducing the air velocity. For the non-choking system (glass beads), the abrupt changes are not observed. The authors conclude that the dominant frequency and standard deviation of the pressure fluctuation can be used to accurately determine the choking transition.

Konrad (1987) has provided a description of the flow pattern and has proposed a method to calculate the pipeline pressure drop in vertical plug conveying of solids. The particles move as discrete plugs that fill the entire cross-section of the pipe at several intervals. Solids are continuously dropped from the bottom of one plug and "rain" down on the front of the next plug. This causes a stress on the plug front which is transmitted through the plug by intergranular forces to the tube wall where it generates a shear stress. The resulting shear force plus the force due to the weight of the particles is

balanced by the pressure drop due to the percolation of air through the particles. Konrad et al. (1980) developed an expression for the pressure drop required to move a single plug of solids through a vertical pipe. The theoretical expression is discussed in Section 3 of this chapter.

Borzone (1985) transported discrete plugs of coal particles vertically through PVC tube (25.4 mm I.D., 3.05 m long). Four different types of coal samples ranging in particle diameter from 9.8 μm to 38.0 μm were used in the experiments. The coal was loaded into the tube and the walls were tapped to consolidate the sample. The air valve was opened allowing the flow rate to reach the desired value. The air flow rate, the pressure drop and plug velocity were measured for a variety of plug lengths. Borzone found that the pressure drop increases linearly with the plug length and is independent of the air velocity in the range studied. The theoretical model of Konrad et al. (1980) represented the data very well (approximately ±5%).

2.3 Theory of Konrad et al. (1980)

Konrad et al. (1980) have proposed a method to calculate the overall pipeline pressure drop in dense-phase horizontal pneumatic conveying. Konrad (1987) extended the analysis to predict the pressure drop in vertical pipes.

The theory is based on the following:

(1) The solids are conveyed in a series of plugs that occupy the entire cross-section of the pipe. The solids move as "packed beds" at about their maximum packing density. Therefore, the Ergun (1952) equation

for flow through a packed bed can be applied with the air velocity replaced by a slip velocity.

(2) For horizontal conveying, there is a stationary layer of material between the plugs. As a plug moves down the pipe, the stationary layer is "swept up" and accelerated to the plug velocity. In vertical conveying, particles are continuously lost from the back of one plug and "rain" down on the front of the next one. In both cases, a stress is applied to the plug front which is transmitted axially through the plug and radially to the pipe wall. The principles of powder (soil) mechanics can be used to calculate the pressure drop required to move a single plug.

(3) For horizontal flow, the flow pattern resembles that of a gas/liquid system. The gas/liquid analogy can be applied to predict the velocity of the interface at the back of the plug.

2.3.1 The Pressure Drop Required to Move a Single Plug of Solids

Konrad et al. (1980) developed a set of theoretical equations for the pressure drop required to move a single plug of solids through both vertical and horizontal pipes. The method assumes that the stress distribution in the granular media can be found from a Janssen (1895) analysis similar to that used in designing hoppers or found in soil mechanics. Since granular materials are frictional, it is only possible to predict the ranges within which the stresses must lie. The two extremes are known as the active and passive

solutions. For the passive case, the principal radial stress is greater than the principal axial stress, whereas the converse is true for the active case.

The equations developed by Konrad et al. (1980) are:

Vertical Plug; Passive Case

$$\frac{\Delta P}{\ell_p} = \rho_b g + \frac{4\mu_w K_w F}{D} + \frac{4\mu_w(K_w+1)c\,\cos\phi\,\cos(\omega+\phi_w)}{D} + \frac{4c_w}{D} \qquad (2.5)$$

Vertical Plug; Active Case

$$\frac{\Delta P}{\ell_p} = \rho_b g + \frac{4\mu_w K_w F}{D} - \frac{4\mu_w(K_w+1)c\,\cos\phi\,\cos(\omega-\phi_w)}{D} + \frac{4c_w}{D} \qquad (2.6)$$

Horizontal Plug; Passive Case

$$\frac{\Delta P}{\ell_p} = 2\rho_b g\,\tan\phi_w + \frac{4\mu_w K_w F}{D} + \frac{4\mu_w(K_w+1)c\,\cos\phi\,\cos(\omega+\phi_w)}{D} + \frac{4c_w}{D} \qquad (2.7)$$

Horizontal Plug; Active Case

$$\frac{\Delta P}{\ell_p} = 2\rho_b g\,\tan\phi_w + \frac{4\mu_w K_w F}{D} - \frac{4\mu_w(K_w+1)c\,\cos\phi\,\cos(\omega-\phi_w)}{D} + \frac{4c_w}{D} \qquad (2.8)$$

where

ΔP is the pressure drop across the plug

ℓ_p is the plug length

ρ_b is the particle bulk density

ϕ_w is the angle of wall friction

μ_w is the coefficient of wall friction ($\mu_w = \tan\phi_w$)

ϕ is the angle of internal friction

K_w is the coefficient of internal friction at the wall

$$= \frac{1 + \sin\phi \cos(\omega+\phi_w)}{1 - \sin\phi \cos(\omega+\phi_w)} \qquad \text{passive case}$$

$$= \frac{1 - \sin\phi \cos(\omega-\phi_w)}{1 + \sin\phi \cos(\omega-\phi_w)} \qquad \text{active case}$$

c is the interparticle cohesion

c_w is the particle/wall cohesion

F is the stress on the plug front

D is the pipe diameter

g is the acceleration due to gravity

$$\omega = \sin^{-1}\left[\frac{\sin\phi_w}{\sin\phi}\right]$$

(Note: strictly this is for cohesionless materials, but is a good approximation for cohesive materials).

For cohesionless particles, only the first two terms on the right hand side are included (i.e. $c=c_w=0$). The theoretical analysis predicts a linear dependence of the pressure drop on the plug length. Also, depending on whether the failure is active or passive, the frontal stress can contribute a significant amount to the pressure drop required to move a plug. One of the objectives of this work is to test the theoretical equations of Konrad et al. (1980) as is outlined in the next chapter.

2.4 Stresses Within a Particulate Mass of Solids: Application of Soil Mechanics

In the analysis of Konrad et al. (1980), the frictional shear properties of the particles are an important element. Therefore, a brief discussion on the stresses that arise within a particulate mass of solids will be given here. Much of the work on the flow of granular material is based upon the principles of soil mechanics, though the stresses in the former are generally lower, being typically 1 - 100 kPa (Bridgwater and Scott, 1983).

The mechanism of stress distribution in solid systems is by particle-to-particle friction. The stresses, or shear forces per unit area, are exerted by the particles on each other (local or internal stresses) and at the boundaries of the bed (boundary or wall stresses) (Delaplaine, 1956). Lambe and Whitman (1979) consider an imaginary plane passing through a particulate mass. At each point where this plane passes through the mass of solids, the transmitted force can be broken up into components normal and tangential to the plane. The tangential components can further be resolved into components lying along a pair of coordinate axes. The summation over the plane of the normal components of all forces, divided by the area of the plane, is the normal stress acting upon the plane. Likewise, the summation over the plane of the tangential components in a particular direction, divided by the area of the plane, is the shear stress in that direction.

If the particles are assumed to be an ideal Coulomb material, the internal yield locus is given by:

$$\tau = \mu\sigma + c \qquad (2.9)$$

where τ is the shear stress, σ is the normal stress, μ is the coefficient of internal friction and c is the cohesion. Similarly, the wall yield locus is

$$\tau_w = \mu_w\sigma_w + c_w \qquad (2.10).$$

The coefficients of friction μ and μ_w are often written as $\tan\phi$ and $\tan\phi_w$ where ϕ and ϕ_w are referred to as the angles of internal and wall friction (Nedderman, 1982). For a cohesionless material, c and c_w are zero. In order to test the theory of Konrad et al. (1980), the angles of friction, ϕ and ϕ_w must be determined for the cohesionless solids.

3.0 EXPERIMENTAL PROGRAM

3.1 Experimental Objectives

An experimental program has been undertaken to gain a more fundamental understanding of dense-phase pneumatic transport of cohesionless solids. As noted previously, the flow pattern in dense-phase pneumatic conveying is quite complex and not very well understood. Konrad (1986) suggests further use of high-speed photography to document all the possible flow patterns in both horizontal and vertical pipes.

In order to design a dense-phase conveying system, the overall pipeline pressure drop must be calculated. This pressure drop is simply the sum of the pressure drops across all the plugs in the pipeline. Since these plugs may vary considerably in length, an understanding of the dependence of the pressure drop on its length (and other parameters such as the frontal stress) is important to any attempt to predict the overall pipeline pressure drop.

A circulating unit with horizontal and vertical sections has been constructed. The pipe material is transparent lexan (polycarbonate). This allows for visual observation of the flow pattern and high-speed photography. Depending on the air velocity used, the flow pattern observed in the pneumatic sections can range from dilute-phase flow to dense-phase plug flow. Pressure drop measurements across a 70 cm length in both the horizontal and vertical sections have been coordinated with the photographic work.

The experimental objectives can be summarized as follows:

1)High-speed photographic documentation of the flow patterns

-Horizontal
Dense-phase plug flow
Dilute-phase flow
Strand flow

-Vertical
Dense-phase plug flow
Dilute-phase flow

2)Analysis of dense-phase films to test the theory of Konrad et al. (1980)

Measurements of:
-Plug length
-Wave front and plug velocities
-Pressure drop across 70 cm section

3.2 Choice of Material

The particles used were a mixture of 5% black and 95% white polyethylene granules. Polyethylene granules have been chosen as the solids investigated because they are cohesionless and free flowing. The black particles were used as tracers to aid the visual observation of the flow pattern. The particle shape can best be described as smooth, rounded cylinders with a diameter of approximately 3.7 mm and a height of approximately 2.1 mm. The particle density is 900 kg/m^3 and the bulk density is 590 kg/m^3. The bulk density and particle size for the black and white particles were measured separately and were found to be the same. The particle shear properties have been measured in an annular shear cell. The angle of internal friction is 24.5° (using the peak shear stress) and the angle of wall friction is 10.3° (using the ultimate

shear stress). The results of the shear measurements are discussed in more detail in the next chapter.

3.3 Description of the Apparatus

3.3.1 Circulating Unit

A schematic diagram of the apparatus is shown in Figure 3.1. The circulating unit consists of a 7.6 m vertical riser section, a 90° elbow leading to a 3 m horizontal section with a disengaging pipe at its end to separate the air (which is vented to the atmosphere) from the solids which flow under gravity into a standpipe returning on an angle to the feed point. The pipe is transparent lexan (50.8 mm internal diameter). The 2.44 m long pipe sections are connected together with metal-supported flexible couplings. Some of the fittings are made of PVC. The 90° elbow is a 2" Schedule 40 PVC conduit with a 1 foot radius. The disengaging pipe is a 4"x4"x2" PVC T-fitting with 4" Schedule 40 pipe sections attached to the top and bottom. A screen is attached to the top to prevent solids from blowing out. This is a suitable air/solids separator for the coarse polyethylene particles used in the experiments. The solids feed point consists of a gate valve (to control solids flow) and two PVC Y-fittings. A screen is also located at the base of the unit just below the solids feed point to prevent solids from entering the air line.

The air supply is filtered to remove entrained liquid and particulate matter from the gas. The air flow is measured by a Ramapo target flow meter. The

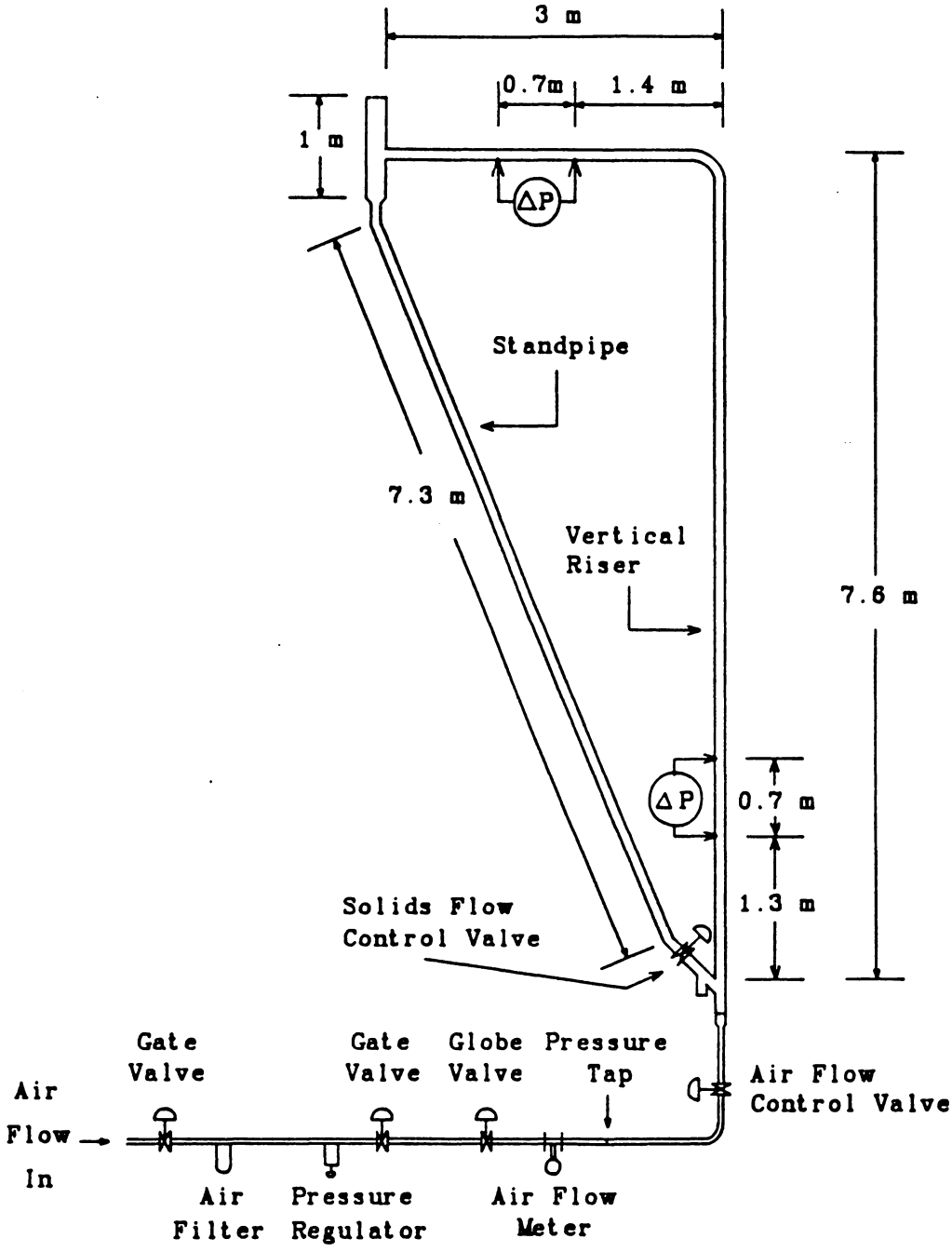

Figure 3.1 Schematic Diagram of the Circulating Unit

pressure in the feed line near the flow meter is measured with an MKS Baratron differential pressure transducer (0-1000 mm Hg). The air flow to the unit is controlled by a gate valve. The air transports the solids up the riser section, into the horizontal section and then to the disengaging point where the solids return to the standpipe. The solids flow pattern can range from dilute-phase flow to dense-phase plug flow.

Pressure taps have been installed 70 cm apart in both the horizontal and vertical sections. The pressure drop across these sections were measured with a differential pressure transducer (0-35 kPa). A HYCAM-II high-speed movie camera was used to film the flow pattern between the pressure taps. Two centimeter rules were attached to the pipe in order to measure distances from the films.

The analog signals from the flow meter and pressure transducers were collected by an IBM-PC data acquisition system using a Data Translation DT2801-A analog and digital input/output board. Labtech Notebook, a menu driven software package, was used to run the data acquisition. In order to distinquish between the individual plugs on both the film and in the data file, a plug counter system was developed, based on the pressure difference between the taps. When only air was flowing over the stationary material between the pressure taps, the pressure drop was negligible compared with that across a plug. But when a plug of material arrived and started to pass the first tap, the pressure drop rose. When the pressure difference reached a pre-set value, a signal was generated that flashed a strobe light once, and incremented both a binary counter, which was collected by the computer, and a mechanical

counter with a pointer system (similar to a clock) which was in the field of view that was filmed. This allowed the pressure profiles of the individual plugs in the data file to be synchronized with the plugs on the film.

3.3.2 Annular Shear Cell

The annular shear cell used to determine the frictional properties of the polyethylene particles is based upon the Carr and Walker (1967/68) design. A schematic diagram of the apparatus is shown in Figure 3.2. The solids are loaded in the annular trough and the lid is placed over the sample. The dimensions of the trough are: inner diameter 142 mm, outer diameter 264 mm; and of the lid: inner diameter 148 mm, outer diameter 260 mm. The lid weight is 10.56 kg. The underside of the lid has eighteen vertical radial stainless steel vanes to grip the sample; their lower sharp edges being flush with the base of the rims. The trough is rotated slowly, at approximately 1.5 revolutions per hour, by a fractional horse-power motor driving through reduction gears. The cell lid is prevented from rotating by a shear torque arm (203.2 mm in length) which pushes against a load cell. The output of the transducer (HBM model U1T universal load cell 0-22.7 kg with model MGT 31 measuring amplifier) is interfaced with the IBM-PC data acquisition system.

The normal load on the shear plane is increased by placing weights symmetrically on the lid, or decreased by partially counterbalancing the lid weight. Diametrically opposite the torque arm is a similar arm to which calibration loads can be applied horizontally via a nylon cord passing over a

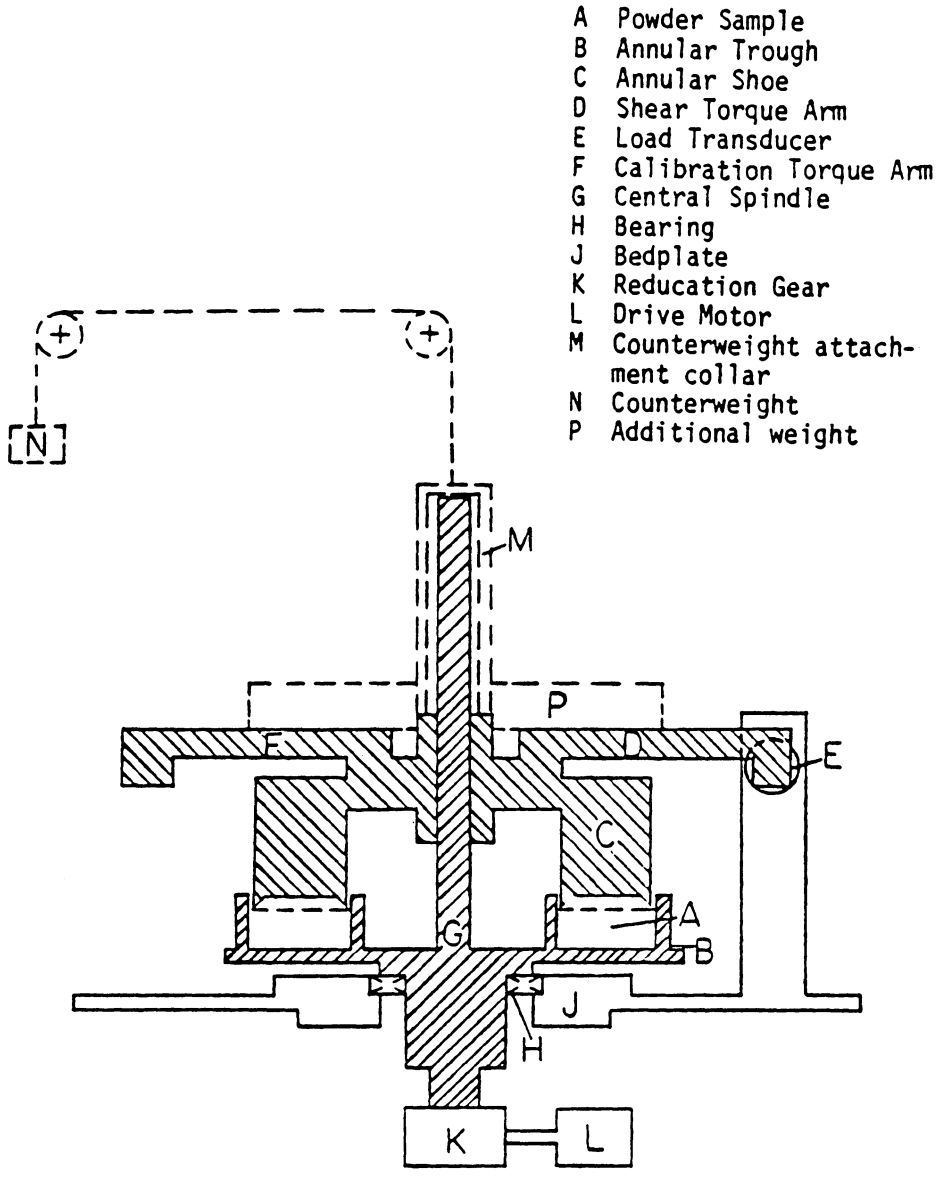

Figure 3.2 Schematic Diagram of the Annular Shear Cell (Source: Lilly, 1984)

pulley to a weight hanger. Wall friction measurements can be made by attaching an annular ring of the wall material to the underside of the lid.

3.4 Experimental Technique

3.4.1 Circulating Unit

A mixture of 5% black and 95% white polyethylene particles was loaded into the standpipe. The black particles were used as tracers to aid the visual observation of the flow pattern. The flow regime (dense, dilute, or strand) and the pipe section (horizontal or vertical) to be filmed were decided upon. The flow meter and pressure transducers were zeroed, the camera was focused and the lighting was checked using an exposure meter. The camera speed was selected by a compromise of two factors. The first factor was to choose a sufficiently high frame rate so that the particles did not move significantly during the exposure time. The second factor was that the maximum length of film that the camera could hold was 122m (400 feet), i.e. 16,000 frames. For the dense-phase flow, a frame rate of 500 frames/sec was decided upon. This gives an exposure time per frame of 0.8 milliseconds with the standard 40% shutter. Since the maximum velocity of the particles and plugs is approximately 3 m/sec, the maximum distance moved by a particle in 0.8 milliseconds would be 2.4 mm, which is less than one particle diameter. For most cases, the velocity, and hence the distance moved was considerably less than this. The total time filmed was approximately 32 seconds. For the

dilute-phase flow, a frame rate of 1500 frames/sec was decided upon. This gives an exposure time per frame of 0.267 milliseconds with the 40% shutter. If the particles travel at 10 m/sec in the dilute phase, a particle would move 2.6 mm, which is less than one particle diameter. The total time filmed was approximately 11 seconds. For the strand flow in the horizontal section, a frame rate of 1250 frames/sec was decided upon. This gives an exposure time per frame of 0.32 milliseconds with the 40% shutter. The total time filmed was approximately 13 seconds. Black and white film (400 ASA) was selected for the horizontal runs and color film (400 ASA) was chosen for the vertical runs.

The computer data acquisition system was set-up to sample from each channel at a rate of 50 Hz (total sample time: 60 seconds for the dense-phase flow and 20 seconds for the dilute-phase and strand flows). The data acquisition system was initialized and placed in a wait mode for a trigger to begin data collection. The plug counter system was re-set to zero. (Note: this system was only used for the films of the dense-phase flow). The air flow was adjusted by the flow control valve. For all these runs, the solids flow control valve was completely open. Therefore, the solids flow rate was determined by the air flow rate. After a few minutes, when a steady state had been reached in the pipeline, the solids flow rate was measured by recording the time required for a particle to travel a distance of 92 cm in the standpipe section near the solids feed point (just prior to the solids flow control valve). Since the solids move as a packed bed in the standpipe, the mass flow rate can be calculated from the bulk density. A couple of readings were taken before the camera was started, and several afterwards.

After a final check to ensure that all was ready, the camera was started. A trigger started the data acquisition system and the plug counter. After the run, the camera was unloaded. The procedure was repeated for different air flow rates (and therefore, different solids flow rates). The ambient pressure was also recorded.

3.4.2 Annular Shear Cell

The general procedure followed for the tests with the annular shear cell is outlined in Carr and Walker (1967/68).

3.4.2.1 Calibration

The load cell that measures the force from the torque arm must be calibrated. With the cell empty and the weight of the lid counterbalanced, known loads are applied to the calibration torque arm causing the shear torque arm to be forced against the load cell. The cell is rotated in both the forward and reverse directions: the mean value of the two readings corresponds to a transducer load equal to that applied to the calibration arm.

First, the amplifier for the load cell was zeroed. The computer acquisition system was set-up to collect the load cell output at a sampling rate of 10 Hz for two minutes with a 30 second delay after the first minute in order to reverse the motor direction. Known weights in ascending order from 0 kg to 21.72 kg were applied successively to the calibration torque arm. The calibration curve is presented in Appendix A.

3.4.2.2 Shear Test

A known weight of material was loosely packed in the trough and the lid was set in place. The highest normal load was applied and the cell was rotated for one full revolution to consolidate the sample. The cell was reversed to remove the shear force. The normal load was reduced to the lowest value and the sample was sheared. When the normal load is less than the consolidation load, the data obtained is for an overconsolidated sample. The computer collected data at a rate of 10 Hz for two minutes. The cell was then reversed and the highest normal load was again applied to reconsolidate the sample. The procedure was repeated for ascending load values up to the consolidation load.

Wall friction measurements were made by attaching an annular piece of lexan to the underside of the lid. The lexan sheet and four screws weighed 0.56 kg. A piece of velvet was fixed to the inner diameter of the lexan ring to prevent particles from creeping up the sides and wedging. The test procedure followed was identical to that outlined above.

Assuming that the shear stress, τ, is developed uniformly over the annular area, it can be calculated from the total shear torque given by the load cell reading (Carr and Walker, 1967/68).

$$\begin{aligned} T &= \int_{R_i}^{R_o} (\tau)(R)(2\pi R)dR \\ &= \frac{2}{3}\pi\tau(R_o^3 - R_i^3) \end{aligned} \qquad (3.1)$$

where T is the torque, τ is the shear stress and R_o and R_i are the outer and inner radii of the shear lid.

4.0 RESULTS and DISCUSSION

4.1 Particle Shear Properties

The angles of internal friction and wall friction for the polyethylene particles have been determined with the annular shear cell. A series of tests with different amounts of material in the cell were made. The consolidation normal stress was 5.27 kPa for the internal friction measurements and 5.42 kPa for the wall friction measurements. A plot of the shear stress versus time (i.e. strain) for an overconsolidated sample is presented in Figure 4.1. This plot is a 13-point moving average of the raw data in order to smooth out the fluctuations due to the vibration of the cell caused by the motor. Notice that the shear stress rises to a maximum value, then levels off to a steady value. This is typical for an overconsolidated sample. The maximum represents the peak stress corresponding to static friction just prior to the failure of the sample. The steady value represents the ultimate stress condition corresponding to kinetic friction. For a sample sheared at the consolidation normal load, the shear stress rises smoothly to the ultimate condition, the peak in the shear stress being virtually eliminated.

The peak and ultimate shear stress values from the internal and wall friction experiments are summarized in Tables 4.1 and 4.2, respectively. The values were obtained from the 13-point moving average; the peak stress was calculated from the maximum value over the two minute run and the ultimate

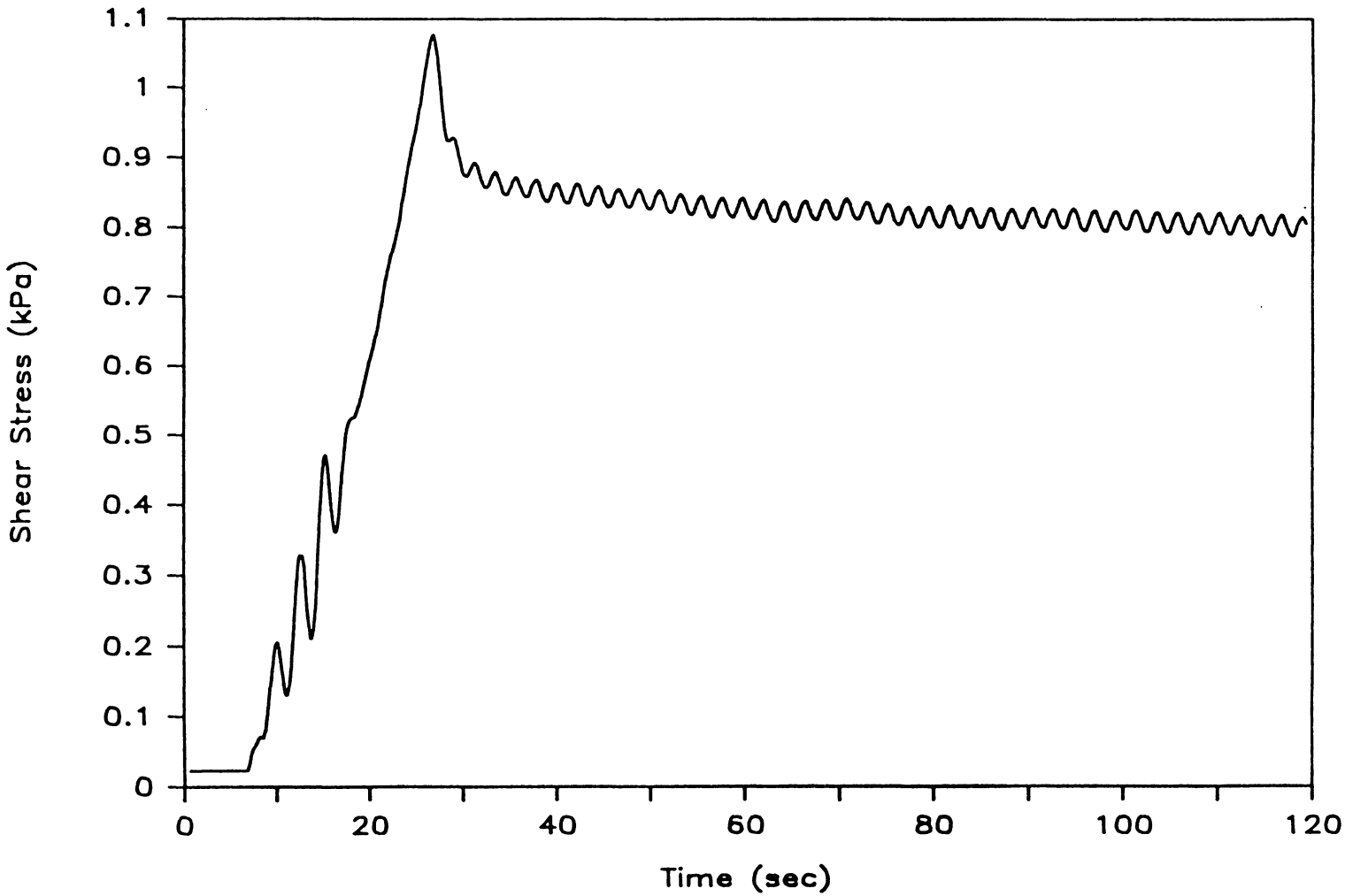

Figure 4.1 Shear Stress versus Time for an Overconsolidated Sample

Table 4.1 Internal Friction Shear Stress Data

	Run 1*		Run 2+		Run 3*		Run 4+	
Normal Stress (kPa)	Peak Shear Stress (kPa)	Ult. Shear Stress (kPa)	Peak Shear Stress (kPa)	Ult. Shear Stress (kPa)	Peak Shear Stress (kPa)	Ult. Shear Stress (kPa)	Peak Shear Stress (kPa)	Ult. Shear Stress (kPa)
0.44	0.32	0.20	0.38	0.25	0.30	0.20	0.35	0.20
1.07	0.55	0.34	0.61	0.45	0.57	0.34	0.55	0.39
1.69	0.75	0.48	0.81	0.61	0.72	0.46	0.78	0.55
2.01	0.78	0.53	0.91	0.69	0.80	0.52	0.90	0.61
2.33	0.84	0.58	1.02	0.76	0.85	0.59	0.94	0.67
2.58	0.87	0.62	1.08	0.81	0.90	0.64	0.98	0.71
2.89	0.90	0.68	1.09	0.84	0.96	0.72	1.00	0.76
4.02	1.01	0.86	1.21	1.04	1.05	0.87	1.09	0.96
5.27	1.13	1.09	1.31	1.26	1.19	1.14	1.24	1.19

* 600 grams of particles in cell
+ 800 grams of particles in cell

Table 4.2 Wall Friction Shear Stress Data

	Run 1*		Run 2+		Run 3+		Run 4*	
Normal Stress (kPa)	Peak Shear Stress (kPa)	Ult. Shear Stress (kPa)	Peak Shear Stress (kPa)	Ult. Shear Stress (kPa)	Peak Shear Stress (kPa)	Ult. Shear Stress (kPa)	Peak Shear Stress (kPa)	Ult. Shear Stress (kPa)
0.60	0.26	0.20	0.20	0.15	0.16	0.13	0.21	0.14
1.22	0.44	0.33	0.26	0.22	0.26	0.24	0.36	0.21
1.85	0.64	0.42	0.39	0.30	0.37	0.35	0.47	0.28
2.16	0.71	0.48	0.43	0.34	0.47	0.42	0.45	0.40
2.48	0.74	0.51	0.48	0.38	0.56	0.46	0.60	0.46
2.73	0.76	0.55	0.51	0.43	0.56	0.49	0.64	0.47
3.04	0.78	0.59	0.61	0.49	0.60	0.52	0.68	0.51
4.18	0.80	0.64	0.80	0.63	0.73	0.62	0.82	0.61
5.42	0.96	0.79	1.00	0.87	0.85	0.79	0.94	0.78

* 400 grams of particles in cell
+ 200 grams of particles in cell

stress from the average over the last 30 seconds of the run. The angle of internal friction was determined from the peak shear measurements because the yielding or failure of the particulate material in dense-phase plug flow occurs at the wall, not internally, hence, the stress state of the material within a plug corresponds to that before failure occurs (i.e. the peak stress). The peak shear stress versus the normal stress for all four runs is presented in Figure 4.2. Since the material is cohesionless, least-squares linear regression was used to calculate the straight line through the origin. Since the calculated frontal stresses for the plug conveying in the present work are all less than 2 kPa, the angle of internal friction was calculated from the data at the lower normal stress values (less than 2 kPa).

For the angle of wall friction, the ultimate shear measurements were used because there is continuous failure at the wall as the plug moves through the pipe. The ultimate shear stress versus the normal stress for all four runs is presented in Figure 4.3. A least-squares linear regression through the origin for the normal stress data less than 3 kPa was used to calculate the angle of wall friction. The particle properties are summarized in Table 4.3.

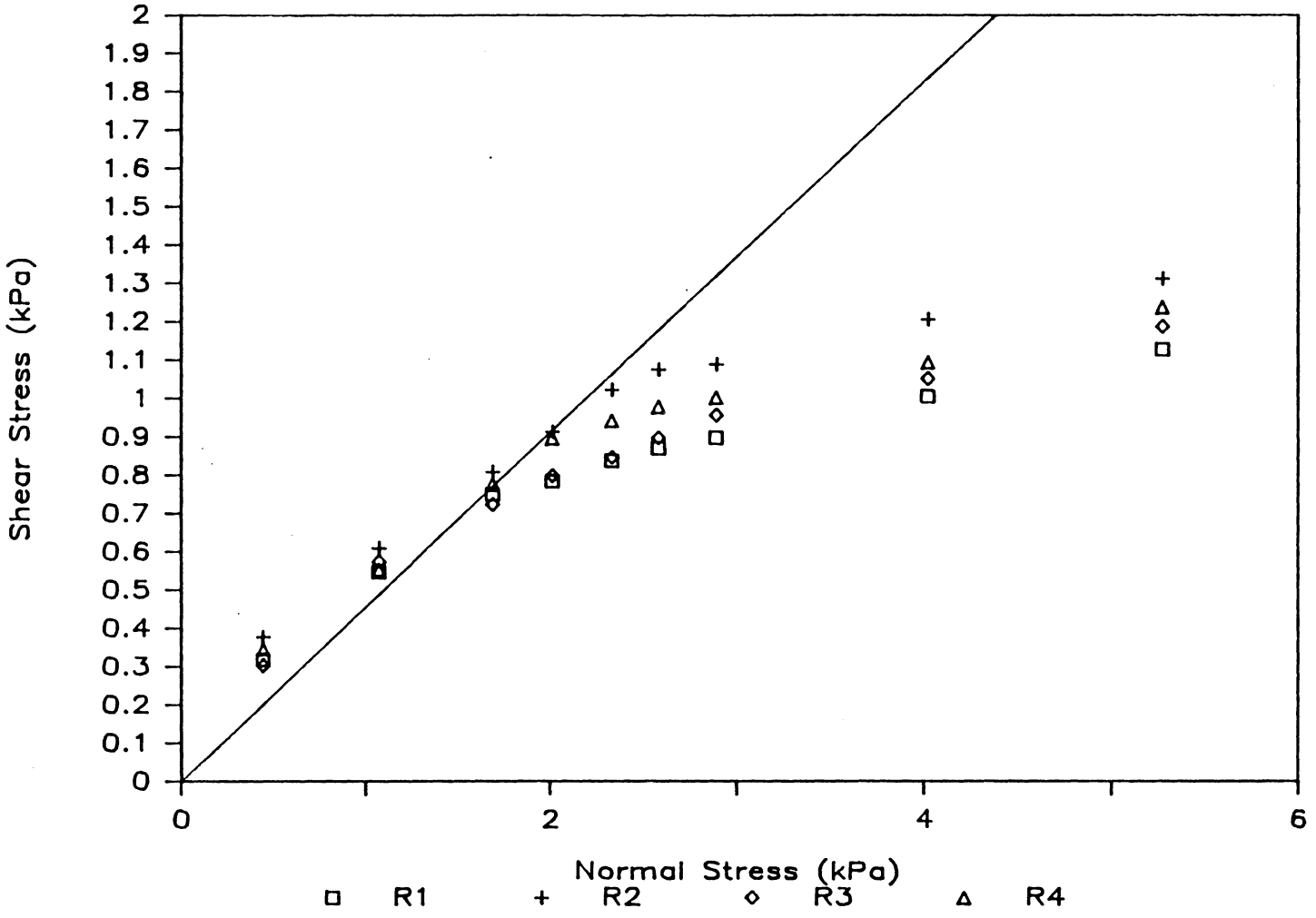

Figure 4.2 Internal Friction: Peak Shear Stress versus Normal Stress

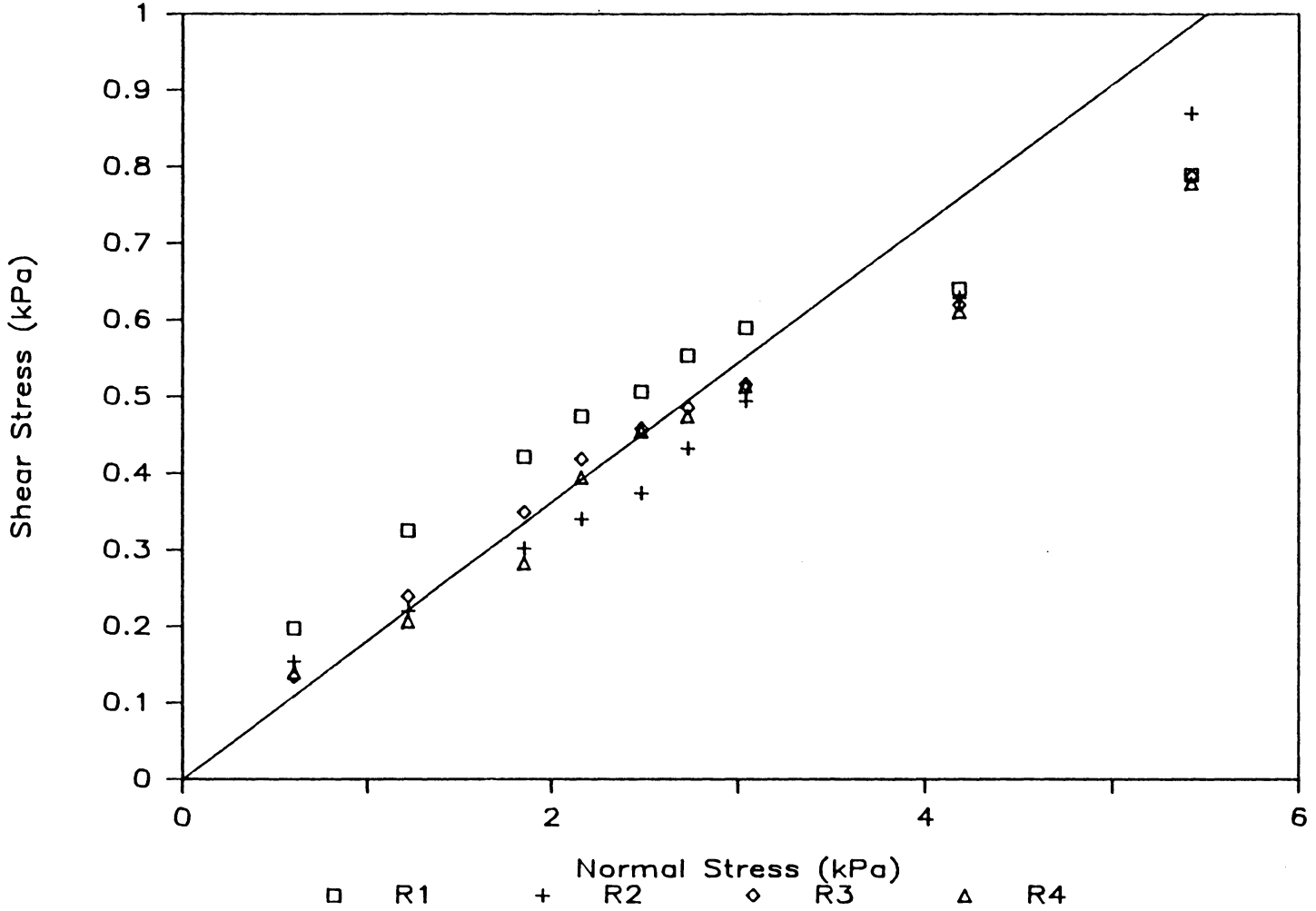

Figure 4.3 Wall Friction: Ultimate Shear Stress versus Normal Stress

Table 4.3 Summary of Particle Properties

Shape: Smooth, rounded cylinders

Diameter: ~ 3.7 mm

Height: ~ 2.1 mm

Particle Density: 900 kg/m^3

Bulk Density: 590 kg/m^3

Angle of Internal
Friction (Peak) : 24.5° *

Angle of Wall
Friction (Ultimate): 10.3° +

* For normal stress data less than 2 kPa.

+ For normal stress data less than 3 kPa.

4.2 Circulating Unit

The operation of the circulating unit was surprisingly trouble free. Upon opening the air supply valve, the solids were introduced into the vertical riser from the standpipe. Depending on the air flow rate and the position of the solids flow control valve, a whole range of flow patterns were observed in the vertical and horizontal sections. For all the experimental runs described in this thesis, the solids flow control valve was completely open. Therefore, the solids flow rate was determined by the air flow rate. At the lower air velocities, dense-phase plug flow was observed. On increasing the air flow rate, the flow pattern changed to dilute-phase flow. The solids in the standpipe flow toward the feed point as a packed-bed (similar to flow pattern f of Figure 1.2). On initial start-up, the solids occasionally bridge in the standpipe which requires a little mechanical vibration (i.e. banging on the pipe by hand) to loosen up the solids. It was also observed that occasionally some air would flow up the standpipe instead of the riser. This usually occurred on start-up or during changes in air velocity. However, once the flow became steady, it appeared that no air flow rose up the standpipe though this is not known for certain. Therefore, the air flow rate measurement may overestimate the true air flow through the pneumatic transport sections.

4.2.1 Horizontal Conveying

A series of five films spanning the operating range of the system were

made of the flow patterns in the horizontal section (see Table 4.4 for the operating conditions for each run). The flow patterns included dense-phase plug flow, strand flow, and dilute-phase flow. Since the main topic of this thesis is dense-phase flow, only a brief description of the dilute-phase and strand flows will be given here.

At the higher air velocities, the solids are maintained in a suspension within the air stream. From the high-speed films, it is observed that there is an increasing solids concentration gradient from the top of the horizontal pipe to the bottom, at the air velocity and solids flow rate used for this run. The solids move in a zig-zag fashion, colliding with each other and the pipe wall. There also appears to be some clustering of the particles along with moving pockets of air. Figure 4.4 shows a series of five consecutive photographs from the film. Notice the three particles located near the top of the pipe at the 57 cm mark in Figure 4.4a. In each subsequent frame, this group moves approximately 0.5 cm. The air/solids structure maintains itself over a relatively long distance in the field of view. The pressure drop across the 70 cm horizontal test section for the dilute-phase flow is presented in Figure 4.5. In this case, the pressure measurements and film were not coordinated. The computer acquisition system was started slightly ahead of the camera (on the order of 1 second). For the dilute-phase flow, approximately 11 seconds were filmed. Therefore, the data presented in the figure spans the entire duration of the film. Notice that the pressure drop fluctuates very rapidly around an average value of 0.12 kPa. This type of pressure profile is expected for dilute-phase flow.

Table 4.4 Horizontal Conveying: Operating Conditions for the Five Experimental Runs

Run	Flow Pattern	Camera Frame Rate (Frames/sec)	Superficial Air Velocity (m/sec)	Solids Mass Flow Rate (kg/sec)
1 (HFILM2)	Dense	500	3.9	0.16
2 (HFILM3)	Dense	500	2.3	0.11
3 (HFILM4)	Dense	500	1.5	0.063
4 (HFILM5)	Dilute	1500	16.1	0.22
5 (HFILM6)	Strand	1250	6.8	0.24

(Note: The ambient absolute pressure was 94 kPa for all these runs.)

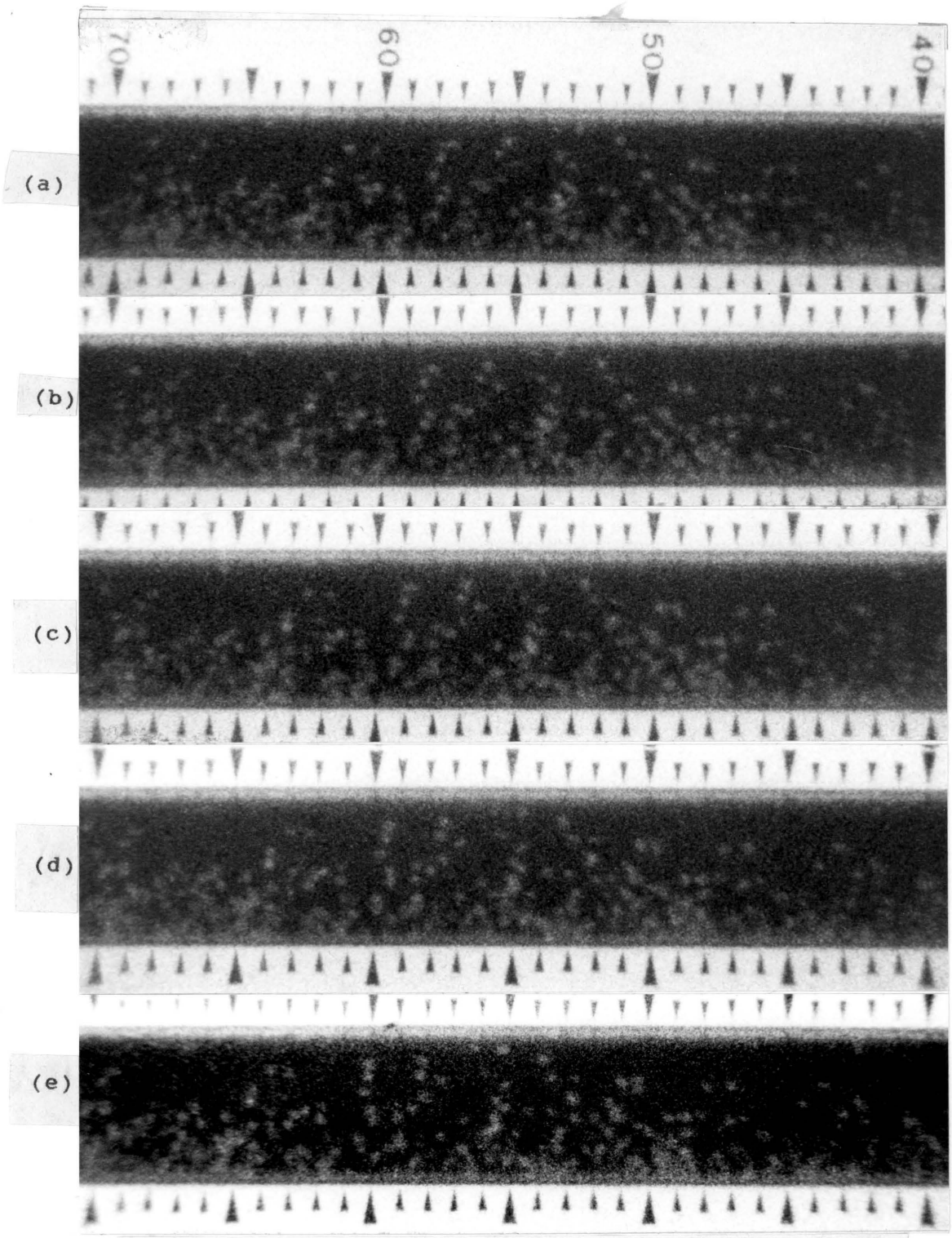

Figure 4.4 Photographs of Horizontal Dilute-Phase Flow.
Flow from right to left.
Time between each frame is 0.67 milliseconds.

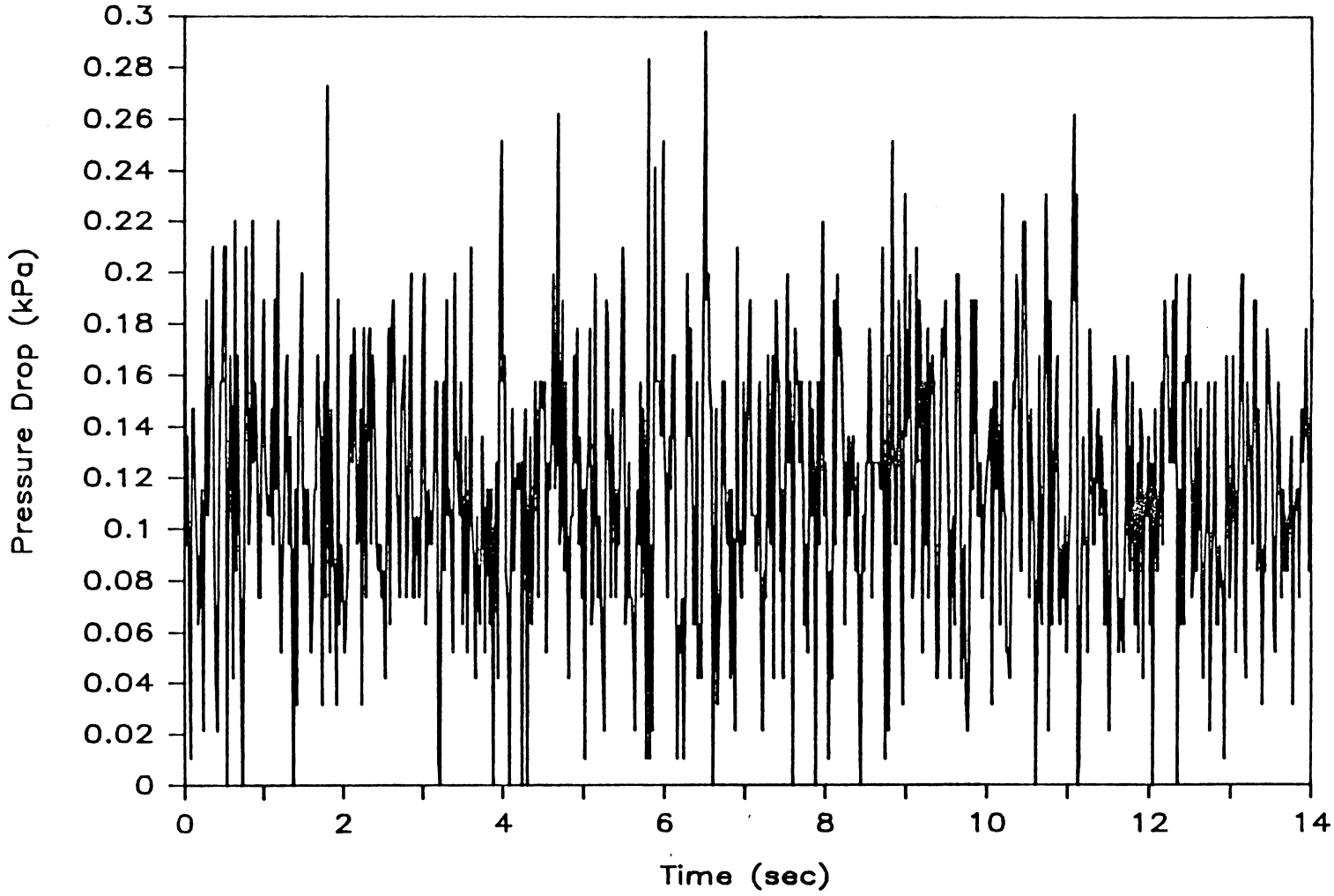

Figure 4.5 Pressure Drop Across 70 cm Section for Horizontal Dilute-Phase Flow

Upon reducing the air velocity, the flow pattern changes to a type of strand flow. Many interesting phenomena are observed for this particular run. For most of the run, there is a stationary layer of solids resting along the bottom of the pipe. The solids are conveyed in a dilute phase above the stationary layer (see Figure 4.6 for a series of photographs of the flow pattern). There is a considerable amount of interaction between the dilute phase and the top of the stationary layer. Particles collide with the stationary layer resulting in a lot of tumbling and rolling. Particles in the dilute phase also collide with each other and the pipe wall. The pressure drop across the 70 cm section is presented in Figure 4.7. Again, the film and pressure data were not coordinated. The computer data acquisition was started about one second before the camera. The total time filmed for this run was approximately 13 seconds, therefore, the data presented in the figure spans the entire run. The pressure drop is significantly different than for the dilute-phase flow. The pressure drop is greater and the rapid fluctuations are no longer present. Also, notice the large pressure spikes. These correspond to an increase in the dilute-phase concentration as observed from the film. Figure 4.6f shows the increasing concentration just entering the field of view. The increase in concentration causes the pressure to rise sharply. Under these conditions, it is occasionally observed that the stationary layer slides along the bottom of the pipe for a certain distance as if it were being dragged by the particles in the dilute phase. Figure 4.8 shows a sequence of photographs depicting this motion. The black particle in the stationary layer at the 42.5 cm mark in Figure 4.8a moves to the 47 cm mark in the next photograph, to the 53.25 cm

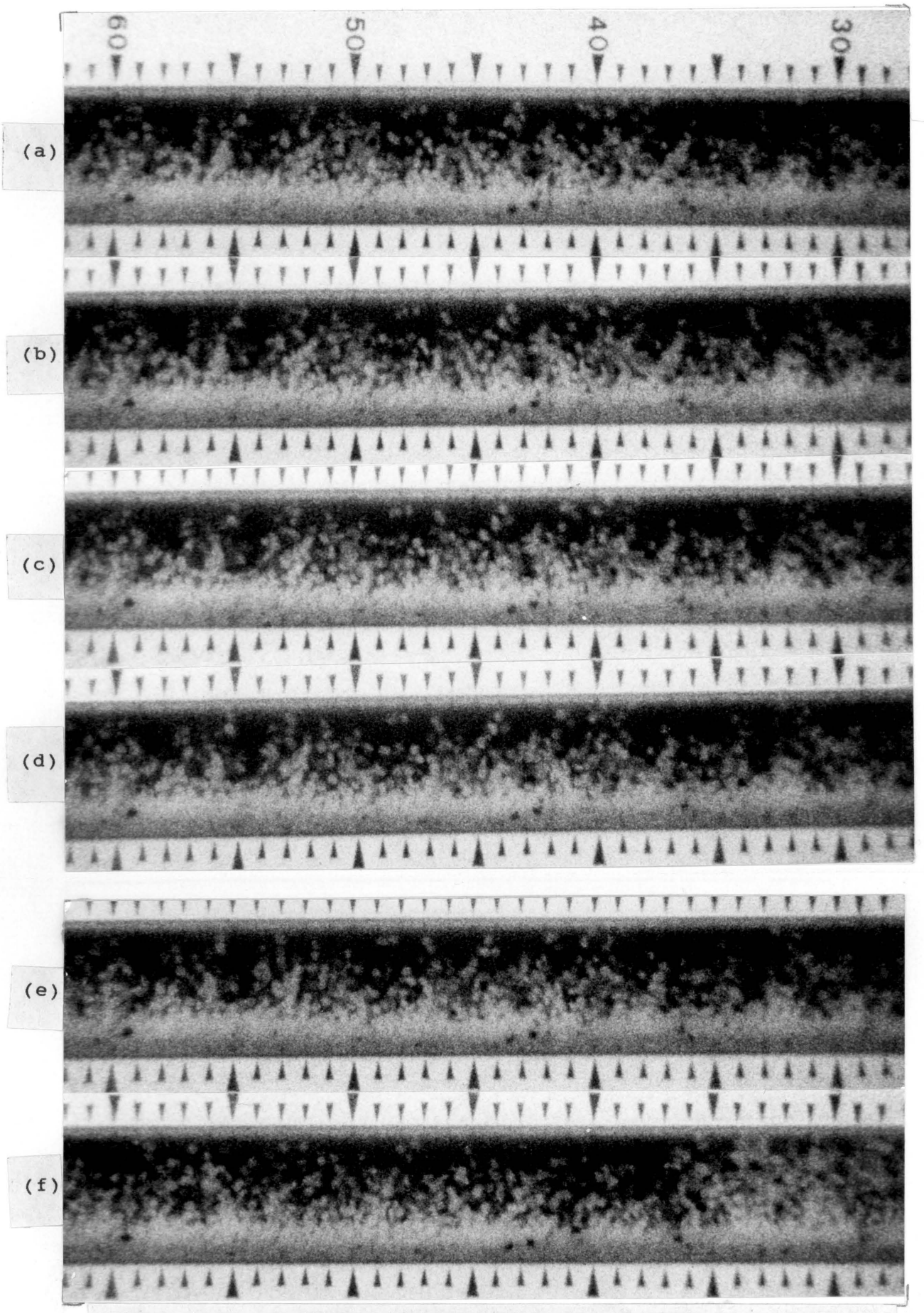

Figure 4.6 Photographs of Horizontal Strand Flow:
Bottom Layer Remains Stationary.
Flow from right to left.
Time between each frame is 0.8 milliseconds for a-e.
Time between frame e and f is 0.0352 seconds.

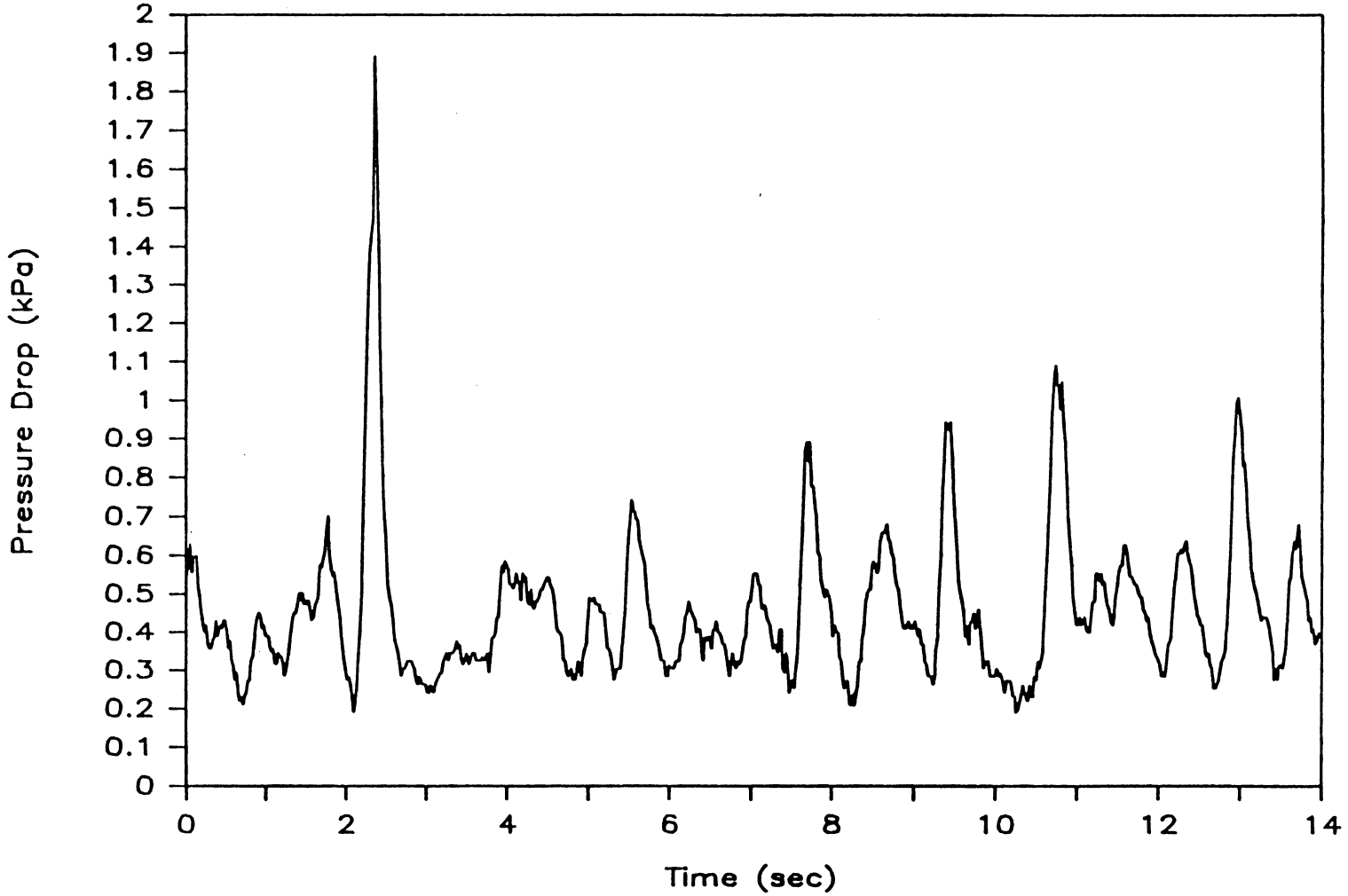

Figure 4.7 Pressure Drop Across 70 cm Section for Horizontal Strand Flow

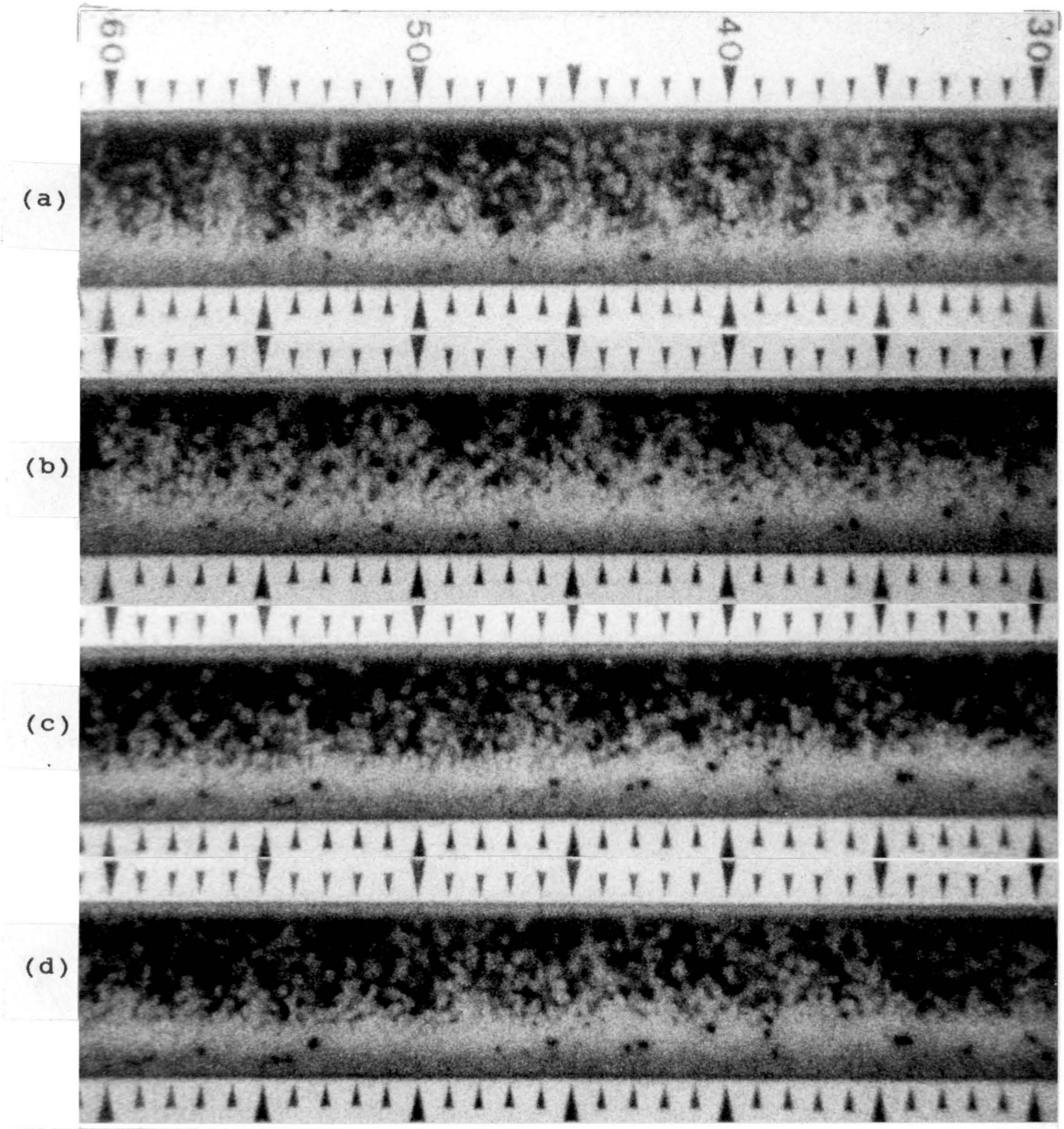

Figure 4.8 Photographs of Horizontal Strand Flow:
Bottom Layer Moves.
Flow from right to left. Time between each frame, from top to bottom, is 0.2488, 0.3112, 0.0920 seconds.

mark in the next and finally to the 53.5 cm mark where it remains. From an industrial standpoint, this type of flow would be undesirable because the particles in the stationary layer would take a very long time to be transported out of the pipe. Also, the effective area for transport is reduced.

The main purpose of the horizontal dense-phase flow film work was to test equations (2.7) and (2.8) for cohesionless particles, which predict a linear dependence of the pressure gradient on the frontal stress. From a momentum balance, Konrad et al. (1980) derived an expression for the frontal stress:

$$F = \rho_b(W_F - u_S)u_S \qquad (4.1)$$

where F is the frontal stress, ρ_b is the bulk density, W_F is the wave front velocity, and u_S is the particle velocity within the plug. The quantities measured from the films were, therefore:

(i) the velocity of the front of a plug W_F,

(ii) the velocity of a particle within the plug u_S by following an individual black particle,

(iii) the length of a plug,

and (iv) the corresponding pressure drop across the plug.

To obtain these quantities, each plug on the films had to be analyzed, frame-by-frame as it passed the two pressure taps. The analysis had to be coordinated with the pressure measurements stored in the computer data file. To illustrate the procedure, consider run 2. In Figure 4.9, the pressure difference between the two taps (70 cm apart) is plotted as a function of time, for run 2. Each peak in the pressure drop data represents a plug passing the pressure taps. Note for this particular run (number 2), the first and last

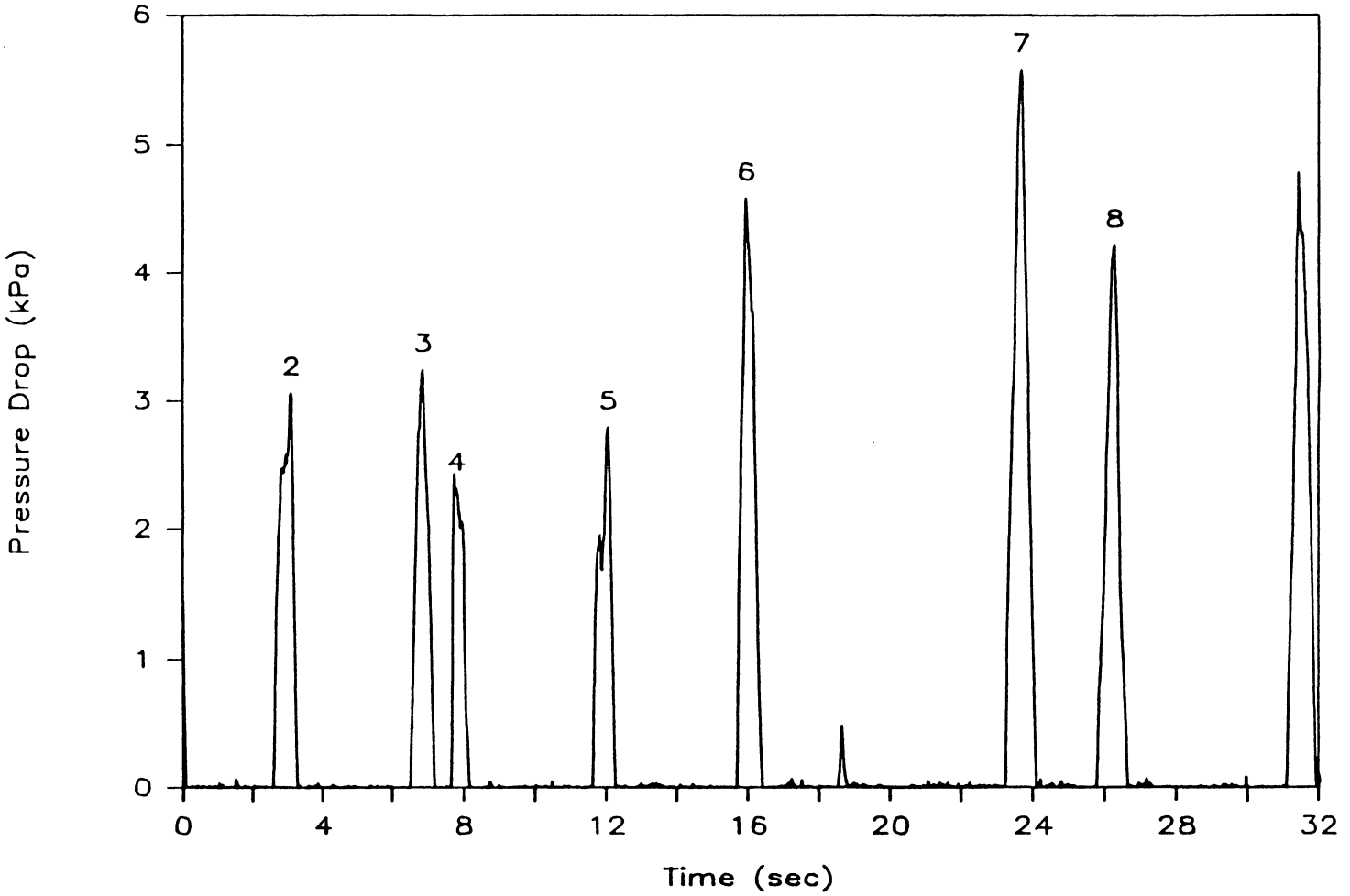

Figure 4.9 Pressure Drop Across 70 cm Section for Horizontal Dense-Phase Flow (Run #2)

plugs were right at the beginning and end of the film, so that only plugs 2 through 8 could be analyzed. The passage of a typical plug (number 5) is shown in Figure 4.10 (where the flow is from right to left), and the corresponding pressure profile is given in Figure 4.11.

First of all, the front of the plug was positioned at the first pressure tap (Figure 4.10(a)), and the frame count was recorded. The film was advanced until the back of the plug reached the first pressure tap (Figure 4.10(b)), and the frame count was again recorded. The plug length in this position was also recorded. The wave front velocity was then calculated by dividing the plug length (i.e. the distance that the wave front moved) by the time required for the plug to pass the pressure tap (as calculated by the number of frames). The particle velocity within the plug was obtained by counting the number of frames required for a particular black particle (within the plug) to travel a 5 cm distance just past the first pressure tap. With these measurements and the bulk density, the frontal stress was calculated by equation (4.1). The film was then advanced until the front of the plug had just reached the second pressure tap (Figure 4.10(c)), at which point the length of the plug at the second tap was recorded. After that, the film was again advanced until the back of the plug had just passed the second pressure tap (Figure 4.10(d)), and the frame count was again recorded. This gave the time required for the plug to pass both pressure taps as measured from the films. The time required for the plug to pass both pressure taps was also obtained from the individual pressure profiles as shown in Figure 4.11. The time for a plug to pass both taps as measured from the films corresponded very well with that measured from the

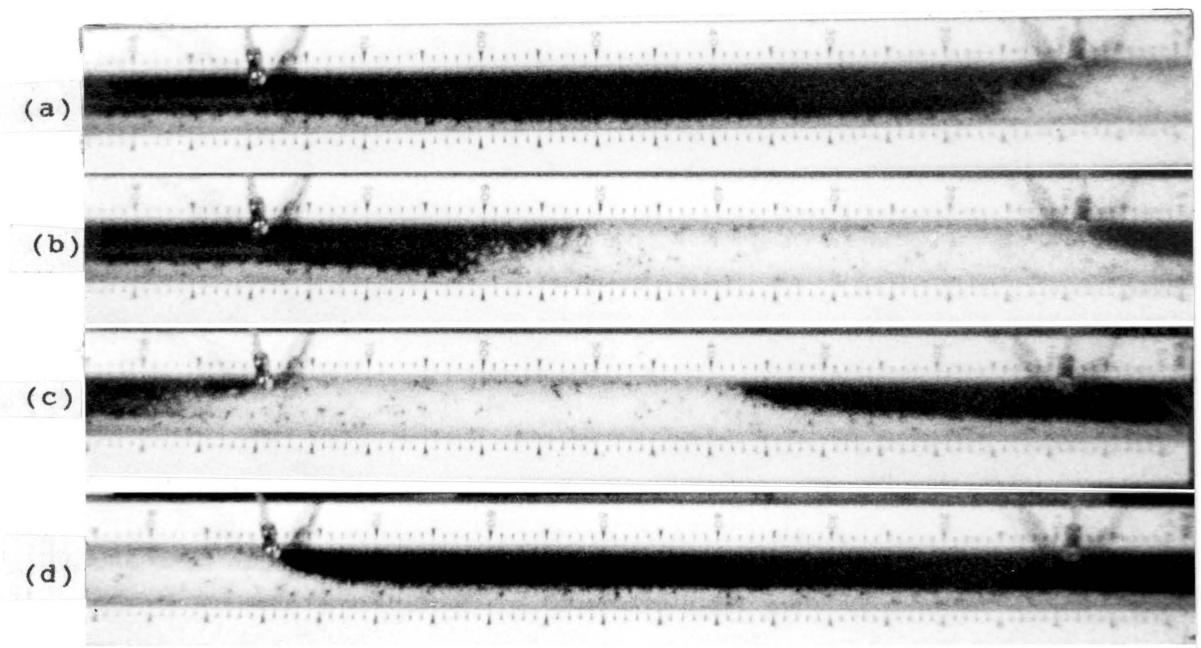

Figure 4.10 Photographs of Horizontal Dense-Phase Flow (Plug #5, Run #2).
Flow from right to left. Time between each frame, from top to bottom, is 0.244, 0.156, 0.252 seconds.

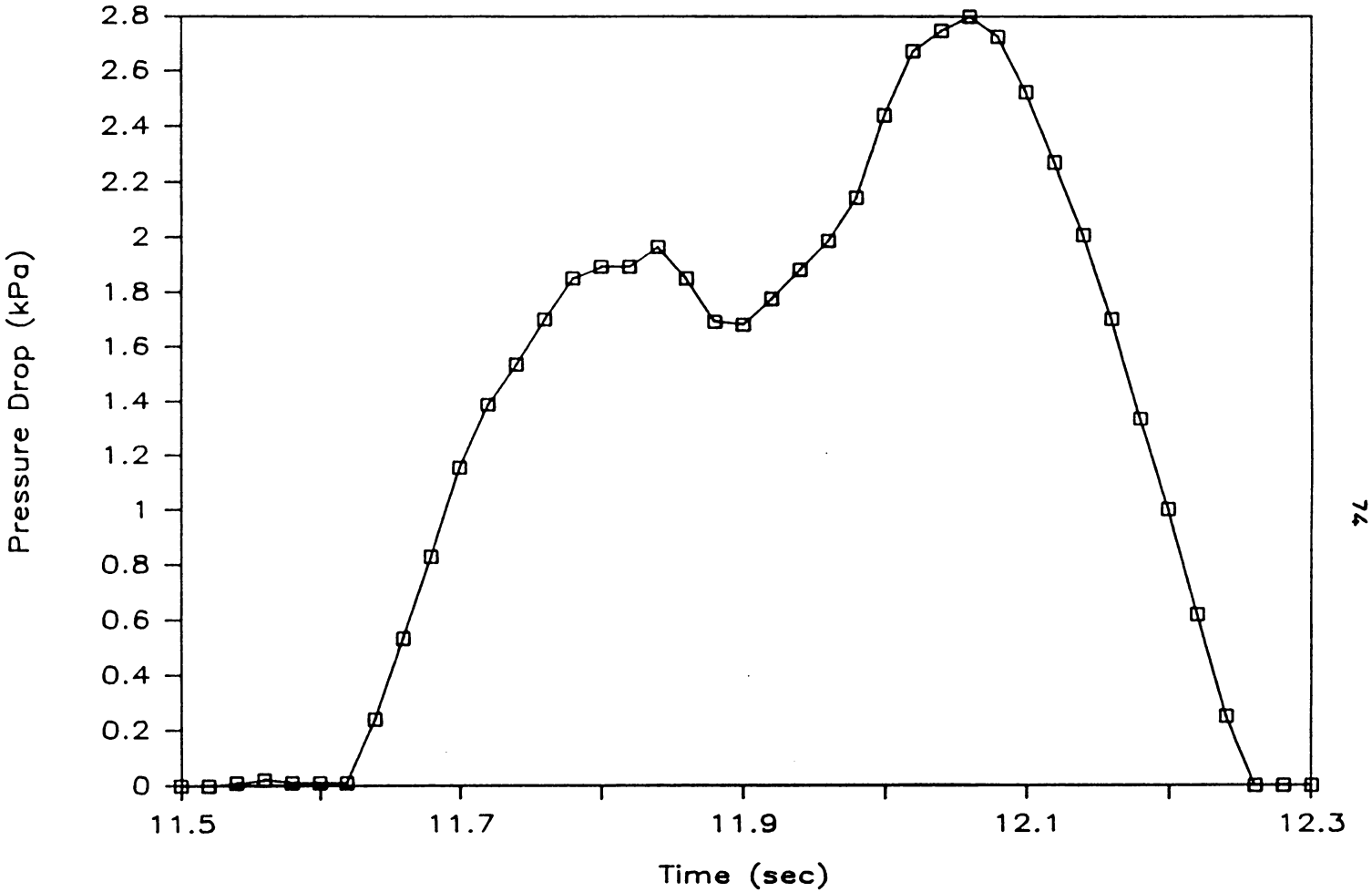

Figure 4.11 Pressure Drop Across 70 cm Section for Plug #5, Run #2

pressure profile: out of 25 plugs, 21 of the times were within 0.01 sec, 24 were within 0.02 sec and all 25 were within 0.04 sec. This is excellent agreement when it is considered that the data were collected at 50 Hz; i.e. one data point every 0.02 sec. The pressure drop across the plug as it had just passed the first tap (Figure 4.10(b)) was obtained from the pressure profile by knowing the time required for the plug to pass the first tap (from the frame count).

The shape of the pressure profile shown in Figure 4.11 requires some comment. For ideal plug conveying, the pressure should rise linearly as a plug passes the first tap, reach a plateau and remain constant while the plug is between the taps and then decrease linearly as the plug passes the second tap. This should be the case if the thickness of the stationary layer is constant, if the plug moves through the pipe at a constant velocity and if the amount of material that is collected by the plug front equals the amount that is dropped off the back. However, this was not the case for the plugs filmed, and, in fact, there were variations in the plug velocity, the plug length, and the amount of material that was left behind. These variations from the ideal condition caused each plug to have a unique (and non-ideal) pressure profile such as that shown in Figure 4.11. Since the plug of Figure 4.11 did not change significantly in length, as it passed between the pressure taps, it follows that some other factor must have been responsible for the change in the pressure across the moving plug. In this case, changes in the frontal stress would explain the profile. A careful study of Figure 4.10(a), reveals that there are variations in the thickness of the stationary layer ahead of the plug.

The stationary layer appears to get thinner and then thicker, moving from right to left. This would cause the plug to encounter a corresponding decrease and increase in the frontal stress, and, hence, the pressure drop required to move the plug would decrease and increase, which is what is observed in Figure 4.11.

Three high-speed films, spanning the dense-phase plug conveying range of the equipment, were made. The experimental results for the pressure drop, etc., are given in Table 4.5, together with the quantities measured from the films. (Note: there is no u_g value given for plug 6 of run 1, since this was a short plug without any black particles that could be tracked.) A plot of the pressure gradient versus the frontal stress, for runs 2 and 3, is presented in Figure 4.12. Also plotted are the active and passive cases as calculated by equations (2.7) and (2.8). It can be seen that the data generally falls between the active and passive lines, although plug 4 of run 2 is some distance above the passive line. Considering the difficulty in obtaining the velocity measurements, the agreement with the theoretical equations to predict the range of stresses is very good. Konrad et al. (1980) found that the data for polyethylene granules followed the passive line.

For run 1, the pressure gradient is plotted against the frontal stress in Figure 4.13. Again, the active and passive cases, as calculated by equations (2.7) and (2.8), are also plotted. In this case there is considerable scatter in the data although the numbers are still in the same range as the predictions. A change in the flow pattern is believed to be the main cause of the scatter.

Table 4.5 Horizontal Conveying: Summary of the Results Obtained from the Dense-Phase Flow Film Work

Plug Number	Plug length ℓ_p (m)	Pressure drop ΔP (kPa)	Pressure gradient $\Delta P/\ell_p$ (kPa/m)	Velocity of plug front w_F (m/s)	Velocity of a particle in the plug u_s (m/s)	Front Stress F (kPa)
Run 1 (HFILM2)						
1	0.32	4.07	12.7	2.78	2.40	0.54
2	0.30	2.33	7.8	2.31	2.23	0.11
3	0.29	2.19	7.6	2.90	1.95	1.09
4	0.39	3.41	8.7	2.59	2.08	0.63
5	0.27	1.73	6.4	2.70	1.95	0.86
6	0.20	1.78	8.9	3.68	—	—
7	0.28	3.73	13.3	2.87	2.84	0.05
8	0.27	3.10	11.5	2.48	1.64	0.81
9	0.25	2.31	9.2	2.69	2.40	0.41
10	0.47	4.82	10.3	2.26	1.74	0.53
11	0.22	1.91	8.7	2.41	2.40	0.014
12	0.34	2.92	8.6	2.76	2.60	0.25
13	0.22	2.13	9.7	2.70	2.40	0.43
Run 2 (HFILM3)						
2	0.40	2.47	6.2	1.69	1.25	0.33
3	0.37	2.72	7.3	1.53	0.98	0.32
4	0.17	2.43	14.3	1.90	1.74	0.16
5	0.42	1.96	4.7	1.75	1.56	0.18
6	0.47	4.57	9.7	1.72	1.12	0.40
7	0.60	5.22	8.7	1.48	0.60	0.31
8	0.55	3.64	6.6	1.38	1.04	0.21
Run 3 (HFILM4)						
1	0.39	3.39	8.7	1.57	0.71	0.36
2	0.52	3.69	7.1	1.23	0.61	0.22
3	0.19	0.96	5.1	1.28	0.68	0.24
4	0.39	3.16	8.1	1.38	1.01	0.22
5	0.32	2.37	7.4	1.55	1.25	0.22

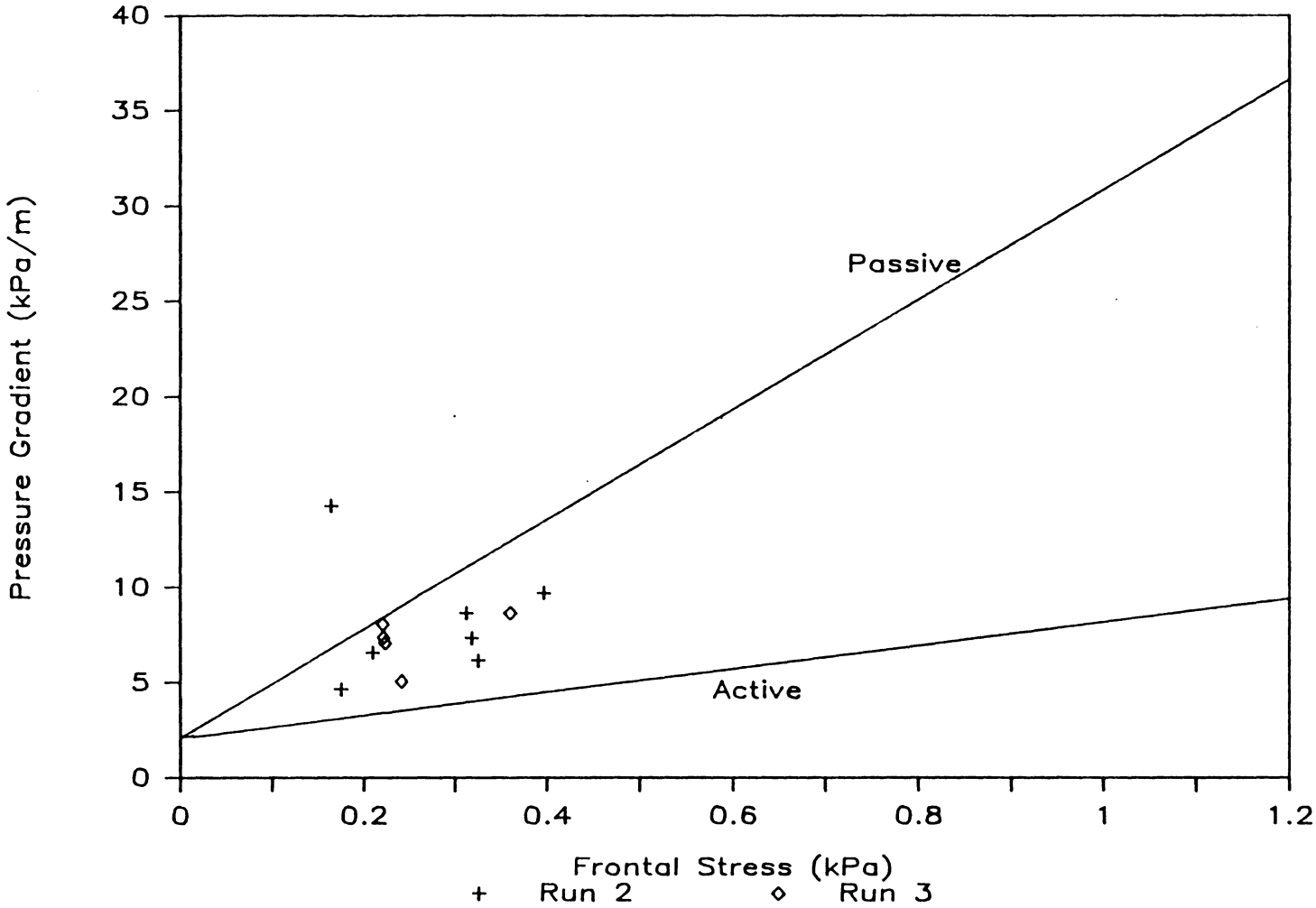

Figure 4.12 Pressure Gradient versus Frontal Stress (Runs 2 & 3)

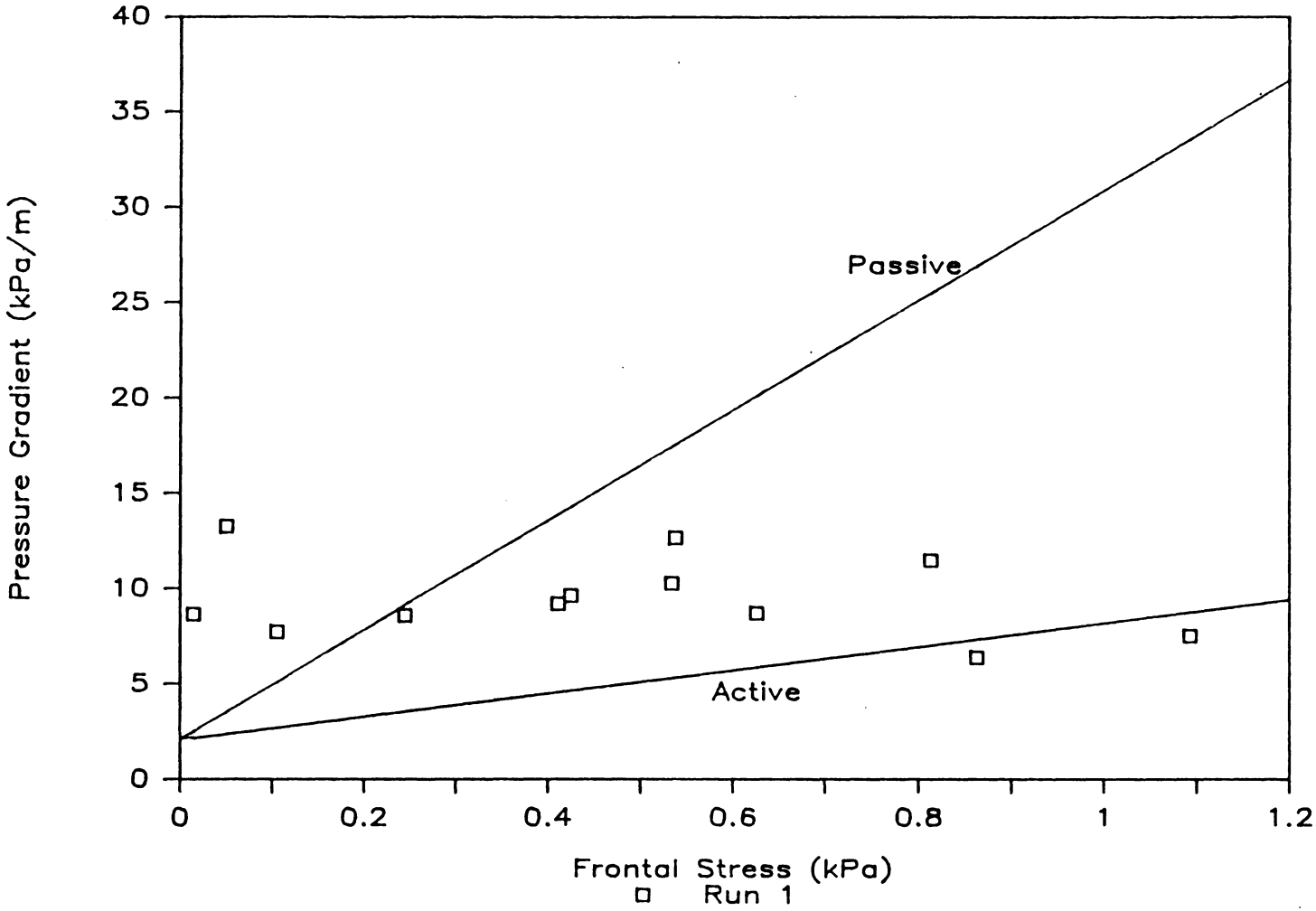

Figure 4.13 Pressure Gradient versus Frontal Stress (Run 1)

Run number one was at the highest superficial air velocity (3.9 m/sec) and, at this velocity, the flow pattern for many of the plugs was not the same as was assumed in deriving the theoretical equations. There was a considerable amount of "rolling" action at the downstream end of a plug. The stationary layer was swept up by the front of a plug, but instead of joining the plug it rolled over like a wave breaking on the sea-shore. Also, for some of the plugs a large amount of material was thrown ahead of the plug as shown in Figure 4.14, which is a photograph of plug 11 of run 1. The length of the rolling section was not constant, but changed as the plug moved through the pipeline. Plug 4, of run 2, also exhibited the rolling behavior which may explain why it is some distance from the passive line. For the other plugs in runs 2 and 3, the flow pattern more closely resembled that observed by Konrad et al. (1980), which is consistent with the good agreement shown by these plugs with the theory.

The superficial air velocity for the strand-flow conveying was 6.8 m/s. The transition velocity between the different flow patterns is not known, but clearly the superficial air velocity employed in run 1 was closer to the transition point than the velocities used in runs 2 and 3. The resulting change in the flow pattern, i.e., the rolling action at the front of a plug, changes the frontal stress so that a new method is needed to calculate the frontal stress in order to apply the theory to the case of a plug with the rolling action.

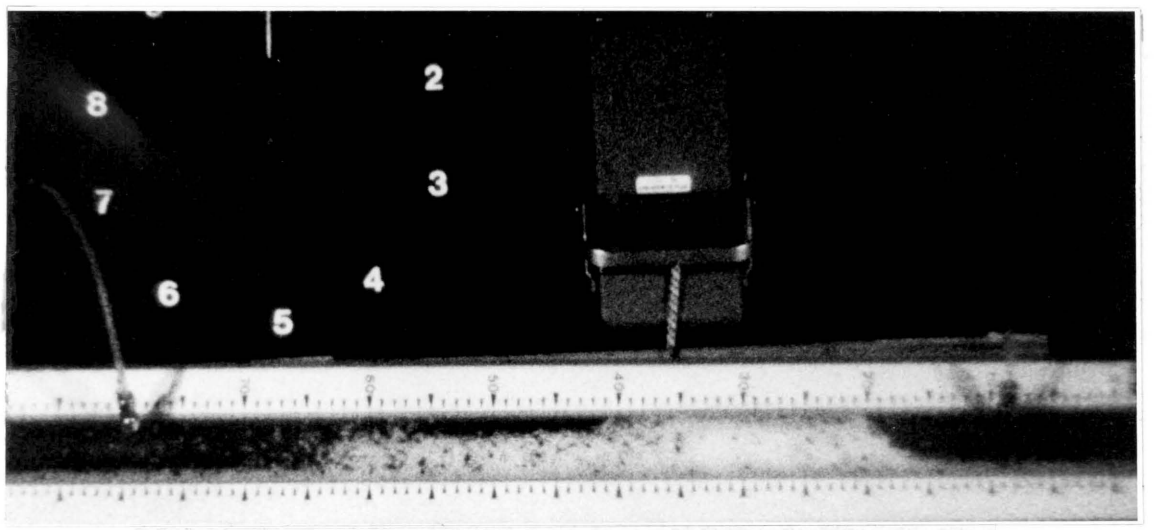

Figure 4.14 Photograph of Plug #11, Run #1 depicting the "Rolling Action". Flow from right to left.

4.2.2 Vertical Conveying

The vertical conveying experimental runs included one dilute-phase flow and three dense-phase plug flow films (see Table 4.6 for the operating conditions for each run). At the higher air velocities, the solids are maintained in a dilute suspension within the air stream (run #9). The superficial air velocity exceeds the single particle terminal velocity (which is about 6 m/sec for these particles). Figure 4.15 is a sequence of photographs showing the gas/solid motion. There is an incredible amount of structure to the flow pattern. The particles remain together as an aggregate or a cluster for a relatively long period of time. Air pockets (or "bubbles") can be seen moving upward. Notice the air bubble at the 34 cm mark on the right side of the pipe in Figure 4.15a. This bubble moves up 1 cm in each succeeding photograph. The total time for this sequence is 0.0053 seconds. The pressure drop across the 70 cm section fluctuates in a similar manner to the horizontal dilute-phase flow except that the mean pressure drop is approximately 0.25 kPa (see Figure 4.16). For this run, the pressure drop measurements were not coordinated with the film. The computer acquisition system was started about one second before the film. The total time filmed was approximately 11 seconds, therefore, the data presented in the figure spans the entire duration of the film. The very rapid pressure fluctuations of small amplitude are expected for the dilute-phase flow pattern observed.

Table 4.6 Vertical Conveying: Operating Conditions for the Four Experimental Runs

Run	Flow Pattern	Camera Frame Rate (Frames/sec)	Superficial Air Velocity (m/sec)	Solids Mass Flow Rate (kg/sec)
6 (VFILM1)	Dense	500	2.9	0.11
7 (VFILM2)	Dense	500	2.4	0.071
8 (VFILM3)	Dense	500	4.1	0.18
9 (VFILM4)	Dilute	1500	15.1	0.23

(Note: The ambient absolute pressure was 93 kPa for all these runs.)

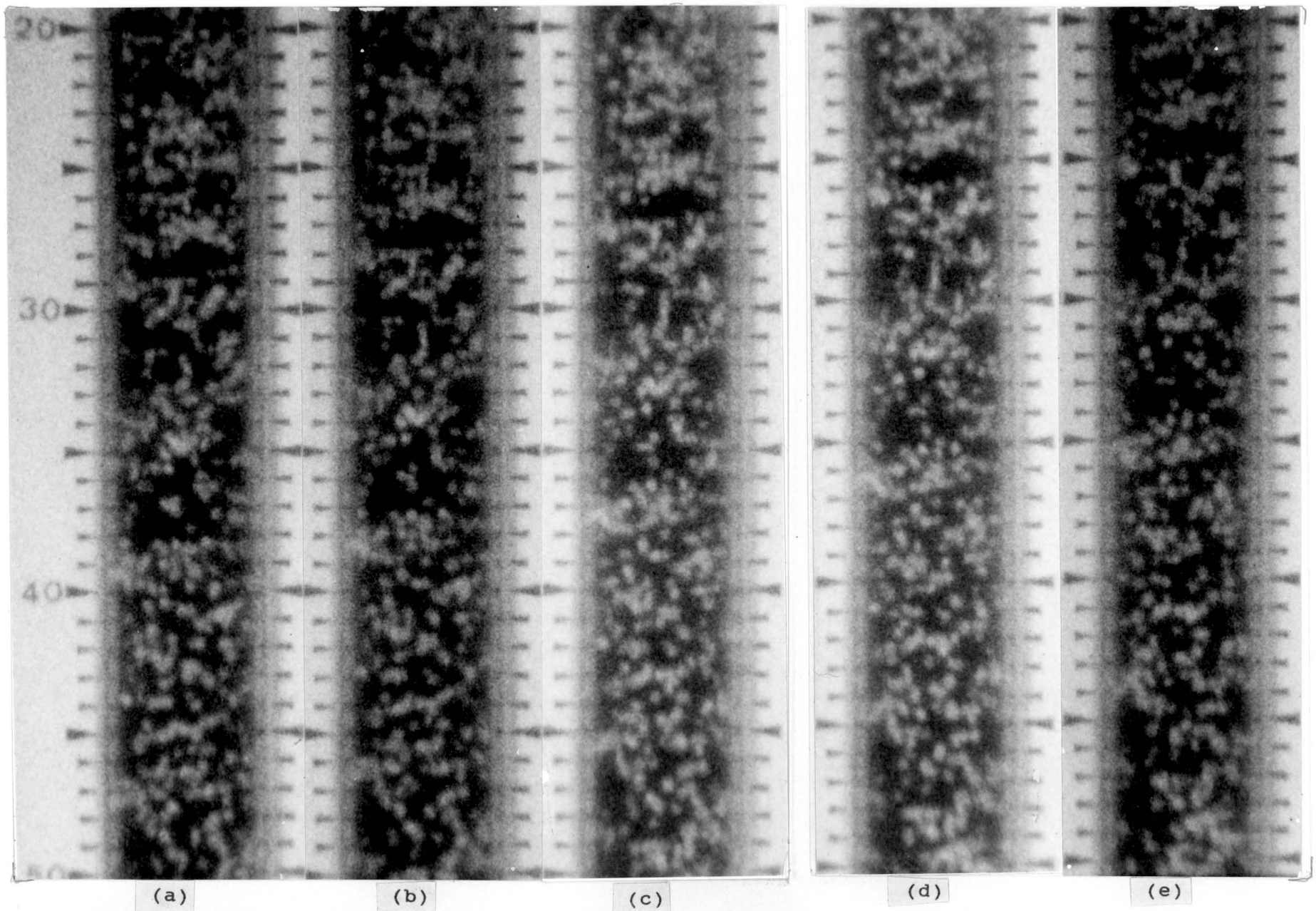

Figure 4.15 Photographs of Vertical Dilute-Phase Flow.
Flow from bottom to top.
Time between each frame is 1.3 milliseconds.

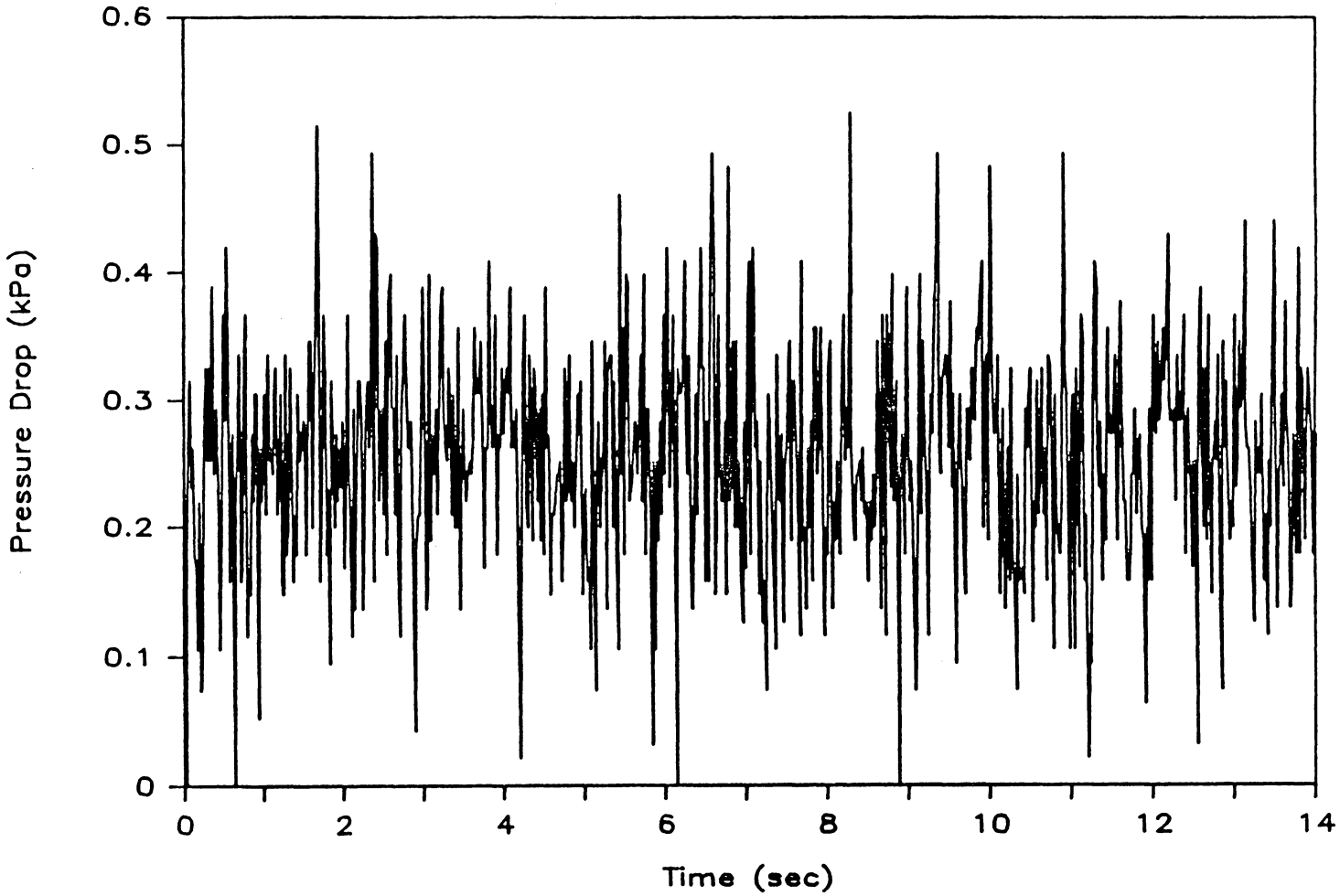

Figure 4.16 Pressure Drop Across 70 cm Section for Vertical Dilute-Phase Flow

For the dense-phase flow at the highest superficial air velocity (run #8), the plug formation region extends into the field of view. The film of this flow pattern is fascinating to observe. The solids shoot up into the field of view like a geyser. There is a considerable amount of solids recirculation. Once enough particles have fallen back down and have compacted together, a plug forms. The plug shoots up through the pipe out of the field of view leaving a trail of particles raining down. The process repeats itself in a cycle. For runs 6 and 7, the plug formation region is below the field of view. The pressure drop across the 70 cm section for run #6 is presented in Figure 4.17. Each numbered peak corresponds to a plug passing the pressure taps.

The analysis of the vertical dense-phase films is not as straightforward as in the horizontal case. First of all, there is always material between the two pressure taps either being suspended as in a turbulent fluidized bed, being transported up in the form of a plug or as particles falling back down from a plug. When viewing the vertical films frame by frame, it is not always possible to precisely determine the back of the plug. Therefore it is difficult to measure the plug length and the time required to pass the pressure taps. Also, in order to calculate the frontal stress according to the method of Konrad (1987), either the particle velocity falling down in the gas slug or the volume fraction of the solids in the gas slug must be measured. It is not possible to obtain the latter from the films, and the former is difficult as well.

However, some of the concepts outlined by Konrad (1987) can be understood by considering the sequence of photographs in Figure 4.18 (plug #4, run #6) and the corresponding pressure profile (Figure 4.19).

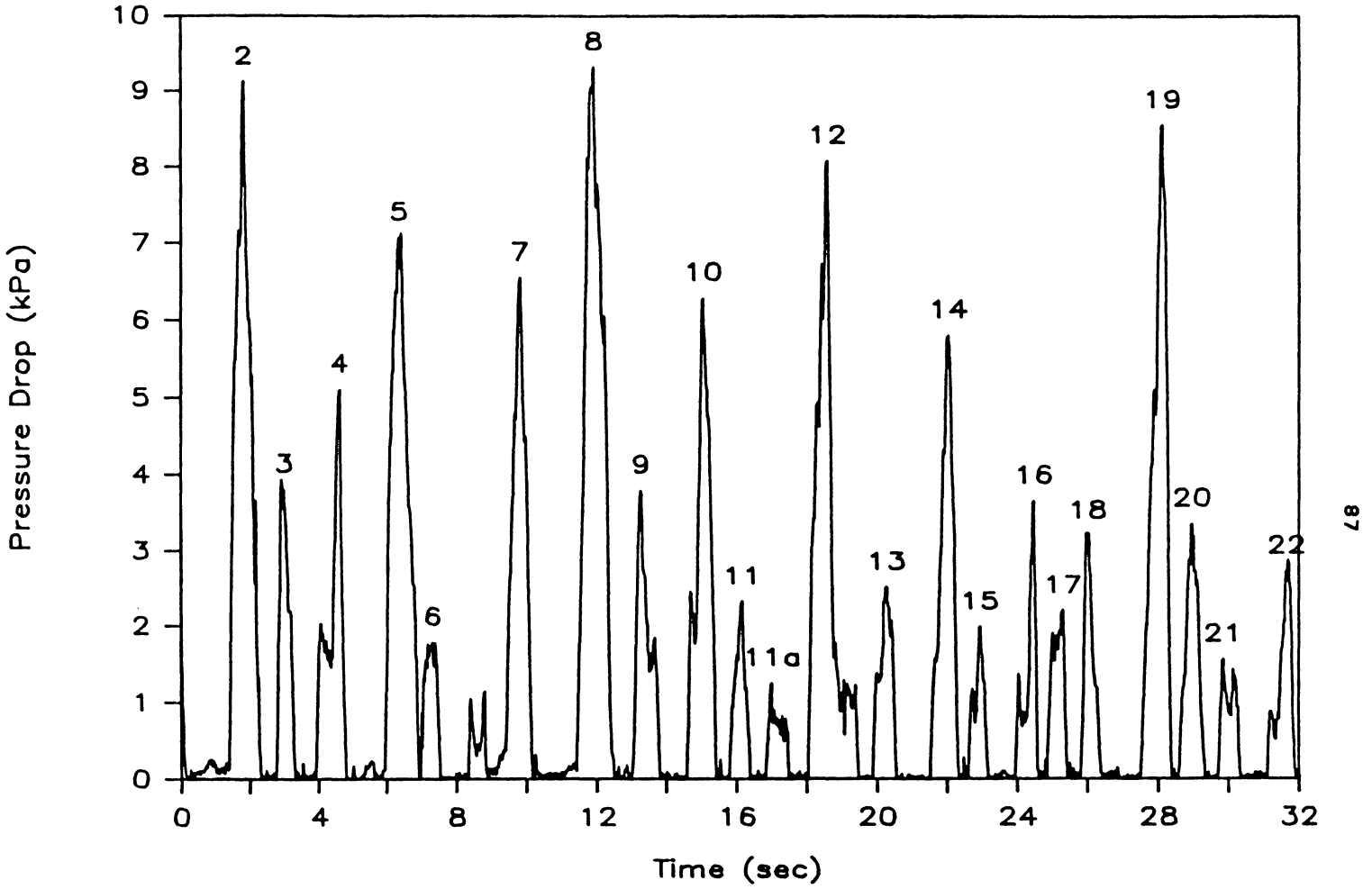

Figure 4.17 Pressure Drop Across 70 cm Section for Vertical Dense-Phase Flow (Run #6)

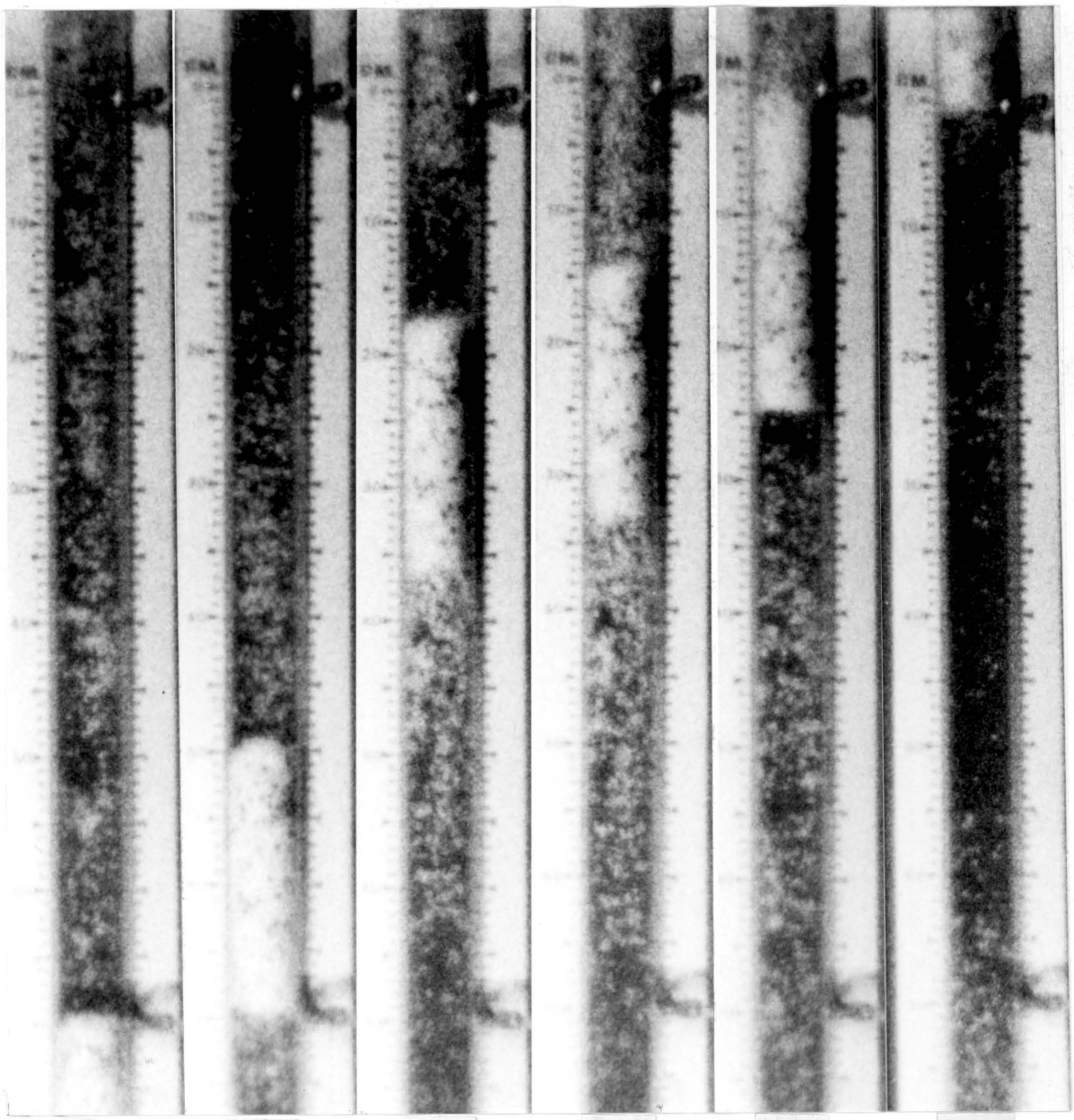

Figure 4.18 Photographs of Vertical Dense-Phase Flow (Plug #4, Run #6). Flow from bottom to top. Time between each frame, from left to right, is 0.150, 0.318, 0.030, 0.174, 0.244 seconds.

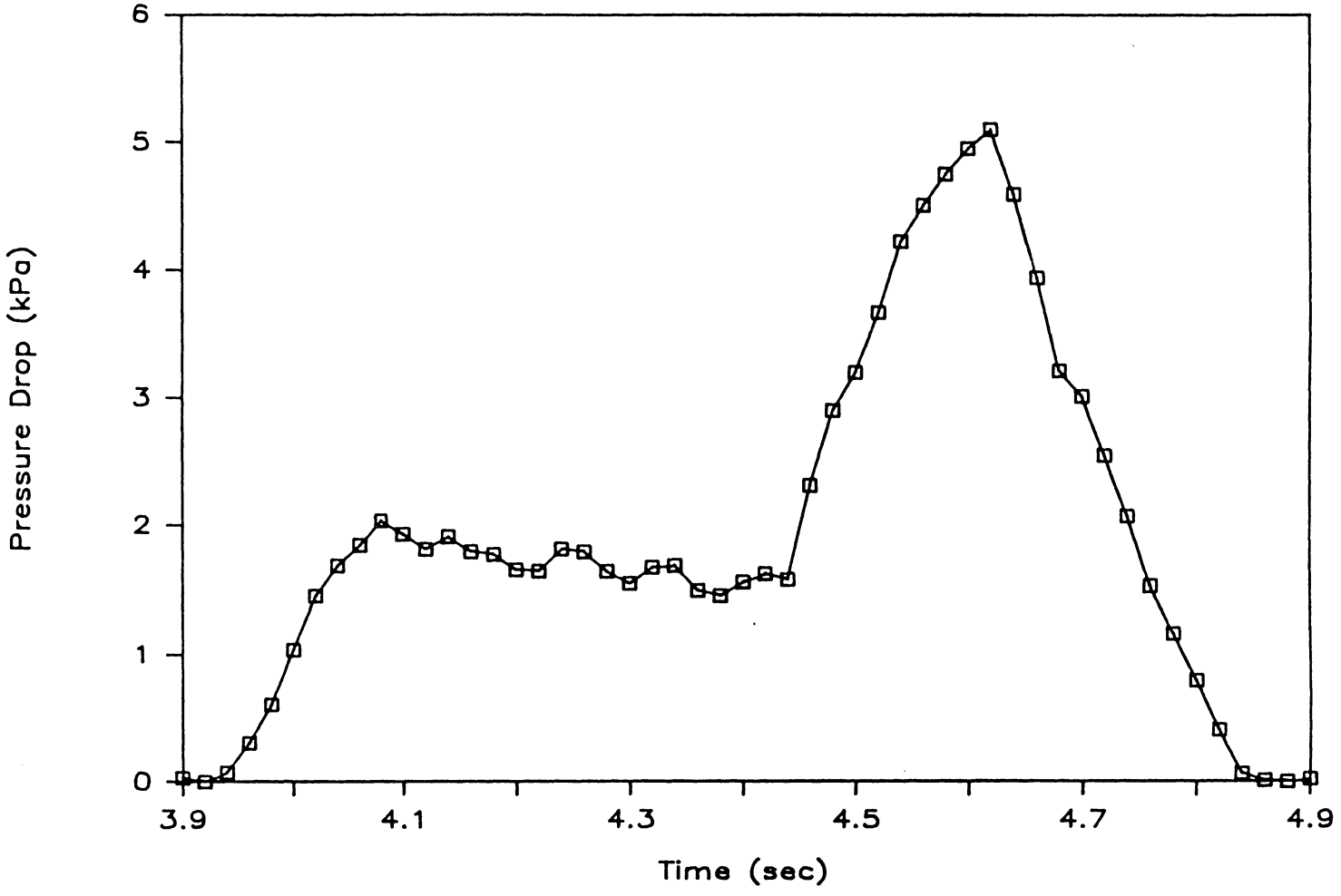

Figure 4.19 Pressure Drop Across 70 cm Section for Plug #4, Run #6

For this particular plug, it is possible to obtain some measurements. In Figure 4.18a, the plug front has just reached the first pressure tap. The particles in the gas slug falling down can be seen hitting the plug front. The next photograph shows the plug just passing the first tap. Notice the particles falling from the back. The time required for the plug to pass the first tap as measured from the film is 0.15 seconds which corresponds to the initial pressure rise observed in Figure 4.19. The plug length in this position is approximately 20 cm. Also notice the void space near the second pressure tap. From Figure 4.19, the pressure drop is observed to remain constant for approximately 0.36 seconds. The photograph of Figure 4.18c was taken 0.318 seconds after the photograph of 4.18b. The plug length is still about 20 centimeters. A large amount of material raining down from the previous plug has come into view at the second pressure tap. In the next photograph (Figure 4.18d), this material is just beginning to hit the plug front. This photograph was taken 0.348 seconds after the photograph of 4.18b and corresponds to the base point of the second pressure rise in Figure 4.19. The plug length is still 20 cm, but by the next photograph (Figure 4.18e), the plug has grown to a length of 25 cm. The plug front positioned at the second tap (Figure 4.18e) corresponds to the peak in the pressure profile. The 20% change in the plug length cannot account for more than doubling the pressure drop. The change in momentum of the particles that were falling down causes a frontal stress to be applied to the plug front which is transmitted axially through the plug and radially to the pipe wall where it generates a shear stress. The resulting wall shear stress must also account for some of the rise

in the pressure drop. The final photograph (Figure 4.18f) shows the back of the plug passing the second tap which corresponds to the pressure drop returning to zero. In order to be more quantitative, a method is needed to calculate the frontal stress.

5.0 CONCLUSIONS AND SUGGESTIONS FOR FURTHER WORK

5.1 Conclusions

1) A circulating unit with both horizontal and vertical sections has been constructed that can easily be operated with cohesionless polyethylene granules (particle diameter ~3 mm) at a variety of flow conditions ranging from dilute-phase flow to dense-phase plug flow.
2) For the dilute-phase flow in both the horizontal and vertical sections, the solids are maintained in a suspension within the air stream (superficial air velocity ~15 m/sec). The pressure drop across the 70 cm test section fluctuates very rapidly around a mean value.
3) Upon reducing the superficial air velocity to 6.8 m/sec, the flow pattern in the horizontal section changes to a type of strand flow. The particles are conveyed in a dilute phase above a stationary layer. Occasionally, the dilute-phase solids concentration increases which drags along the particles in the stationary layer for a certain distance. When this occurs, there is a corresponding increase in the pressure drop across the 70 cm test section.
4) For horizontal dense-phase conveying, the solids move in plugs that occupy the entire pipe cross-section. The flow pattern at the lower superficial air velocities (2.3 and 1.5 m/sec) resembles that described by Konrad et al. (1980). For the highest superficial air velocity (~4

m/sec) and for thin stationary layers, the flow pattern at the front of the plug changes to a "rolling" behavior.

5) For each plug that passes the pressure taps in horizontal conveying, there is a corresponding peak in the pressure profile. If no plug is between the pressure taps, only air is flowing over the stationary layer and the pressure drop across the 70 cm test section is effectively zero.

6) The pressure gradient required for a plug of cohesionless material to move through a horizontal pipeline is a linear function of the frontal stress. The pressure gradient range can be predicted from the active and passive equations of Konrad et al. (1980), if no "rolling" behavior is observed at the front end of the plug.

7) For plugs exhibiting the "rolling" behavior at the front of a plug, a new method is needed to calculate the frontal stress.

8) For vertical dense-phase conveying, the solids move in plugs that occupy the entire pipe cross-section. Particles fall from the back of one plug and "rain" down on the front of the next as described by Konrad (1987).

9) The analysis of the vertical dense-phase films is not as straightforward as the horizontal ones. However, by observing the motion of a particular plug and the corresponding pressure profile, some of the concepts outlined by Konrad (1987) can be understood in a qualitative sense. The particles "raining" down from the back of one plug results

in a stress on the next plug front which is transmitted axially through the plug and radially to the pipe wall. If a large amount of material hits the plug front, the stress increases which results in a corresponding increase in the pressure drop required to move the plug.

5.2 Suggestions for Further Work

1) Further theoretical work is necessary to devise a method to calculate the frontal stress in horizontal conveying for plugs exhibiting the "rolling" behavior.
2) In order to test the method of Konrad (1987) to calculate the pressure drop in vertical dense-phase transport, a method is needed to measure the frontal stress.
3) The work described in this thesis was for coarse, cohesionless particles. An experimental program with fine, cohesive powders is necessary in order to test the theoretical equations of Konrad et al. (1980). With slight modifications, it might be possible to convey finer materials in the circulating unit.
4) The differences in the pressure fluctuations corresponding to the various flow patterns deserves more investigation. Following the lead of Tsuji and Morikawa (1982b) and Satija et al. (1985), the Fast Fourier Transform technique should be used to obtain a fingerprint of the pressure fluctuations for the various flow patterns.

References

Albright, C.W., J.H. Holden, H.P. Simons, and L.D. Schmidt, 1951.
"Pressure Drop in Flow of Dense Coal-Air Mixtures," *Industrial and Engineering Chemistry*, Vol. 43, No. 8, August 1951, pp. 1837-1840.

Borzone, L.S., 1985.
"Dense Phase Transport: The Vertical Plug Flow," M.S. Thesis, University of Pittsburgh, Pittsburgh, Pennsylvania, 1985.

Bridgwater, J., and A.M. Scott, 1983.
"Flow of Solids in Bunkers," in *Handbook of Solids in Motion*, edited by N.P. Cheremisinoff and R. Gupta, Ann Arbor Science, 1983, pp. 807-846.

Cardoso, V.M.R., 1978.
"An Investigation Into Pneumatic and Mechanical Transport of a Granular Plug in a Horizontal Straight Pipe," report submitted to the School of Mechanical Engineering, University of the Witwatersrand, Johannesburg, South Africa, November, 1978.

Carr, J.F. and D.M. Walker, 1967/68.
"An Annular Shear Cell for Granular Materials," *Powder Technology*, Vol. 1, 1967/68, pp. 369-373.

Chan, S., D. Remple, C.A. Shook, and M.N. Esmail, 1982.
"A One-Dimensional Model of Plug Flow Pneumatic Conveying," *The Canadian Journal of Chemical Engineering*, Vol. 60, October 1982, pp. 581-588.

Colijn, H., 1981.
"Mechanical conveyors and elevators," in *Solids Handling*, edited by Kenneth McNaughton and The Staff of Chemical Engineering, McGraw-Hill Publications Co., New York, N.Y., 1981, pp. 97-112.

Delaplaine, J.W., 1956.
"Forces Acting in Flowing Beds of Solids," *A.I.Ch.E. Journal*, Vol. 2, No. 1, March 1956, pp. 127-138.

Dickson, A.J., B.W. Skews, and R.D. Marcus, 1978.
"Plug Phase Conveying," *Proceedings of Pneumotransport* 4, paper D6, Organized by BHRA Fluid Engineering, Cranfield, Bedford, U.K., June 1978.

Ergun, S., 1952.
"Fluid Flow Through Packed Columns," *Chemical Engineering Progress*, Vol. 48, 1952, pp. 89-94.

Janssen, H.A., 1895.
"Versuche uber Getreidedruck in Silozellen," *Z. ver. deut. Ing.*, Vol. 39, 1895, pp. 1045-1049.

Kano, T., F. Takeuchi, H. Sugiyama, and E. Yamazaki, 1984.
"A Study of the Optimum Conditions for Plug-type Pneumatic Conveying of Granular Materials," *International Chemical Engineering*, Vol. 24, No. 4, October 1984, pp. 702-709.

Kano, T., 1986.
"Reduction of Power Consumption in Pneumatic Conveying of Granular Materials," in *The Best of Bulk Solids Handling - Pneumatic Conveying of Bulk & Powder*, edited by R.H. Wohlbier, Trans Tech Publications, Clausthal-Zellerfeld, Federal Republic of Germany, 1986, pp. 185-191.

Klintworth, J. and R.D. Marcus, 1986.
"A Review of Low-Velocity Pneumatic Conveying Systems," in *The Best of Bulk Solids Handling - Pneumatic Conveying of Bulk & Powder*, edited by R.H. Wohlbier, Trans Tech Publications, Clausthal-Zellerfeld, Federal Republic of Germany, 1986, pp. 25-31.

Konrad, K., D. Harrison, R.M. Nedderman, and J.F. Davidson, 1980.
"Prediction of the Pressure Drop for Horizontal Dense Phase Pneumatic Conveying of Particles," *Proceedings of Pneumotransport* 5, paper E1, Organized by BHRA Fluid Engineering, Cranfield, Bedford, U.K., April 1980.

Konrad, K., 1981.
"Dense Phase Pneumatic Conveying of Particles," PhD dissertation, University of Cambridge, U.K., 1981.

Konrad, K., 1986.
"Dense-Phase Pneumatic Conveying: A Review," *Powder Technology*, Vol. 49, 1986, pp. 1-35.

Konrad, K., 1987.
"An Exploratory Analysis of Dense Phase Pneumatic Conveying Through Vertical Pipelines," *Journal of Pipelines*, Vol. 6, 1987, pp. 99-104.

Krauss, M.N., 1986.
"Pneumatic Conveying Systems," *Chemical Engineering*, Vol. 93, No. 19, October 13, 1986, pp. 50-61.

Lambe, T.W., and R.V. Whitman, 1979.
Soil Mechanics, SI Version, John Wiley & Sons, New York, N.Y., 1979.

Legel, D., and J. Schwedes, 1984.
"Investigation of Pneumatic Conveying of Plugs of Cohesionless Bulk Solids in Horizontal Pipes," *Bulk Solids Handling*, Vol. 4, No. 2, June 1984, pp. 399-405.

Leung, L.S., 1980.
"Vertical Pneumatic Conveying: A Flow Regime Diagram and a Review of Choking versus Non-Choking Systems," *Powder Technology*, Vol. 25, 1980, pp. 185-190.

Lilly, K., 1984.
"Horizontal Dense Phase Pneumatic Conveying of Particles, M.S. Thesis, Virginia Polytechnic Institute and State University, Blacksburg, Virginia, July 1984.

Lippert, A., 1966.
"Pneumatic Conveyance of Solids at High Concentrations," *Chemie-Ingenieur-Technik*, Vol. 38, No. 3, 1966, pp. 350-355. (Original in German)

Marcus, R.D., 1986.
Introduction to *The Best of Bulk Solids Handling - Pneumatic Conveying of Bulk & Powder*, edited by R.H. Wohlbier, Trans Tech Publications, Clausthal-Zellerfeld, Federal Republic of Germany, 1986.

Nedderman, R.M., 1982.
"The Theoretical Prediction of Stress Distributions in Hoppers," *Trans IChemE*, Vol. 60, 1982, pp. 259-275.

P.E.C. (Physics Engineering Chemistry Corporation) Report, 1966.
"Characteristics of Confined Dense Phase Flow of Granular Solids Driven by Compressed Air," U.S. Report No. A.D. 642845, prepared by P.E.C. Research Associates, Inc., 1001 Mapleton Avenue, Boulder, Colorado 80302, 1966.

Ramachandran, P.S., D.G. Burkhard, and B.E. Lauer, 1970.
"Studies of Dense Phase Horizontal Flow of Solids-Gas Mixtures," *Indian Journal of Technology*, Vol. 8, June 1970, pp. 199-204.

Reece, E.V., 1985.
"Bulk Solids Handling," *Chemical Engineering*, Vol. 92, No. 9, April 29, 1985, pp. 38-52.

Rizk, F., 1986.
"Pneumatic Transport in Dilute and Dense Phase," in *The Best of Bulk Solids Handling - Pneumatic Conveying of Bulk & Powder*, edited by R.H. Wohlbier, Trans Tech Publications, Clausthal-Zellerfeld, Federal Republic of Germany, 1986, pp. 9-15.

Sandy, C.W., T.E. Daubert, and J.H. Jones, 1970.
"Vertical Dense-Phase Gas-Solids Transport," *Chemical Engineering Progress Symposium Series*, Vol. 66, No. 105, 1970, pp. 133-142.

Satija, S., J.B. Young, and L.-S. Fan, 1985.
"Pressure Fluctuations and Choking Criterion for Vertical Pneumatic Conveying of Fine Particles," *Powder Technology*, Vol. 43, 1985, pp. 257-271.

Stoess, H.A., 1983.
Pneumatic Conveying, John Wiley & Sons, New York, N. Y., 1983.

Tomita, Y., S. Yutani, and T. Jotaki, 1980.
"Pressure Drop in Vertical Pneumatic Transport Lines of Powdery Material at High Solids Loading," *Powder Technology*, Vol. 25, 1980, pp. 101-107.

Tomita, Y., T. Jotaki, and H. Hayashi, 1981.
"Wavelike Motion of Particulate Slugs in a Horizontal Pneumatic Pipeline," *International Journal of Multiphase Flow*, Vol. 7, 1981, pp. 151-166.

Tsuji, Y., and Y. Morikawa, 1982a.
"Plug Flow of Coarse Particles in a Horizontal Pipe," *ASME Journal of Fluids Engineering*, Vol. 104, June 1982, pp. 198-206.

Tsuji, Y., and Y. Morikawa, 1982b.
"Flow Pattern and Pressure Fluctuation in Air-Solid Two-Phase Flow in a Pipe at Low Air Velocities," *International Journal of Multiphase Flow*, Vol. 8, No. 4, 1982, pp. 329-341.

Tsuji, Y., and Y. Morikawa, 1982c.
"Plug Conveying of Coarse Particles in a Horizontal Pipe with Secondary Air Injection," *International Journal of Multiphase Flow*, Vol. 8, No. 6, 1982, pp. 657-667.

Wen, C-Y, and H.P. Simons, 1959.
"Flow Characteristics in Horizontal Fluidized Solids Transport," *AIChE Journal*, Vol. 5, No. 2, June 1959, pp. 263-267.

Wilson, K.C., 1986.
"Analysis of Slip of a Particulate Mass in a Horizontal Pipe," in *The Best of Bulk Solids Handling - Pneumatic Conveying of Bulk & Powder*, edited by R.H. Wohlbier, Trans Tech Publications, Clausthal-Zellerfeld, Federal Republic of Germany, 1986, pp.67-71.

Wirth, K.E. and O. Molerus, 1984.
"Critical Solids Transport Velocity in Horizontal Pipelines," *Proceedings of Pneumatech* 2, Canterbury, U.K., 1984, pp. 99-125.

Appendices

Appendix A

Equipment Specifications

1) Ramapo Target Flow Meter

Model:	Mark V-1-F01ED
Serial No.:	9953
Flow Range:	15 to 150 SCFM
Calibration:	Flow Rate (SCFM) = 15*Voltage(VDC)
	(Calibrated with air at 70°F and 2 atm)

2) MKS Baratron Differential Pressure Transducer

Model:	Type 220BH-2A1-B-1000
Serial No.:	28225-1
Pressure Range:	0 to 1000 mm Hg
Calibration:	Pressure (mm Hg) = 100*Voltage(VDC)

3) Omega Differential Pressure Transducer

Model:	PX142-005D5V
Pressure Range:	0 to 35 kPa (0 to 5 psi)
Calibration:	Pressure (kPa) = 4.31*Voltage(VDC)
	(see Figure A.1 for calibration curve)

4) HBM Load Cell

Model:	U1T
Serial No.:	165958
Load Range:	0 to 22.7 kg (0 to 50 lbs)
Calibration:	Force(Newtons) = 23.013*Voltage(VDC) + 0.421
	(see Figure A.2 for calibration curve)

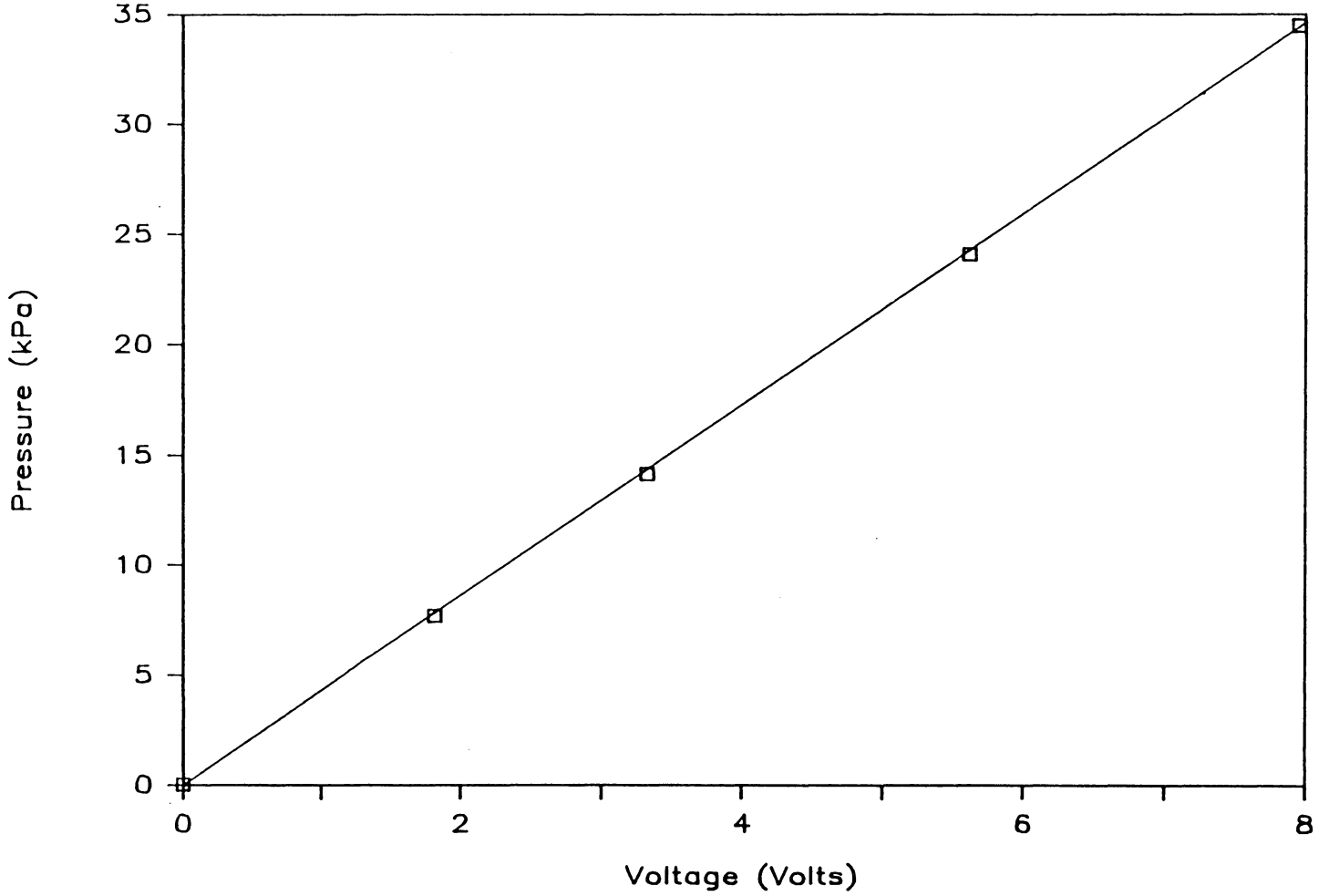

Figure A.1 Calibration Curve: Omega Differential Pressure Transducer

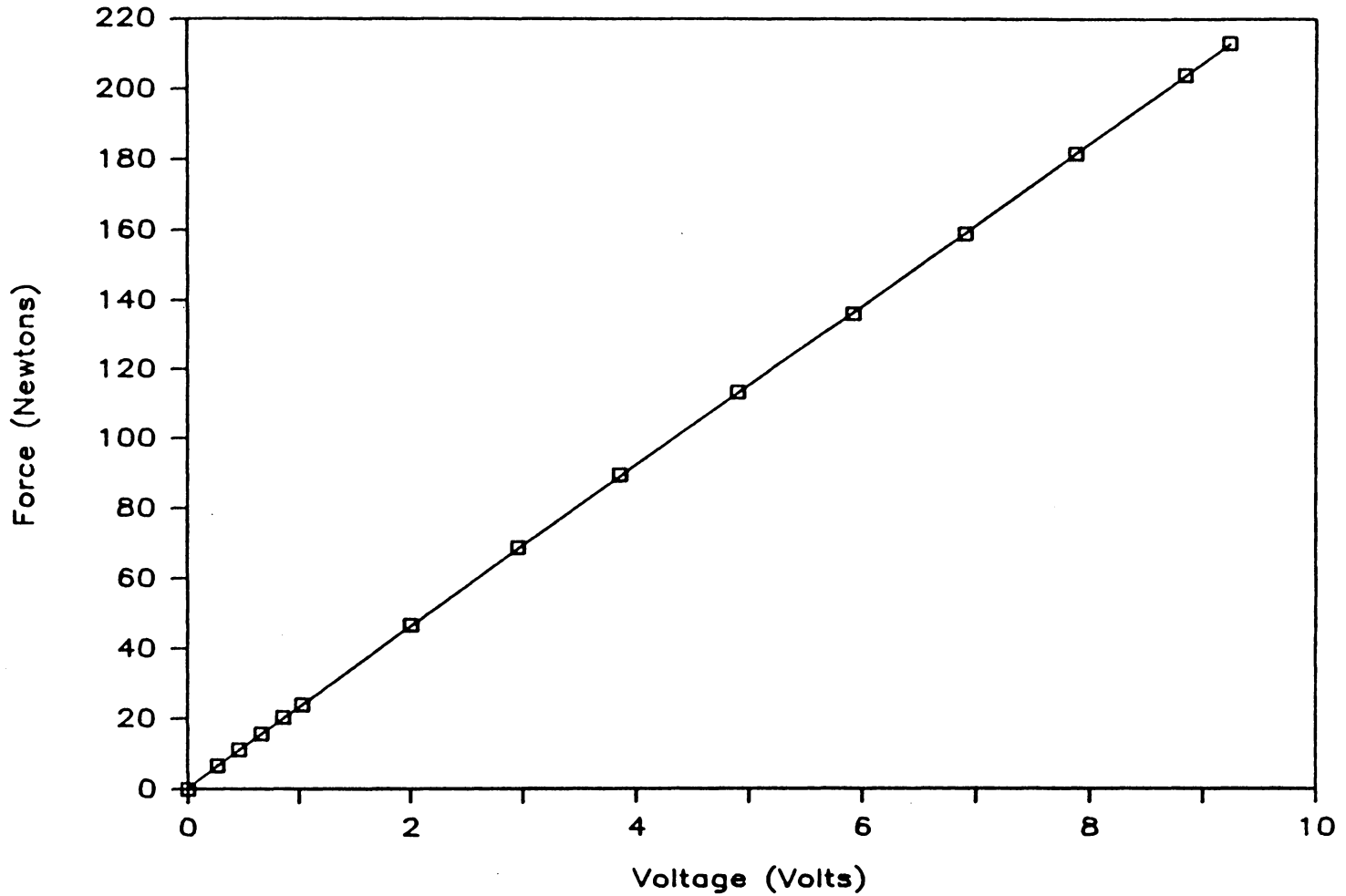

Figure A.2 Calibration Curve: HBM Load Cell

Appendix B

Internal Friction:
Peak Shear Stress versus Normal Stress

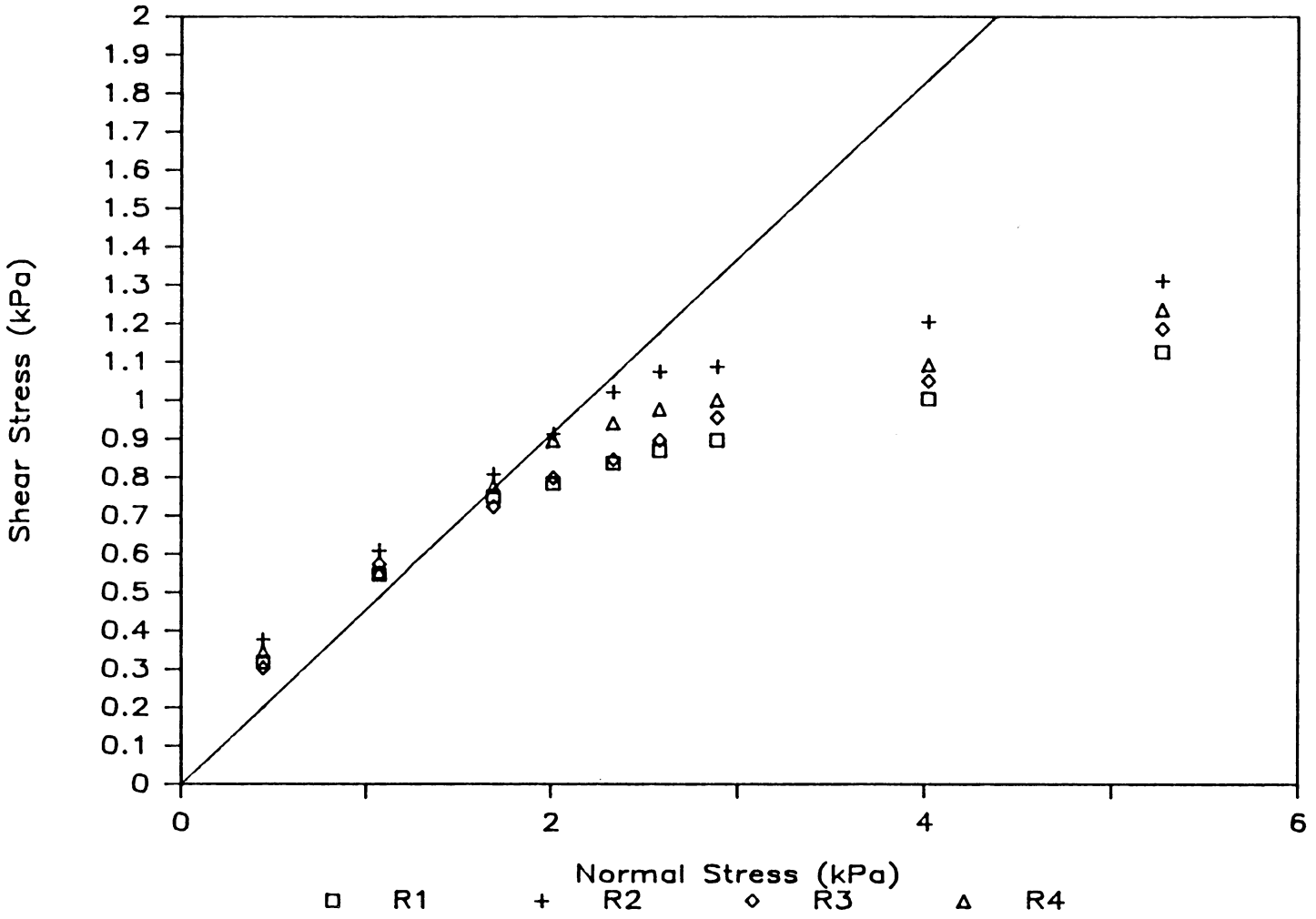

Figure B.1 Internal Friction: Peak Shear Stress versus Normal Stress

Appendix C

Wall Friction:
Ultimate Shear Stress versus Normal Stress

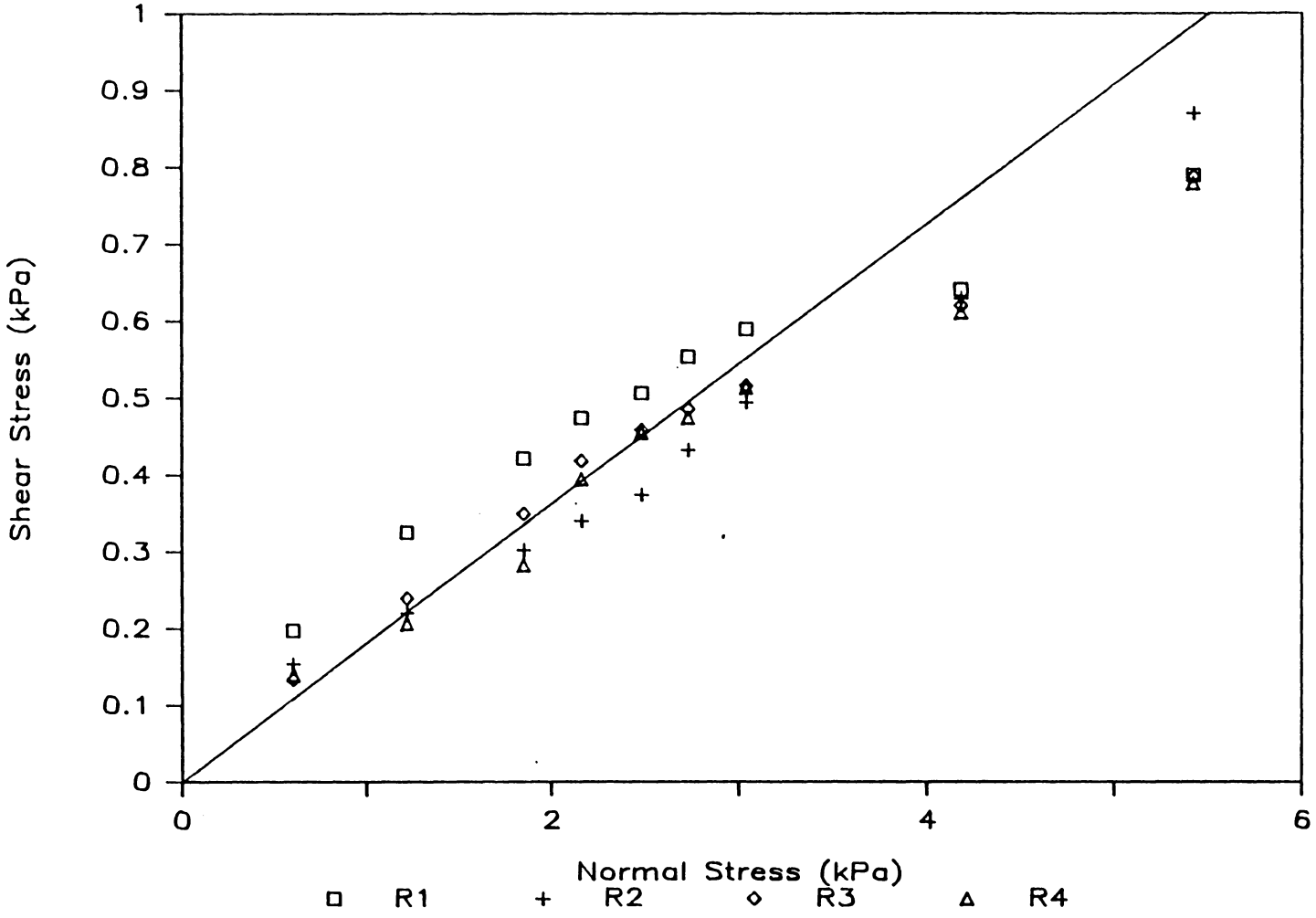

Figure C.1 Wall Friction: Ultimate Shear Stress versus Normal Stress

Appendix D

Pressure Profiles for all the Experimental Runs

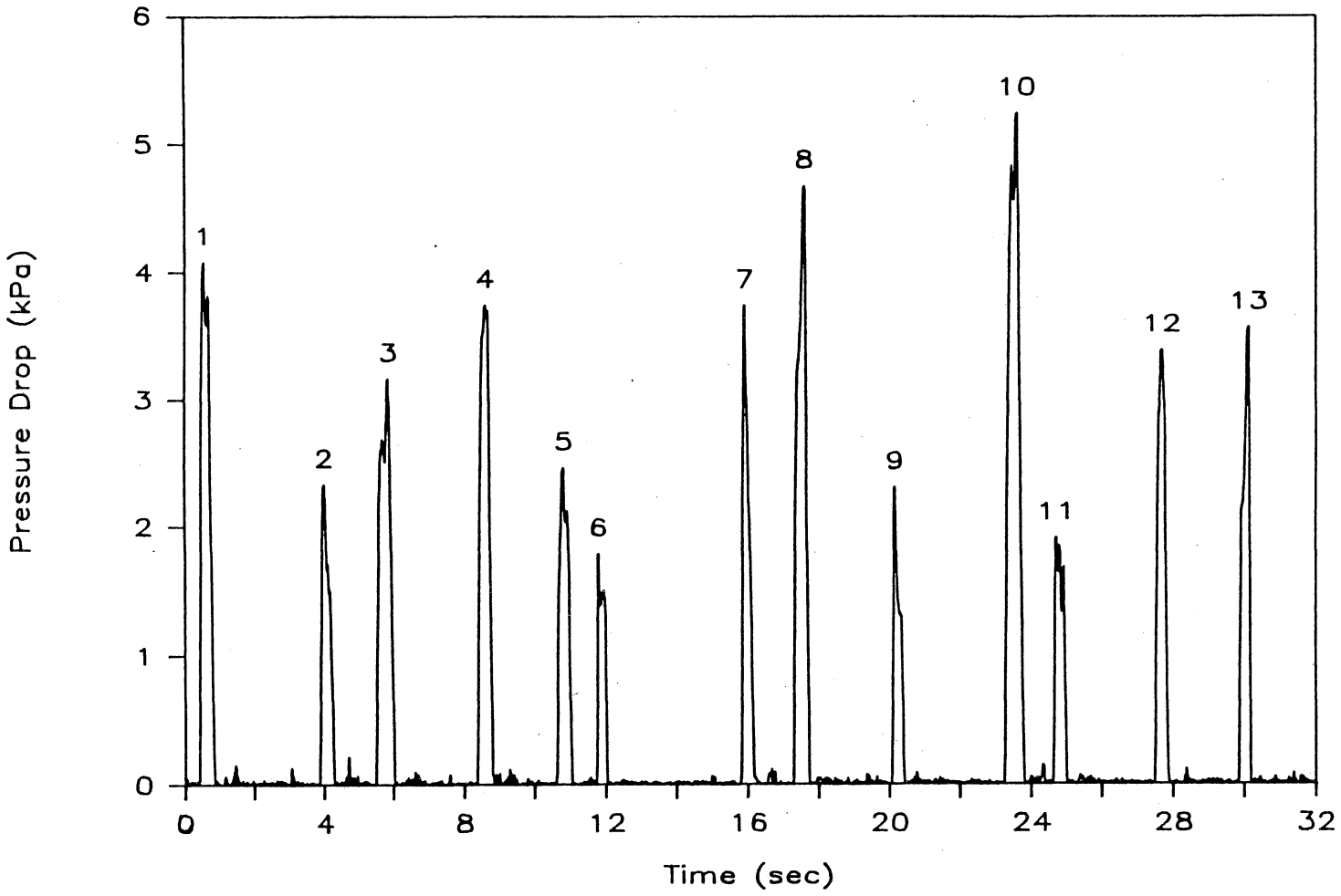

Figure D.1 Overall Pressure Profile: Run 1

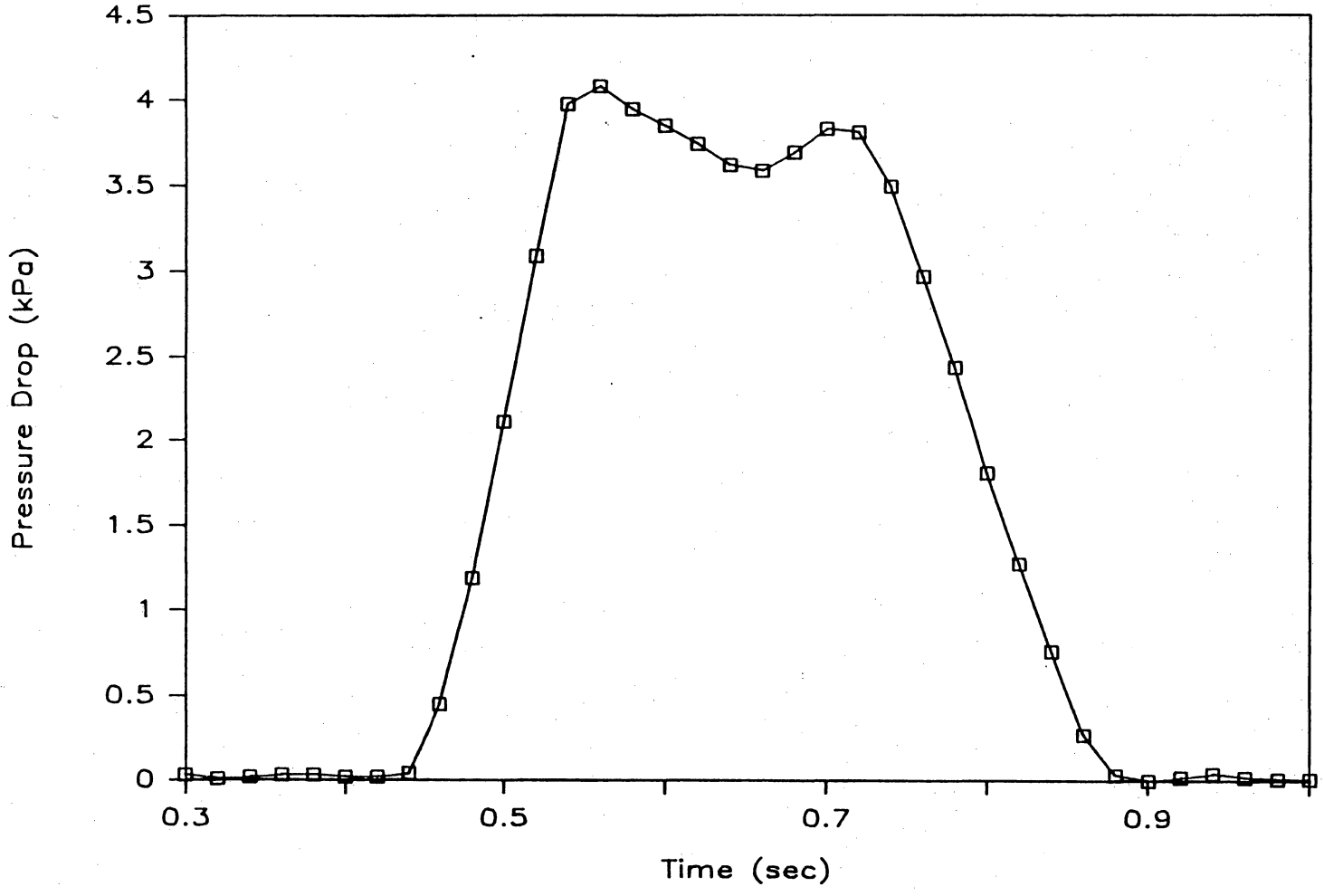

Figure D.2 Pressure Profile: Run 1, Plug #1

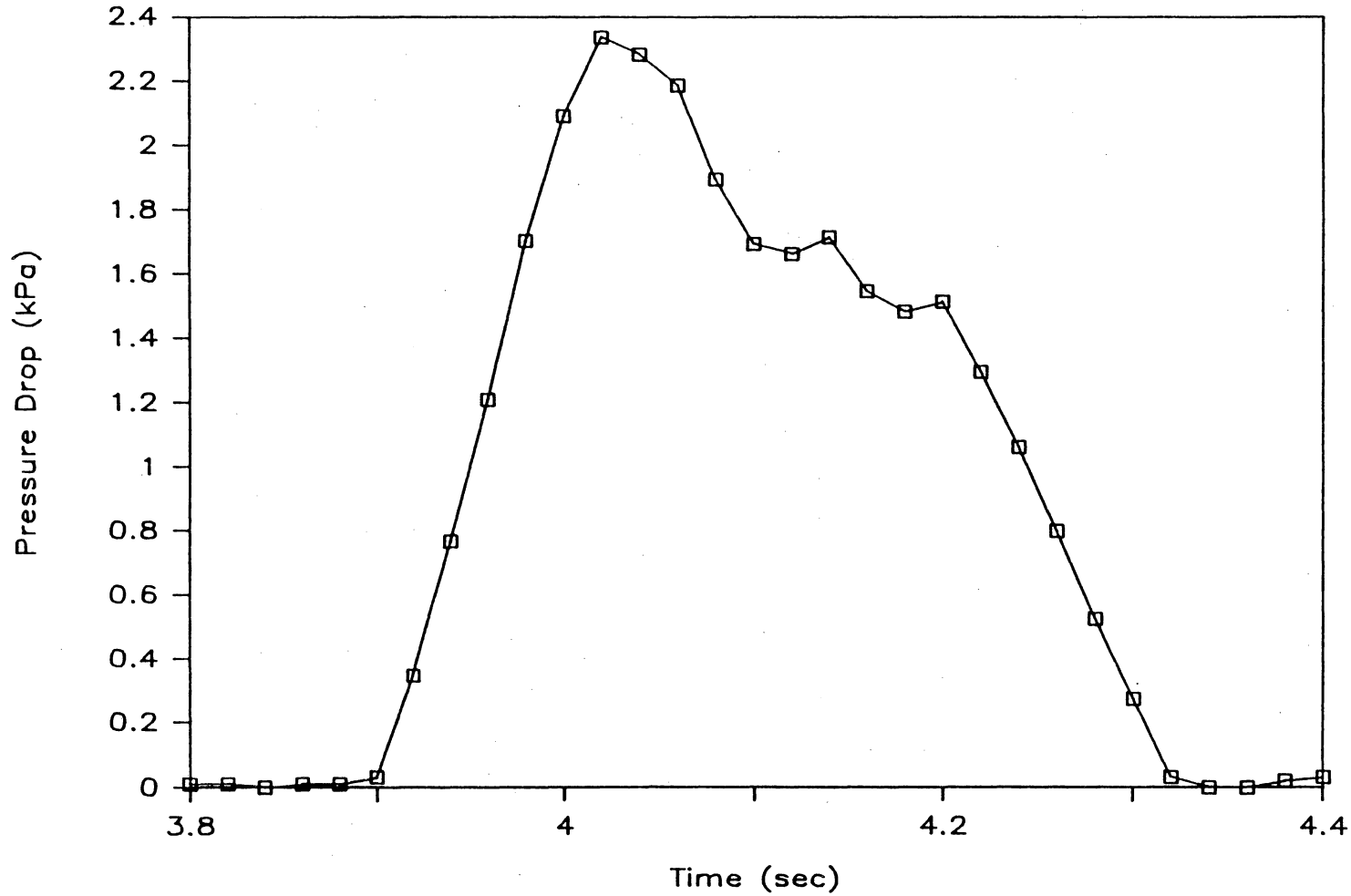

Figure D.3 Pressure Profile: Run 1, Plug #2

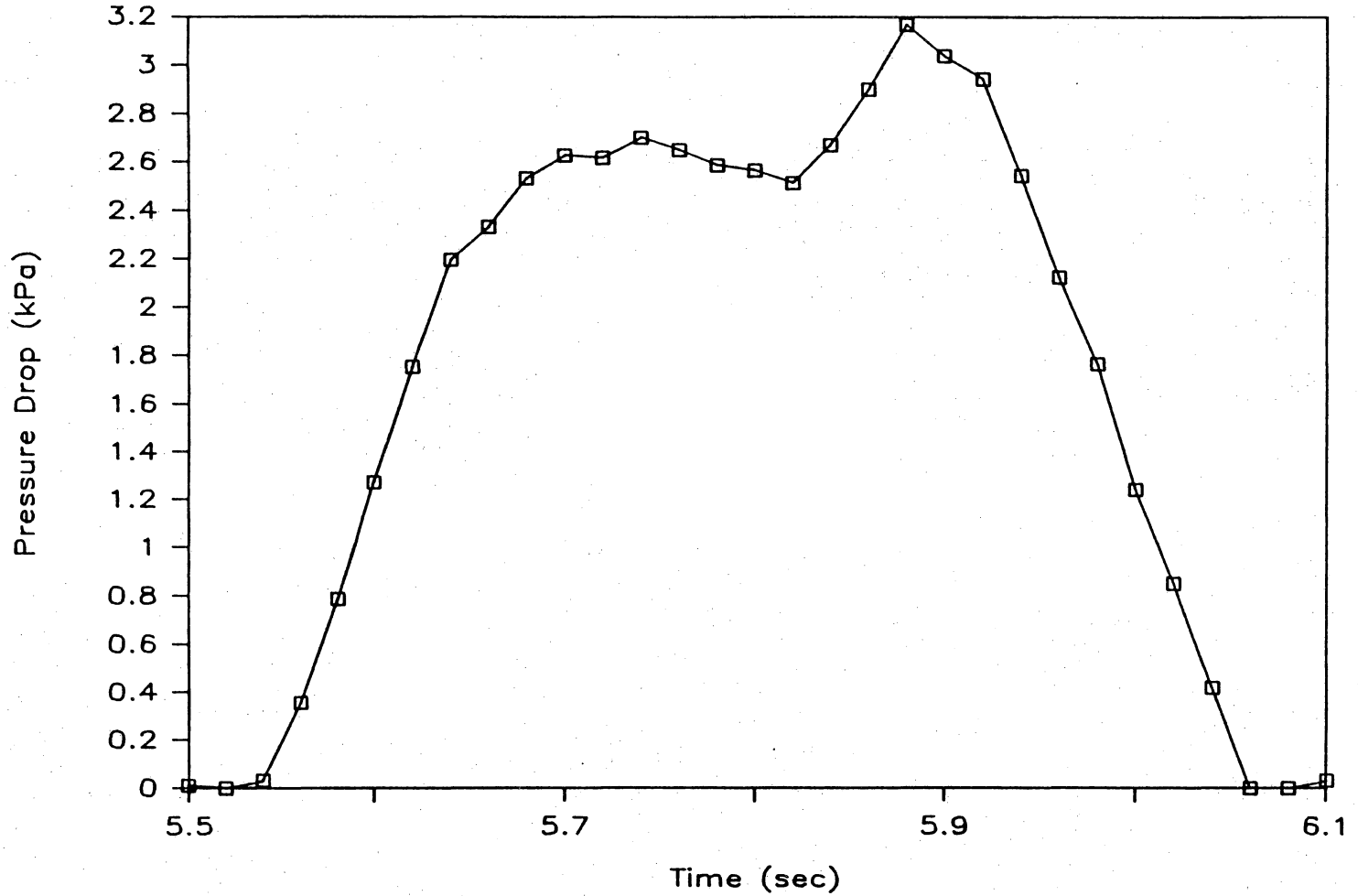

Figure D.4 Pressure Profile: Run 1, Plug #3

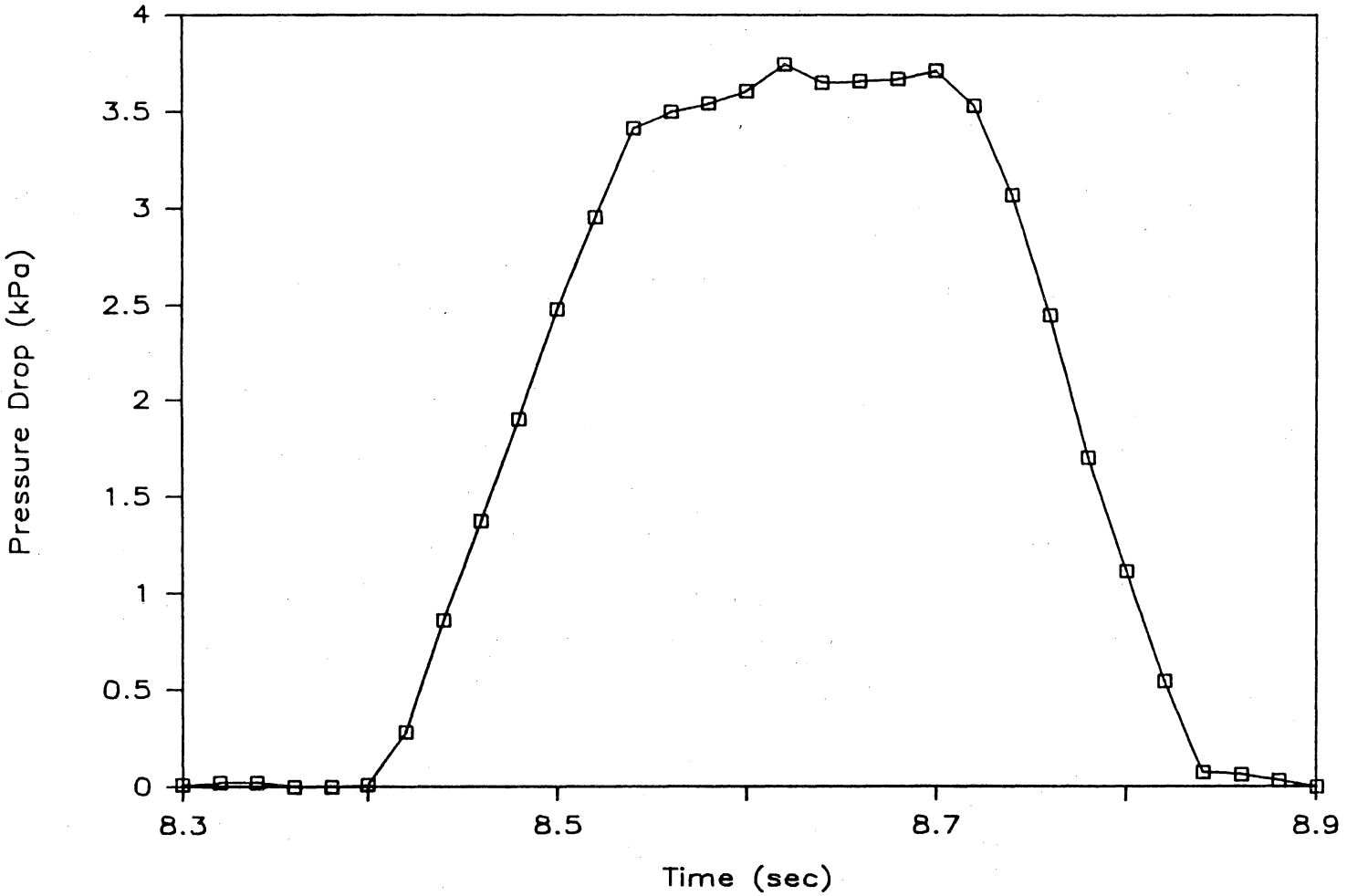

Figure D.5 Pressure Profile: Run 1, Plug #4

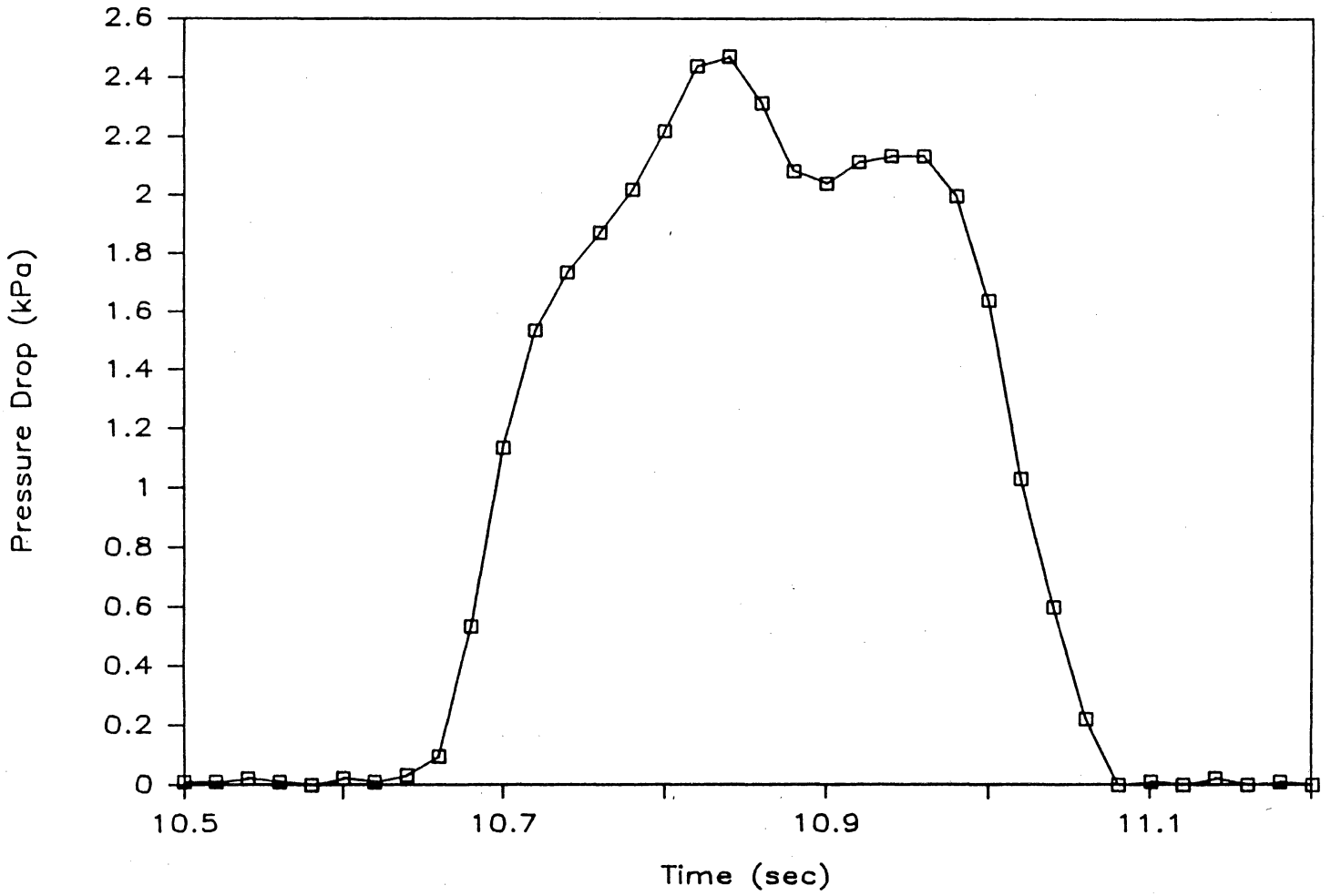

Figure D.6 Pressure Profile: Run 1, Plug #5

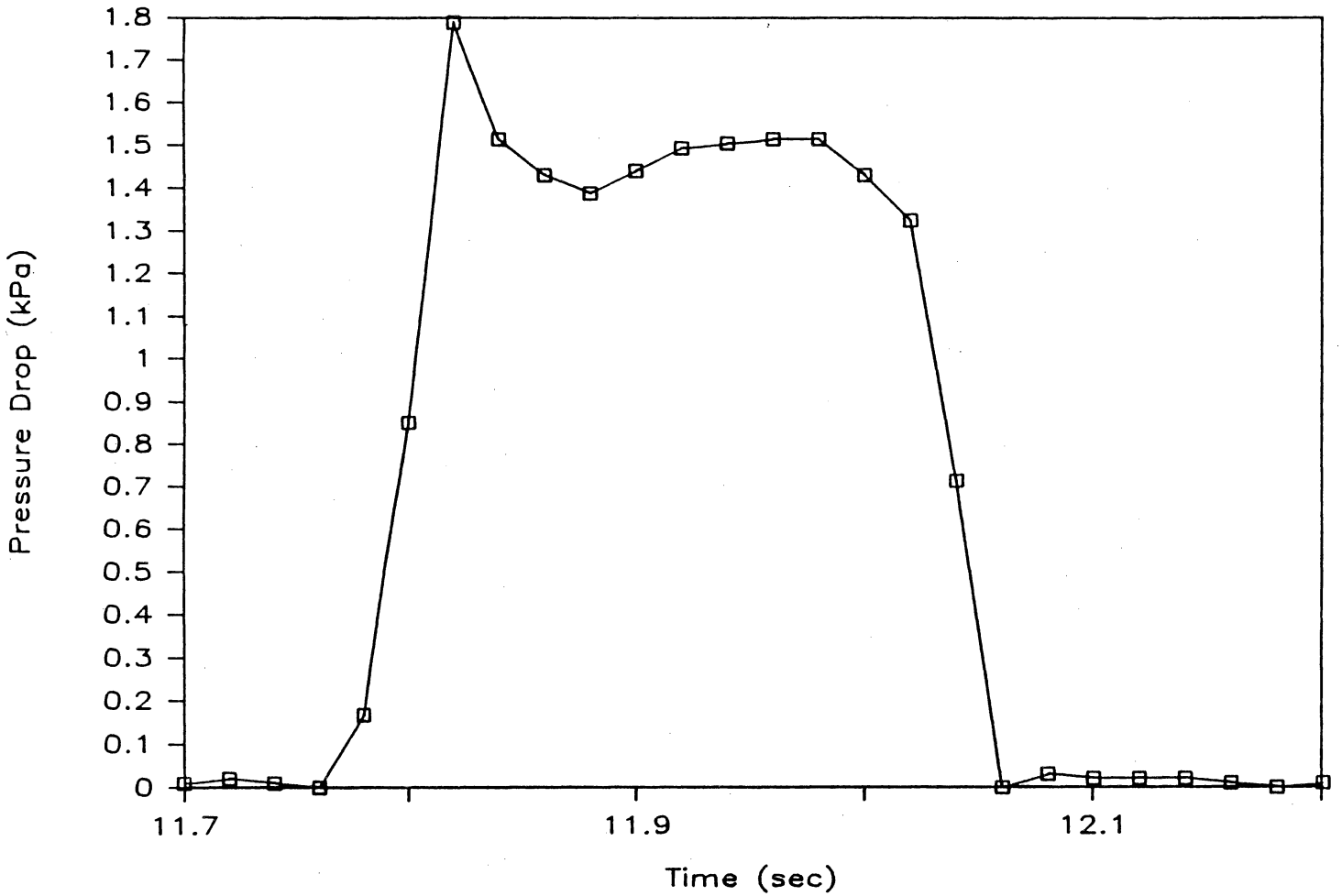

Figure D.7 Pressure Profile: Run 1, Plug #6

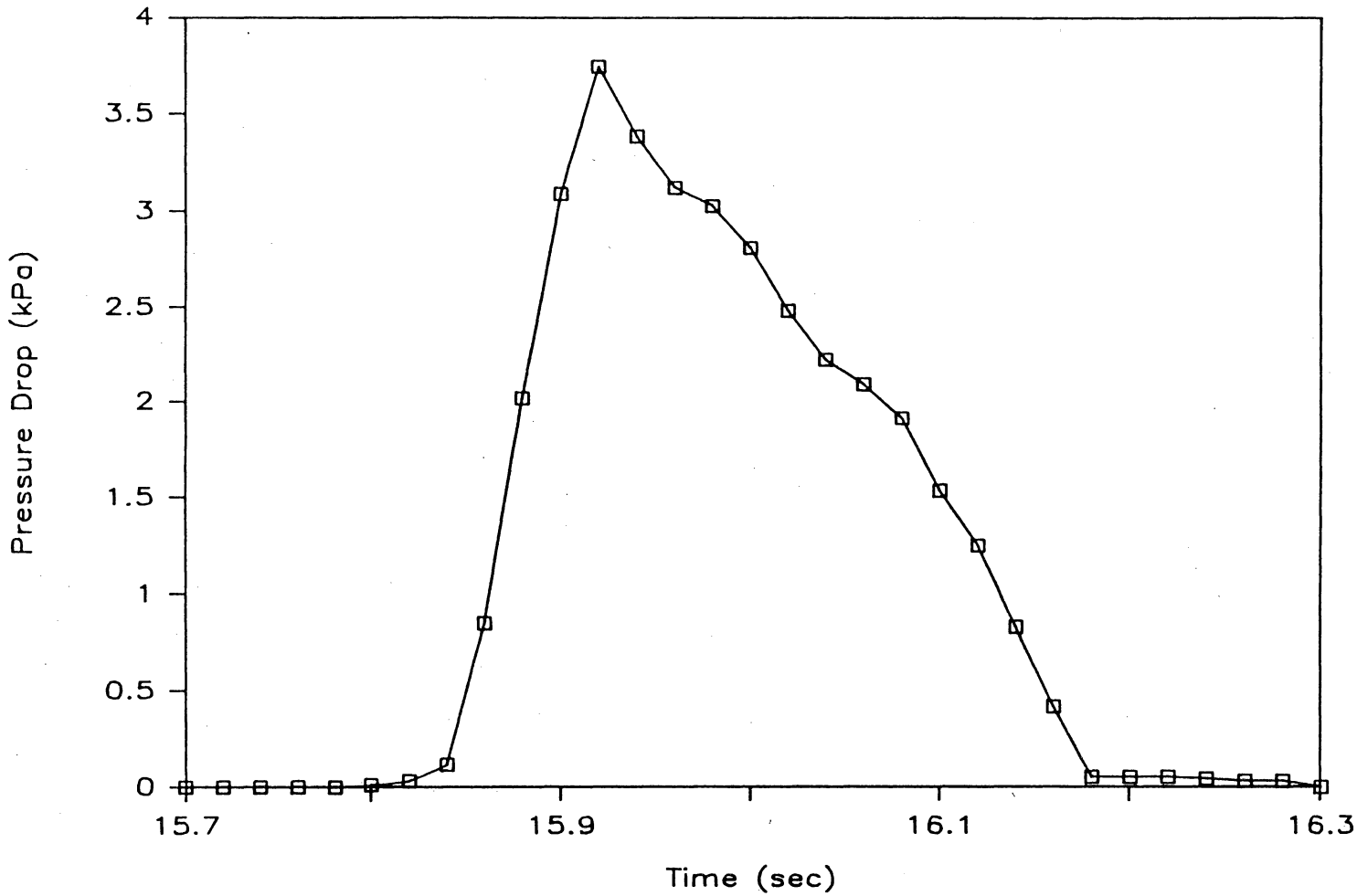

Figure D.8 Pressure Profile: Run 1, Plug #7

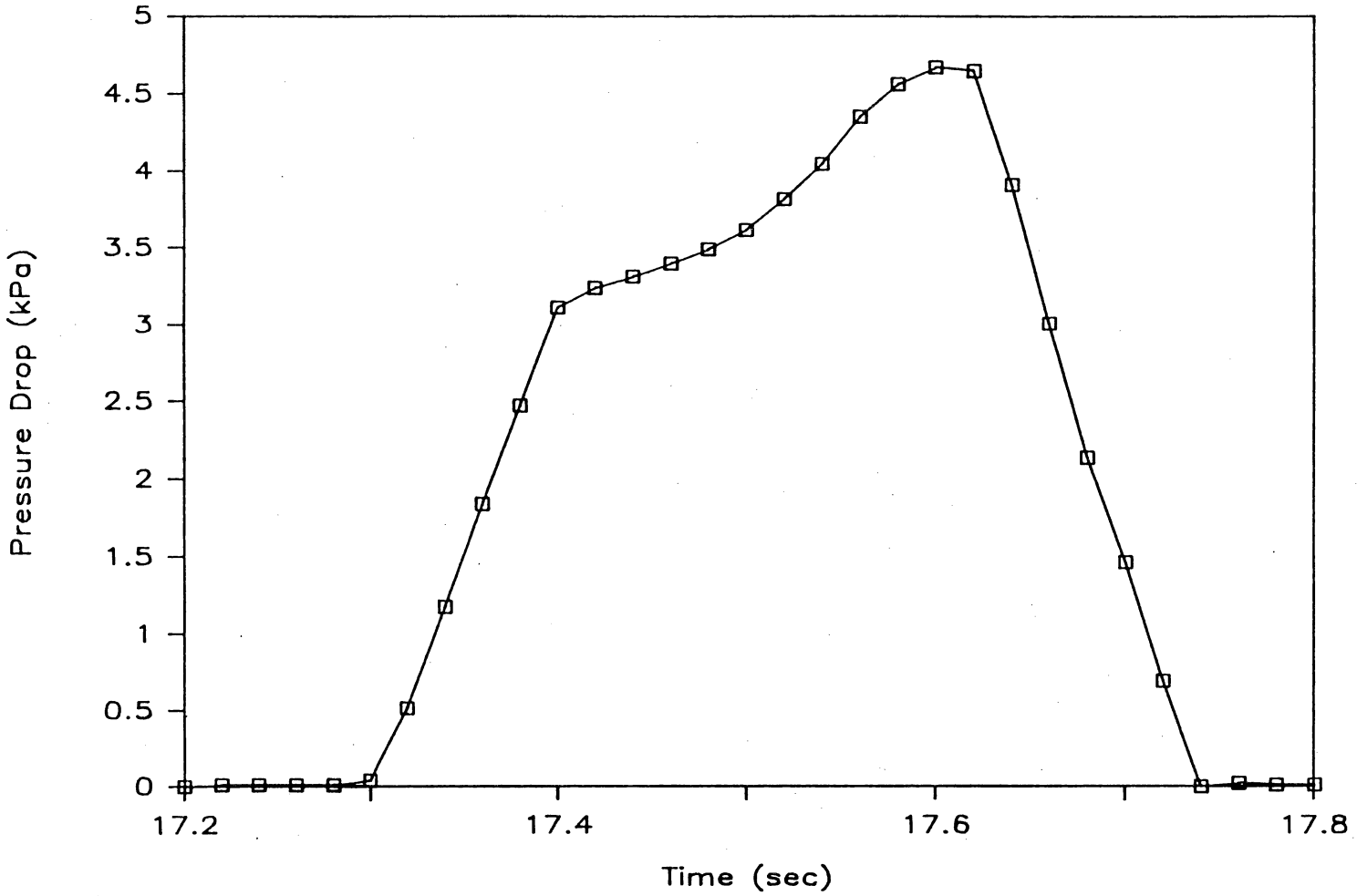

Figure D.9 Pressure Profile: Run 1, Plug #8

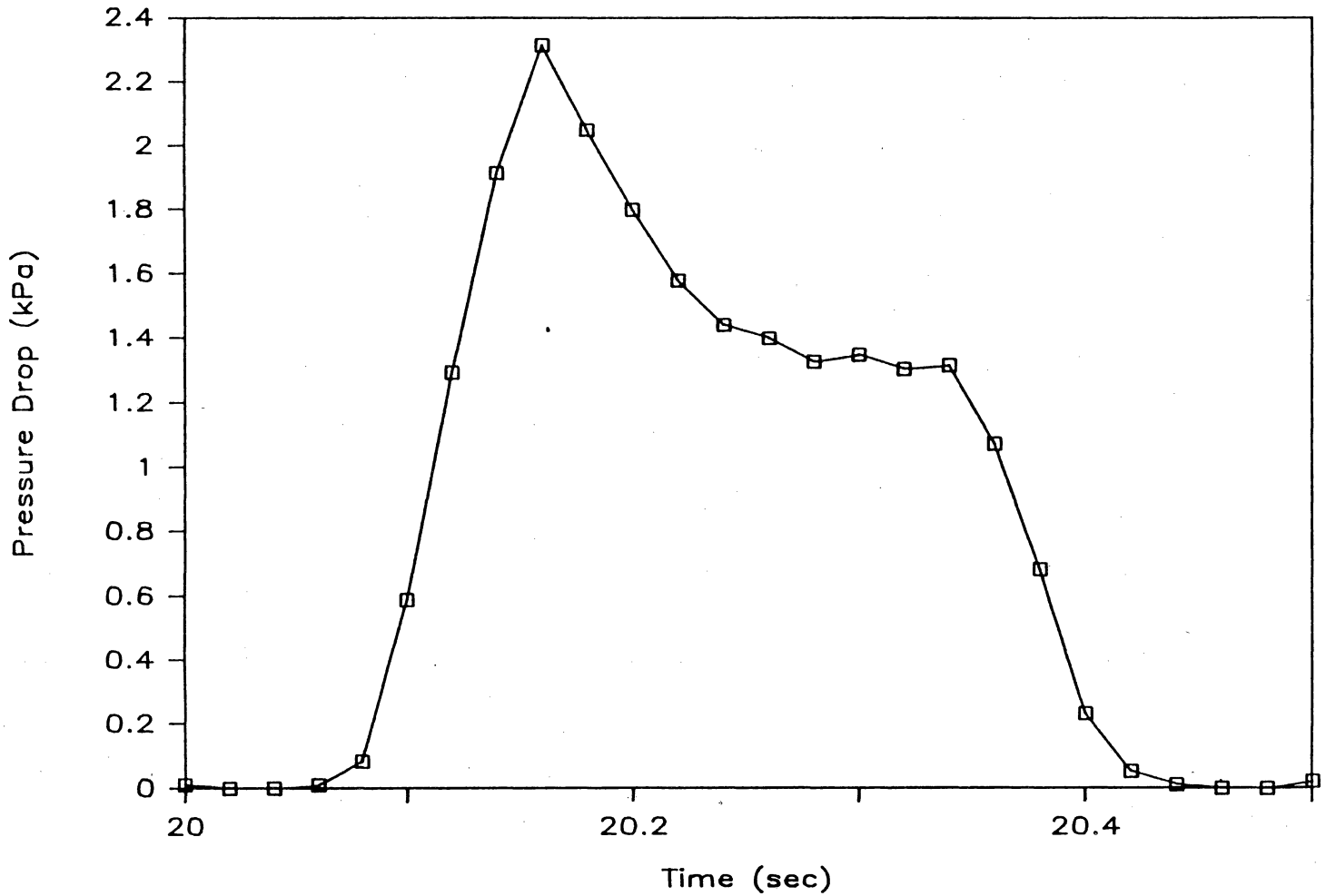

Figure D.10 Pressure Profile: Run 1, Plug #9

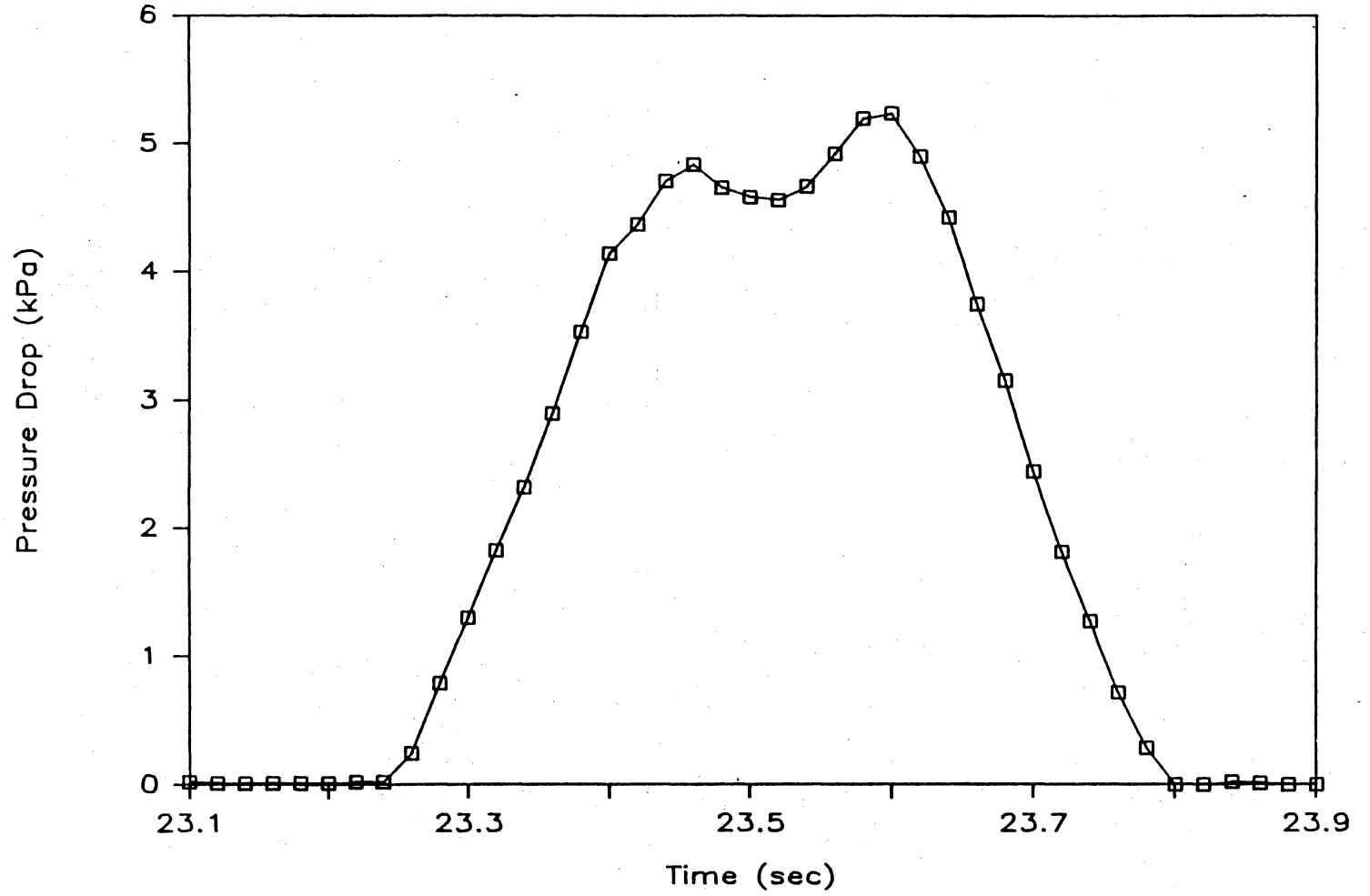

Figure D.11 Pressure Profile: Run 1, Plug #10

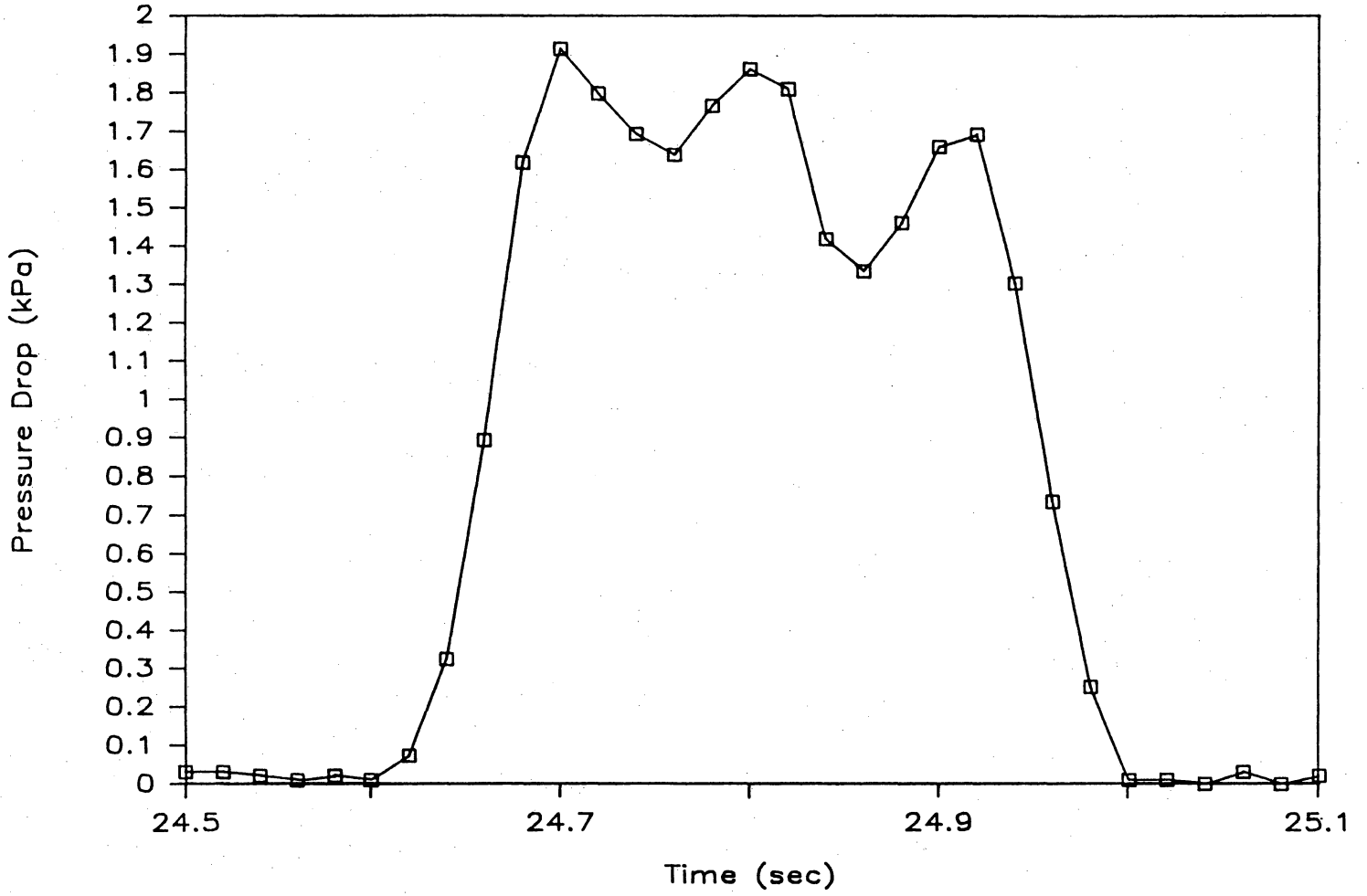

Figure D.12 Pressure Profile: Run 1, Plug #11

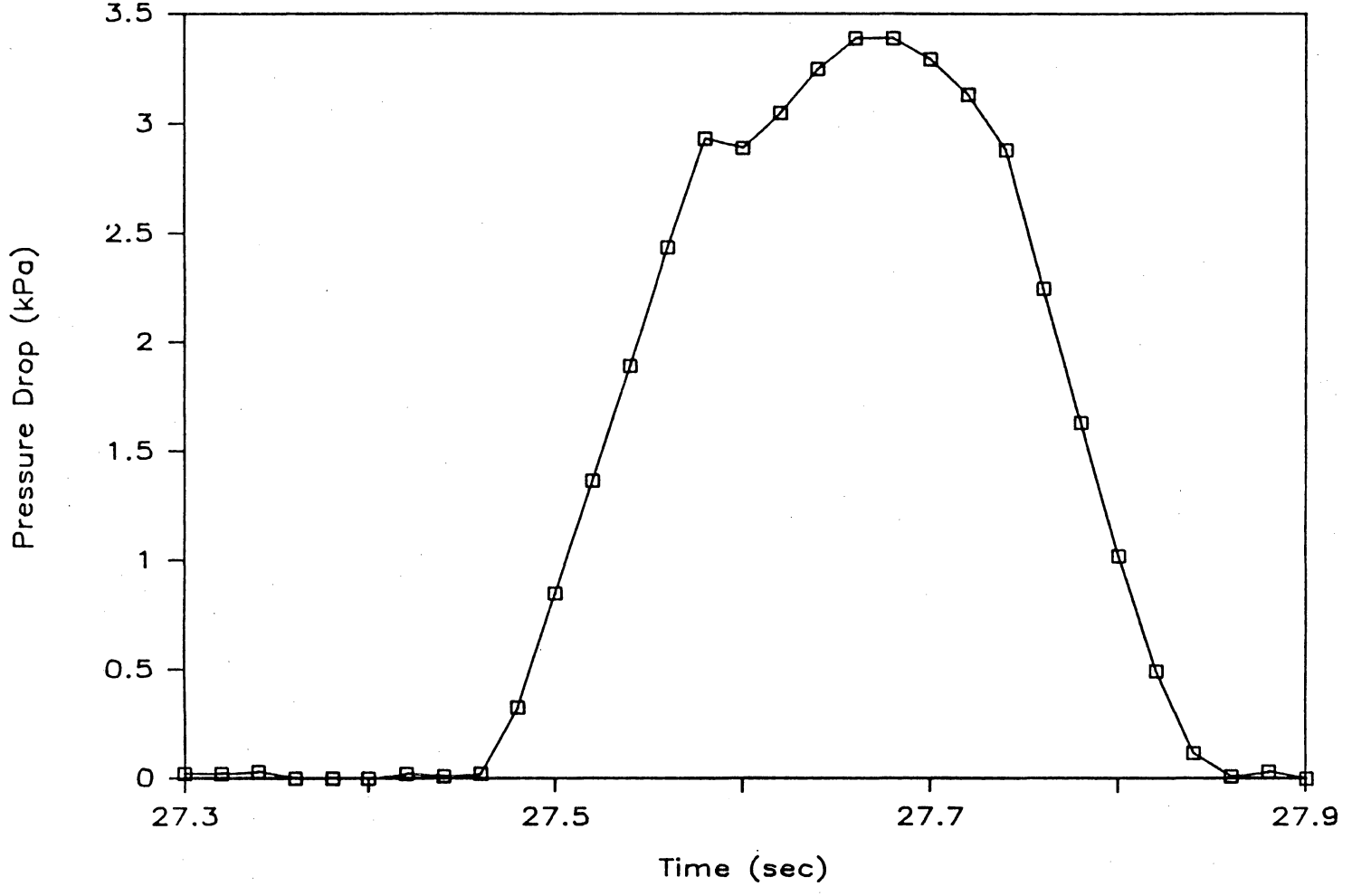

Figure D.13 Pressure Profile: Run 1, Plug #12

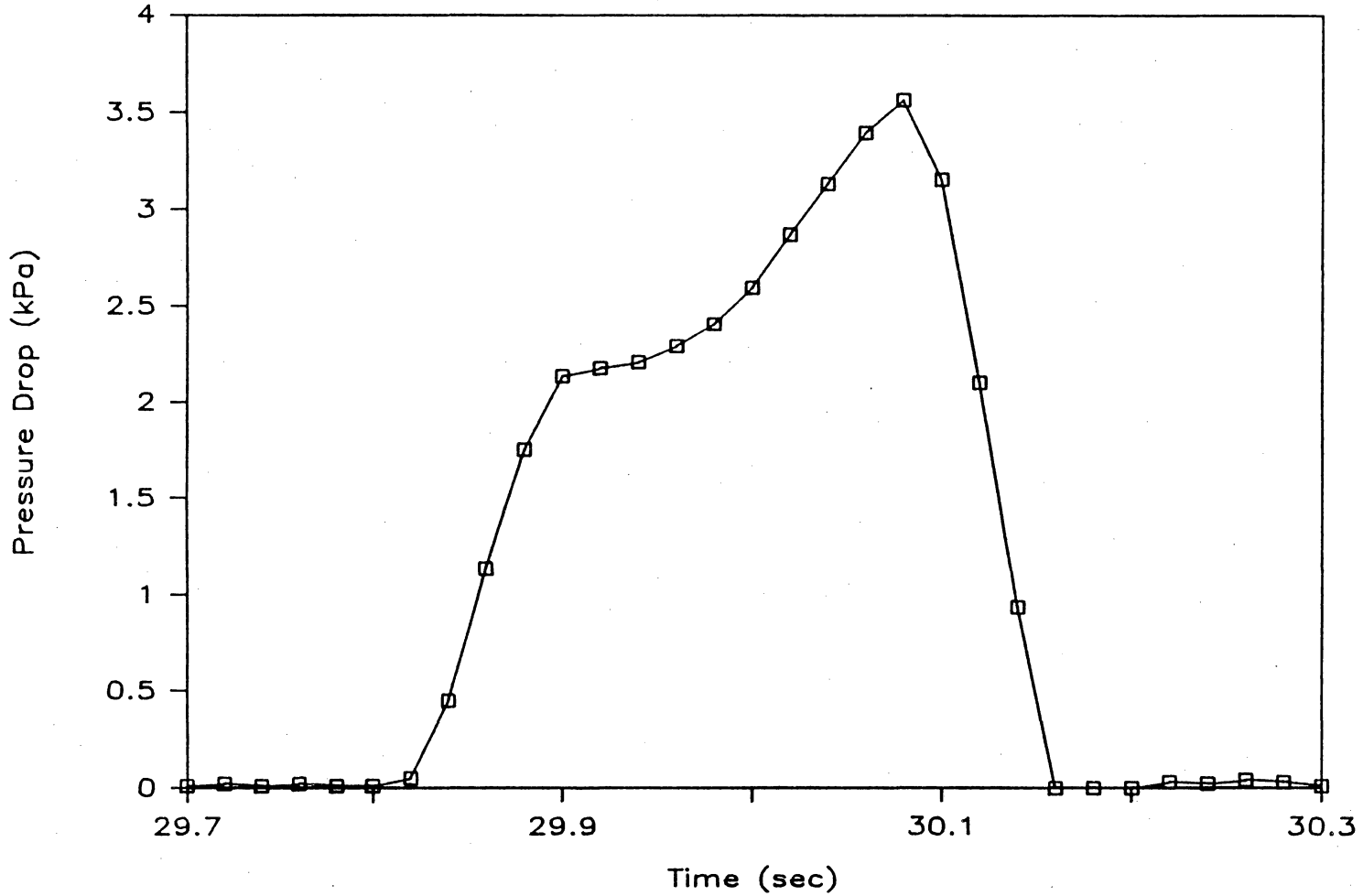

Figure D.14 Pressure Profile: Run 1, Plug #13

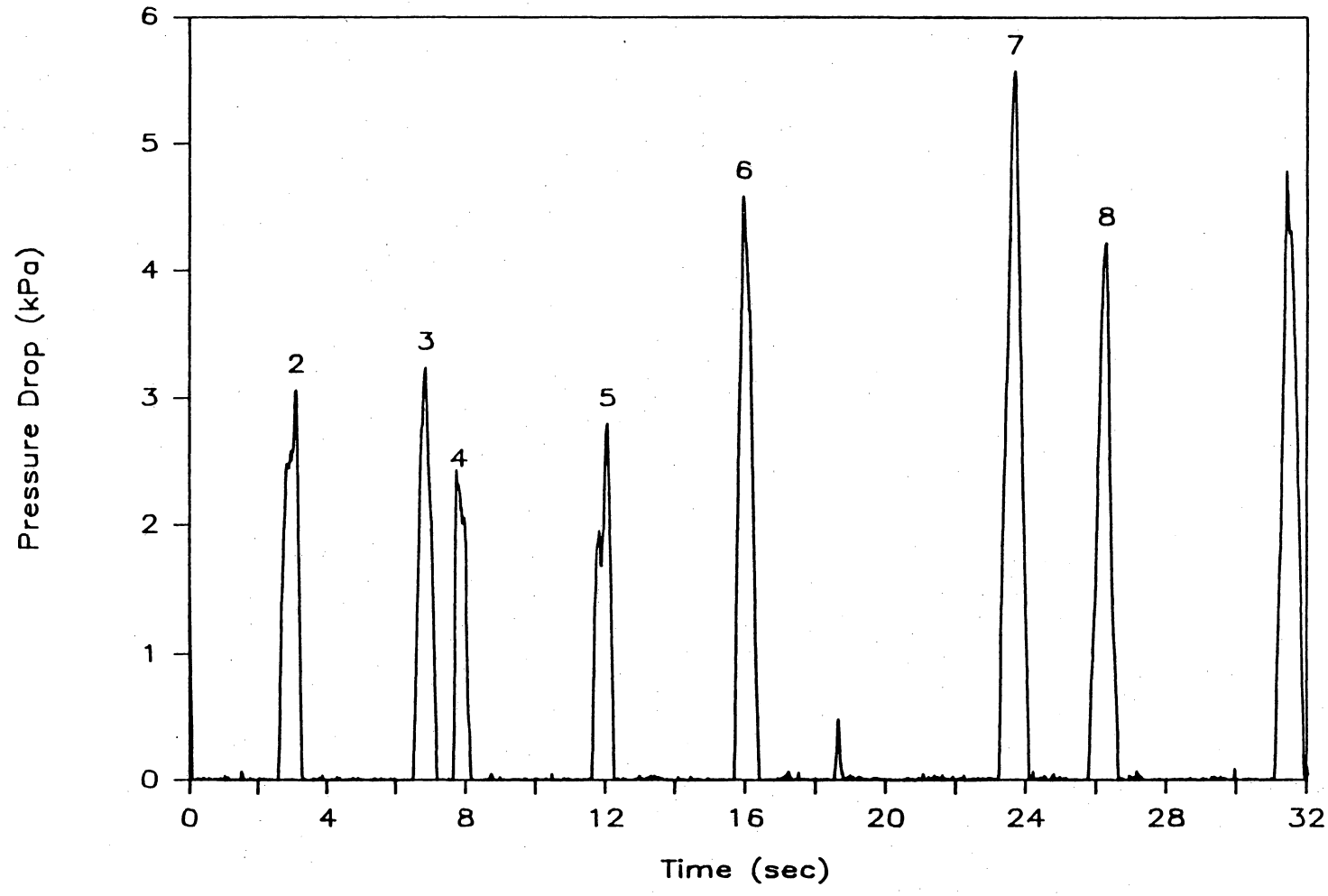

Figure D.15 Overall Pressure Profile: Run 2

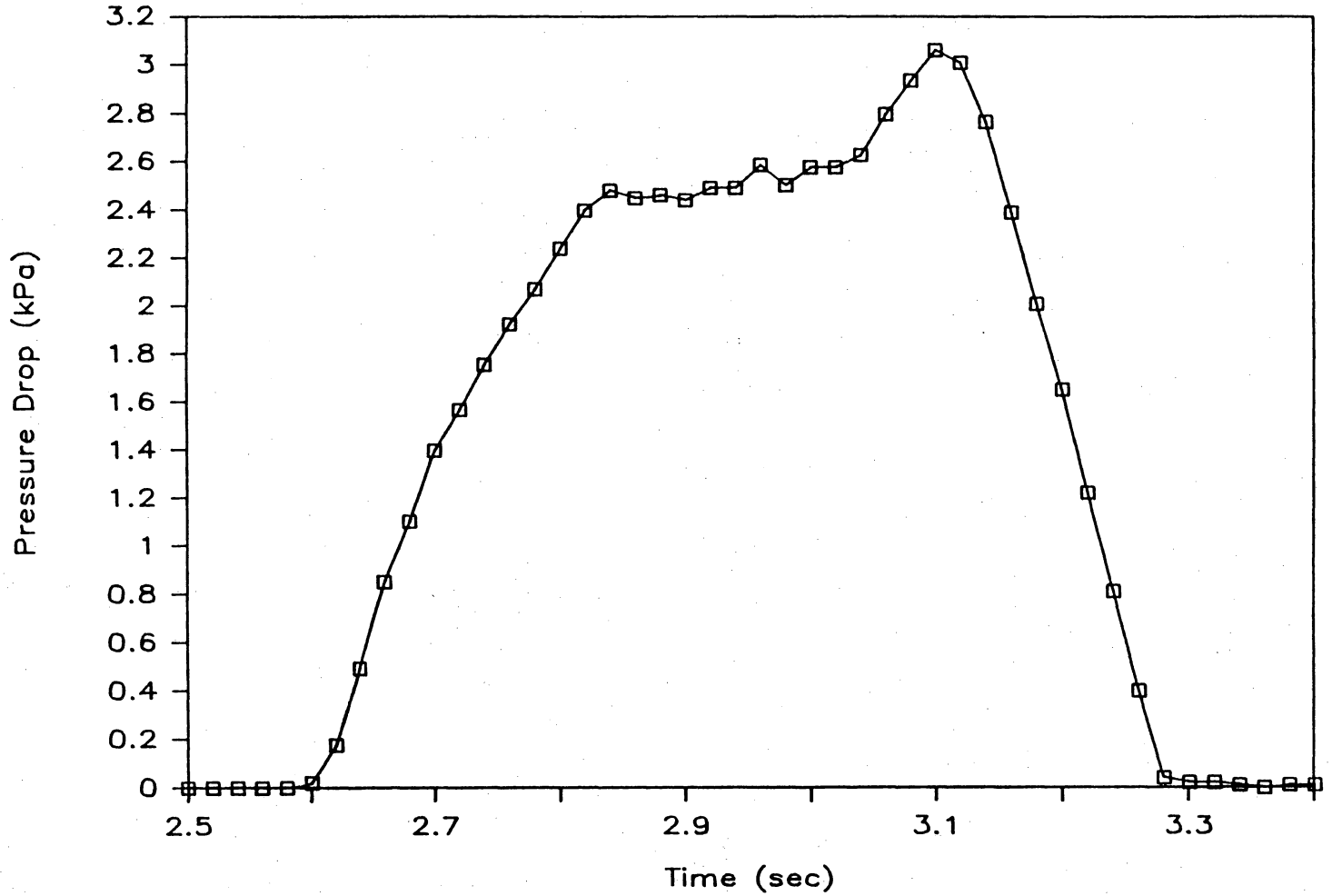

Figure D.16 Pressure Profile: Run 2, Plug #2

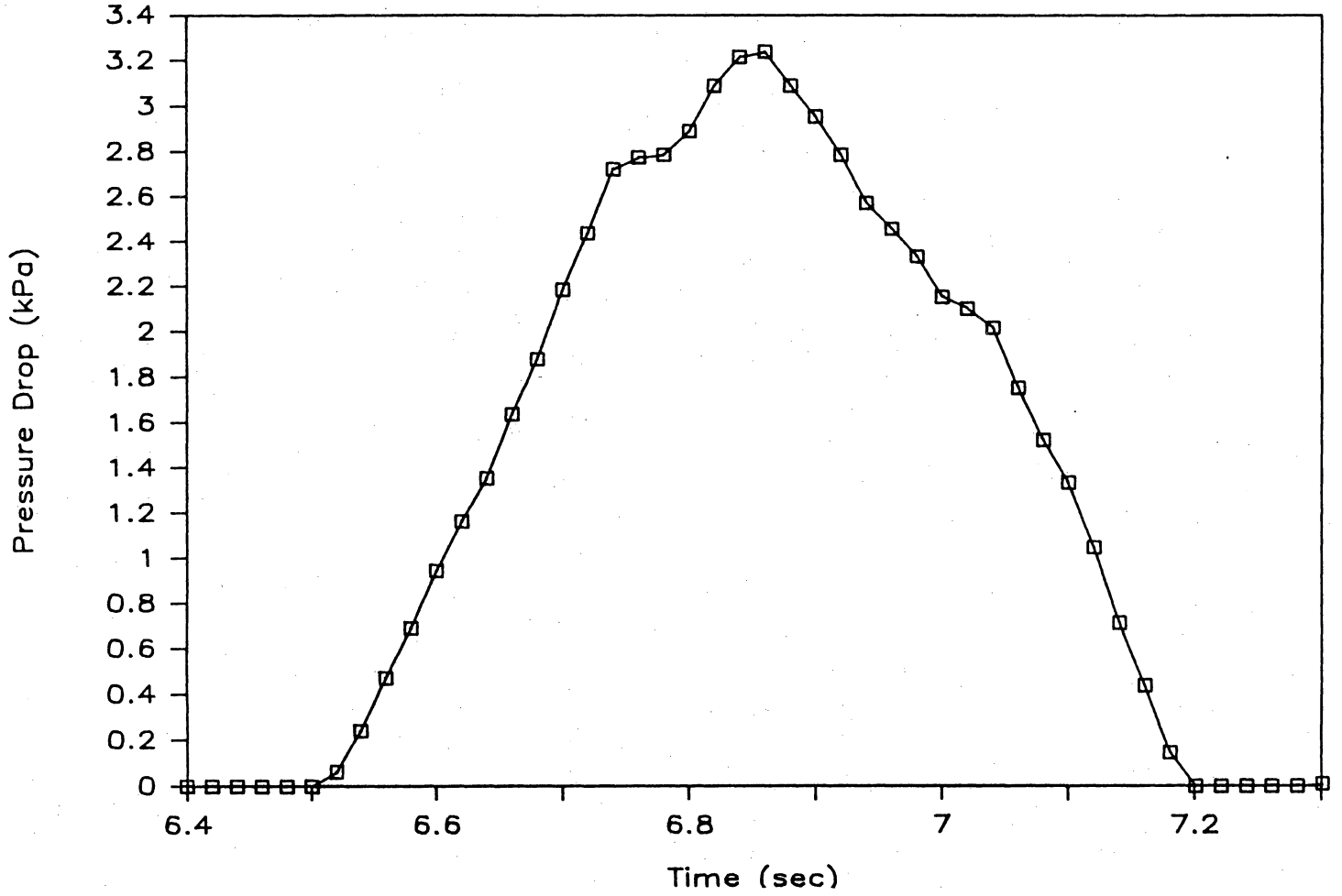

Figure D.17 Pressure Profile: Run 2, Plug #3

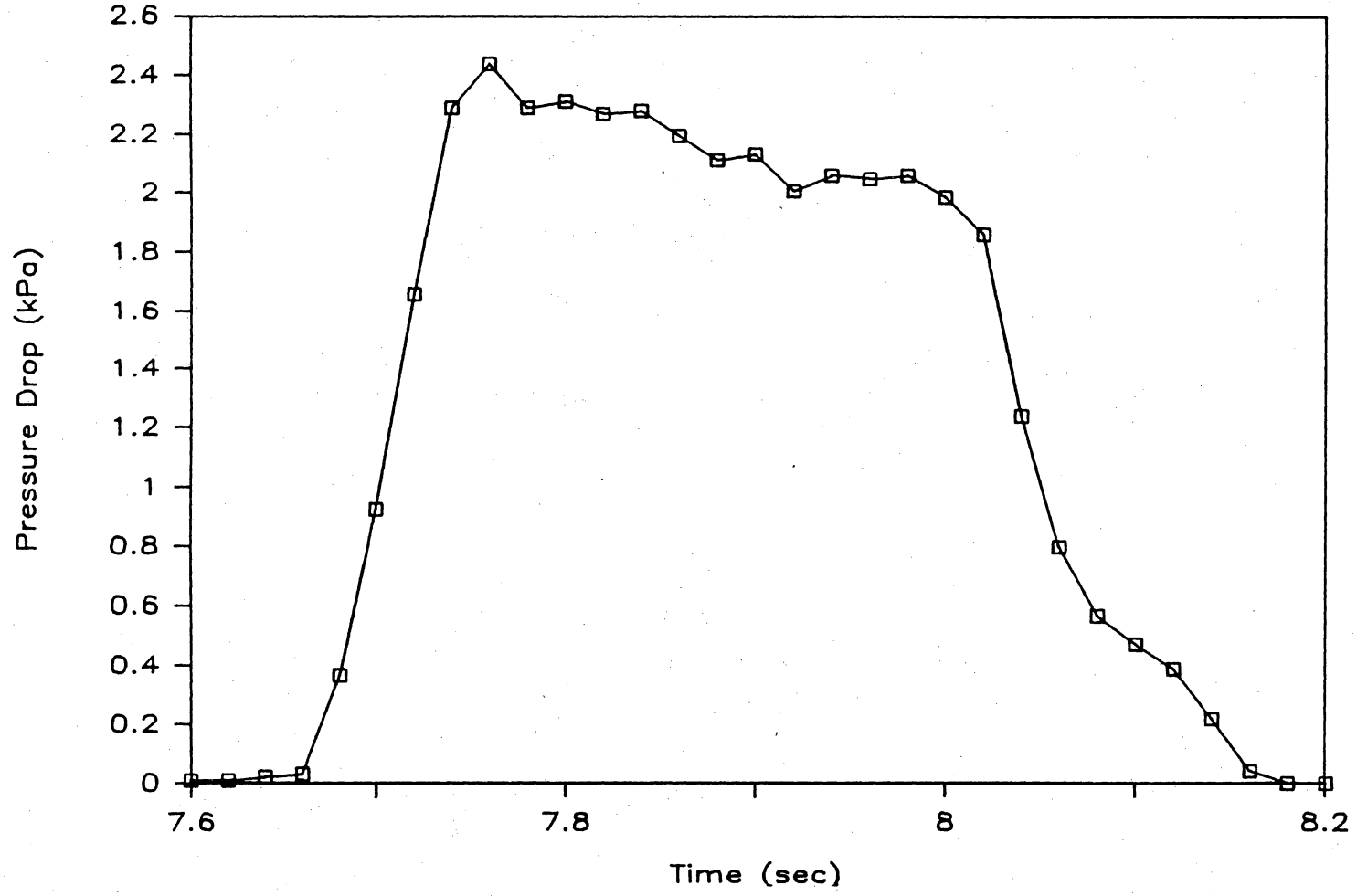

Figure D.18 Pressure Profile: Run 2, Plug #4

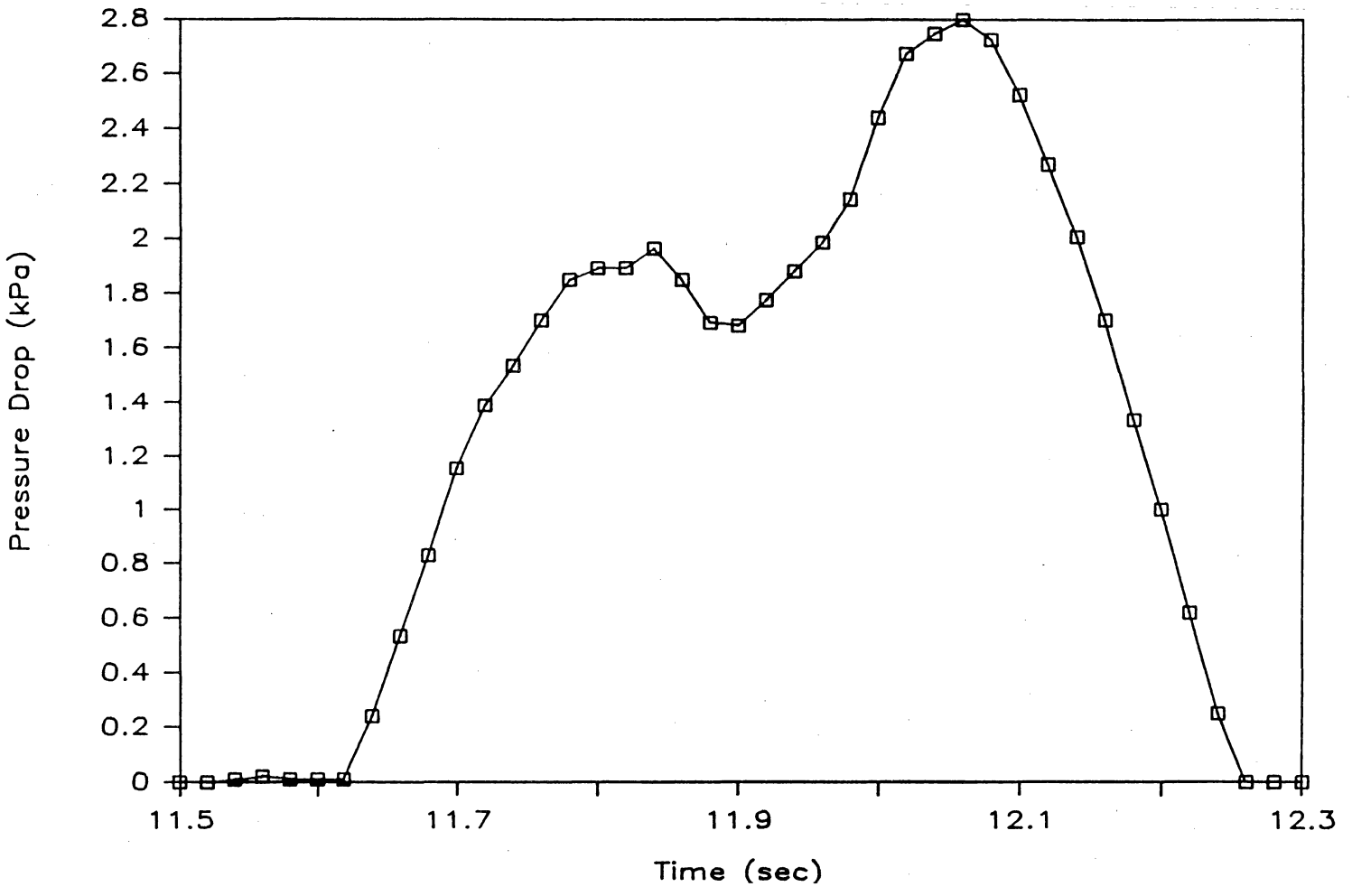

Figure D.19 Pressure Profile: Run 2, Plug #5

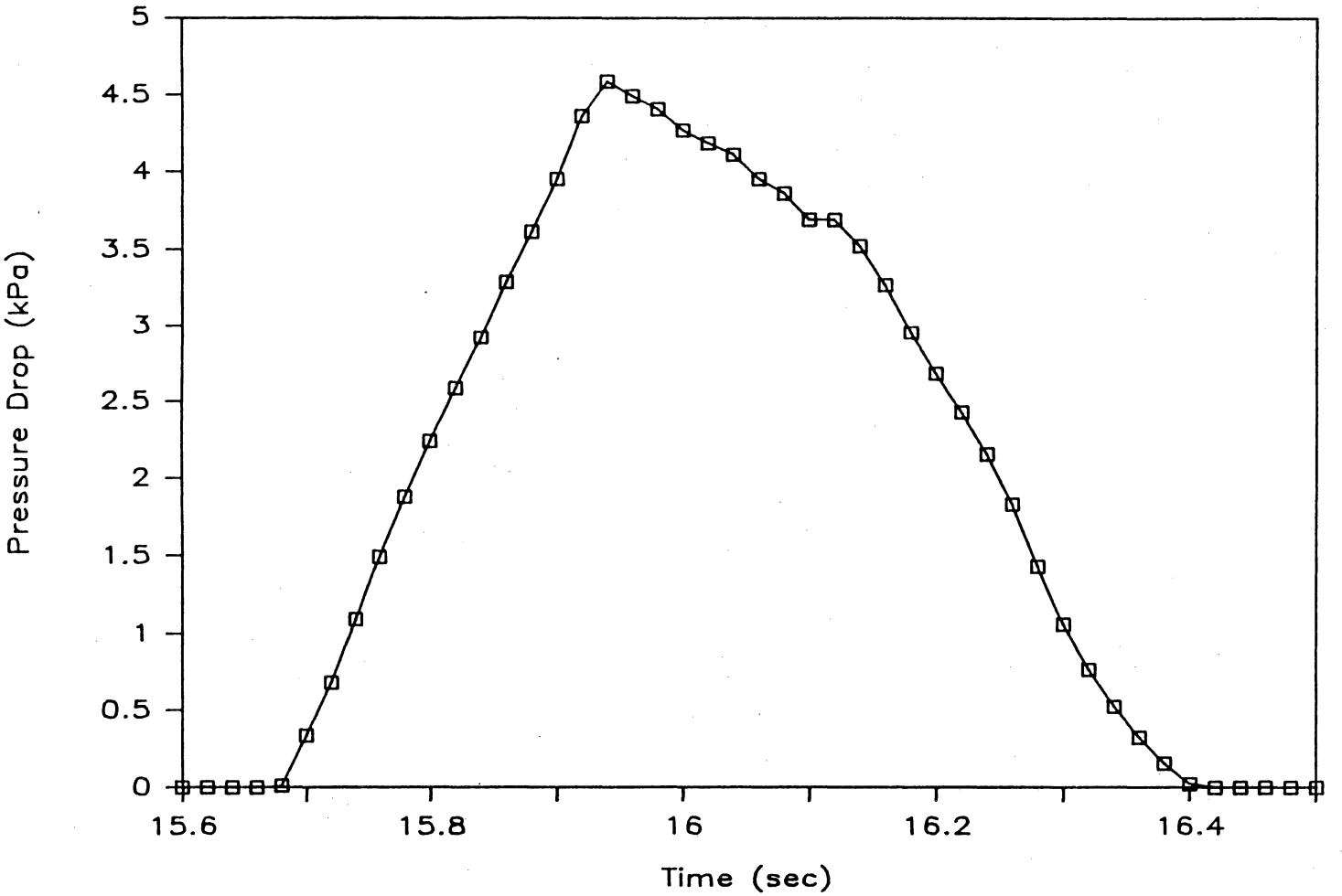

Figure D.20 Pressure Profile: Run 2, Plug #6

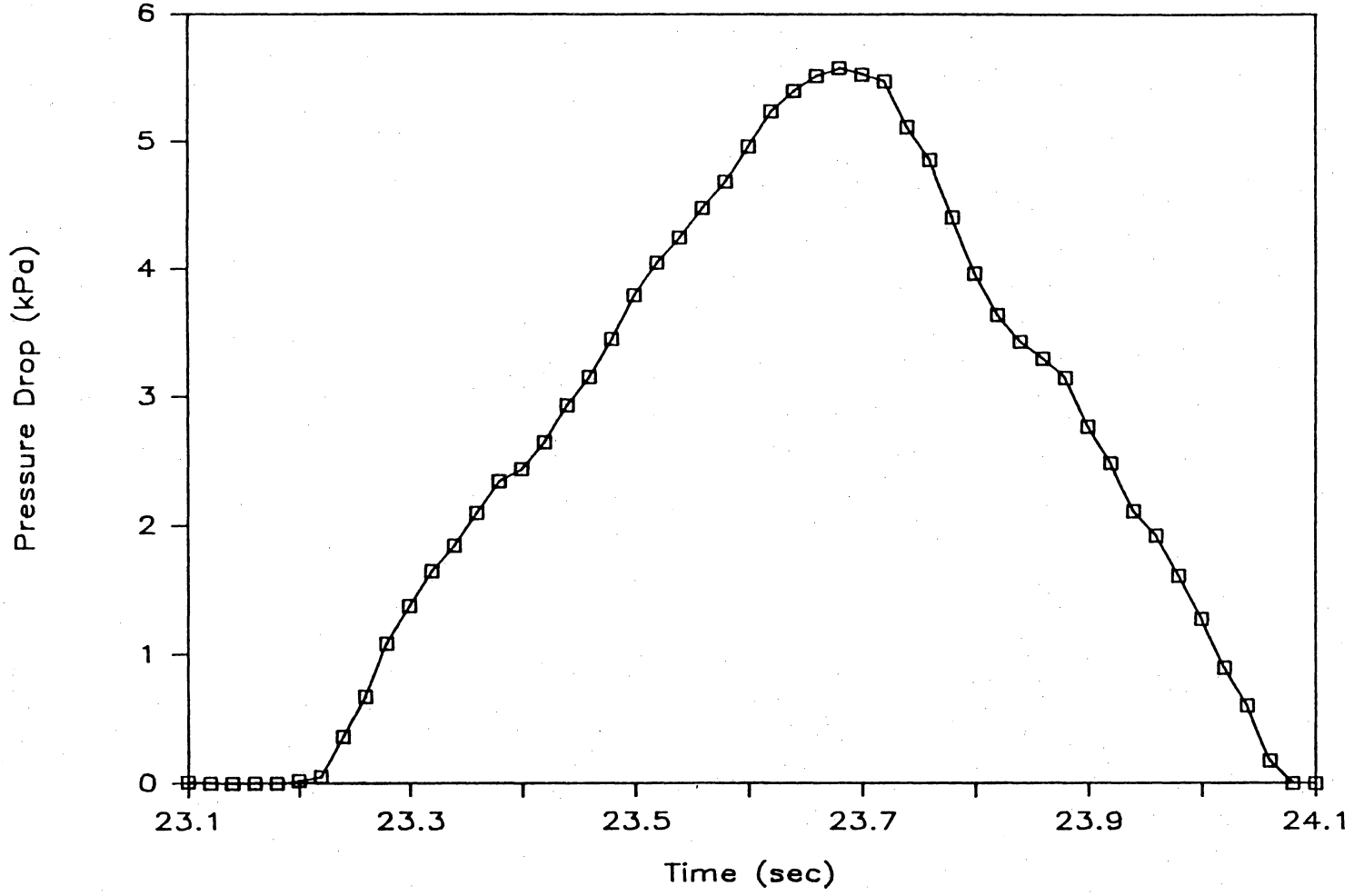

Figure D.21 Pressure Profile: Run 2, Plug #7

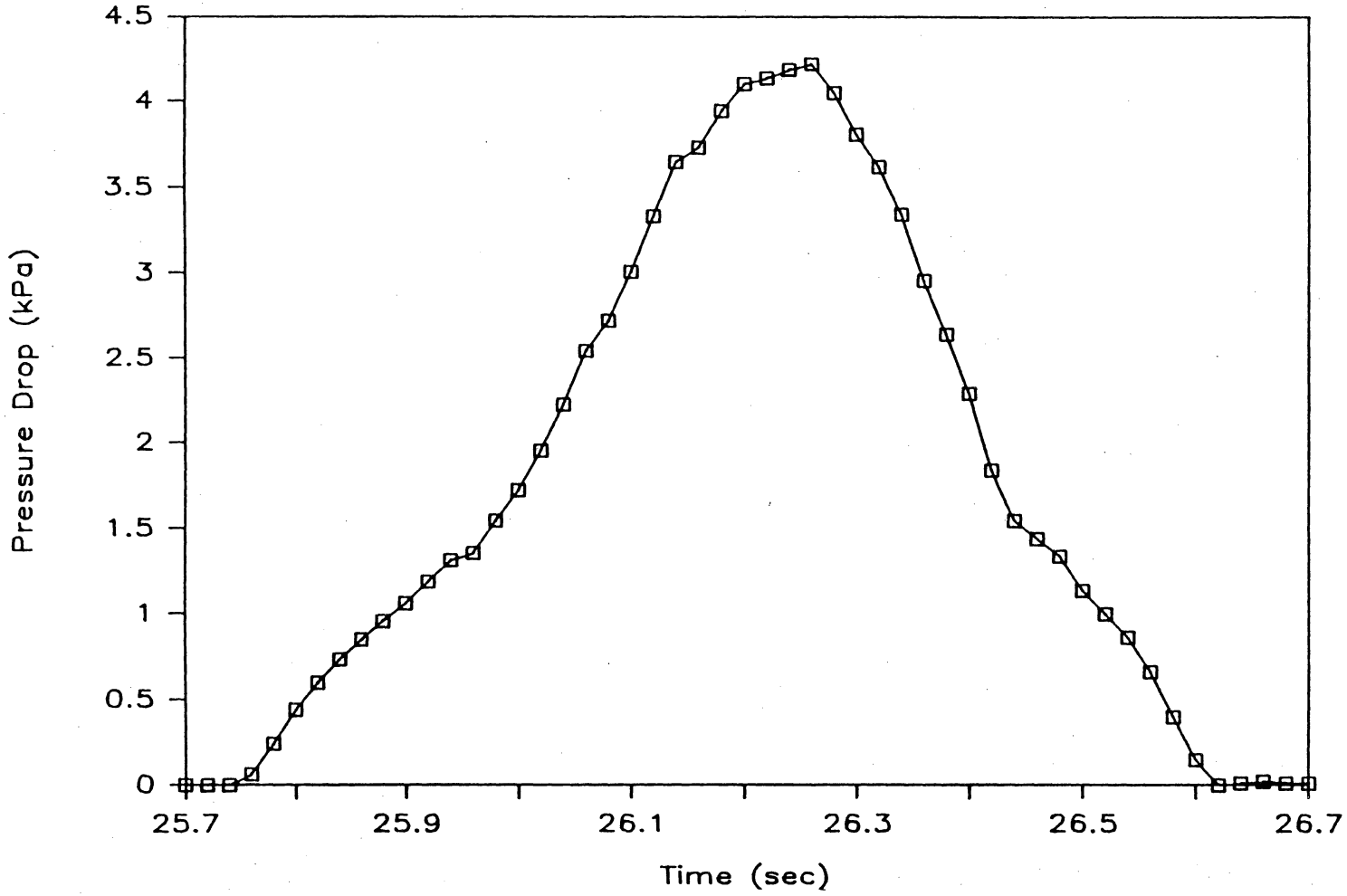

Figure D.22 Pressure Profile: Run 2, Plug #8

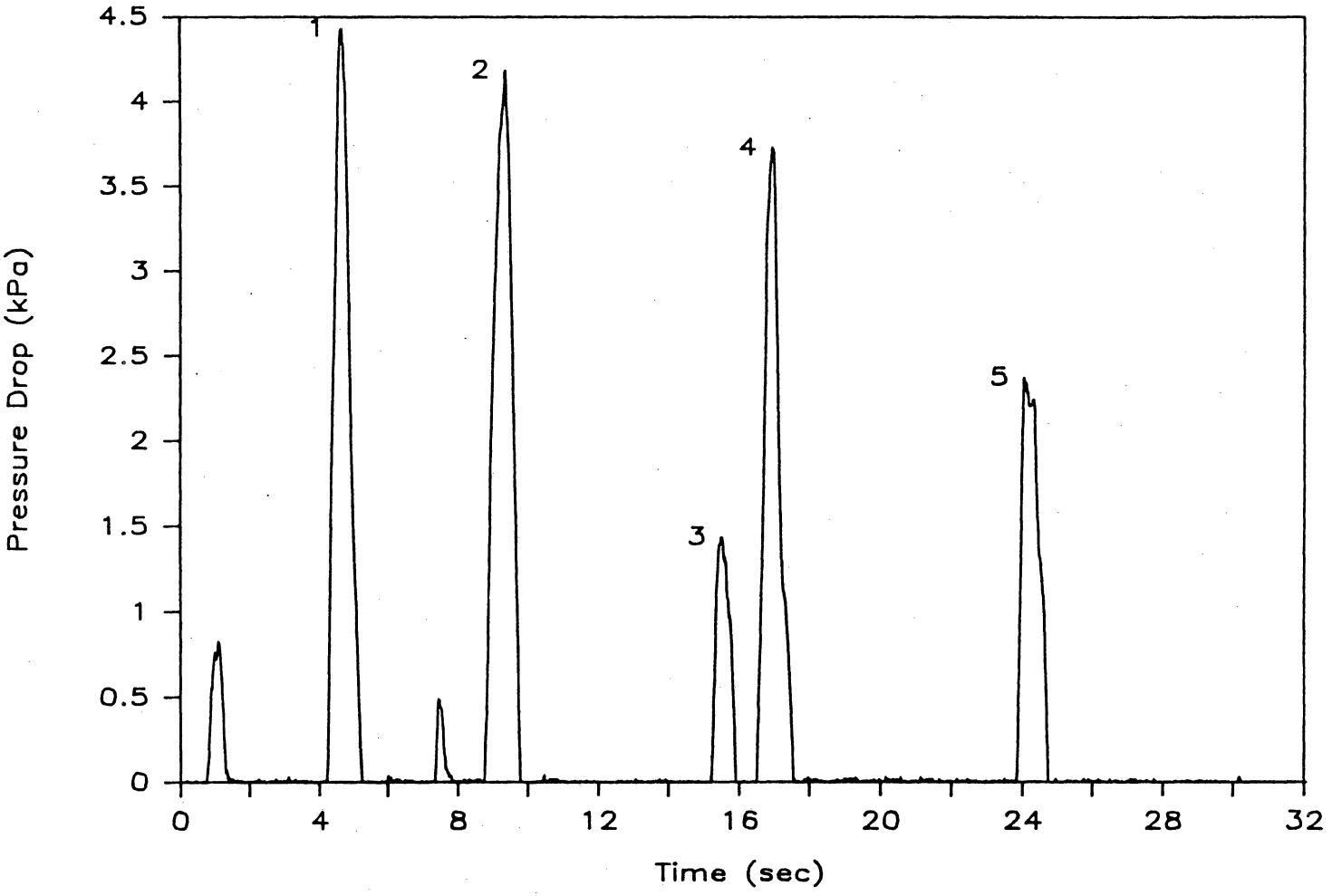

Figure D.23 Overall Pressure Profile: Run 3

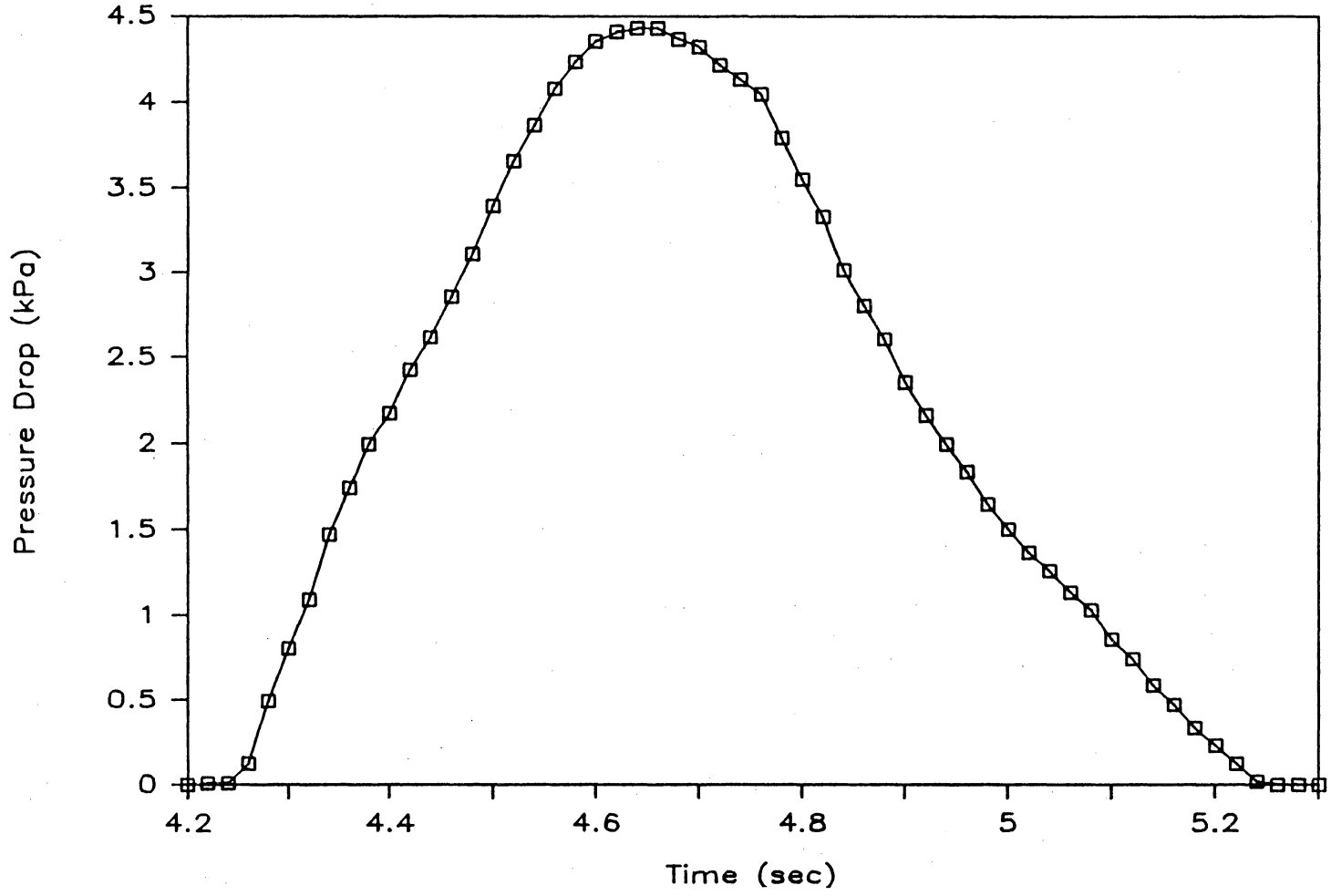

Figure D.24 Pressure Profile: Run 3, Plug #1

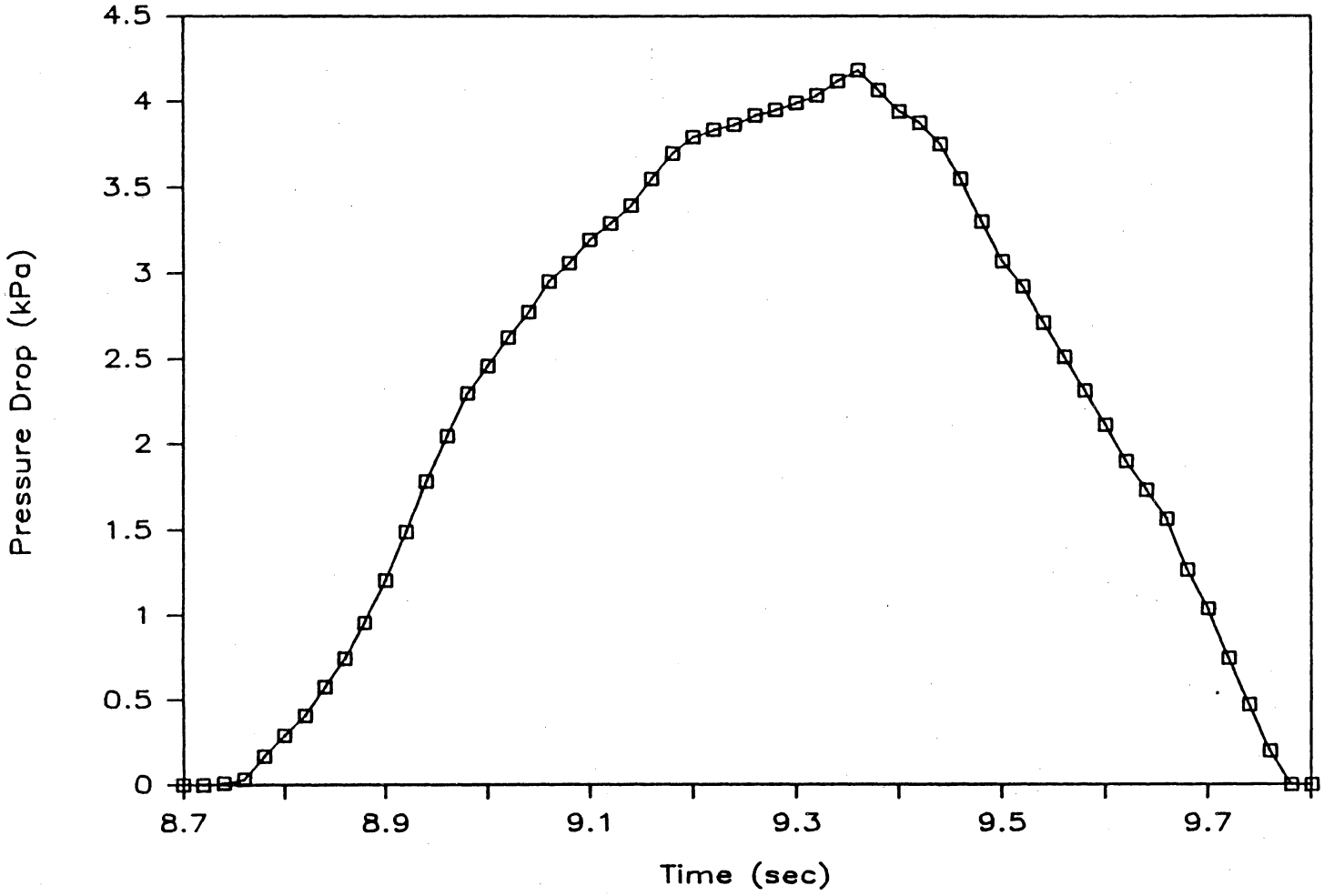

Figure D.25 Pressure Profile: Run 3, Plug #2

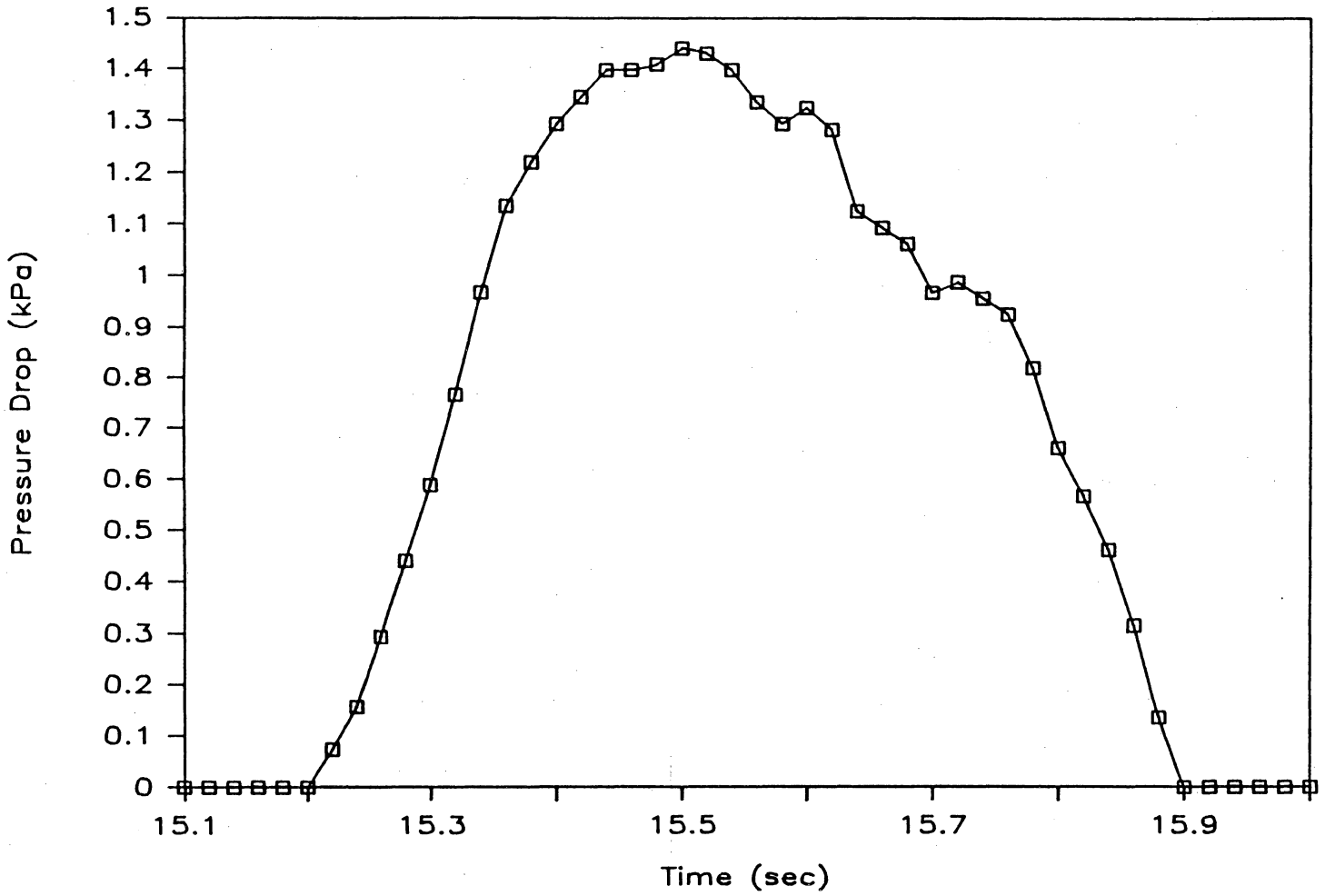

Figure D.26 Pressure Profile: Run 3, Plug #3

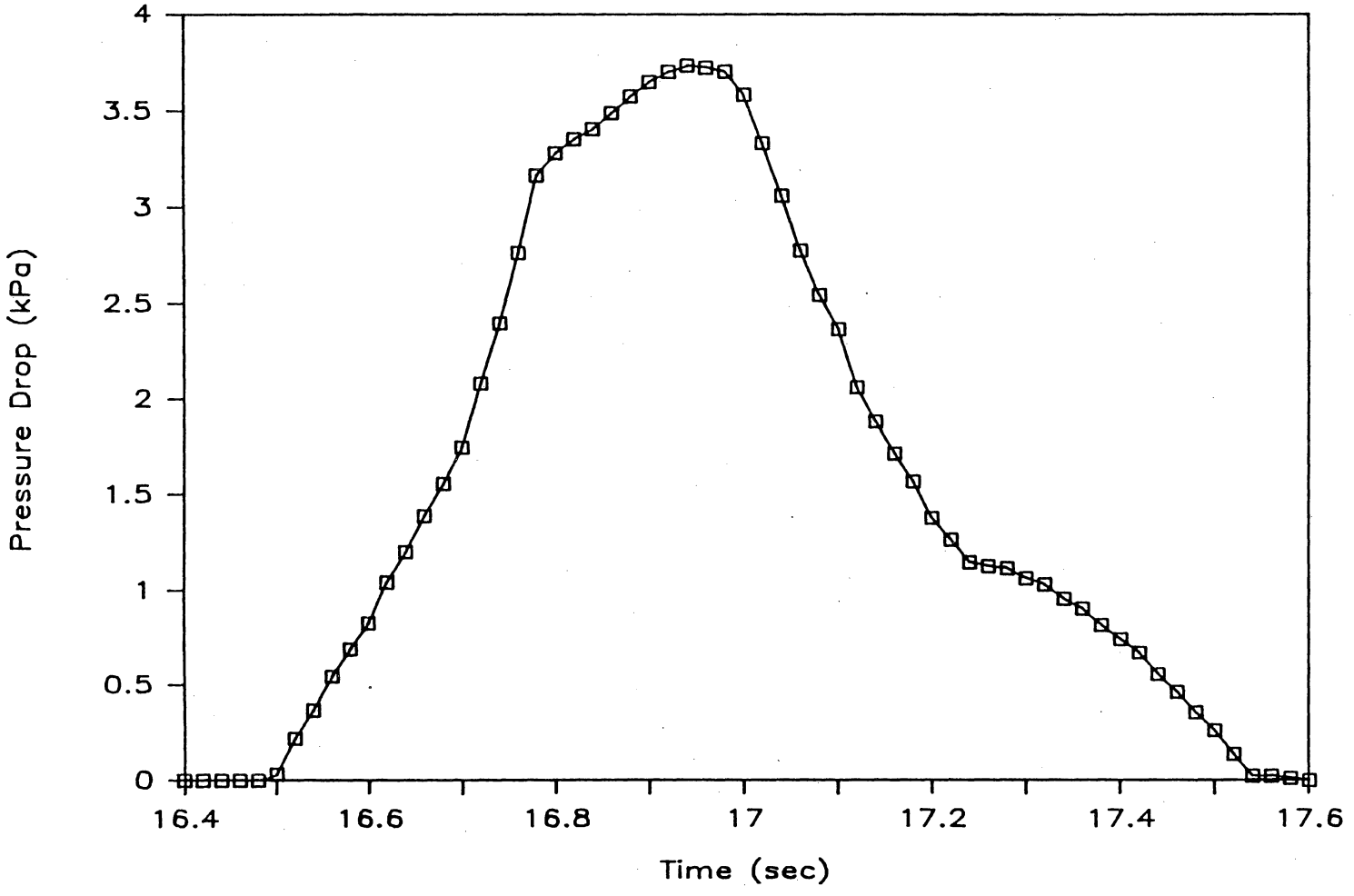

Figure D.27 Pressure Profile: Run 3, Plug #4

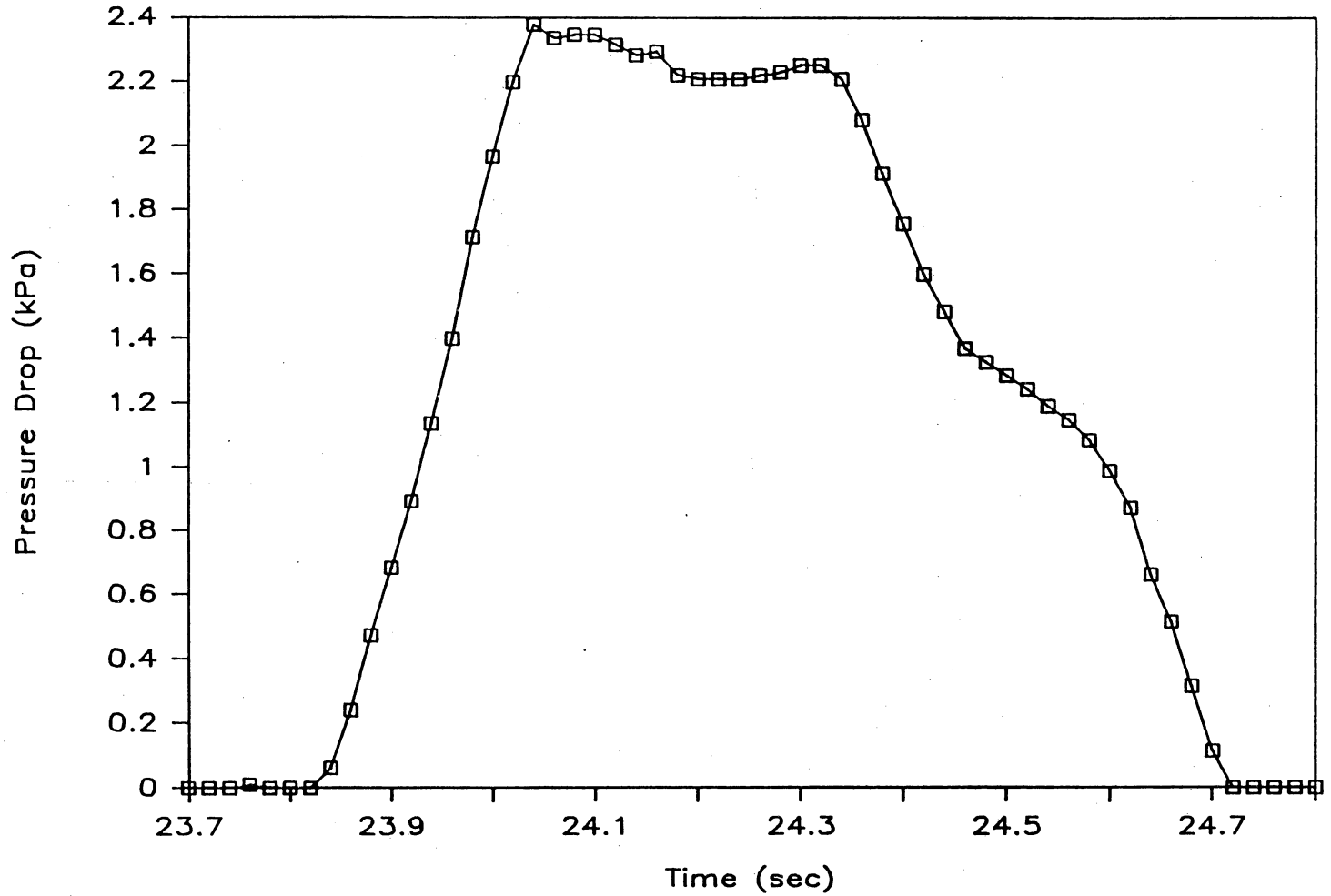

Figure D.28 Pressure Profile: Run 3, Plug #5

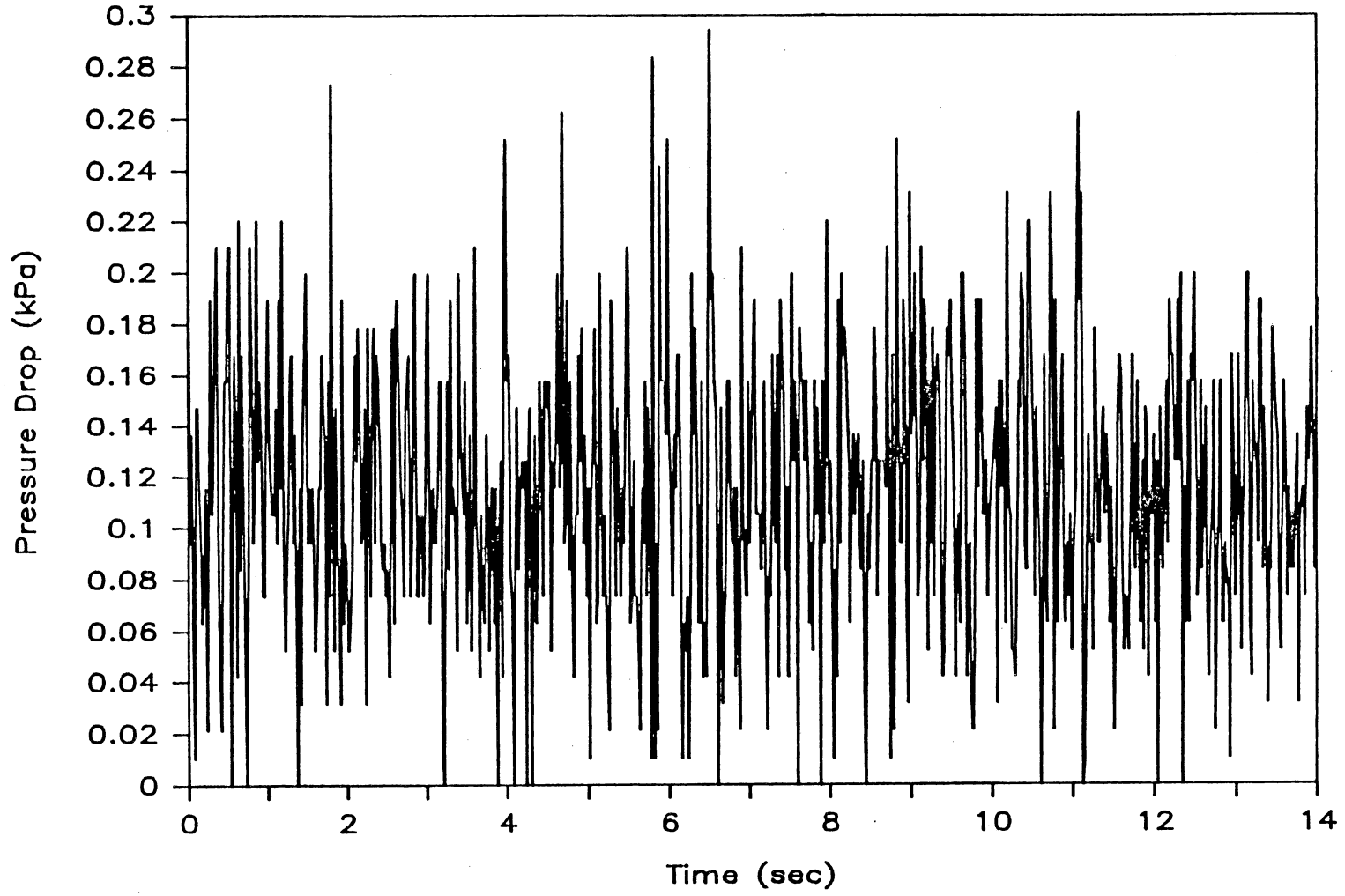

Figure D.29 Overall Pressure Profile: Run 4

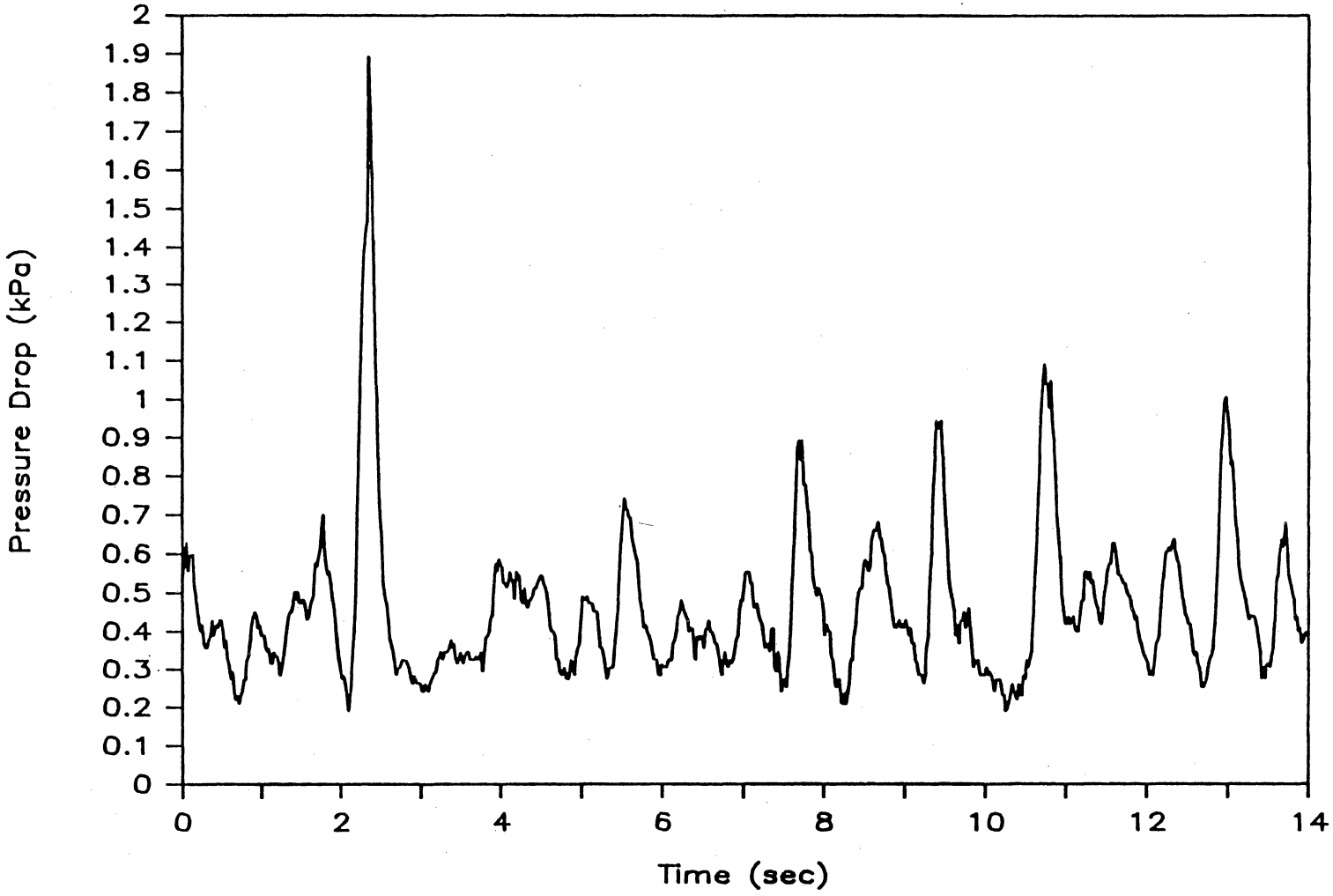

Figure D.30 Overall Pressure Profile: Run 5

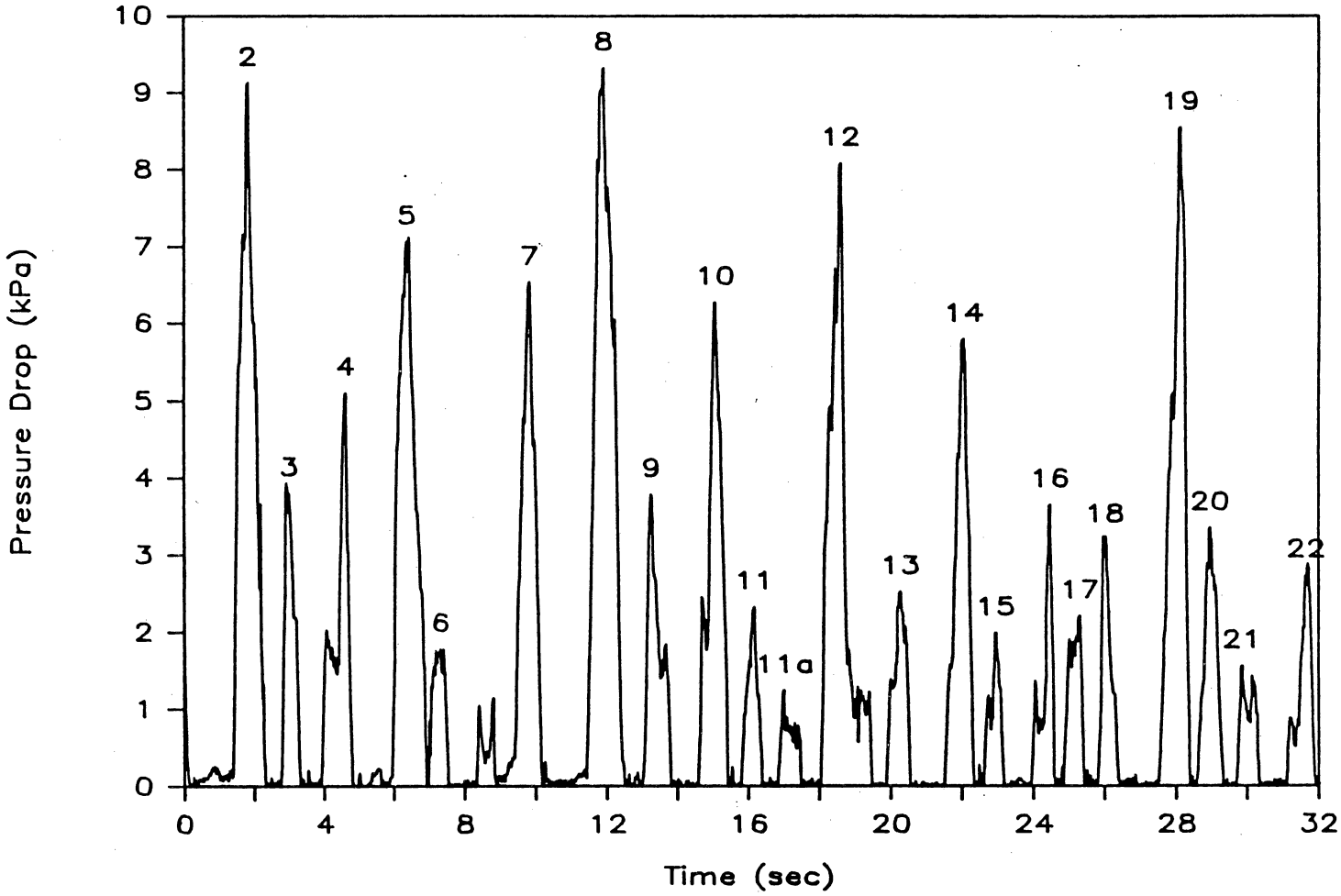

Figure D.31 Overall Pressure Profile: Run 6

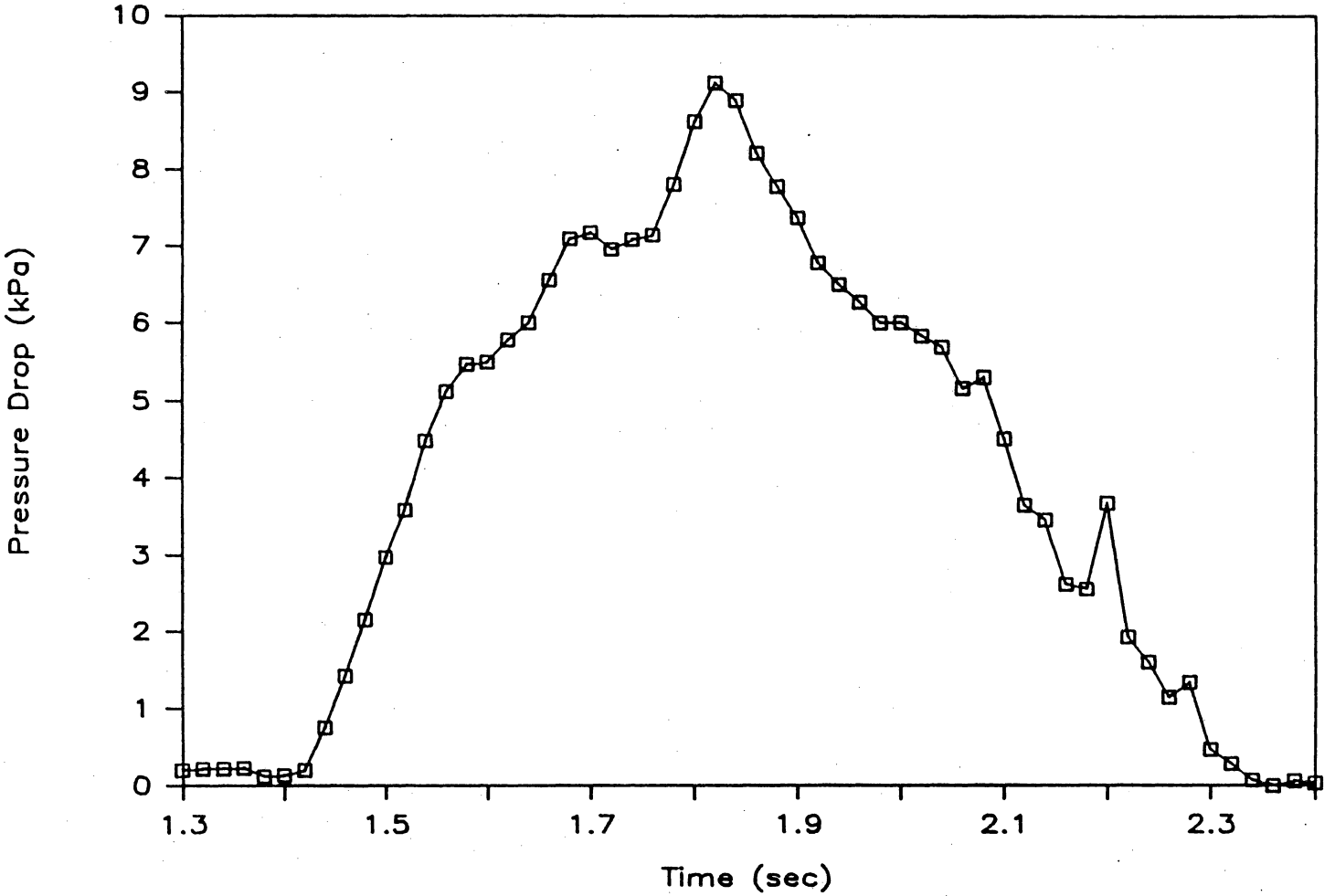

Figure D.32 Pressure Profile: Run 6, Plug #2

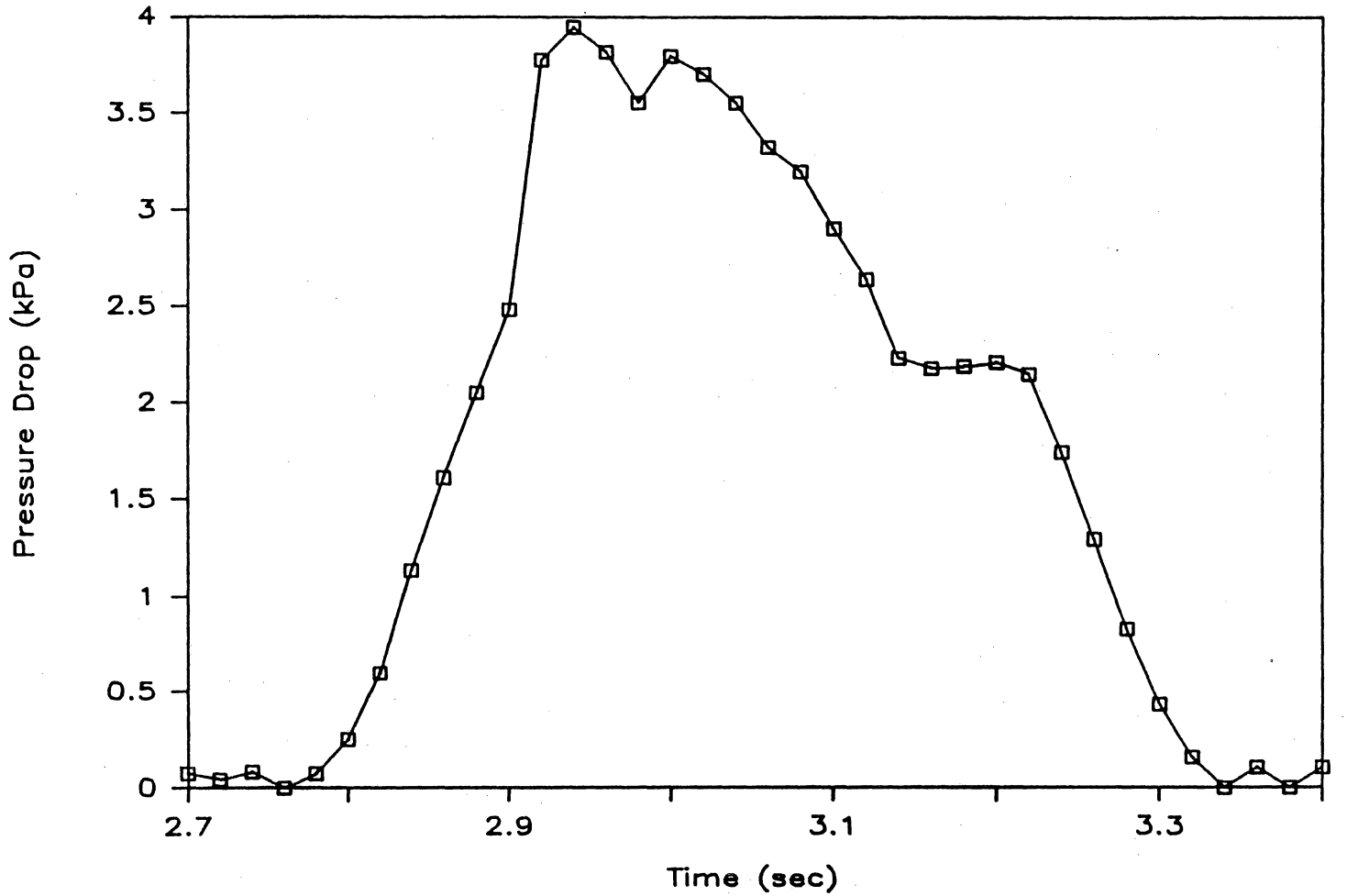

Figure D.33 Pressure Profile: Run 6, Plug #3

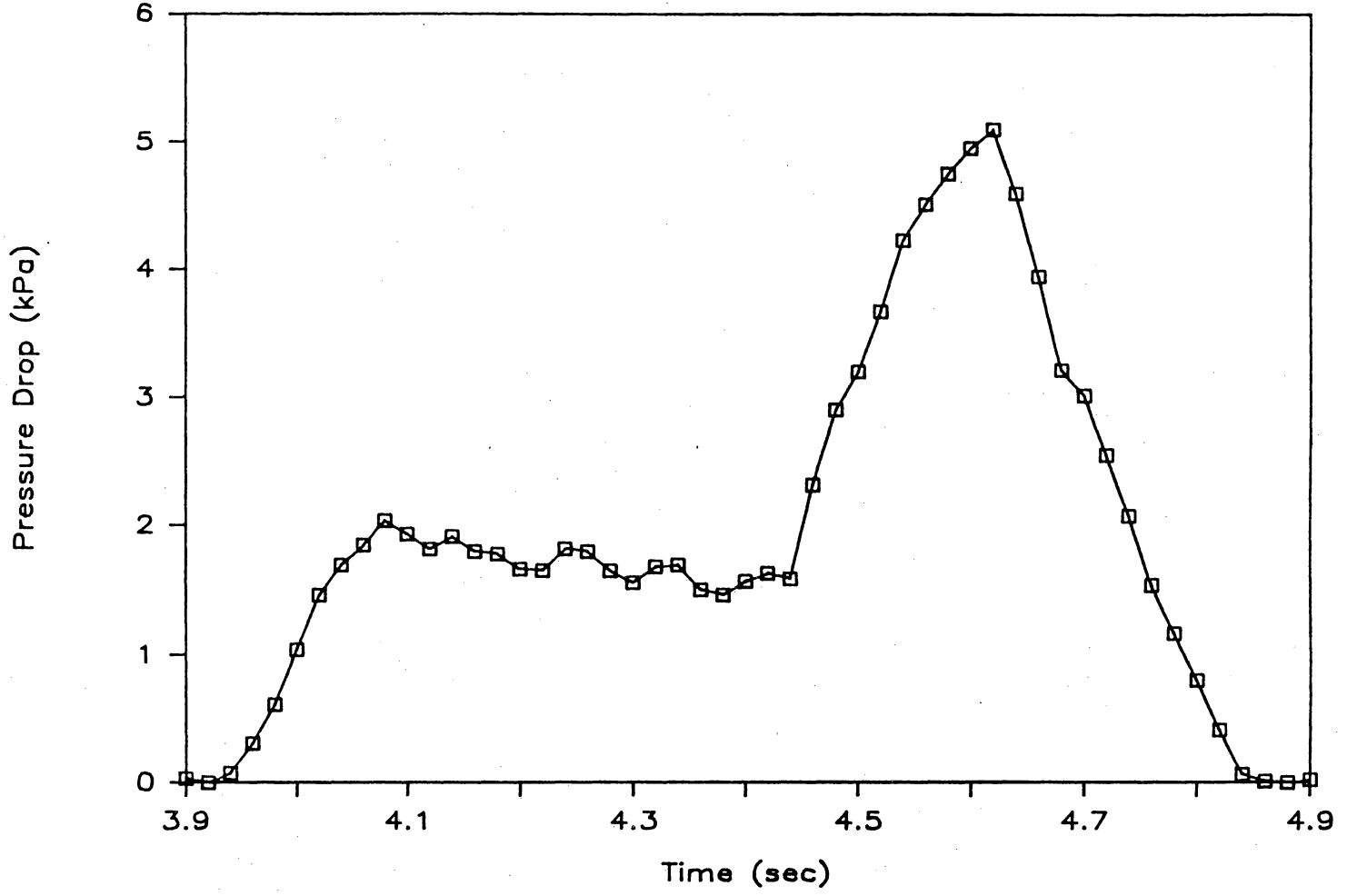

Figure D.34 Pressure Profile: Run 6, Plug #4

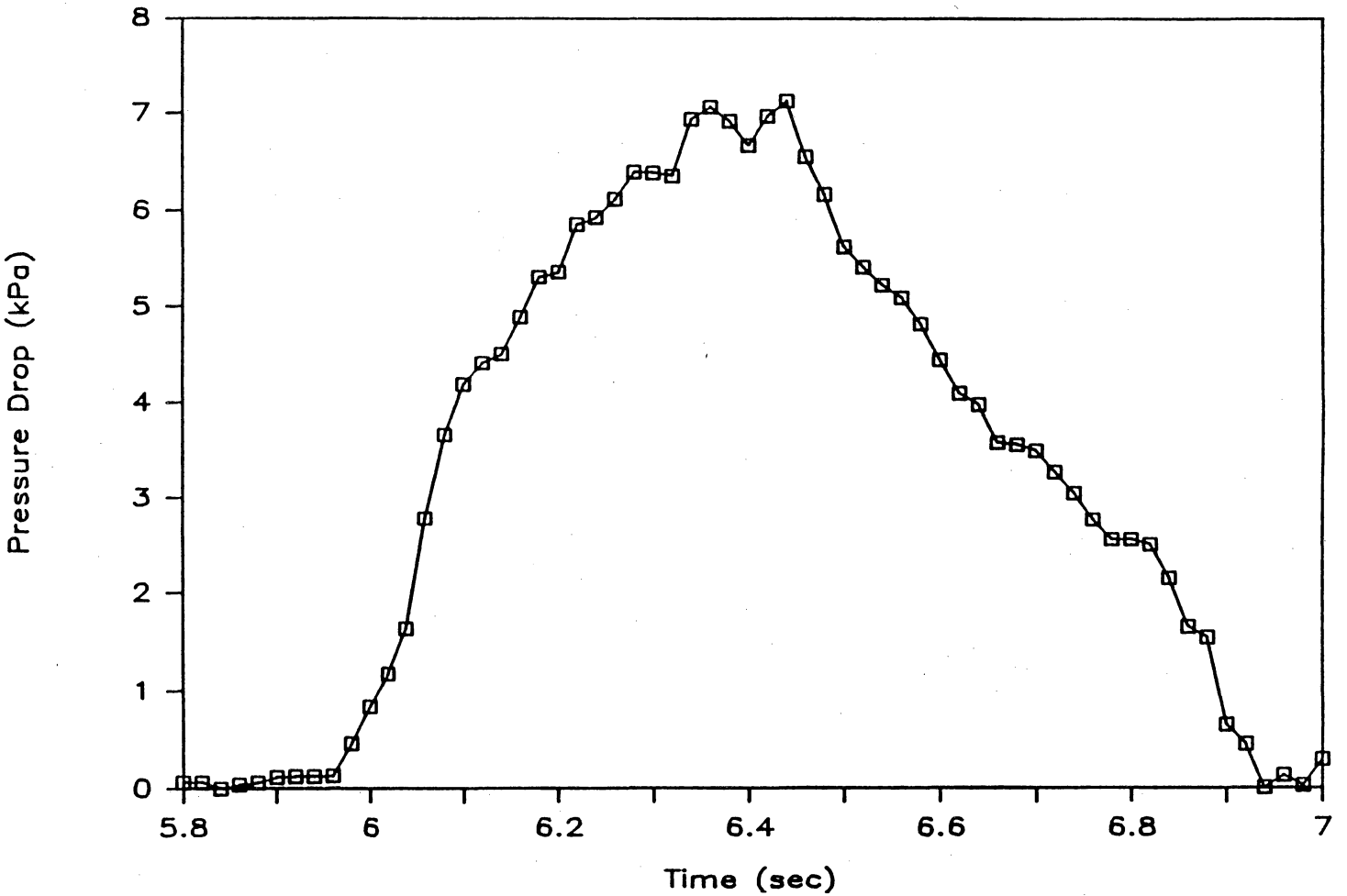

Figure D.35 Pressure Profile: Run 6, Plug #5

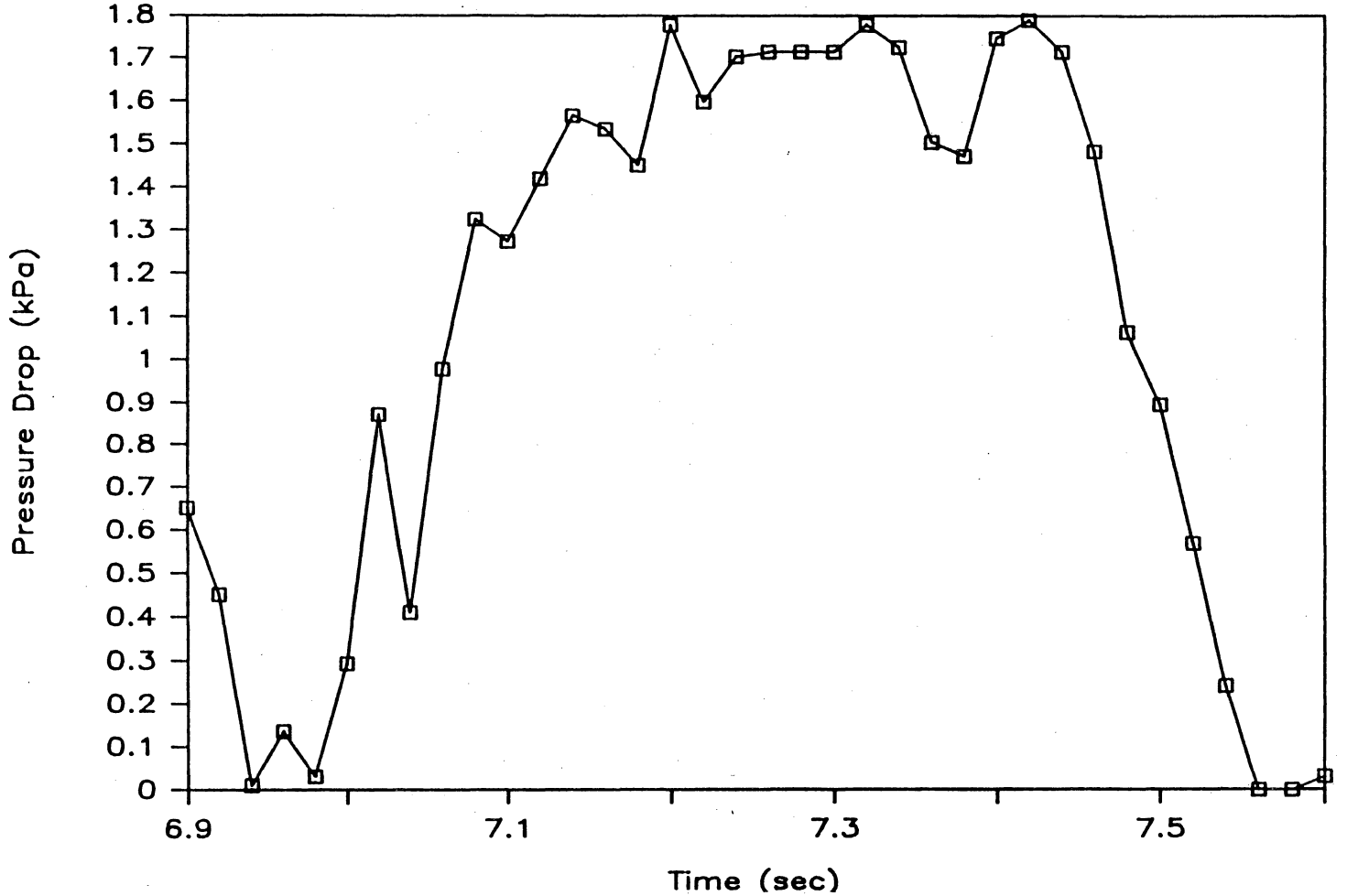

Figure D.36 Pressure Profile: Run 6, Plug #6

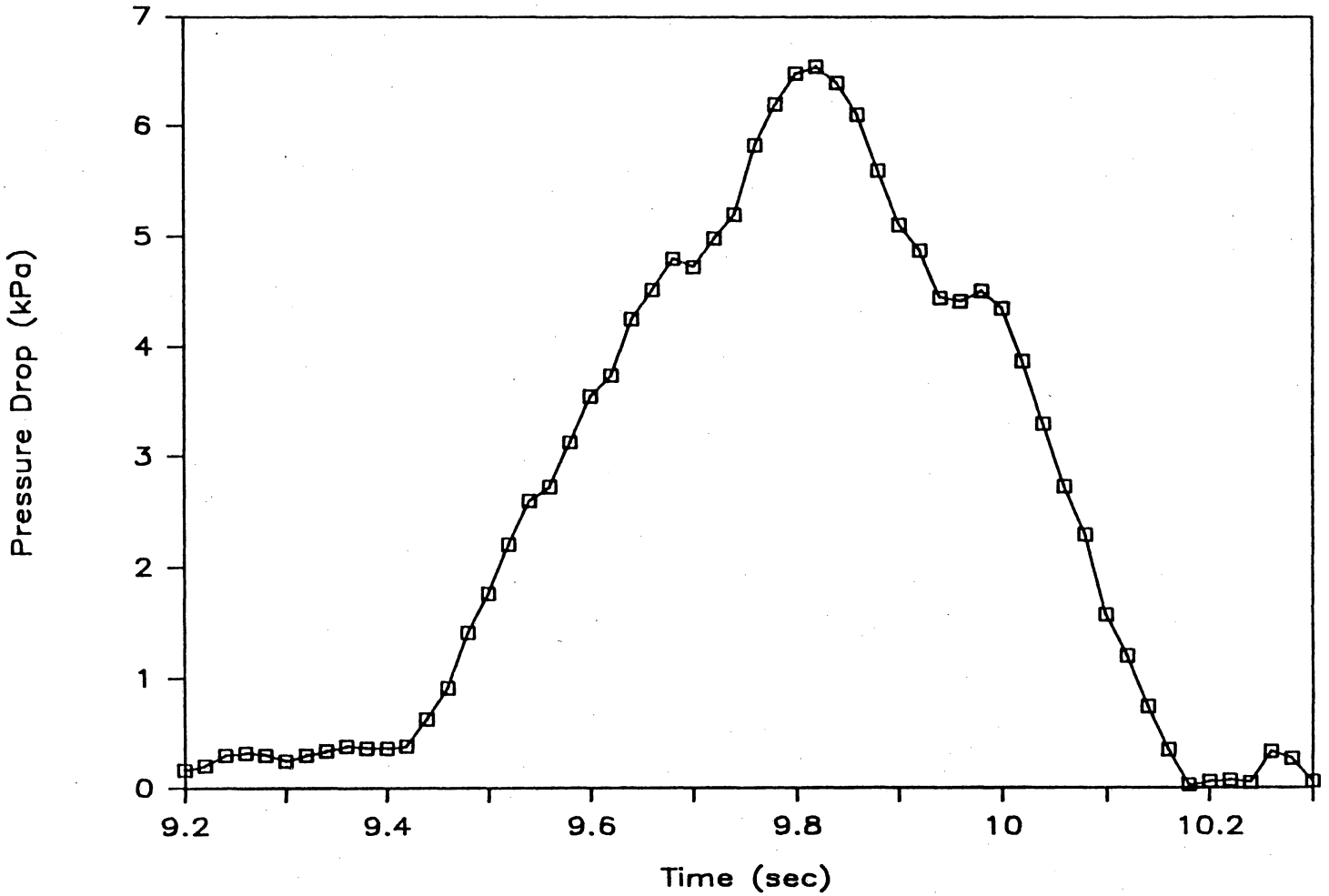

Figure D.37 Pressure Profile: Run 6, Plug #7

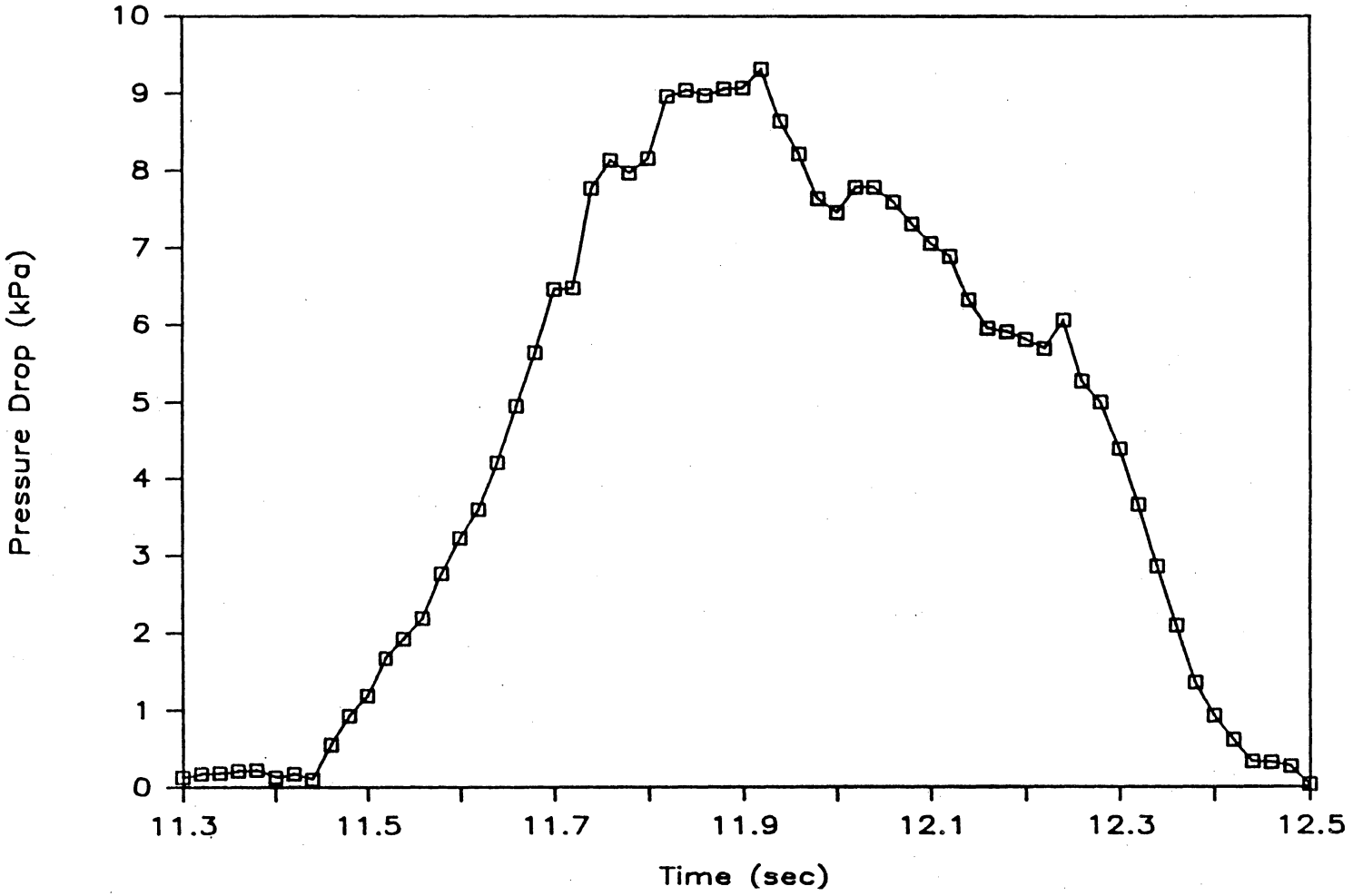

Figure D.38 Pressure Profile: Run 6, Plug #8

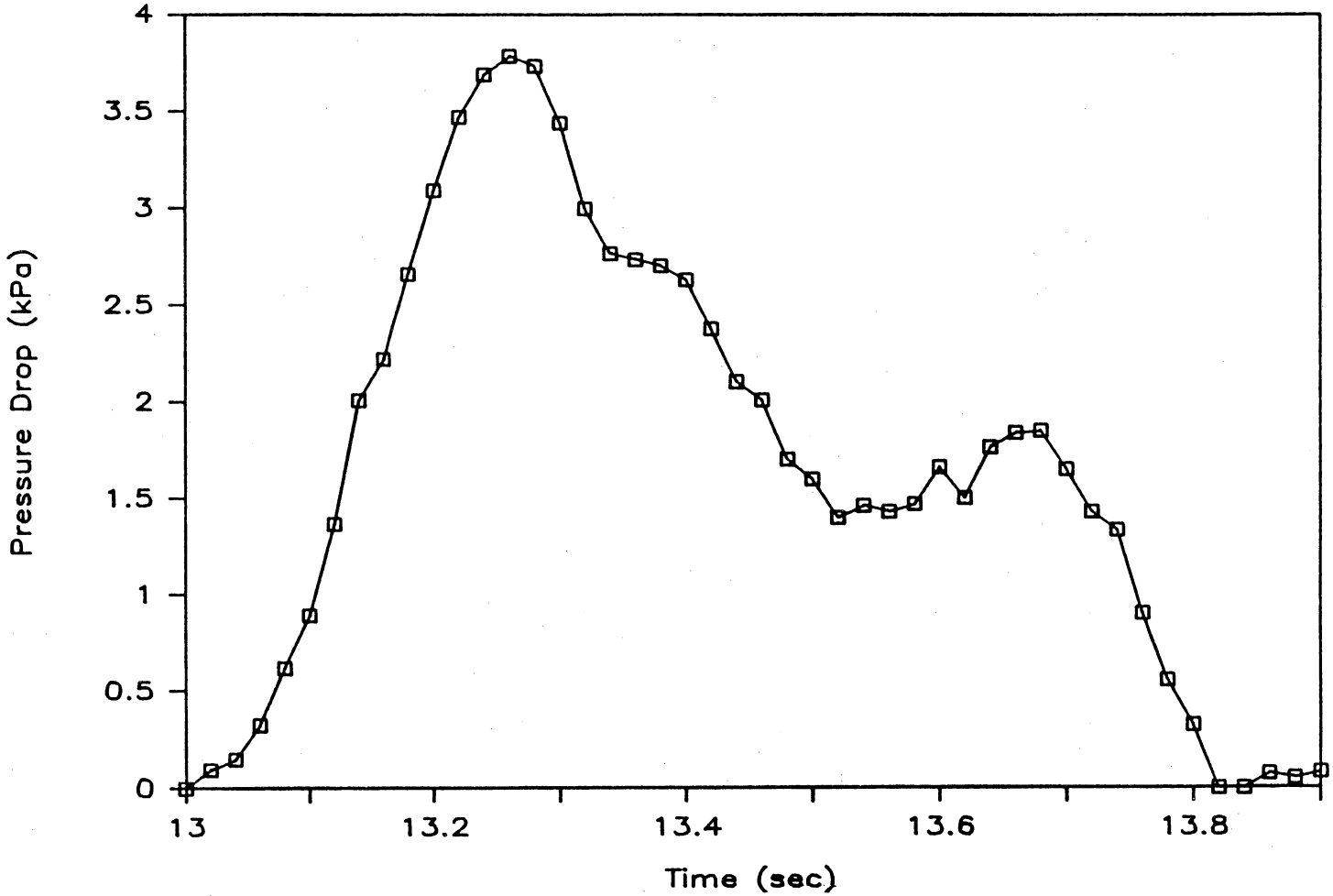

Figure D.39 Pressure Profile: Run 6, Plug #9

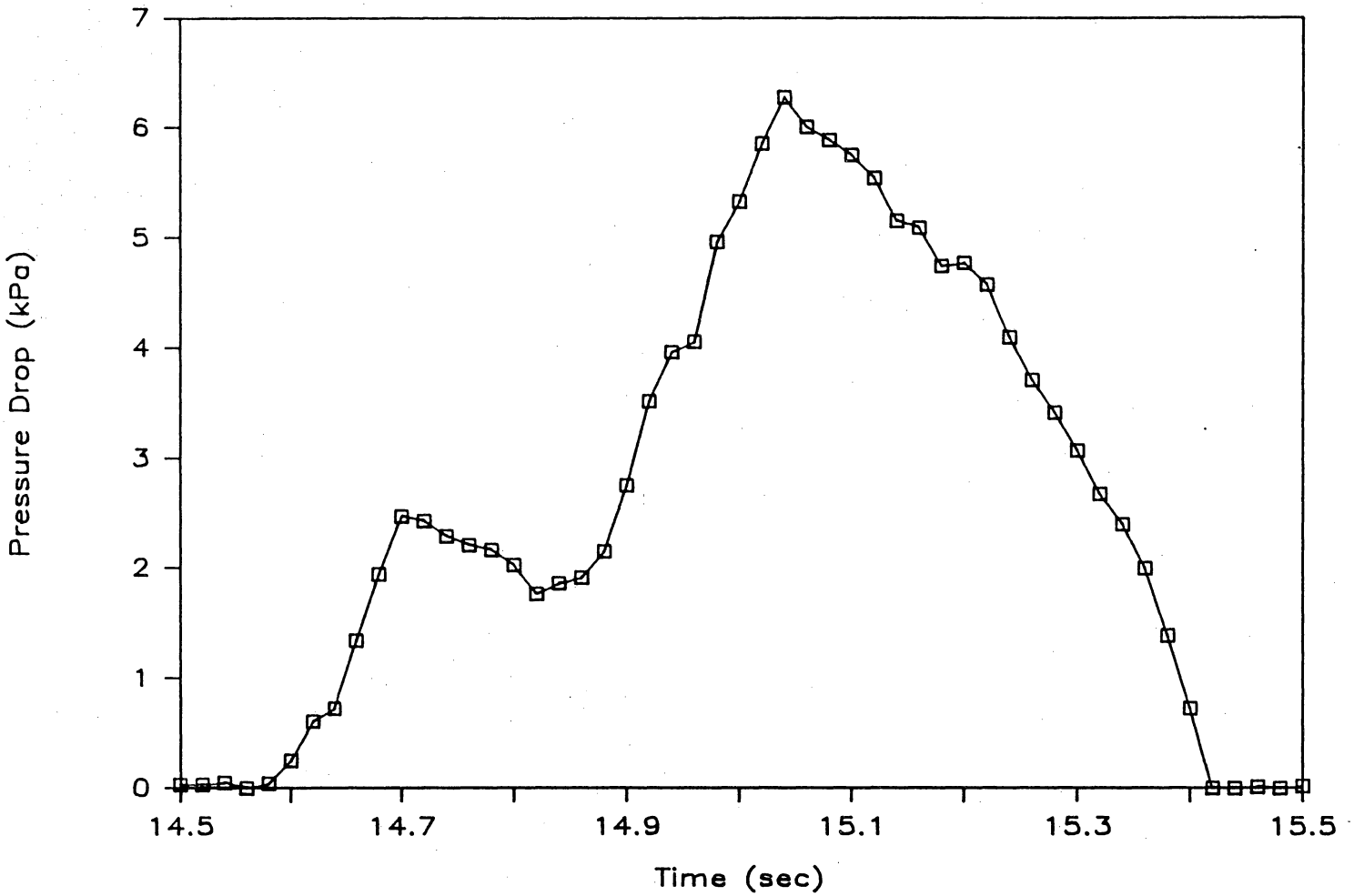

Figure D.40 Pressure Profile: Run 6, Plug #10

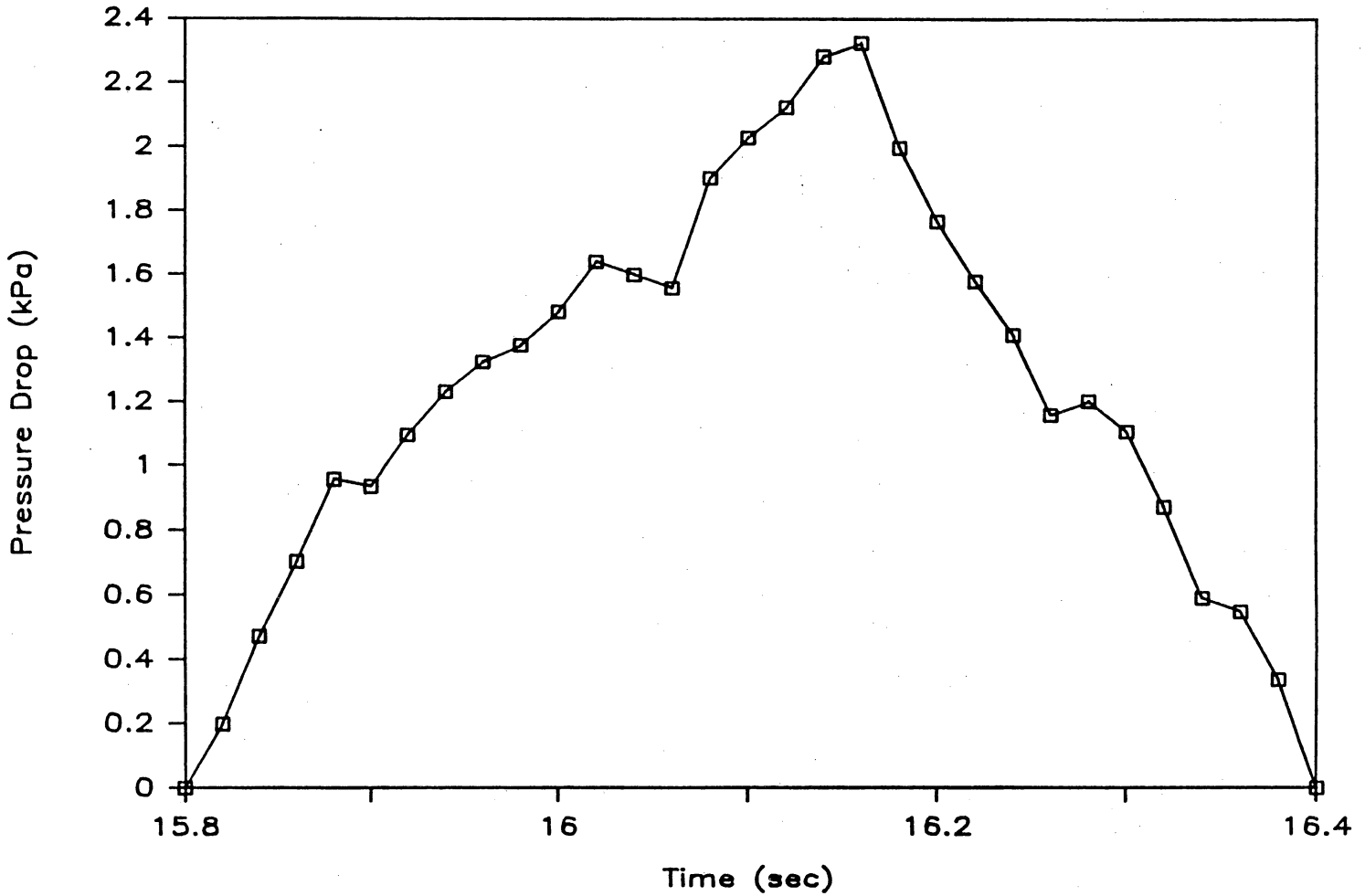

Figure D.41 Pressure Profile: Run 6, Plug #11

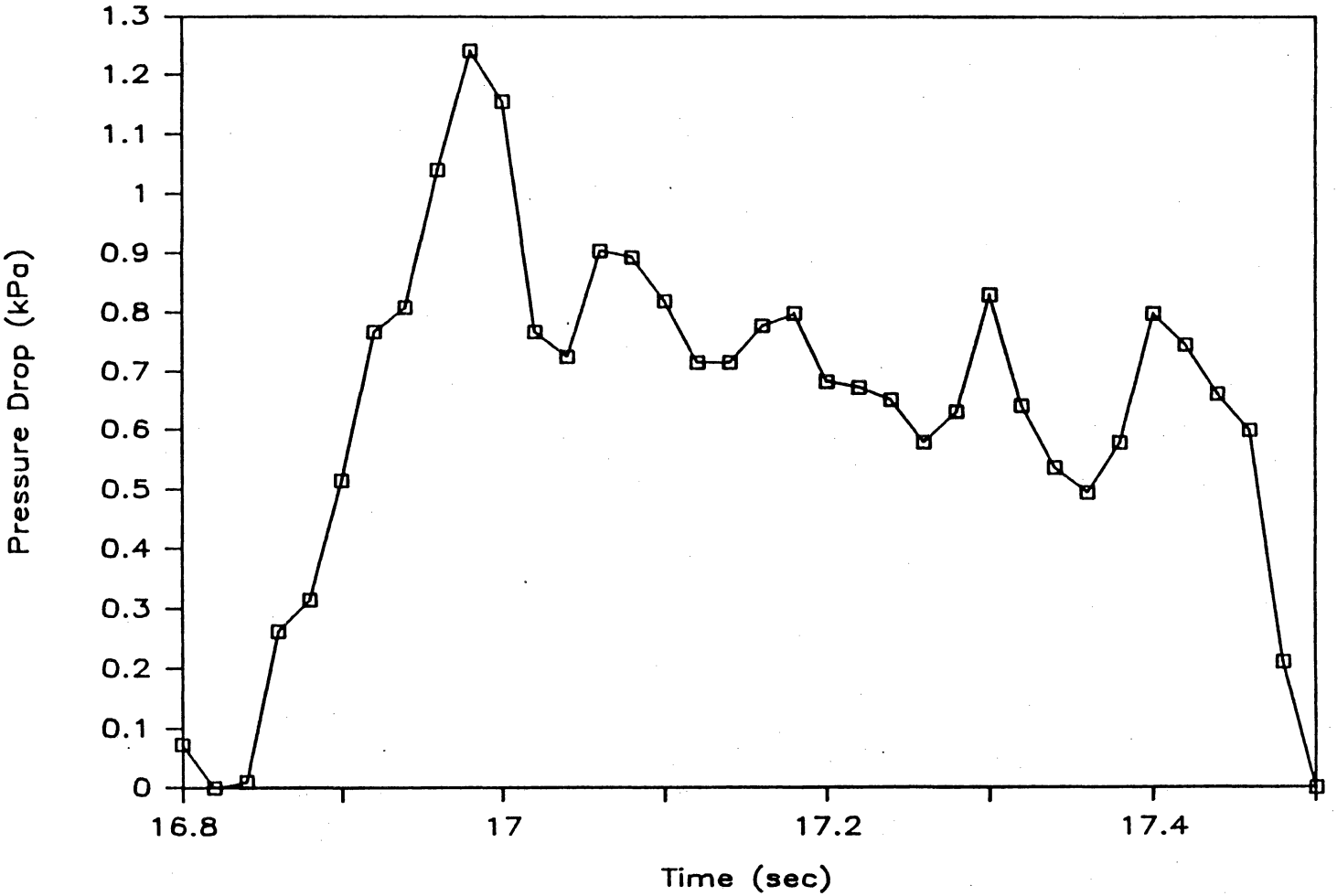

Figure D.42 Pressure Profile: Run 6, Plug #11a

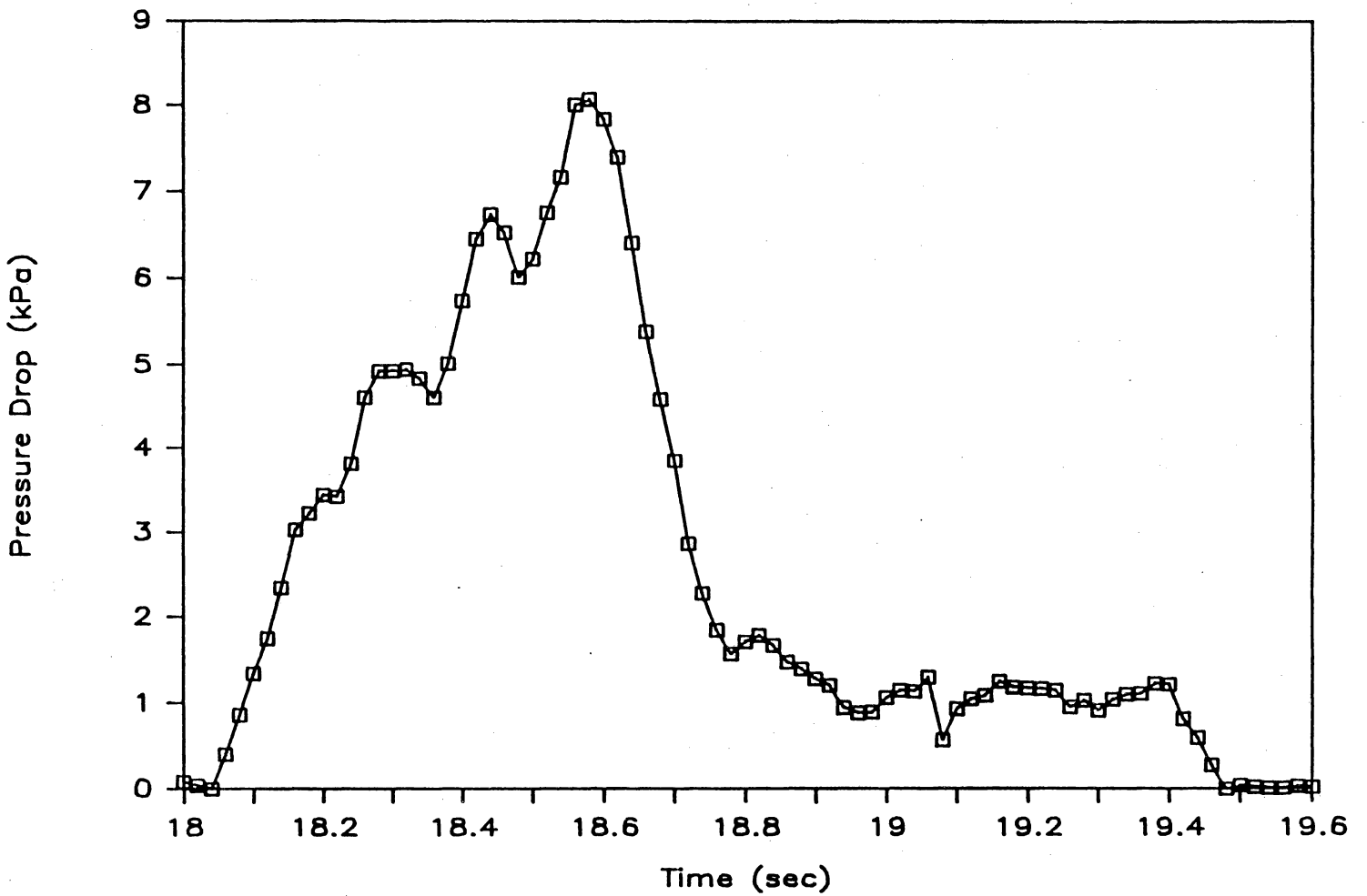

Figure D.43 Pressure Profile: Run 6, Plug #12

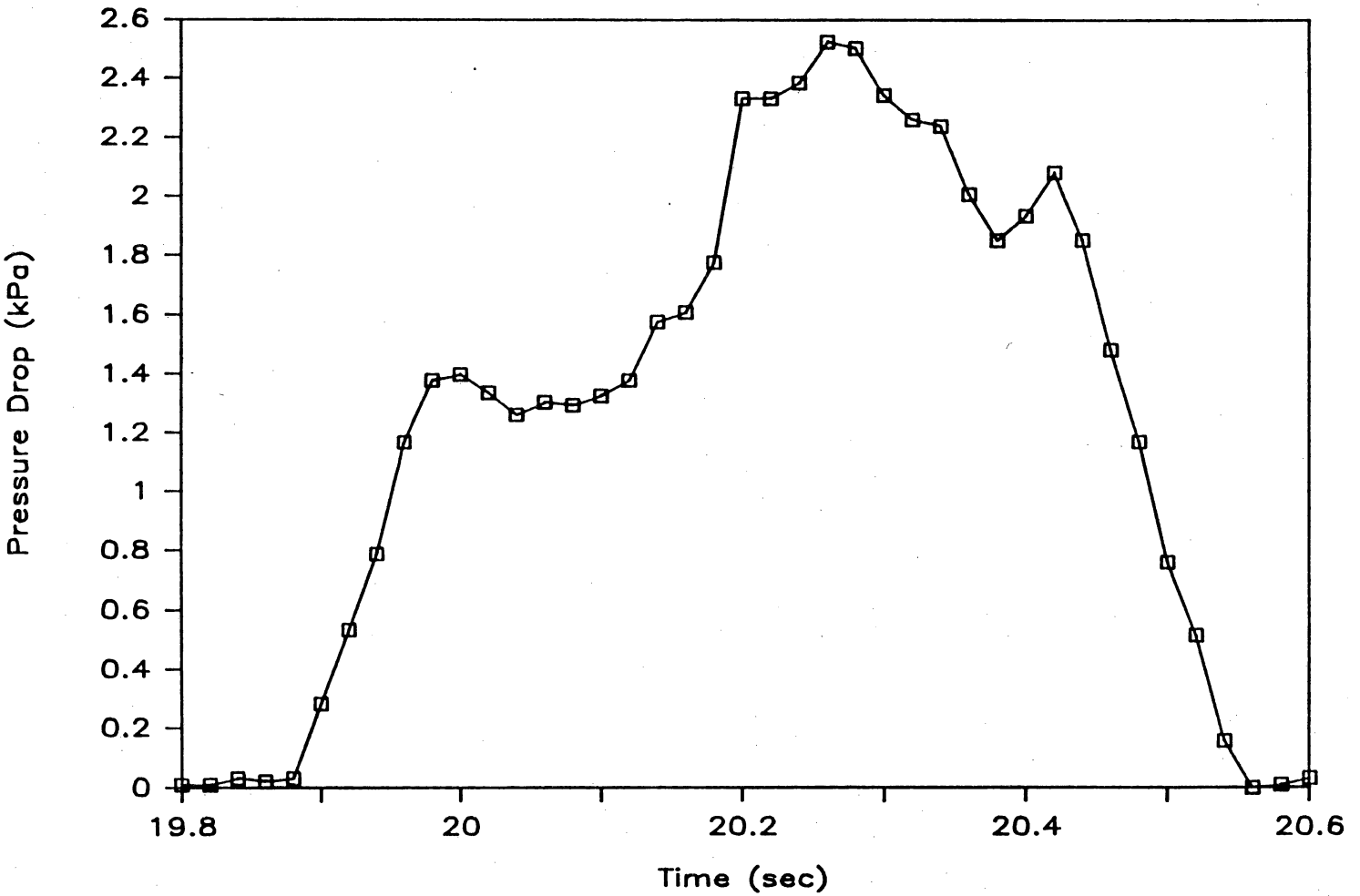

Figure D.44 Pressure Profile: Run 6, Plug #13

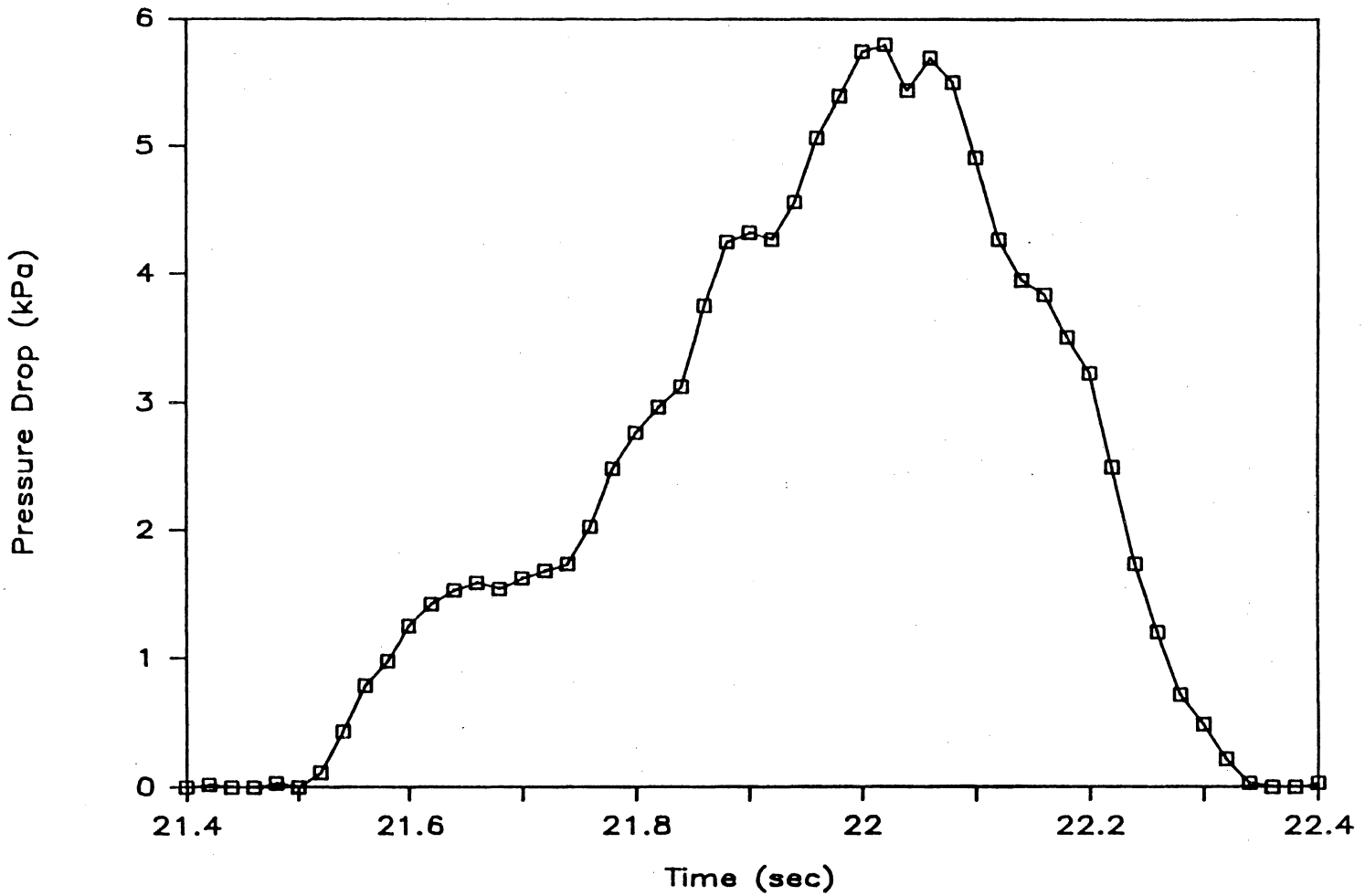

Figure D.45 Pressure Profile: Run 6, Plug #14

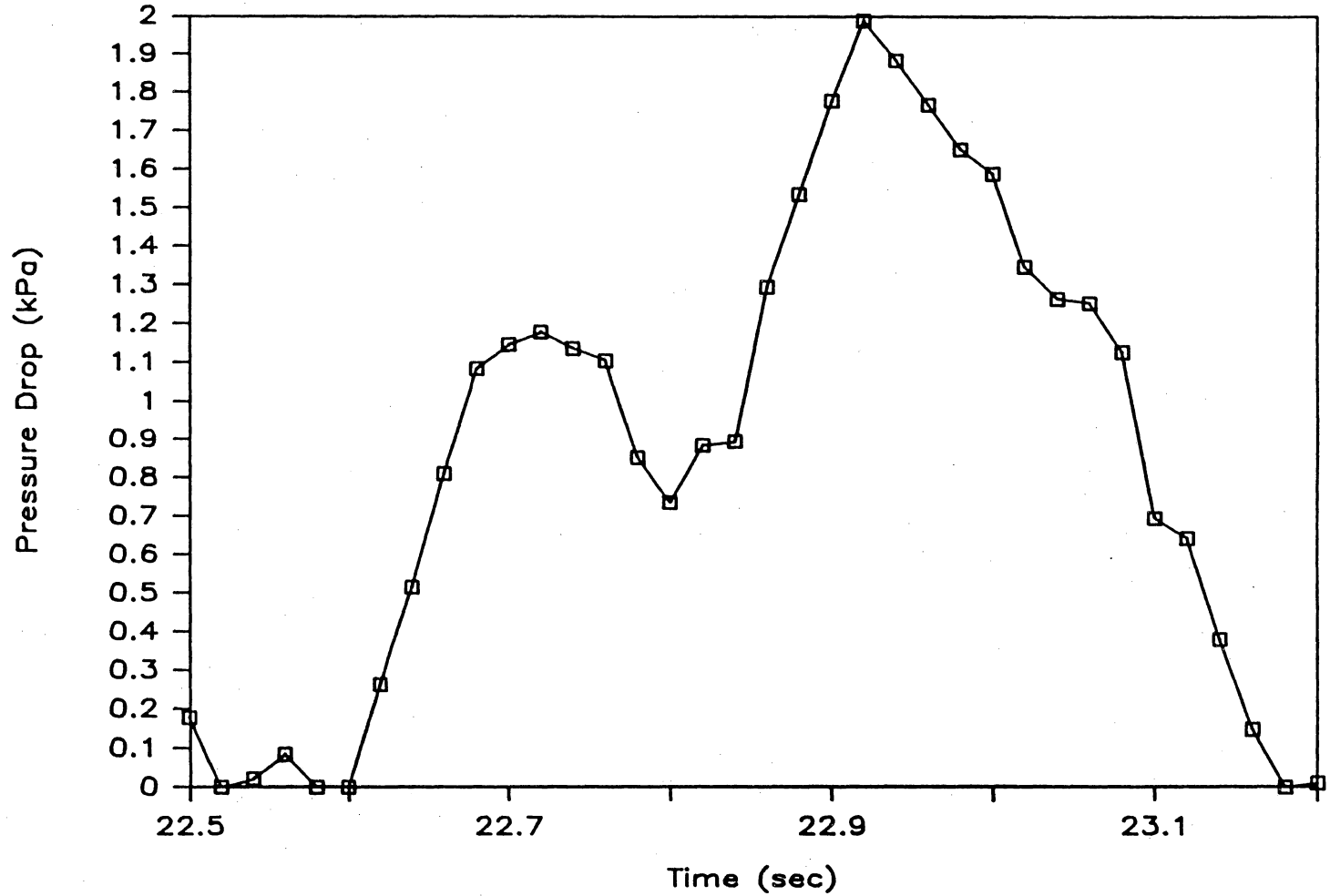

Figure D.46 Pressure Profile: Run 6, Plug #15

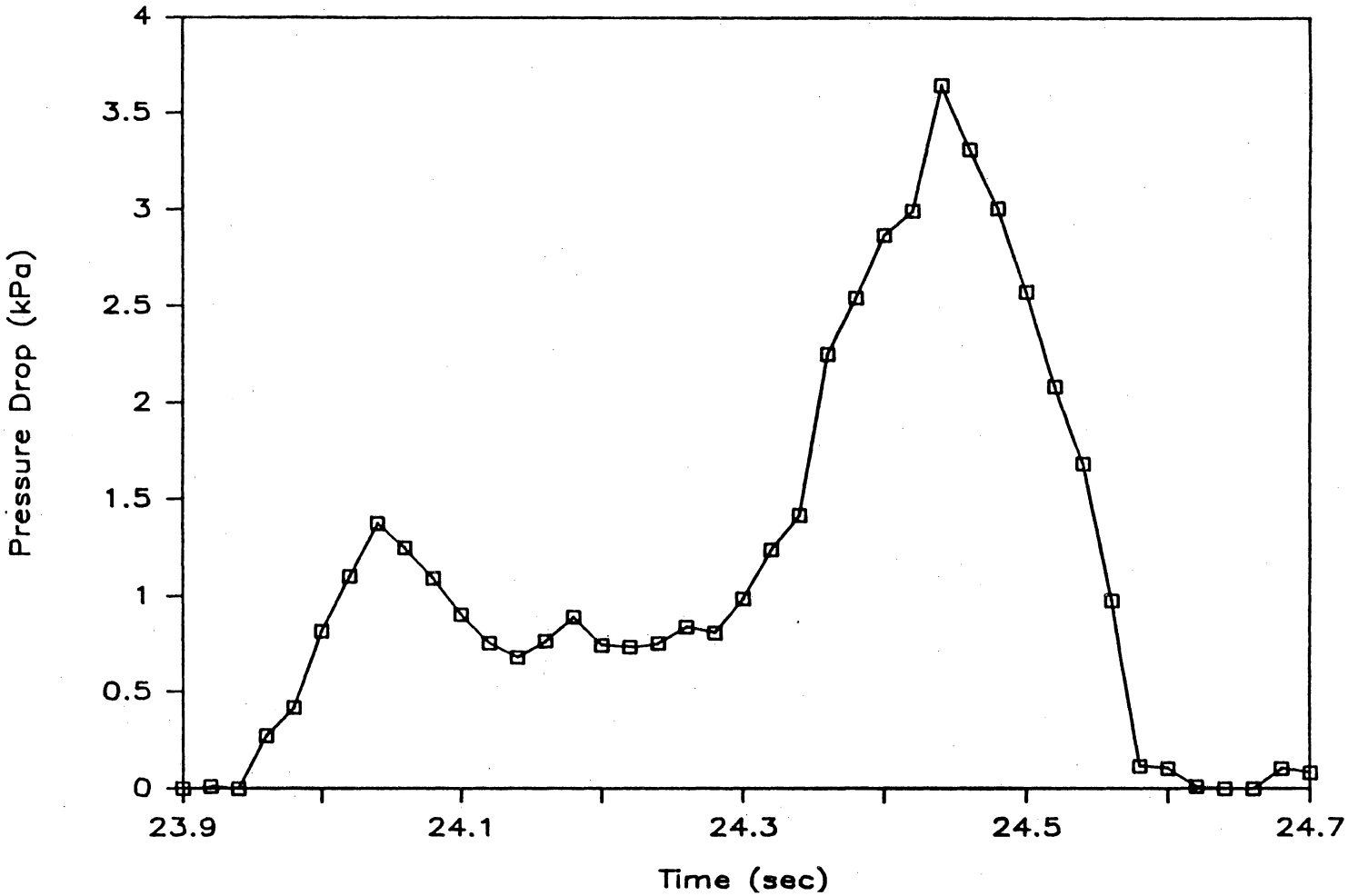

Figure D.47 Pressure Profile: Run 6, Plug #16

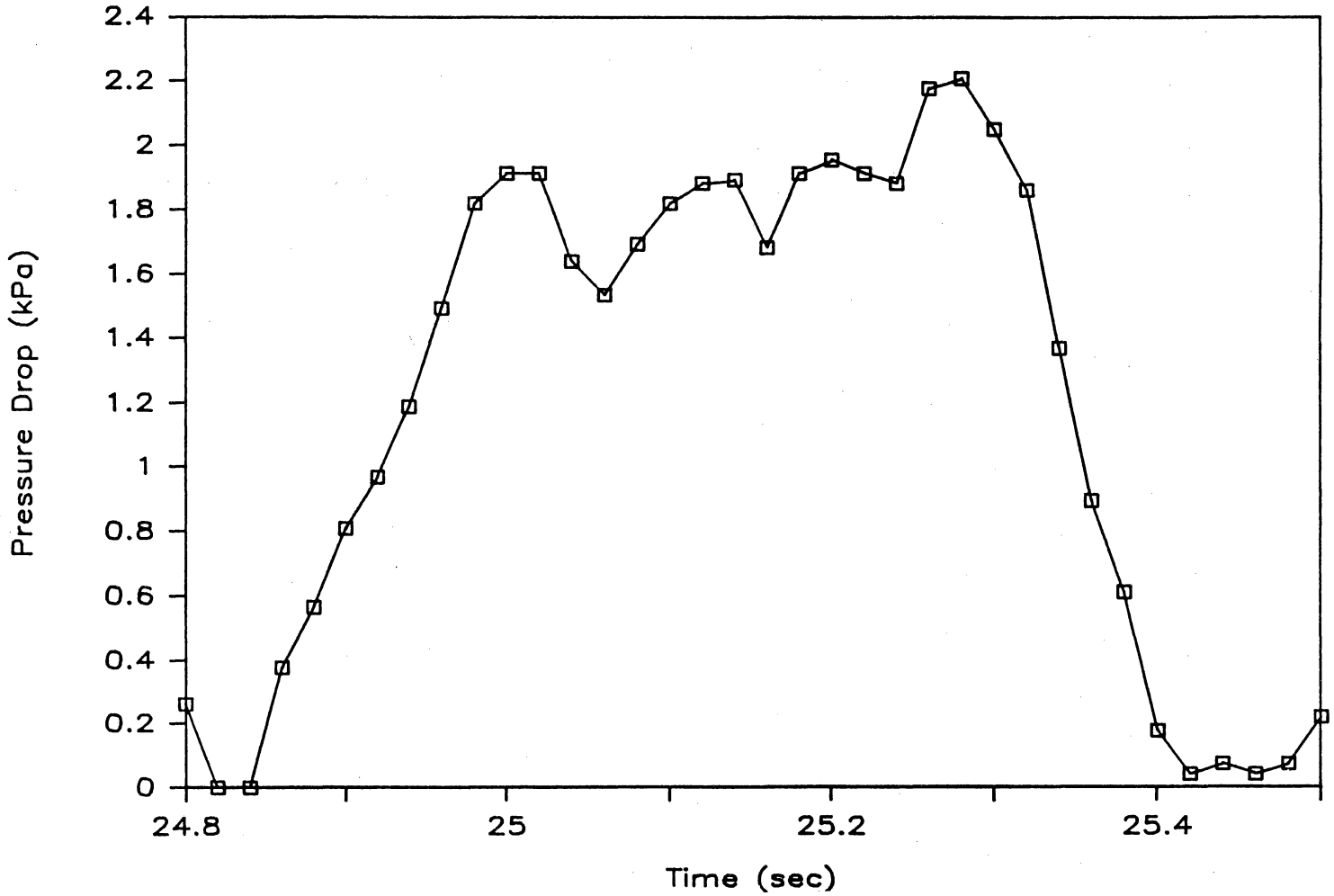

Figure D.48 Pressure Profile: Run 6, Plug #17

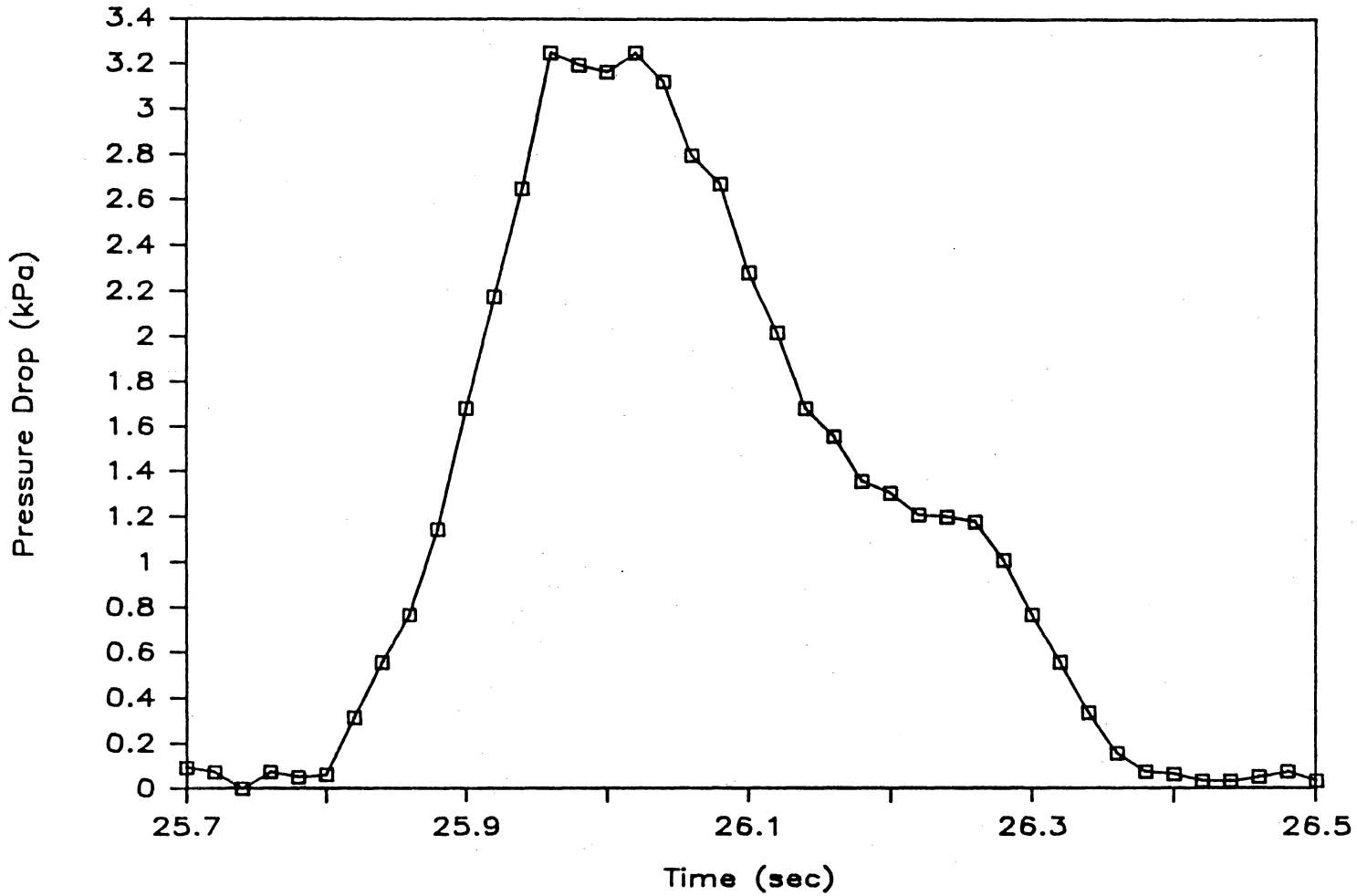

Figure D.49 Pressure Profile: Run 6, Plug #18

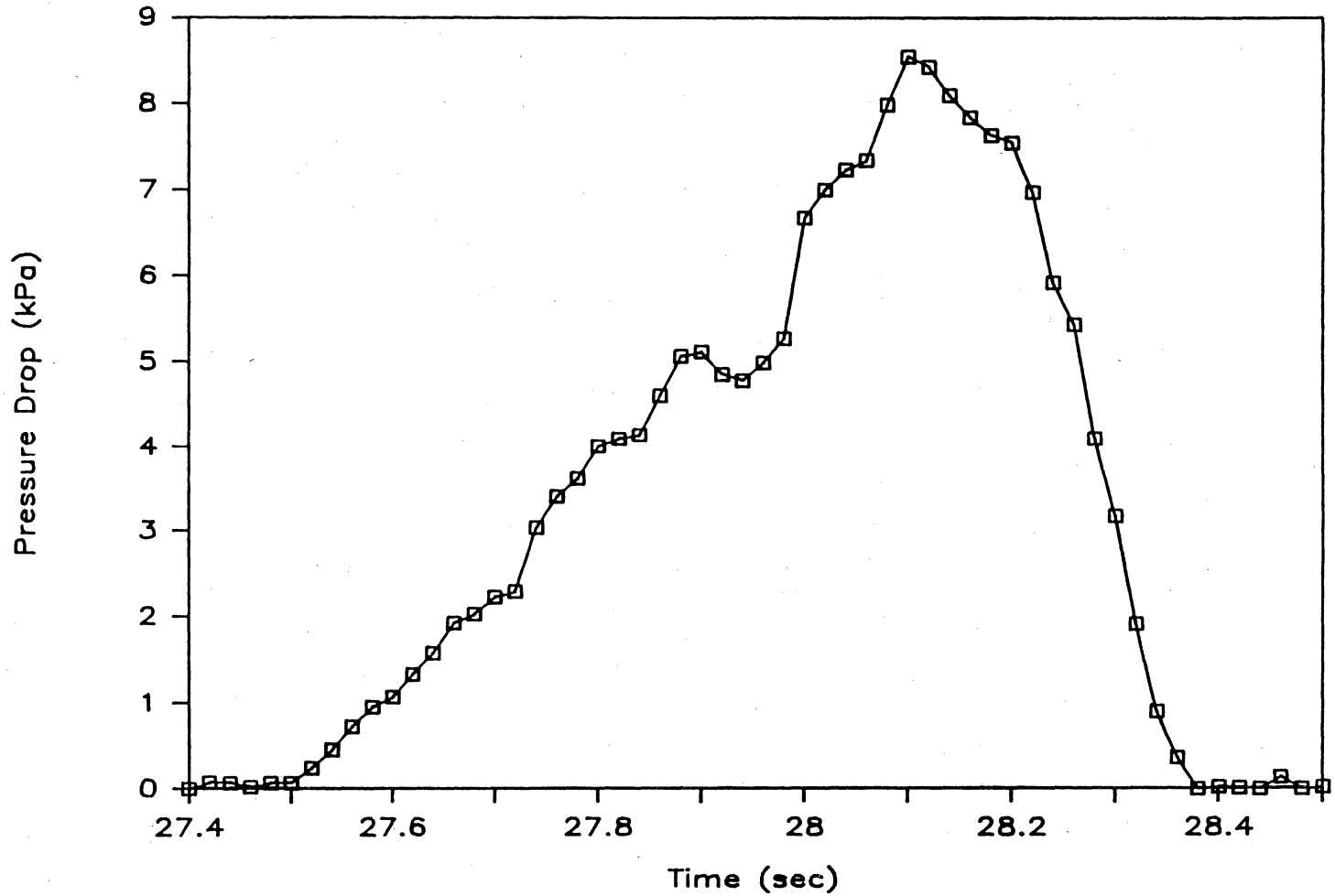

Figure D.50 Pressure Profile: Run 6, Plug #19

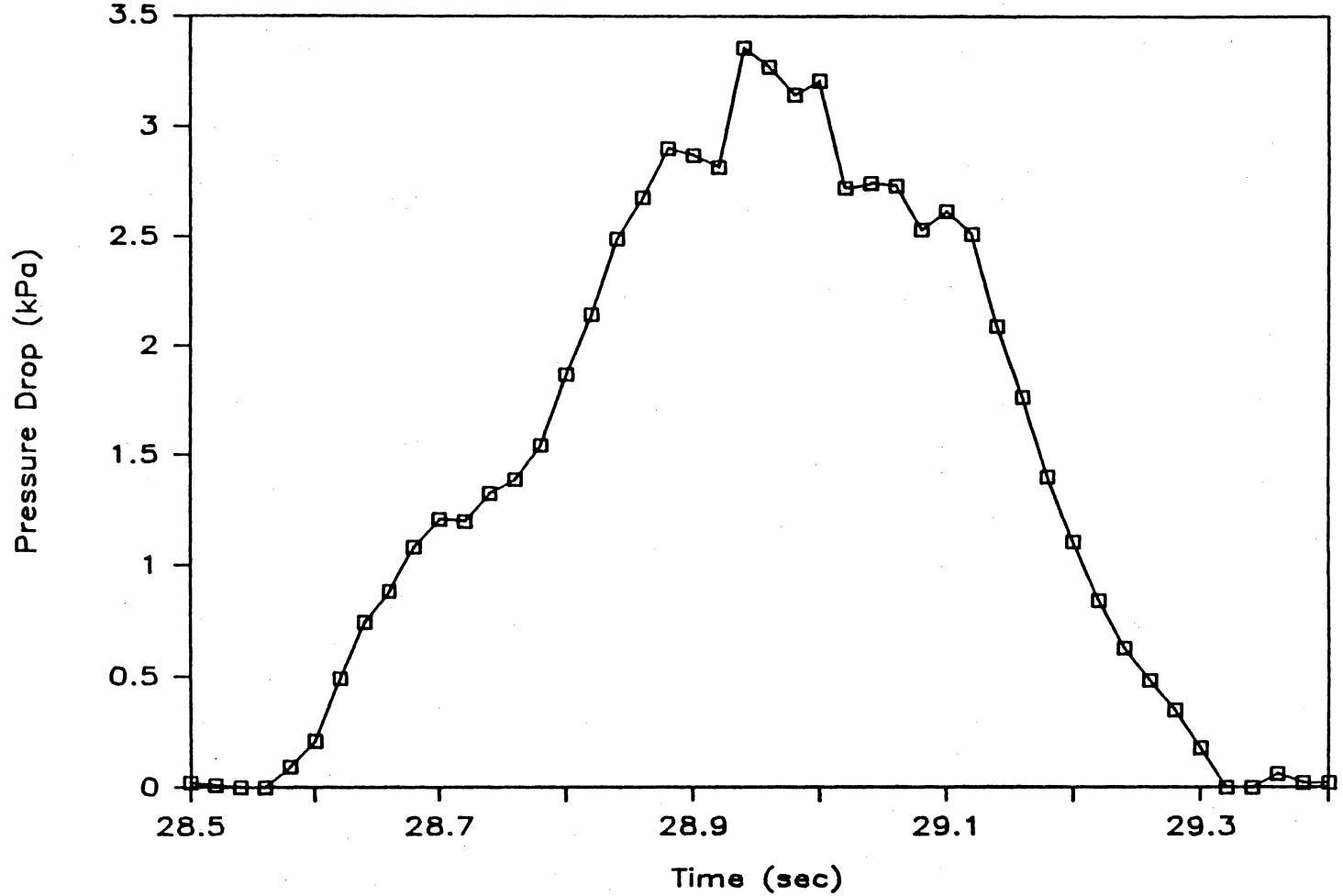

Figure D.51 Pressure Profile: Run 6, Plug #20

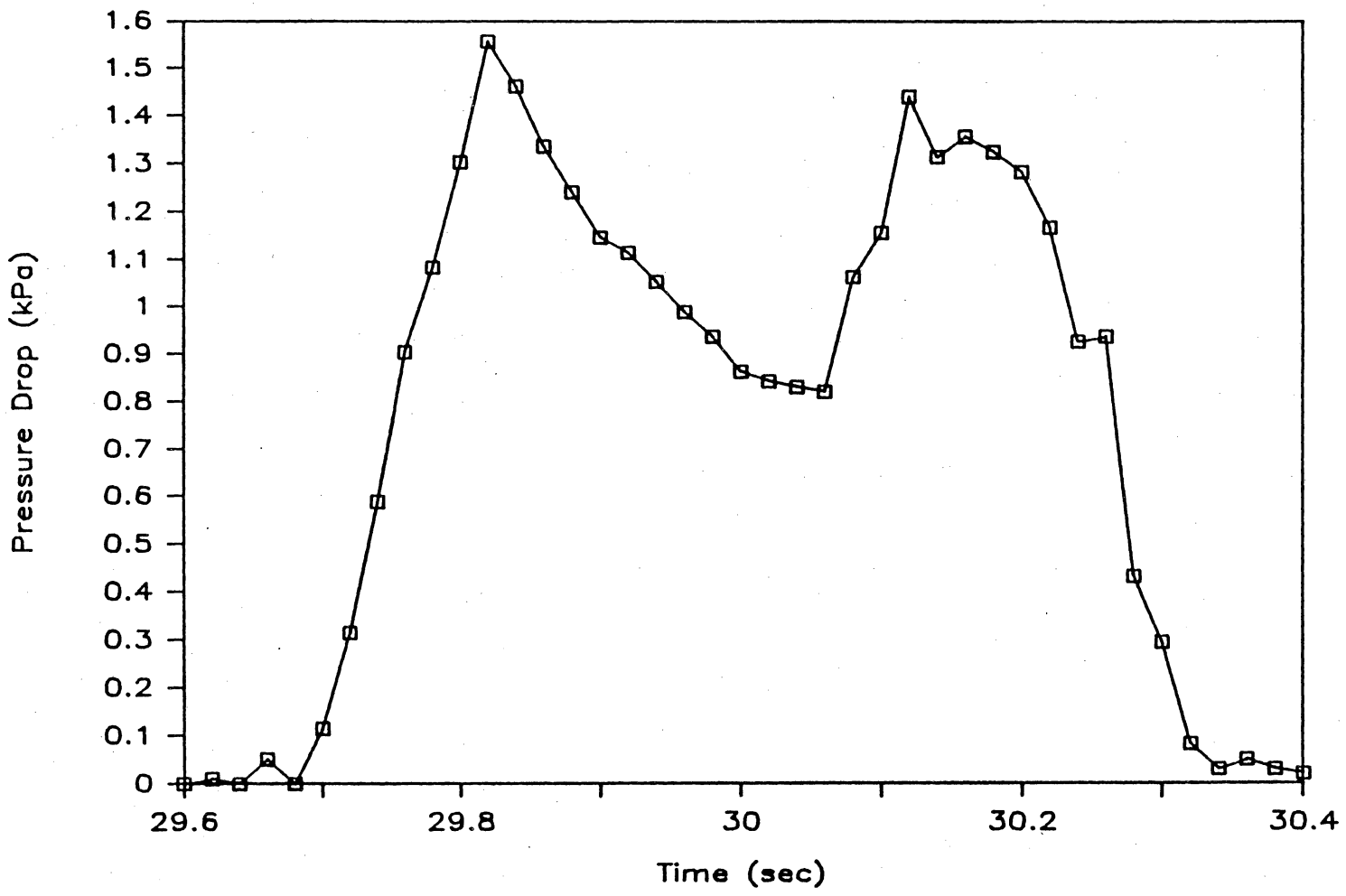

Figure D.52 Pressure Profile: Run 6, Plug #21

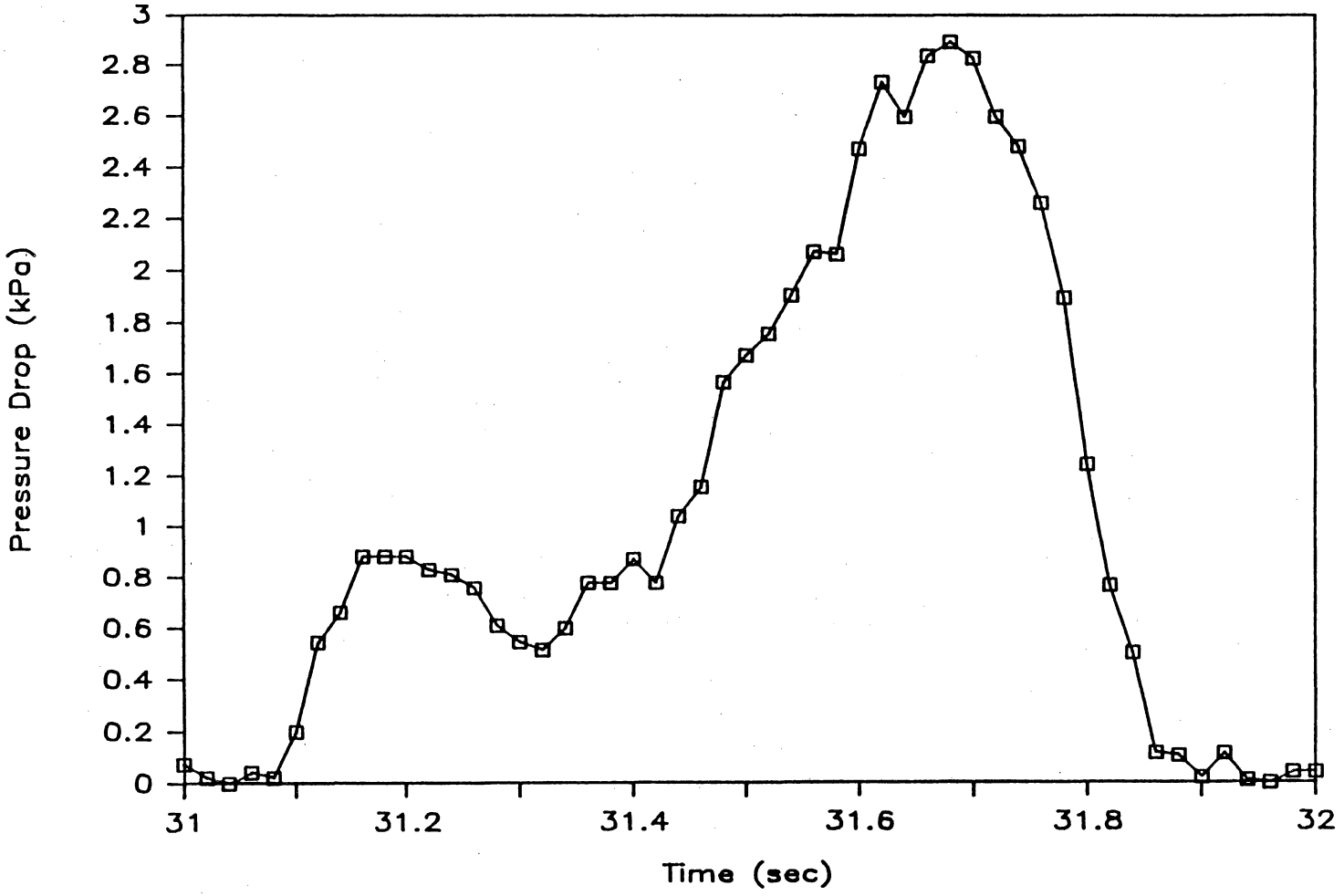

Figure D.53 Pressure Profile: Run 6, Plug #22

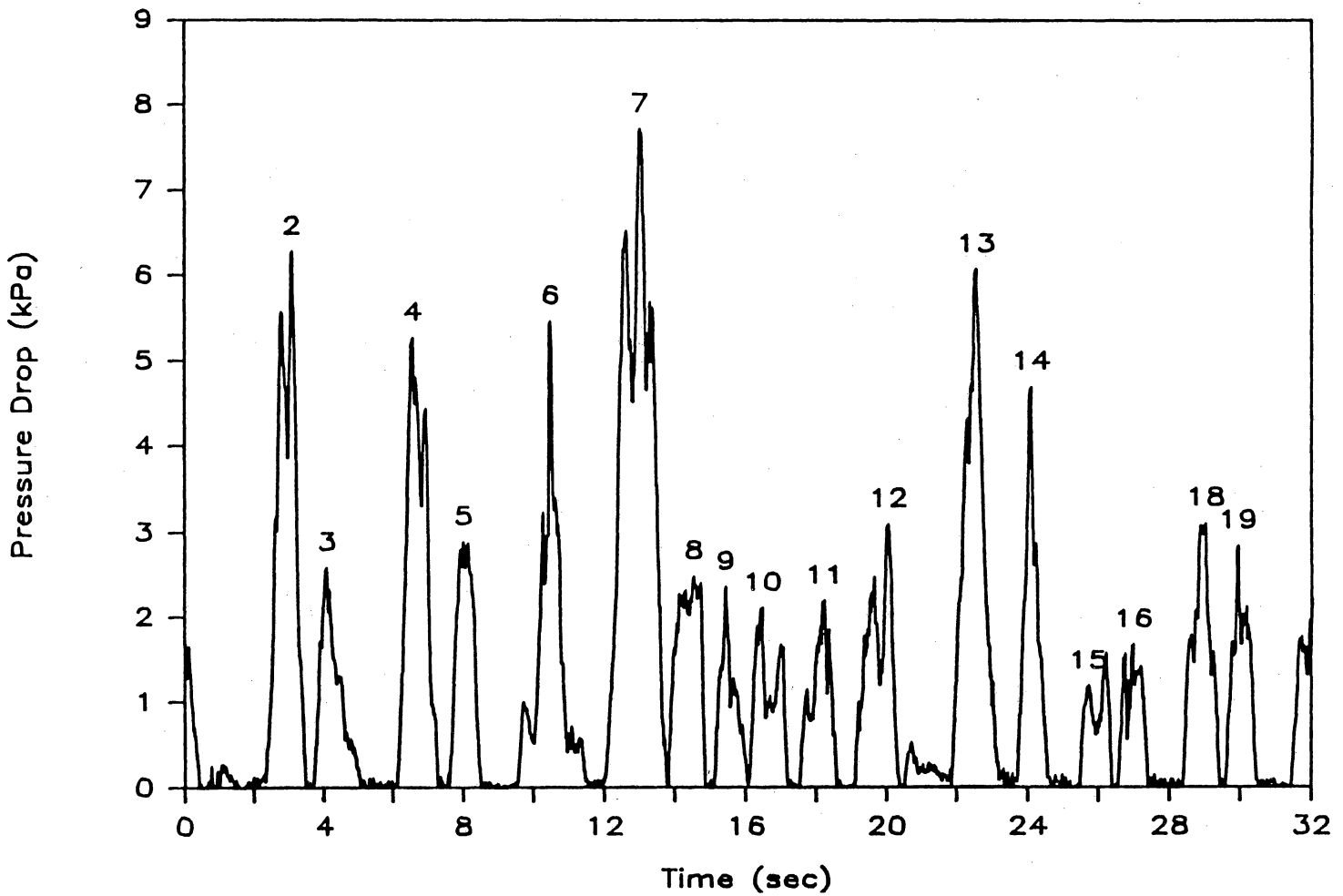

Figure D.54 Overall Pressure Profile: Run 7

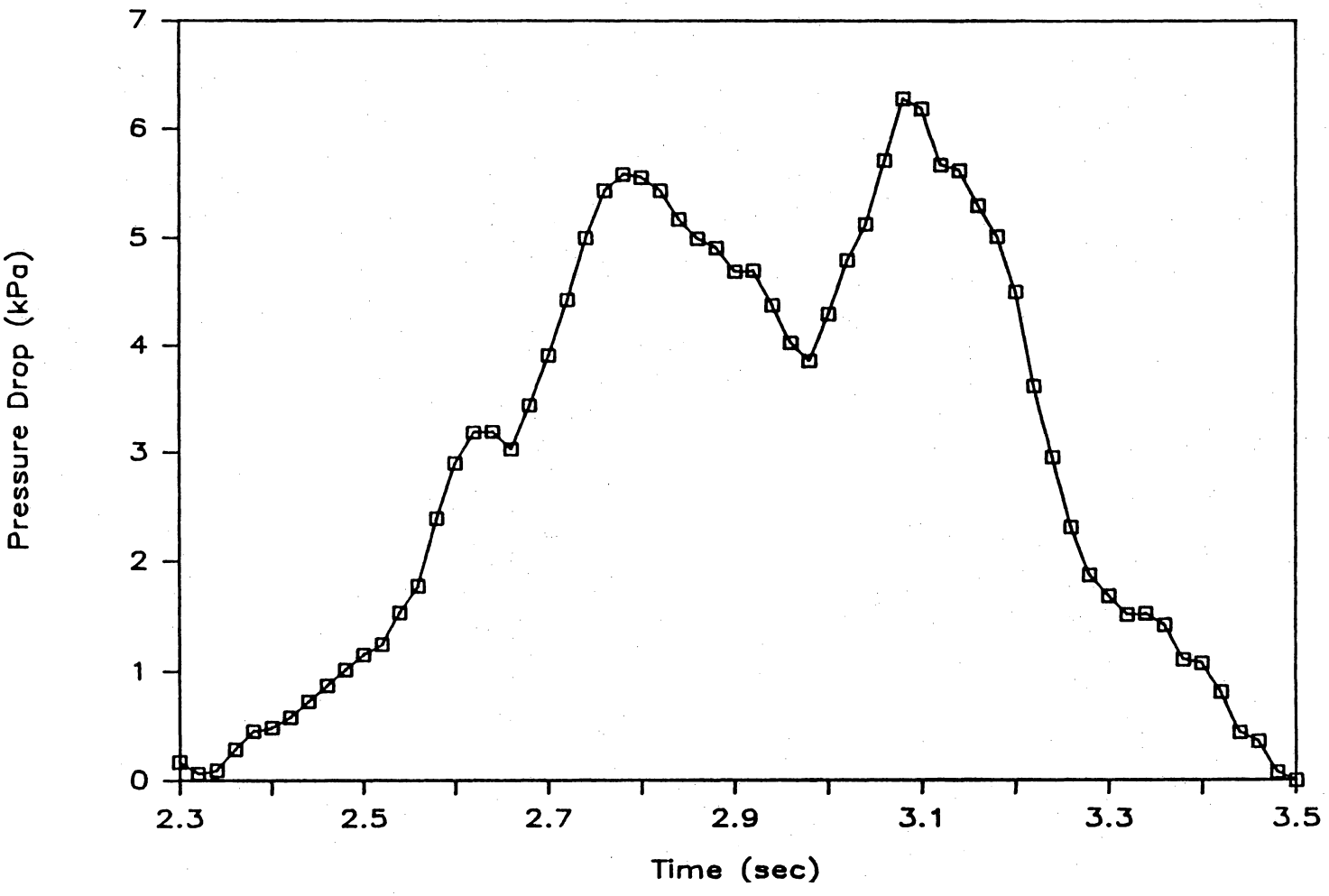

Figure D.55 Pressure Profile: Run 7, Plug #2

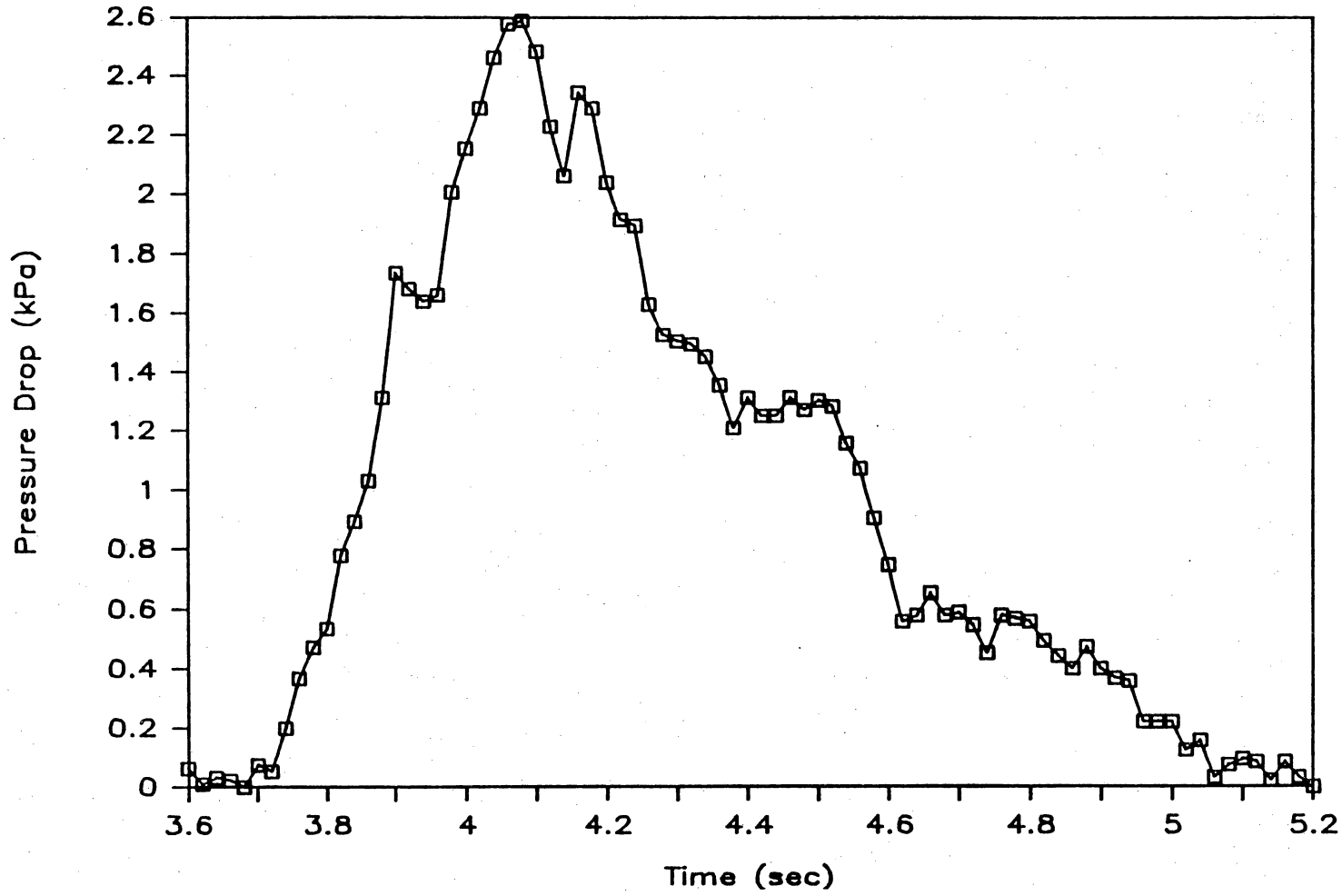

Figure D.56 Pressure Profile: Run 7, Plug #3

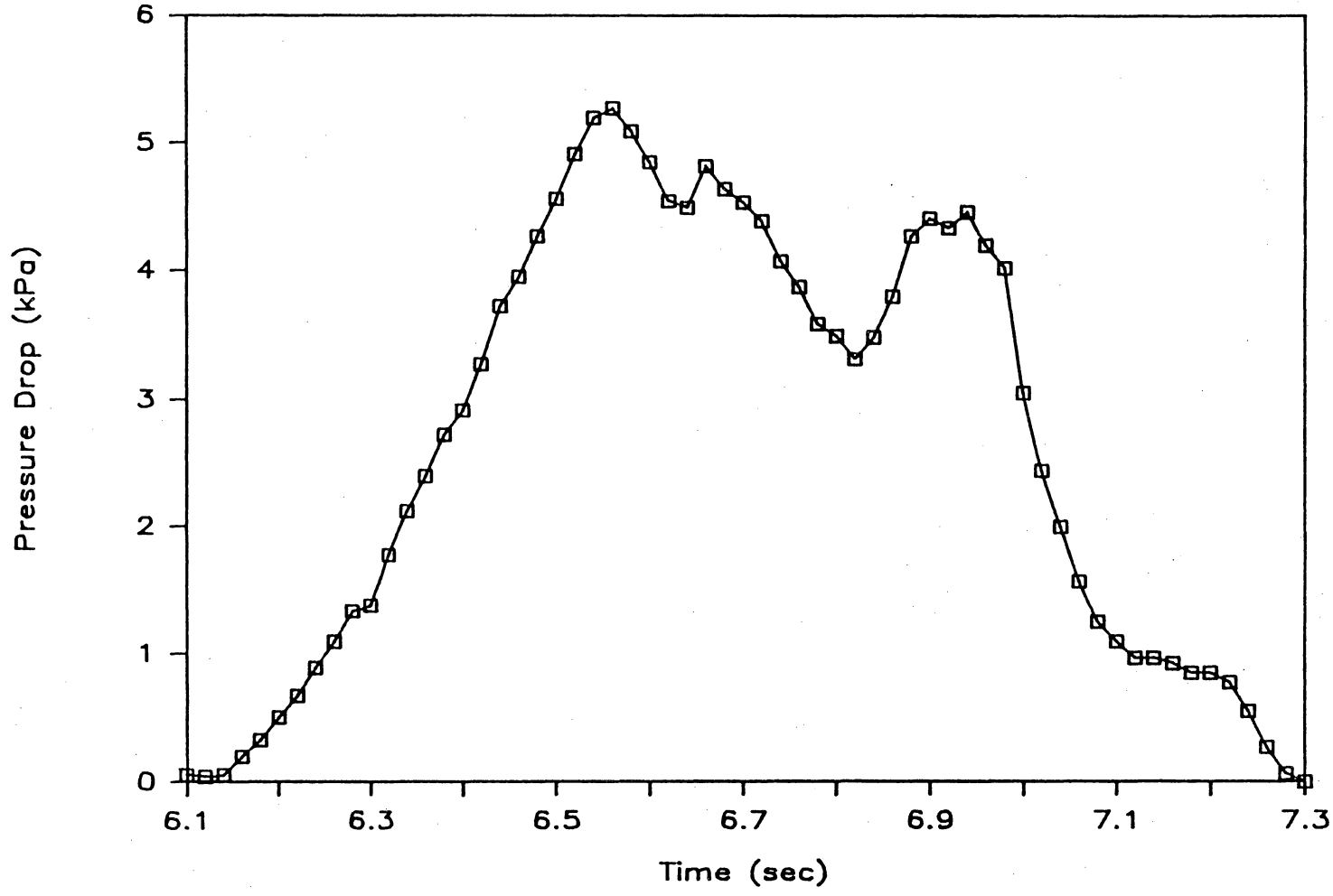

Figure D.57 Pressure Profile: Run 7, Plug #4

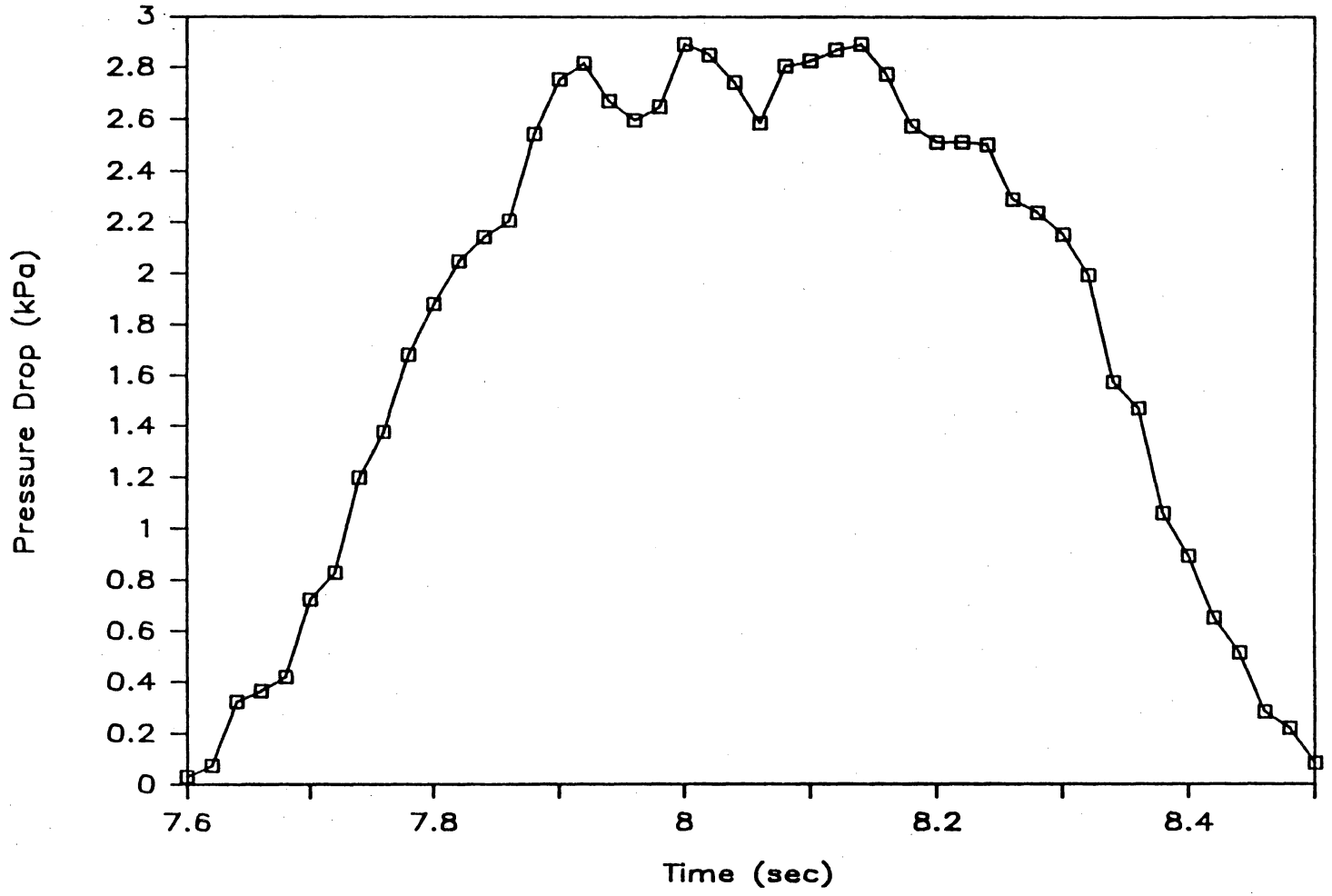

Figure D.58 Pressure Profile: Run 7, Plug #5

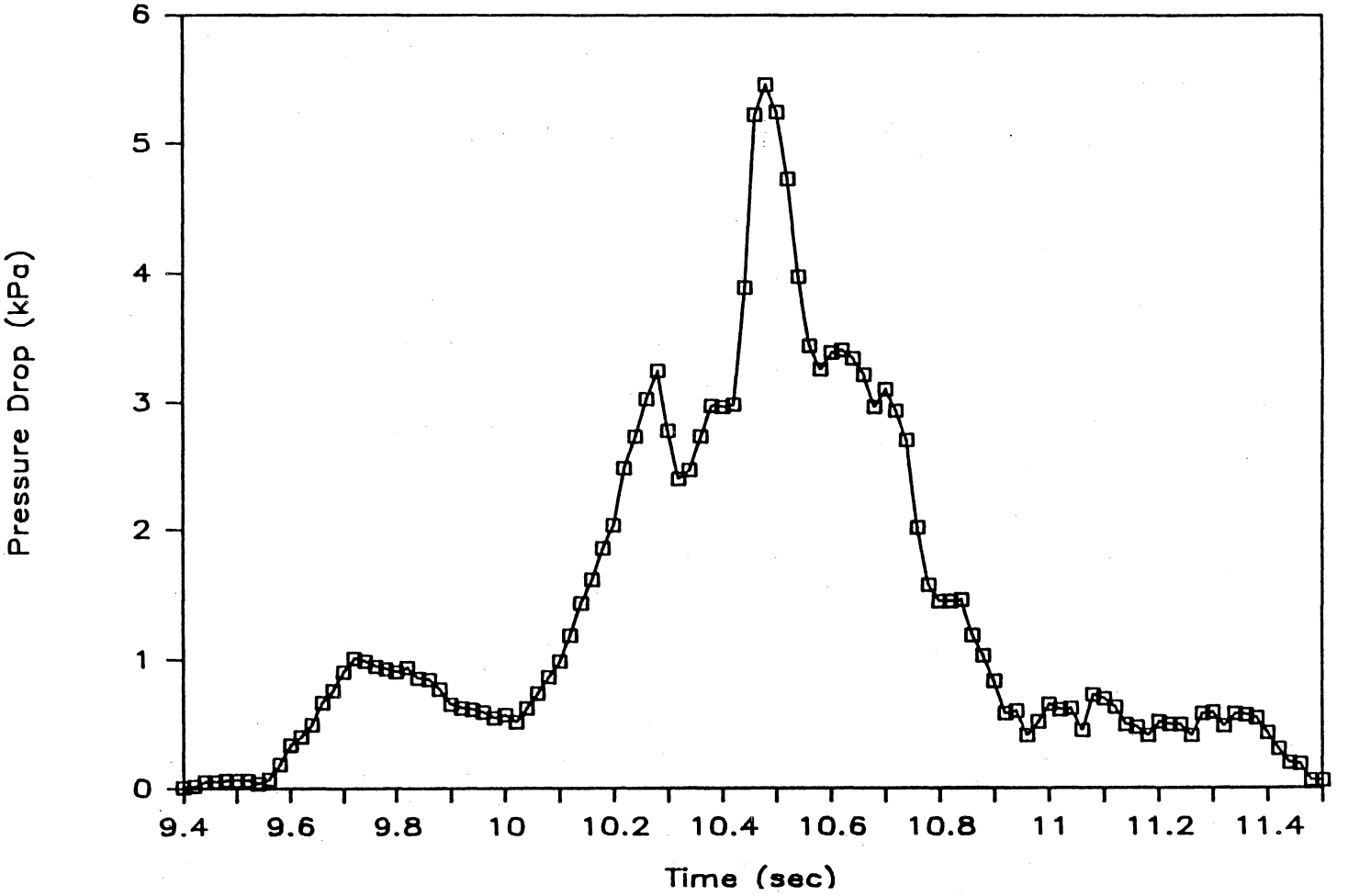

Figure D.59 Pressure Profile: Run 7, Plug #6

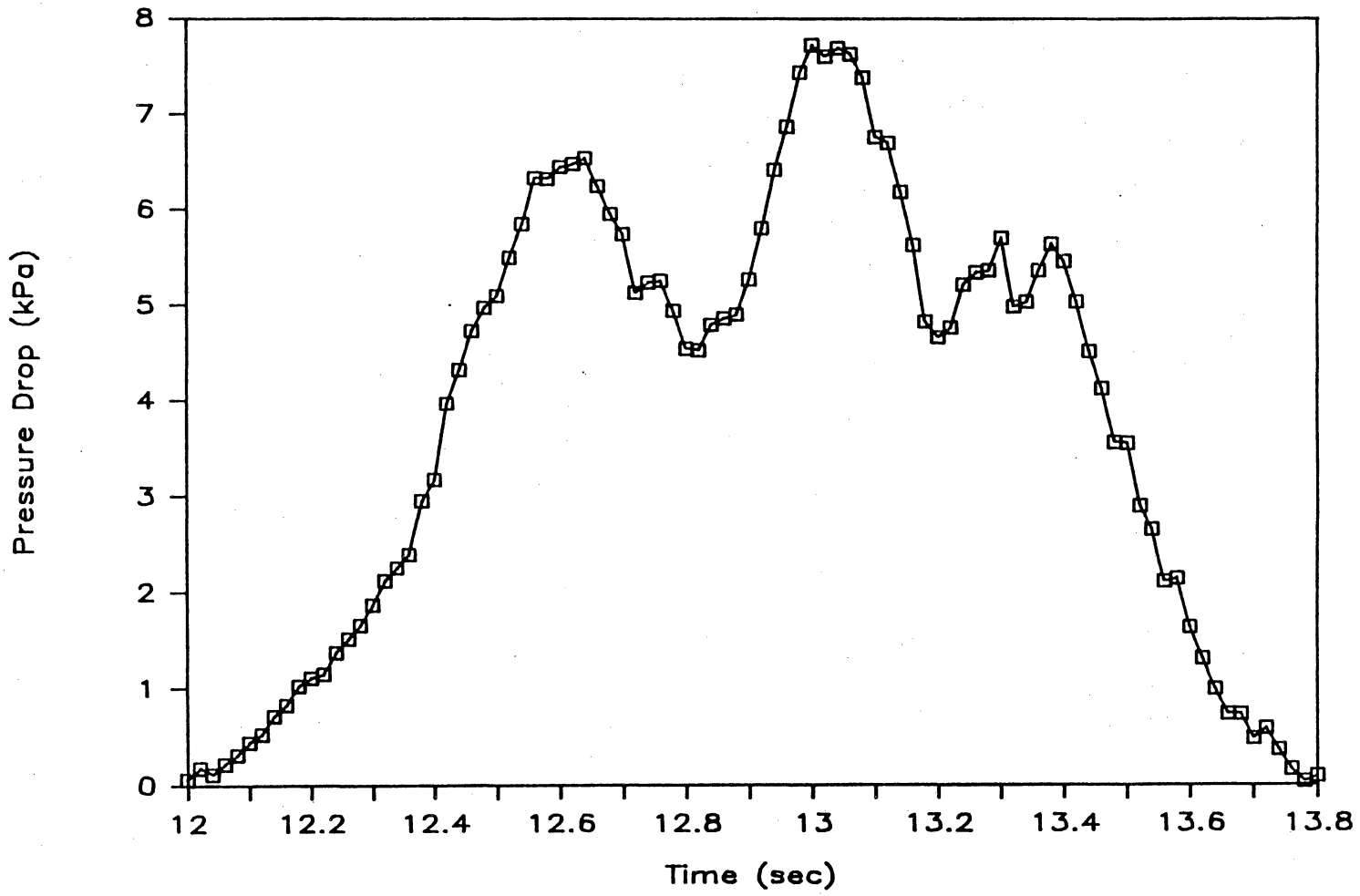

Figure D.60 Pressure Profile: Run 7, Plug #7

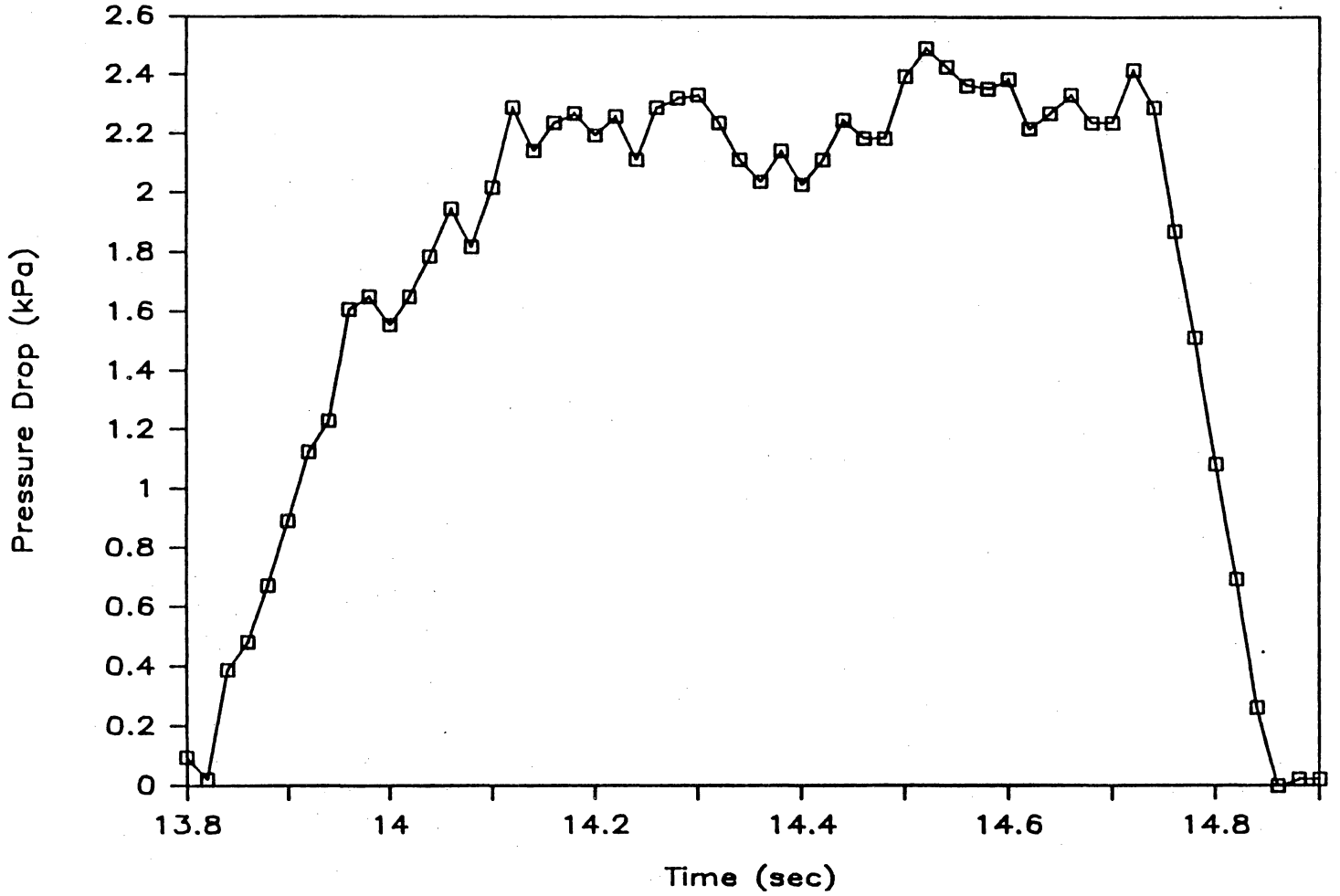

Figure D.61 Pressure Profile: Run 7, Plug #8

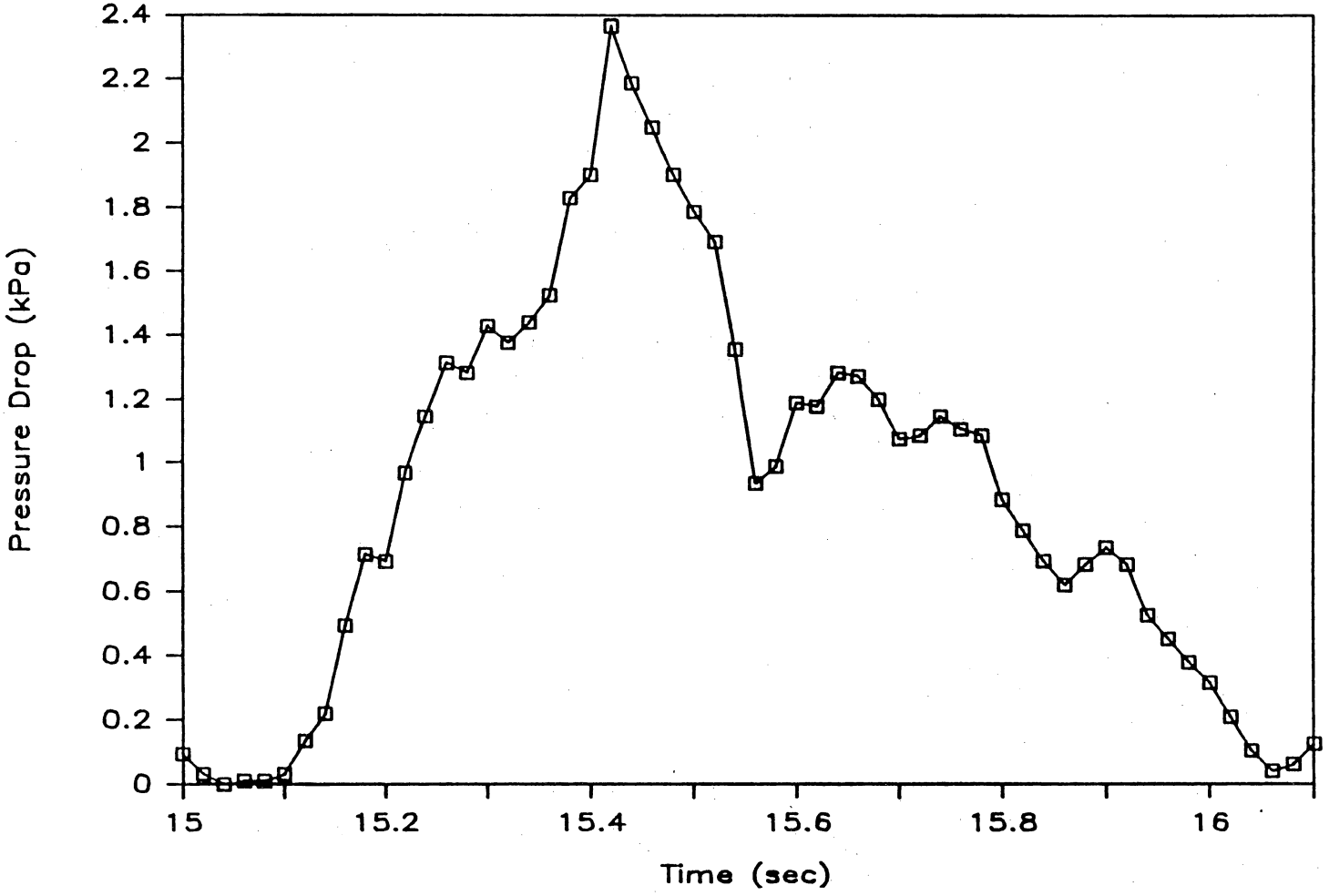

Figure D.62 Pressure Profile: Run 7, Plug #9

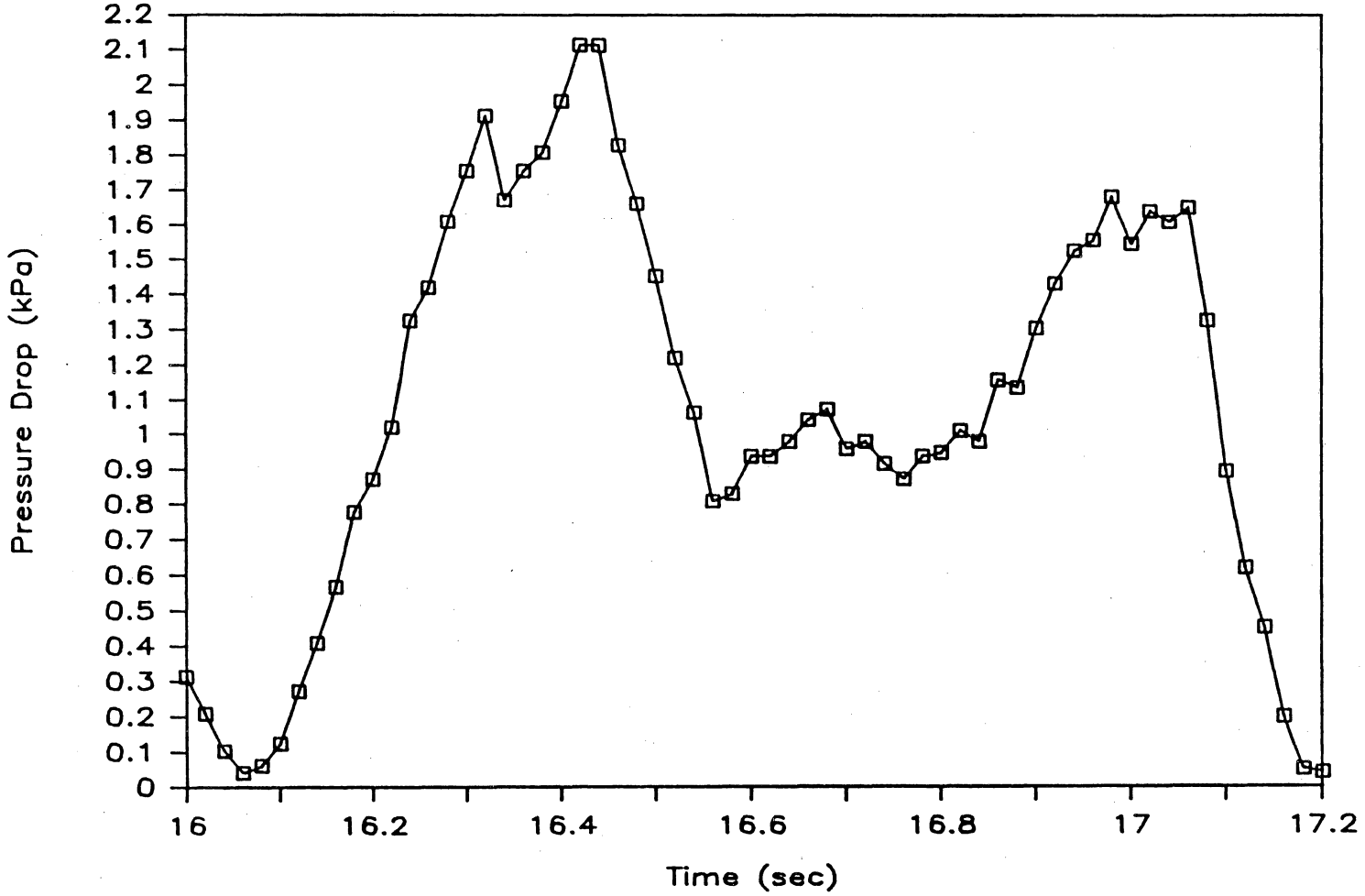

Figure D.63 Pressure Profile: Run 7, Plug #10

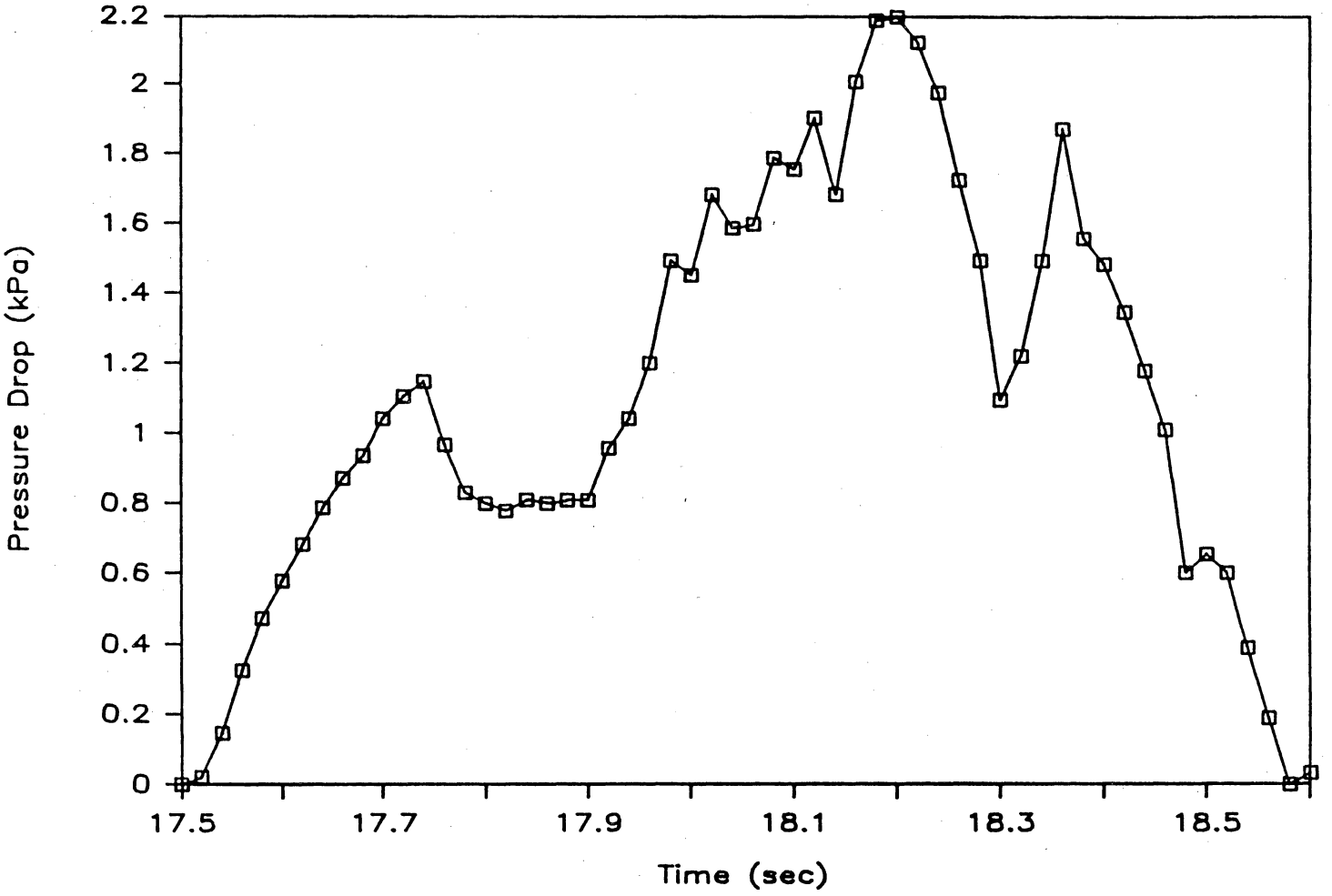

Figure D.64 Pressure Profile: Run 7, Plug #11

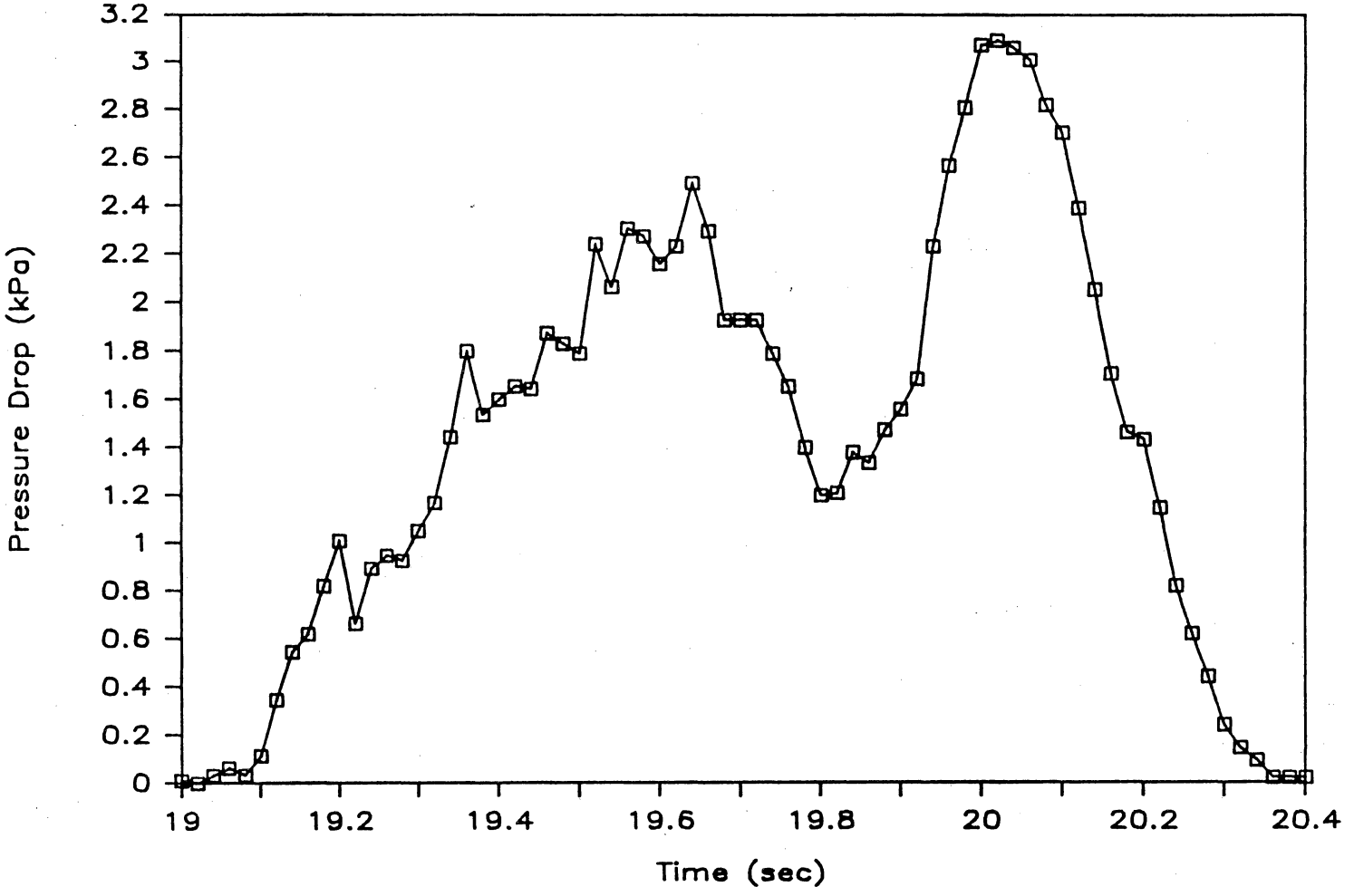

Figure D.65 Pressure Profile: Run 7, Plug #12

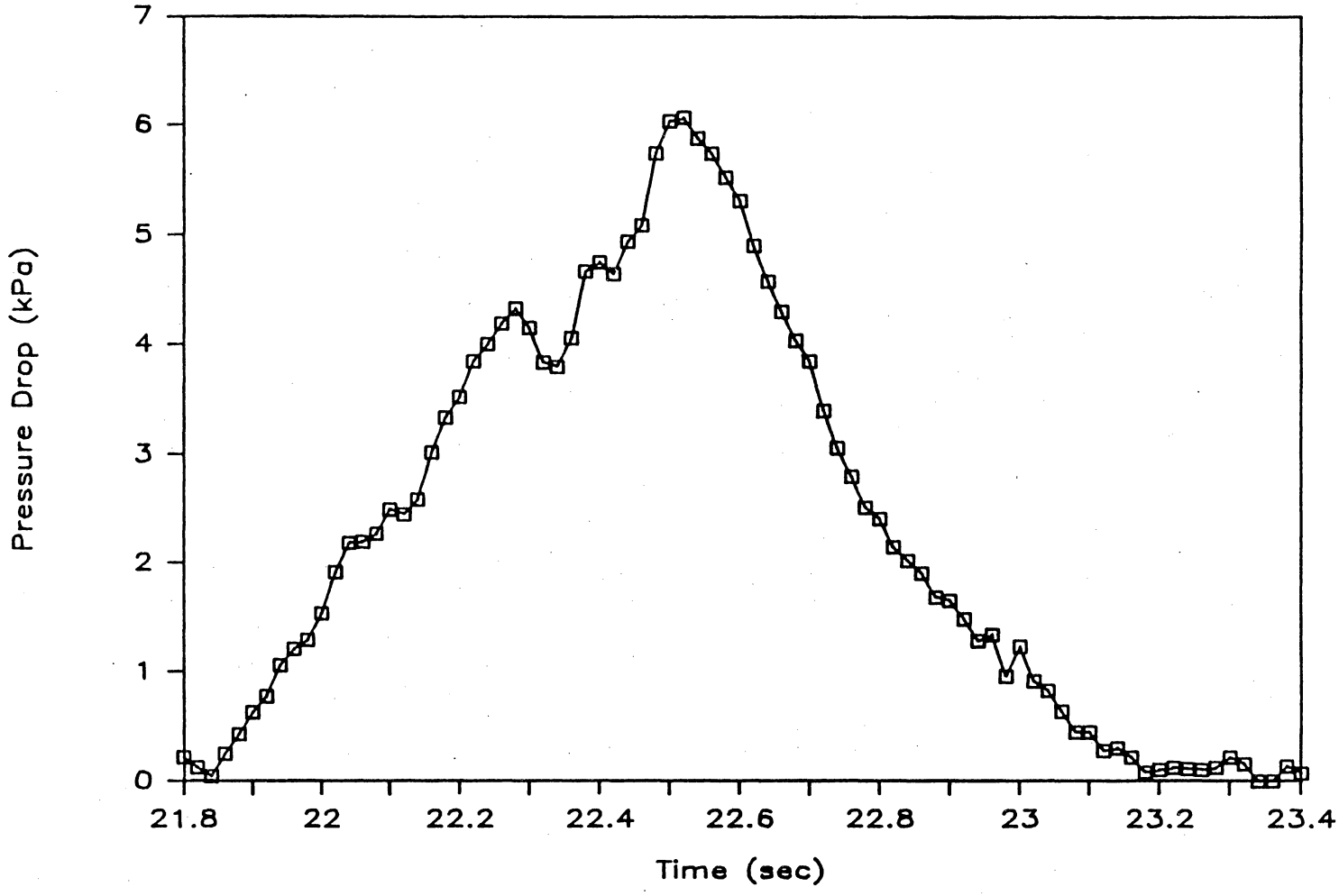

Figure D.66 Pressure Profile: Run 7, Plug #13

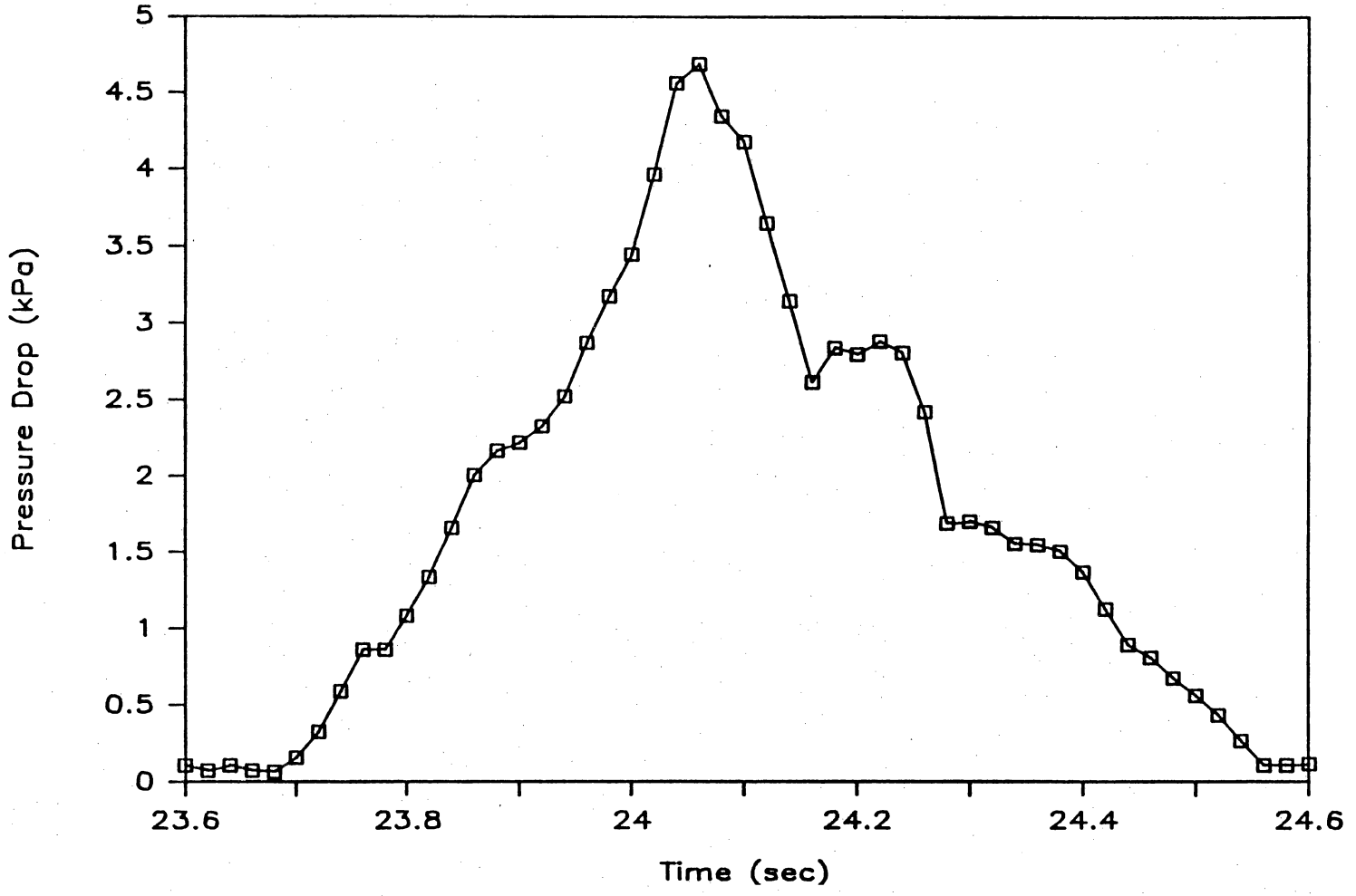

Figure D.67 Pressure Profile: Run 7, Plug #14

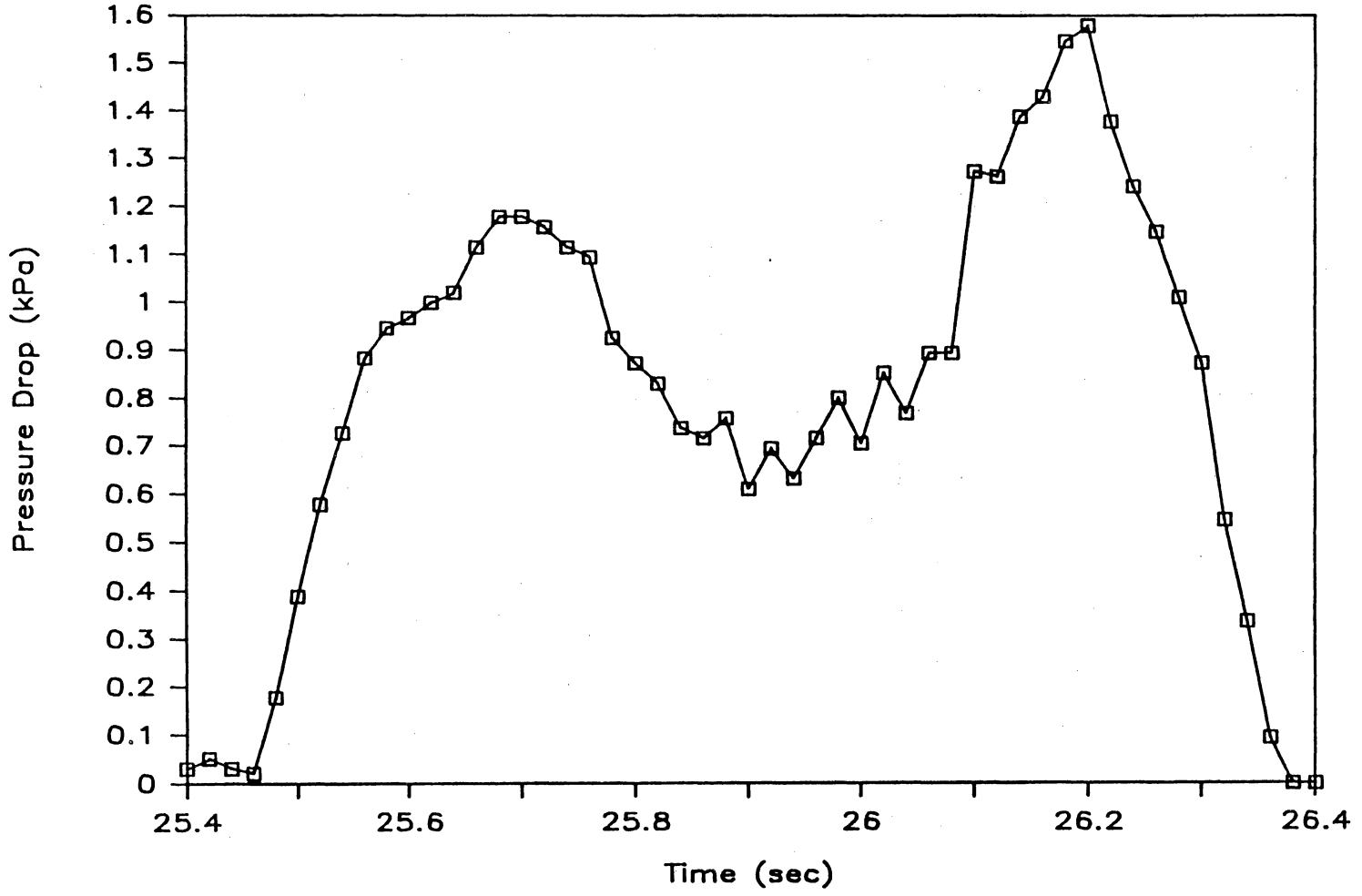

Figure D.68 Pressure Profile: Run 7, Plug #15

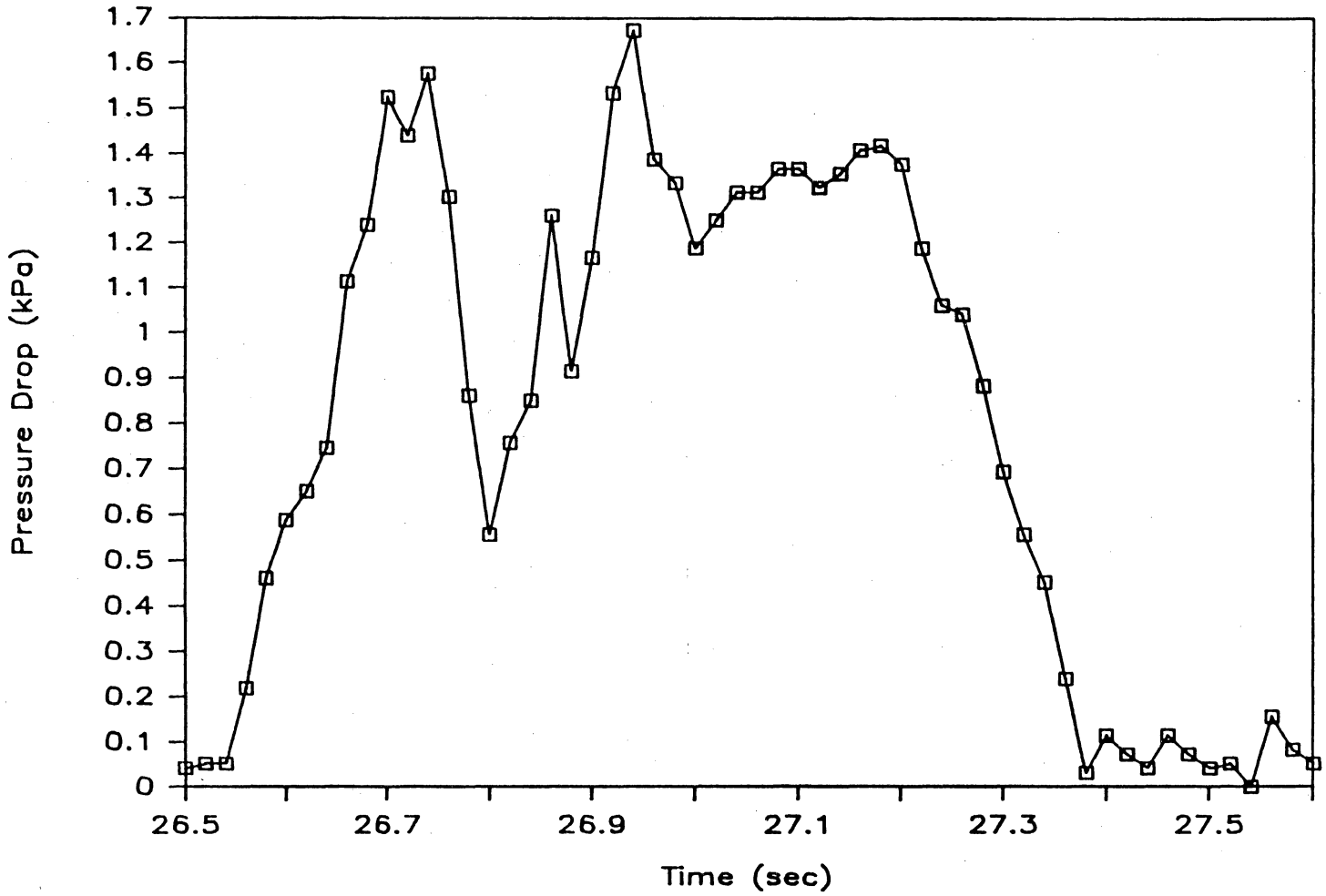

Figure D.69 Pressure Profile: Run 7, Plugs #16 & 17

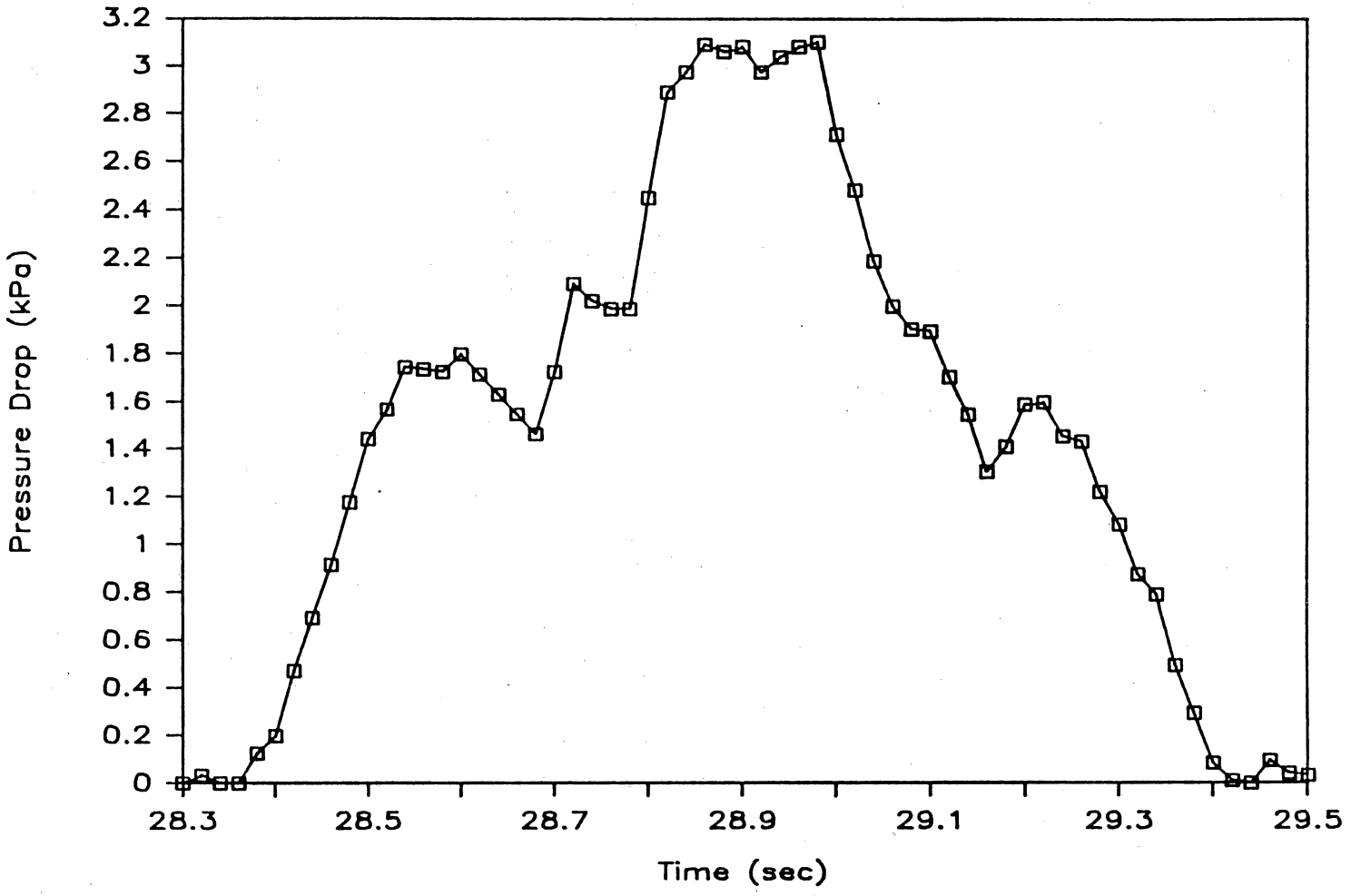

Figure D.70 Pressure Profile: Run 7, Plug #18

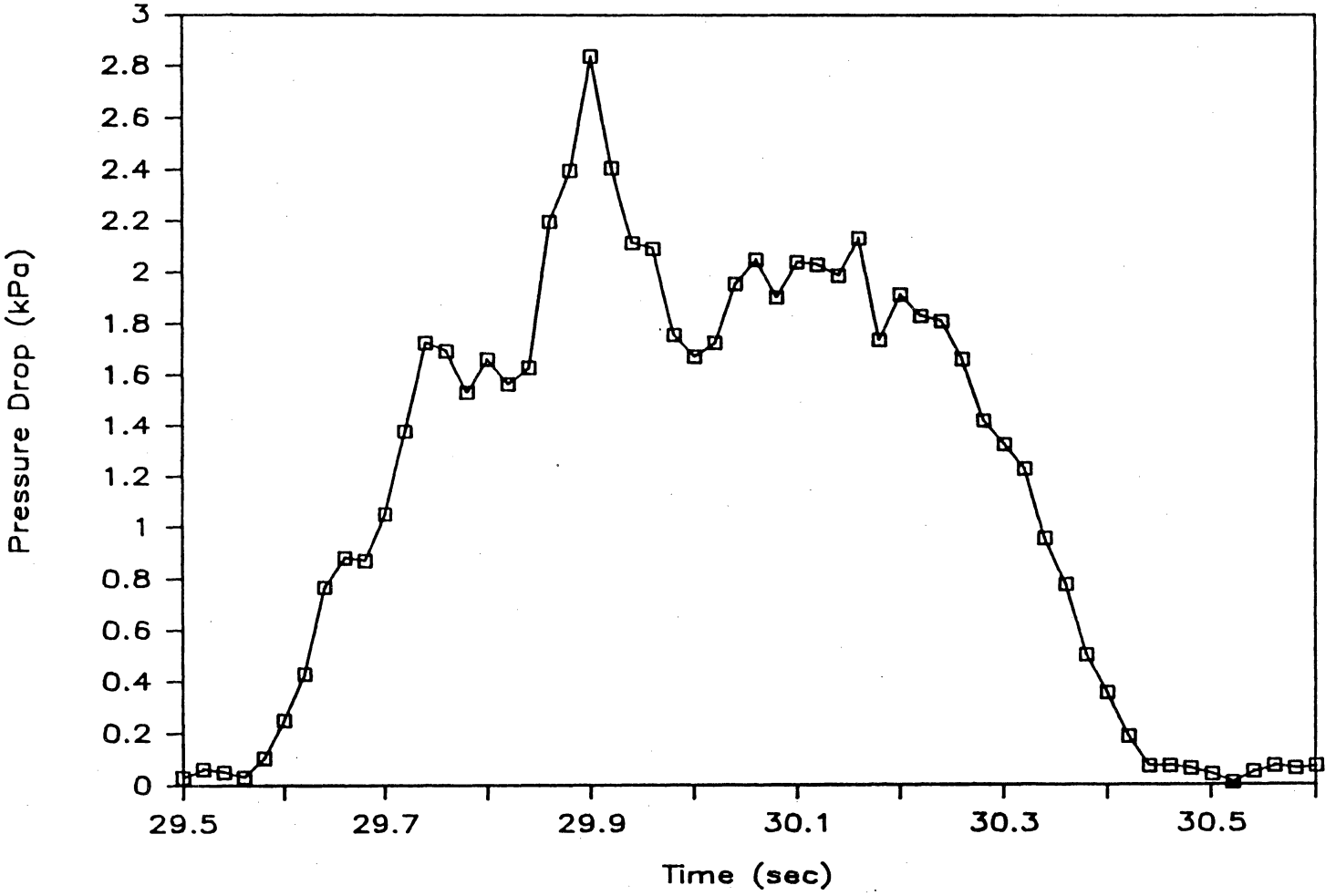

Figure D.71 Pressure Profile: Run 7, Plug #19

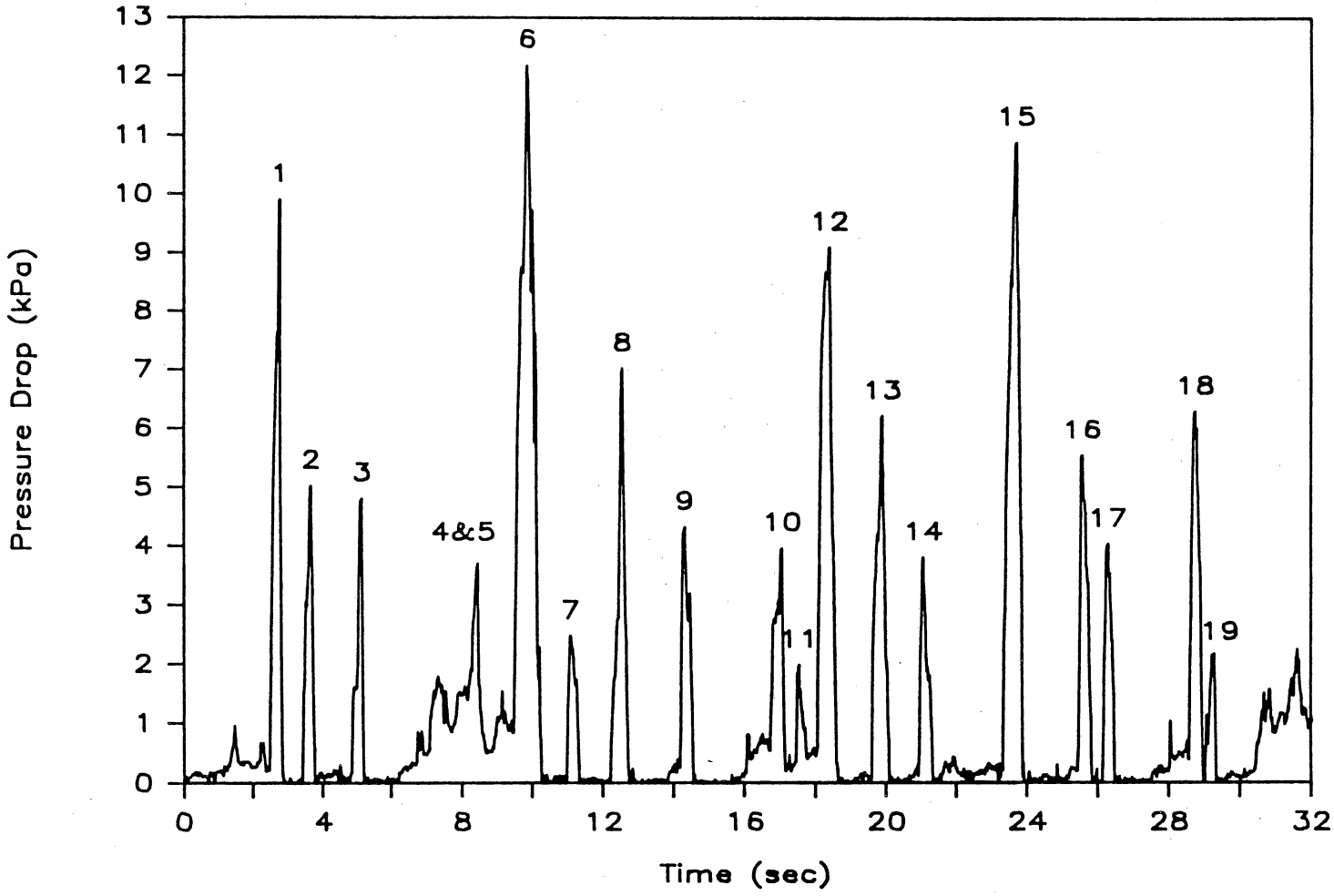

Figure D.72 Overall Pressure Profile: Run 8

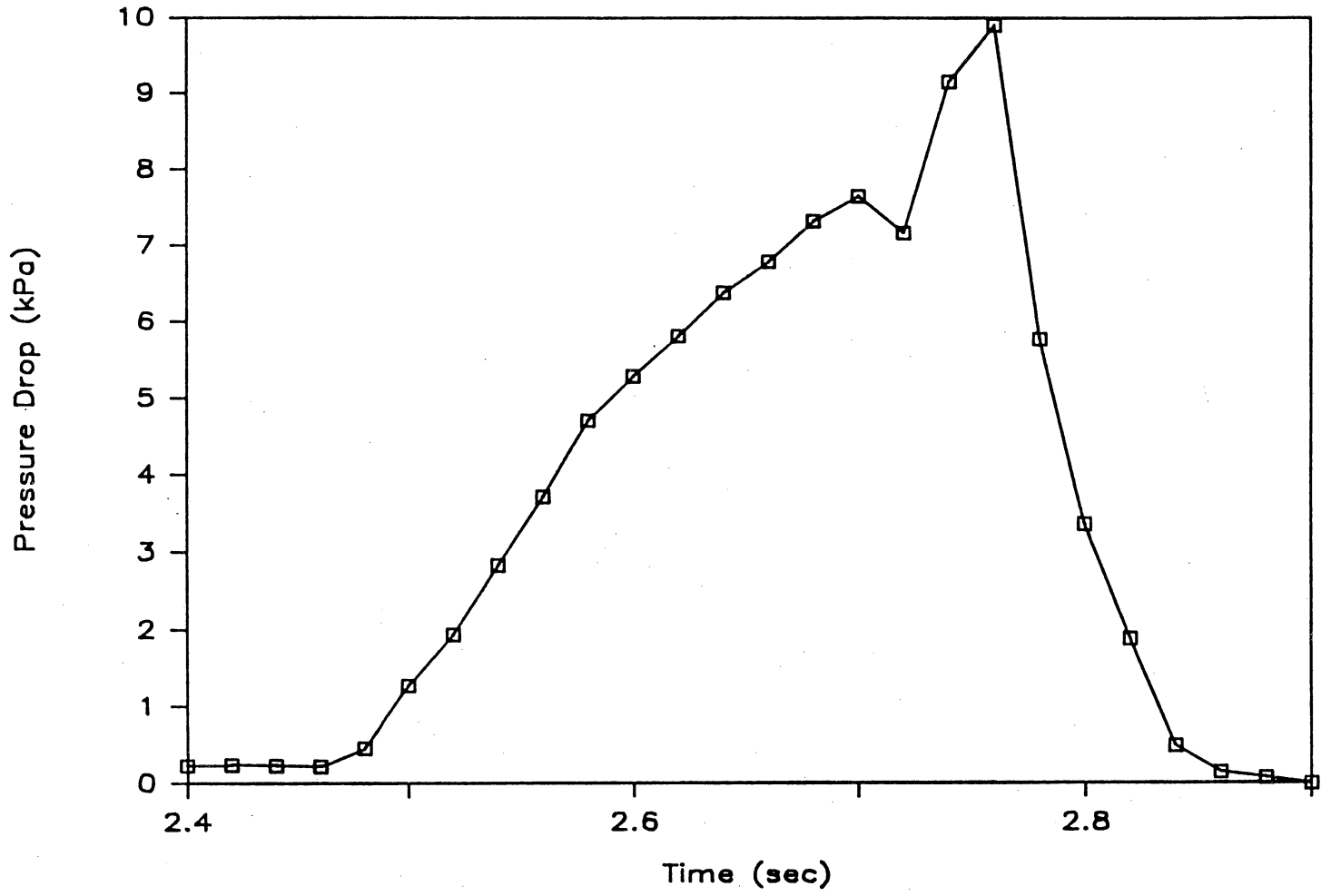

Figure D.73 Pressure Profile: Run 8, Plug #1

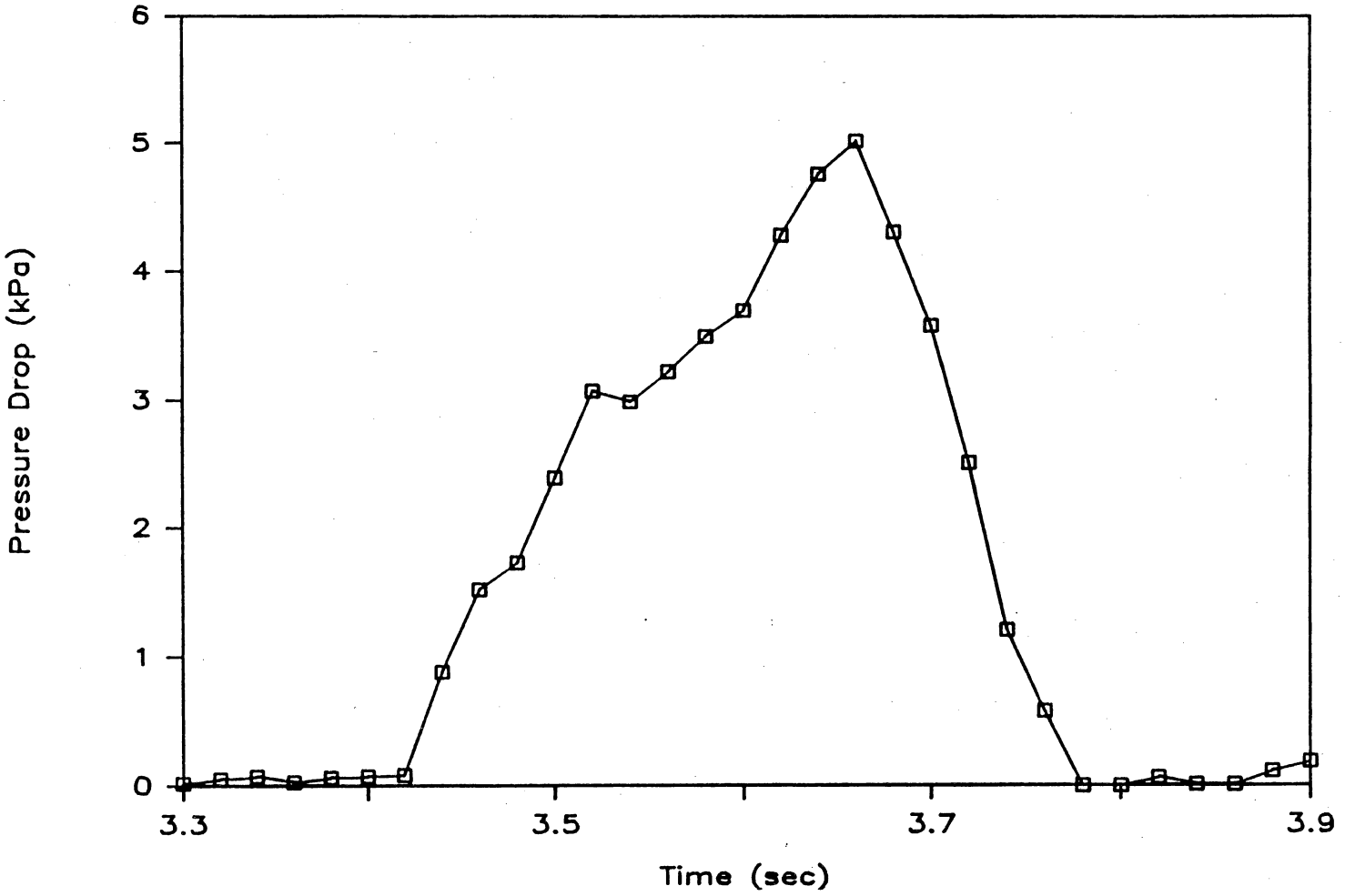

Figure D.74 Pressure Profile: Run 8, Plug #2

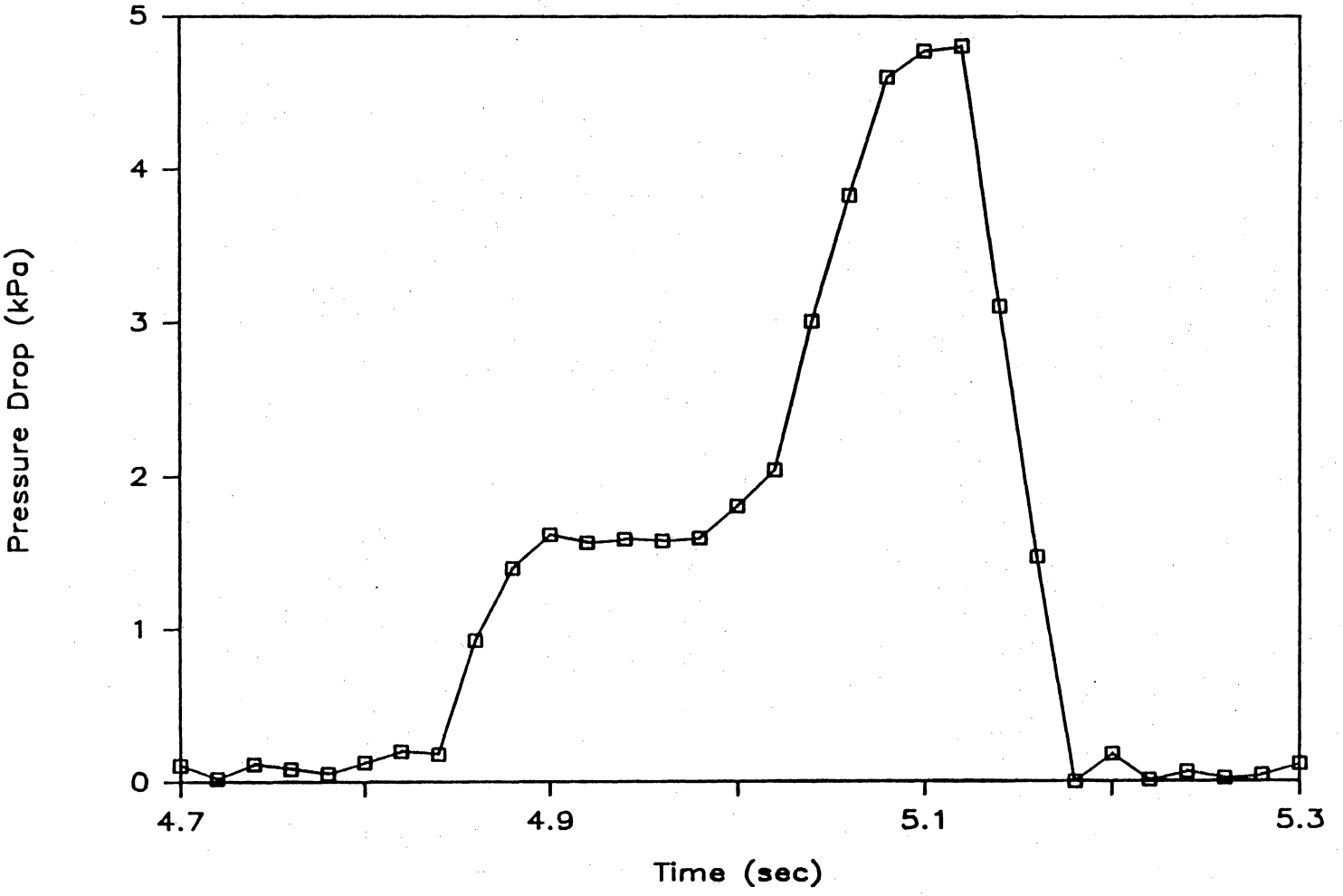

Figure D.75 Pressure Profile: Run 8, Plug #3

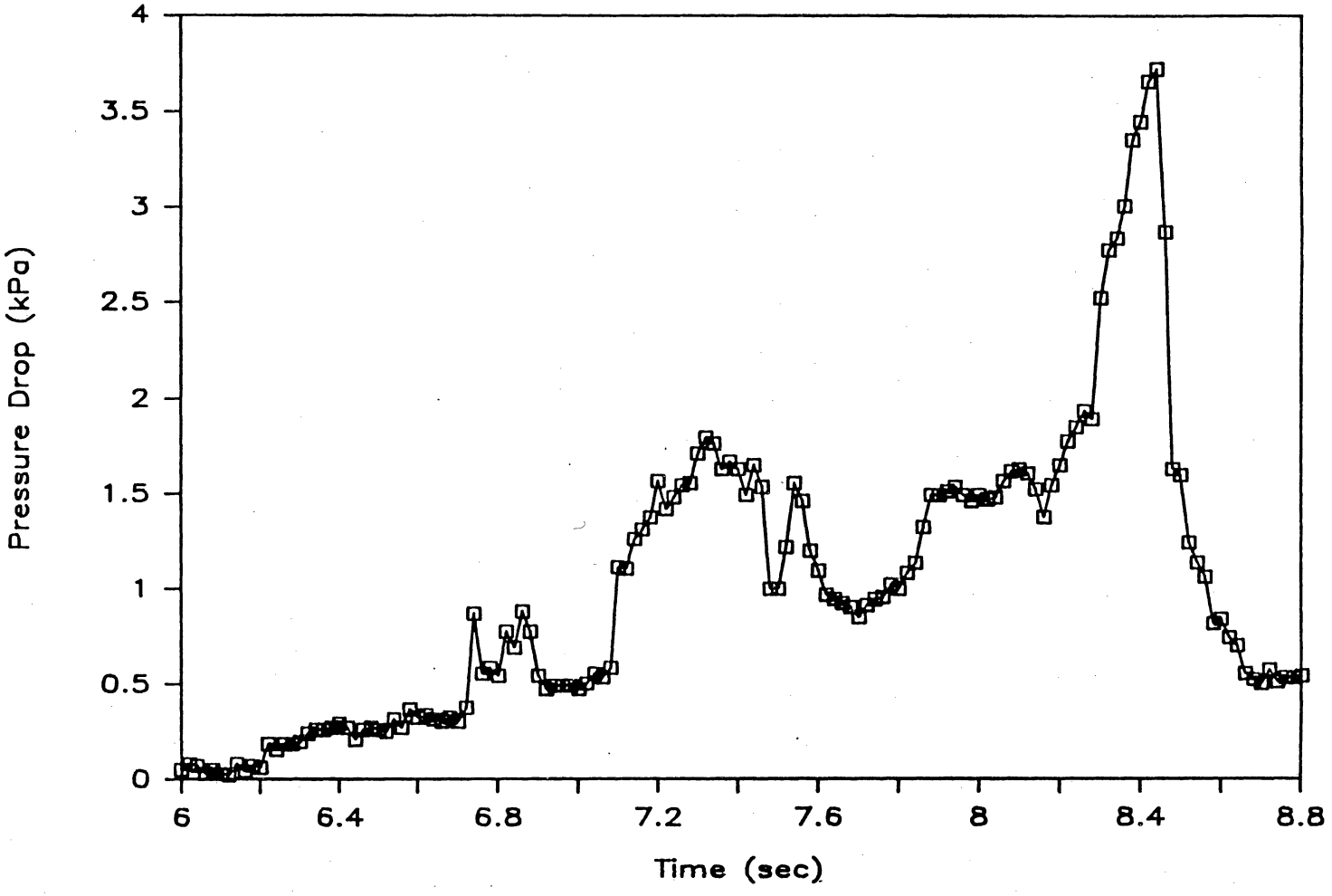

Figure D.76 Pressure Profile: Run 8, Plugs #4 & 5

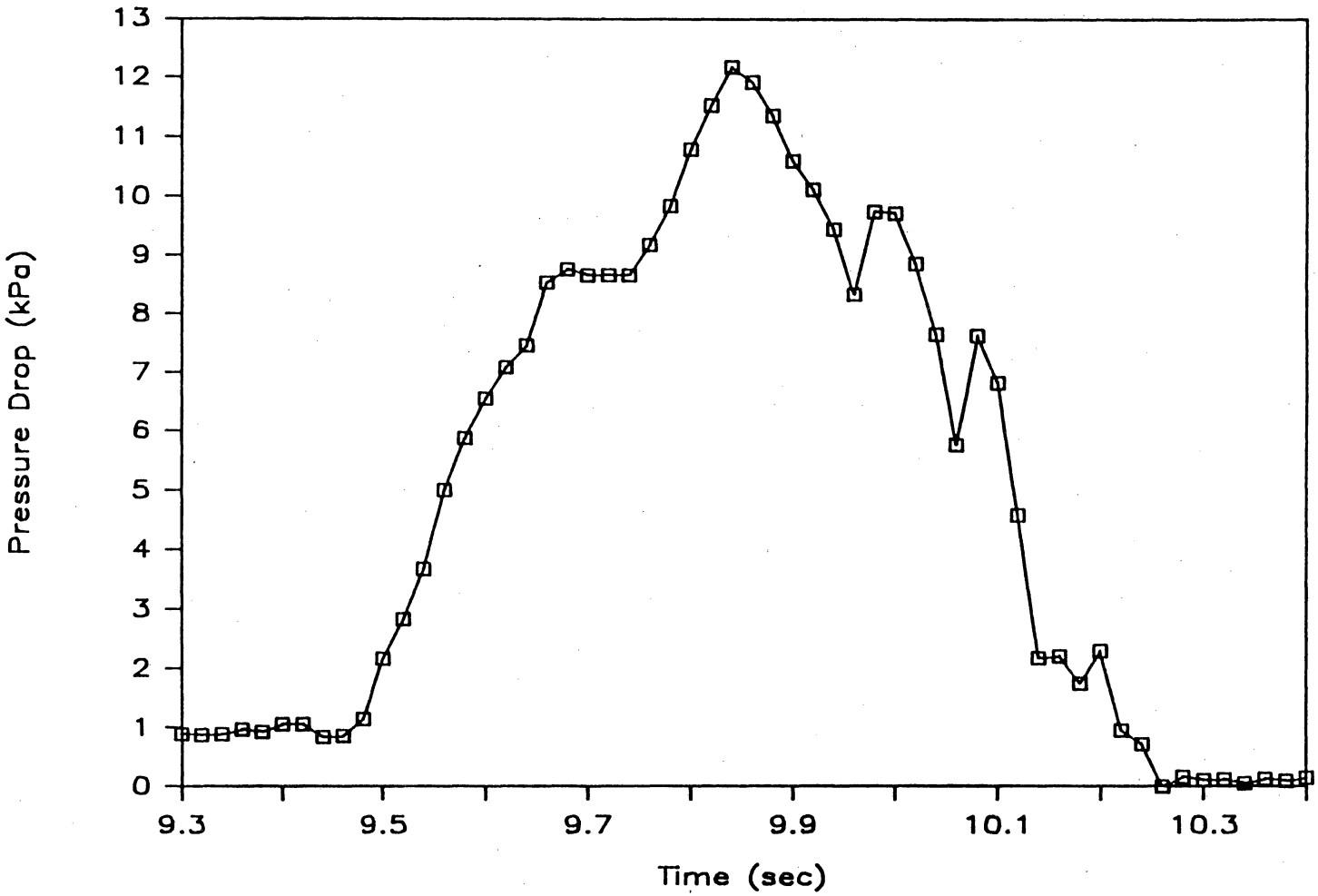

Figure D.77 Pressure Profile: Run 8, Plug #6

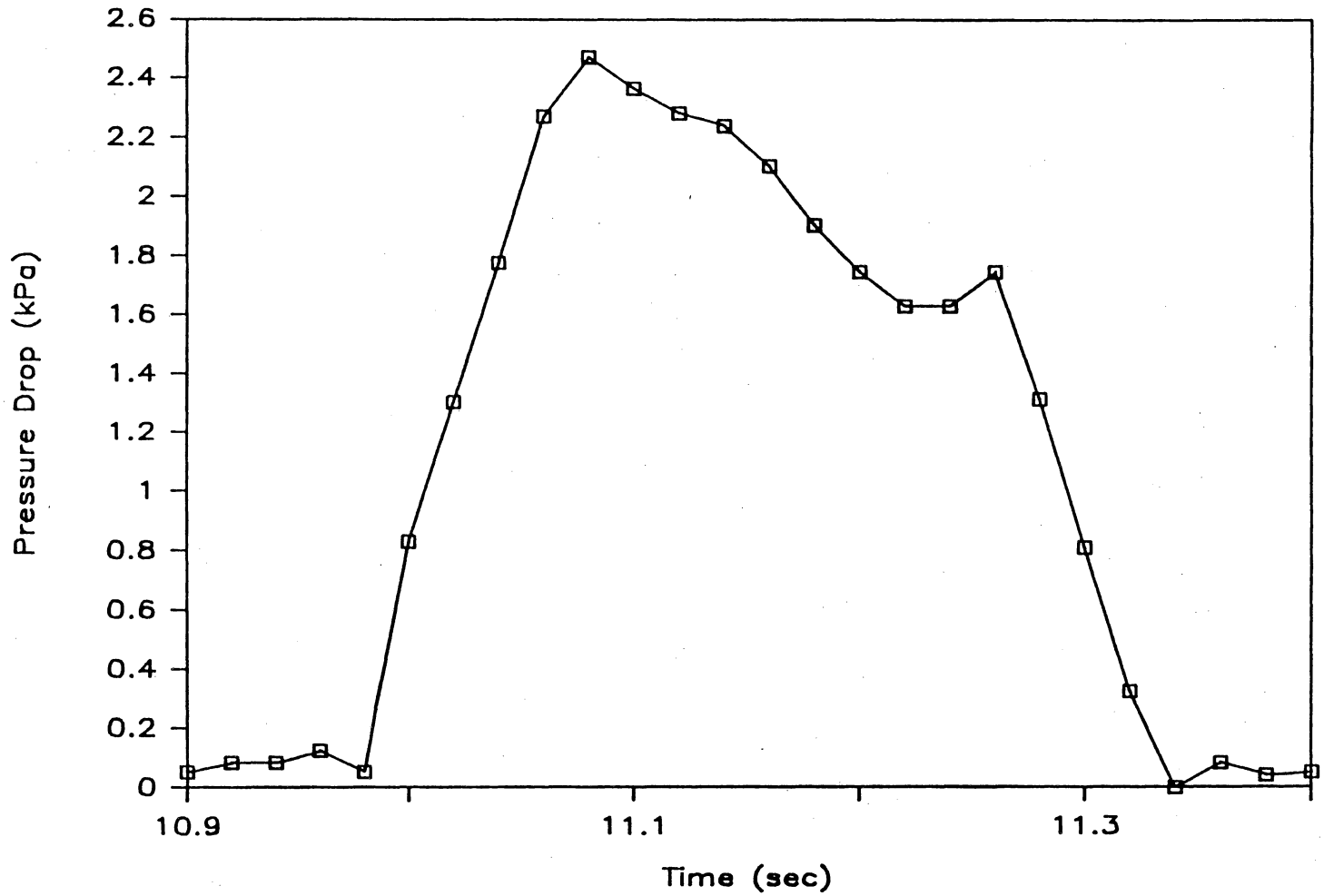

Figure D.78 Pressure Profile: Run 8, Plug #7

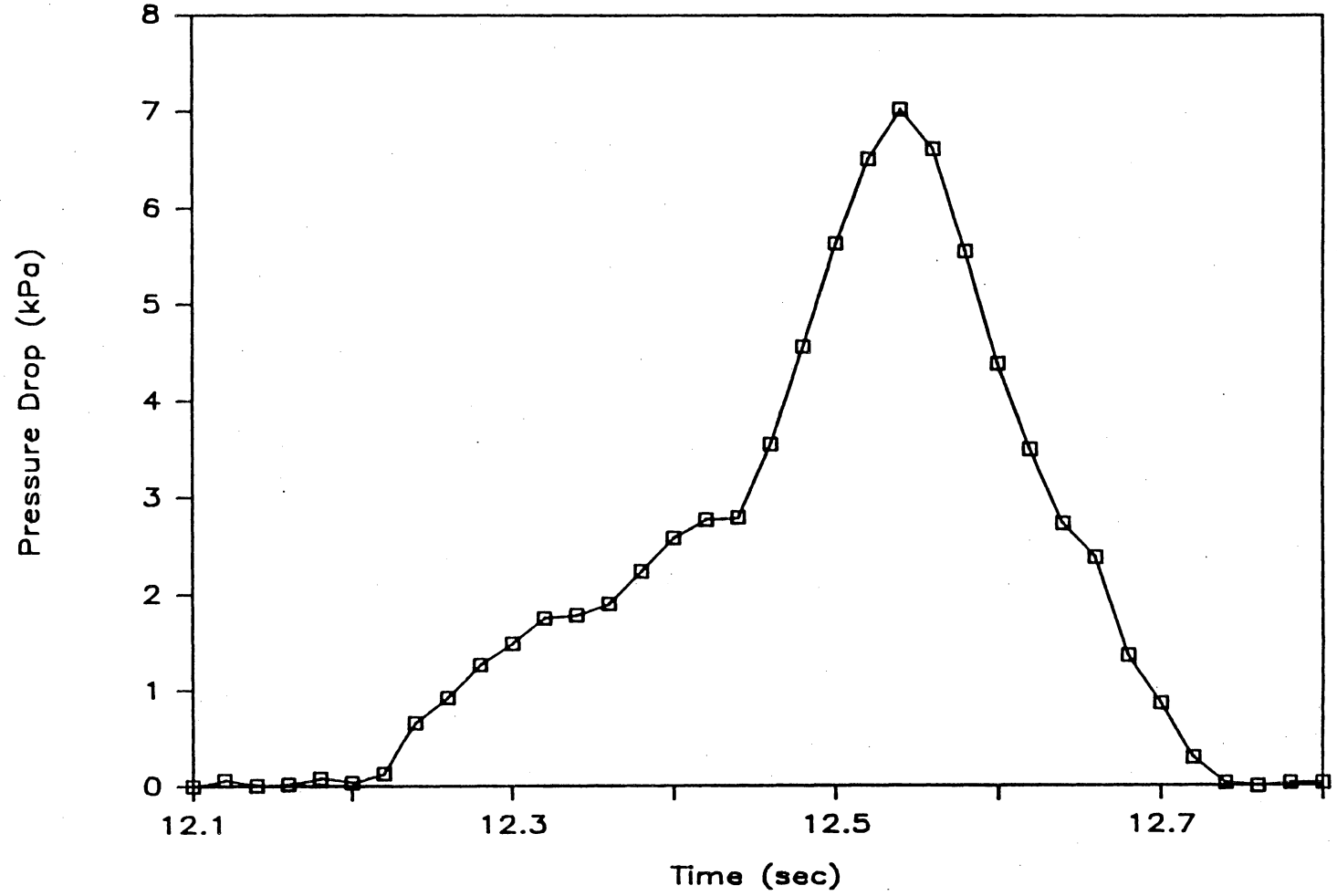

Figure D.79 Pressure Profile: Run 8, Plug #8

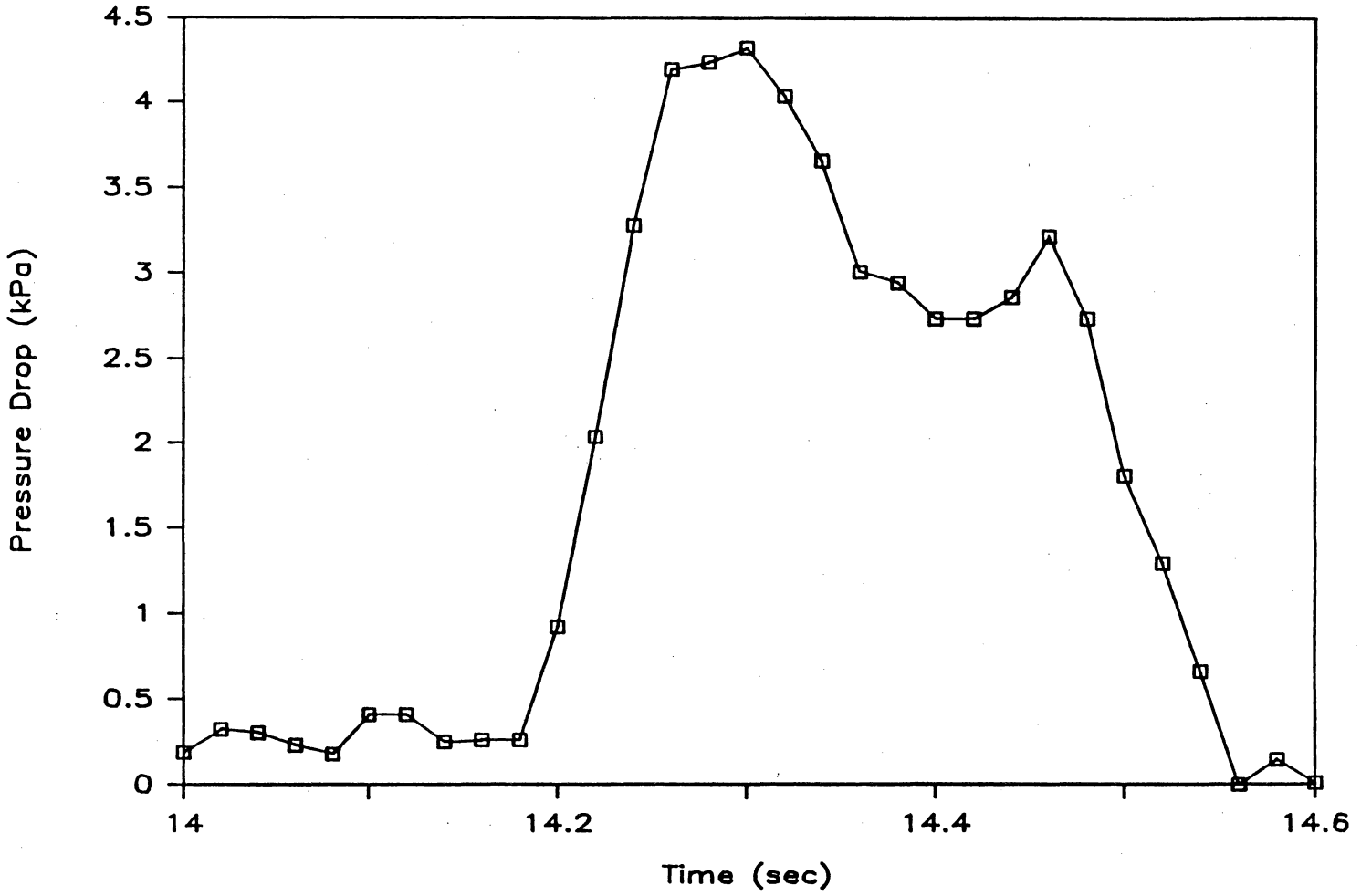

Figure D.80 Pressure Profile: Run 8, Plug #9

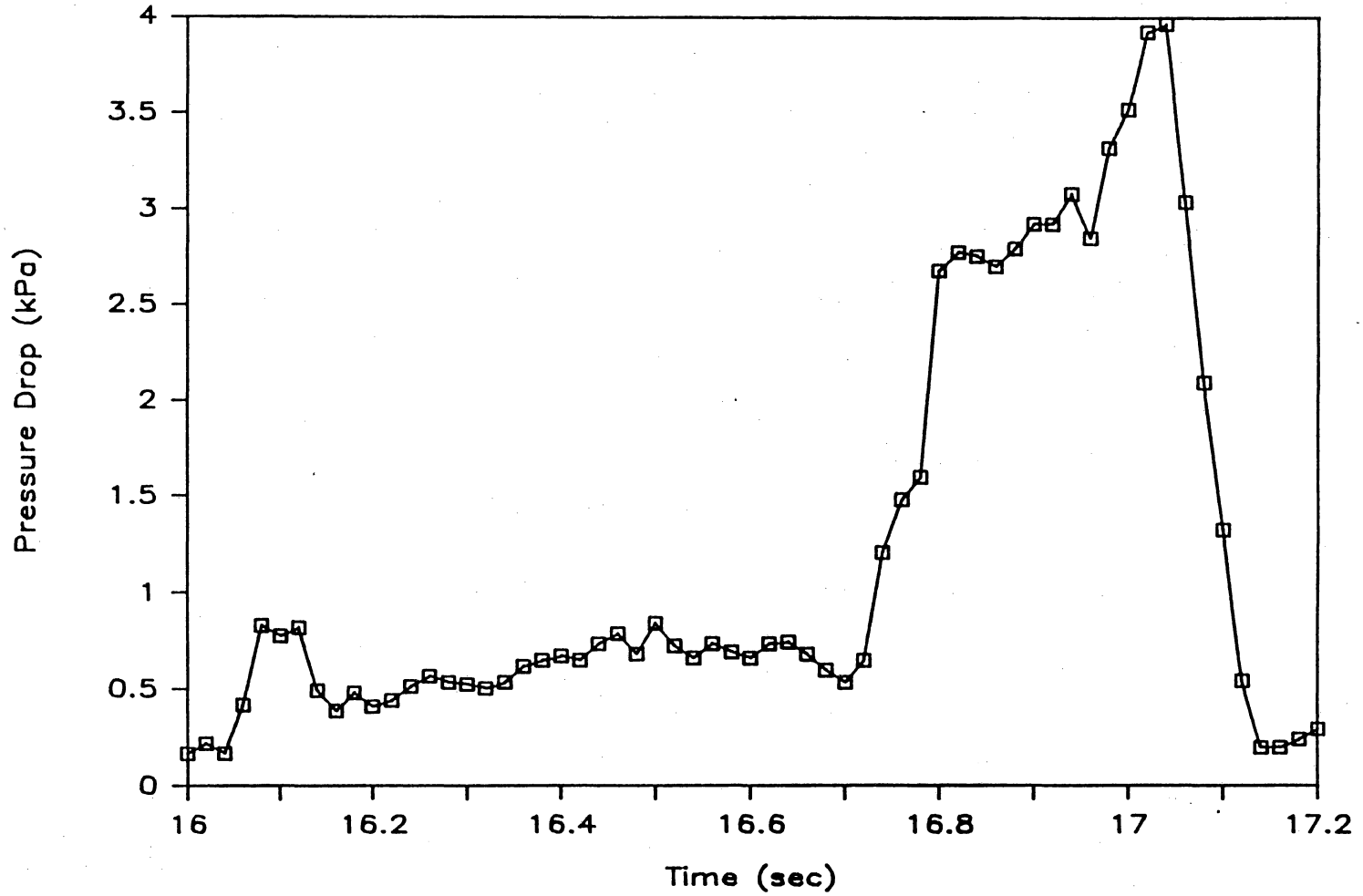

Figure D.81 Pressure Profile: Run 8, Plug #10

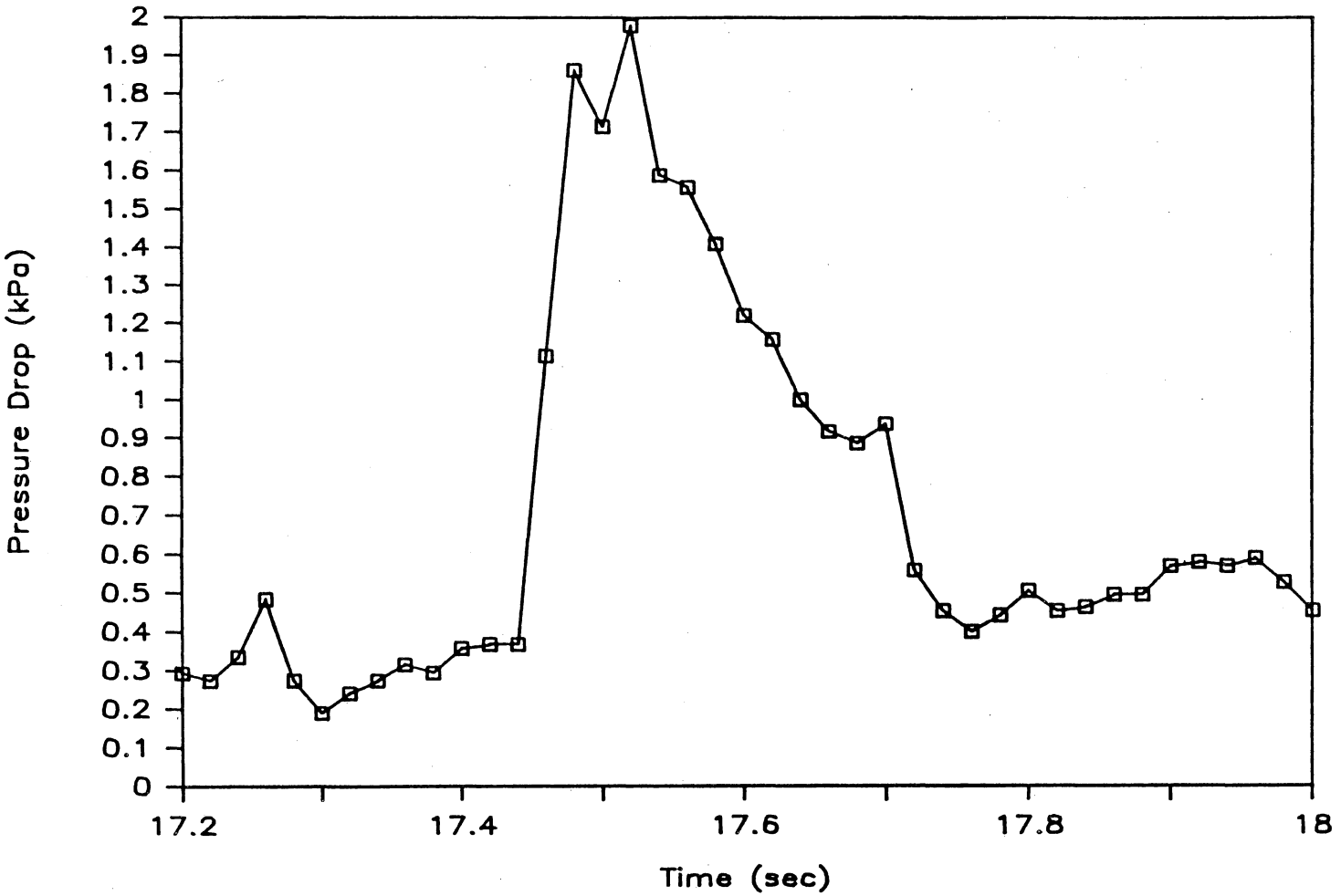

Figure D.82 Pressure Profile: Run 8, Plug #11

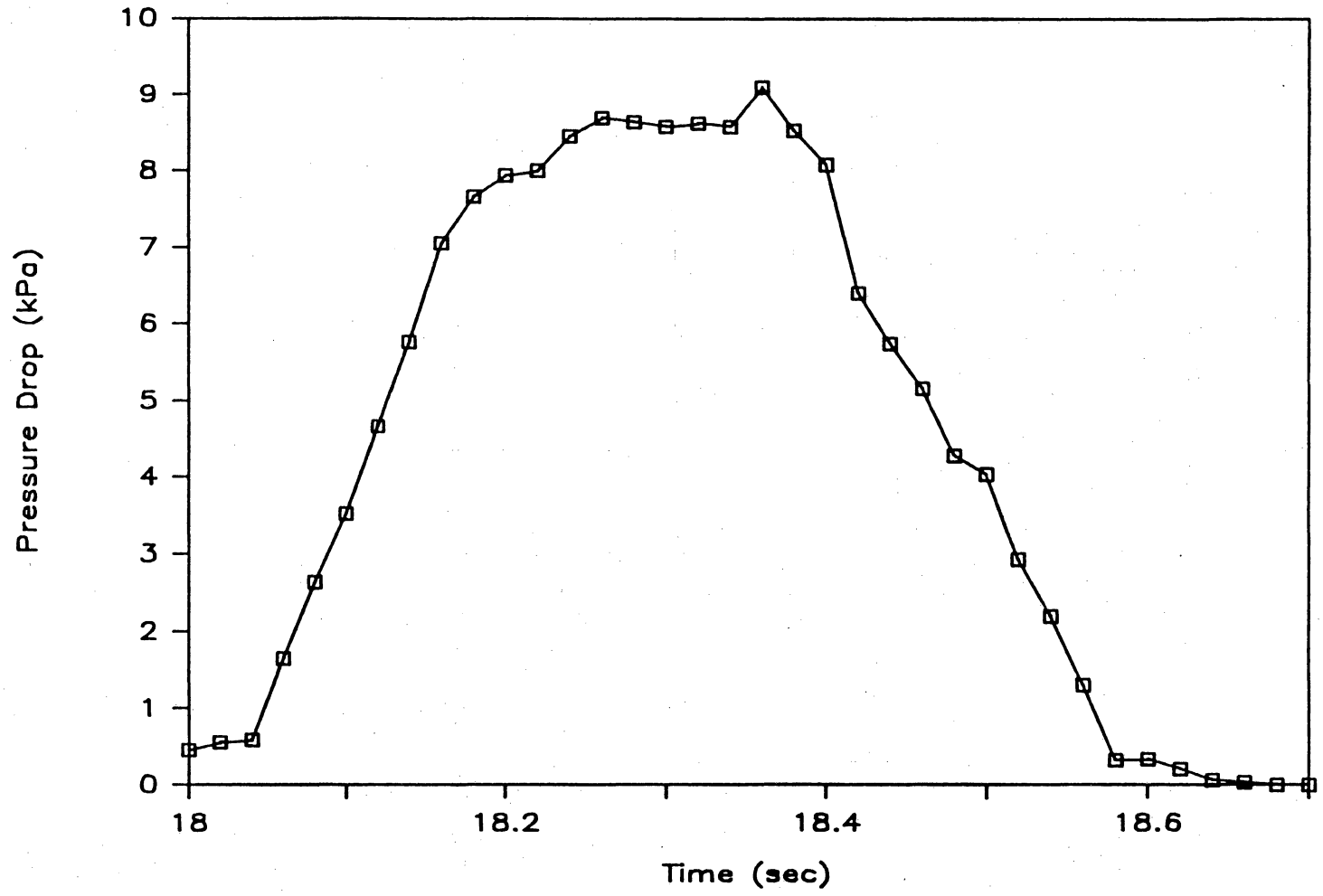

Figure D.83 Pressure Profile: Run 8, Plug #12

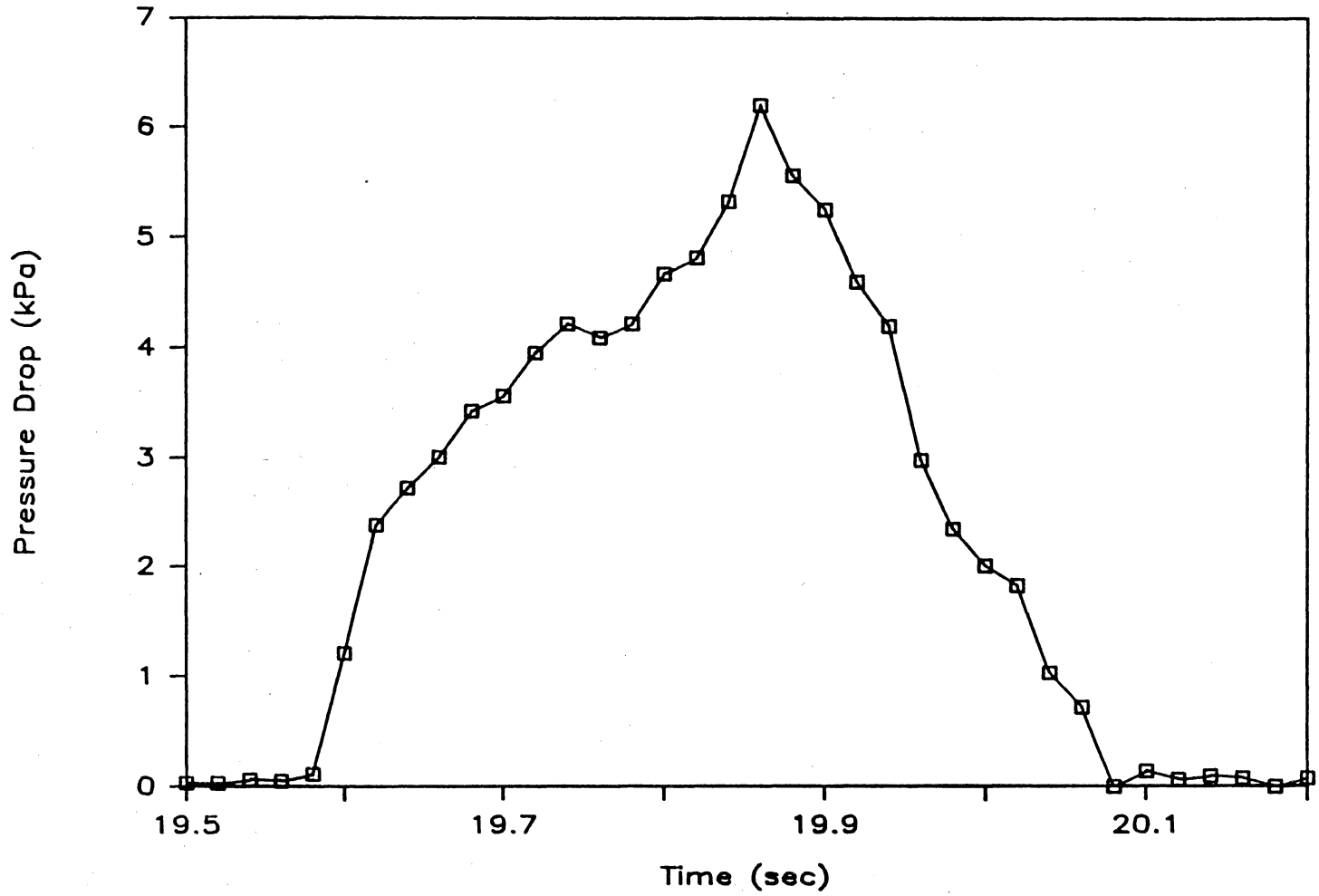

Figure D.84 Pressure Profile: Run 8, Plug #13

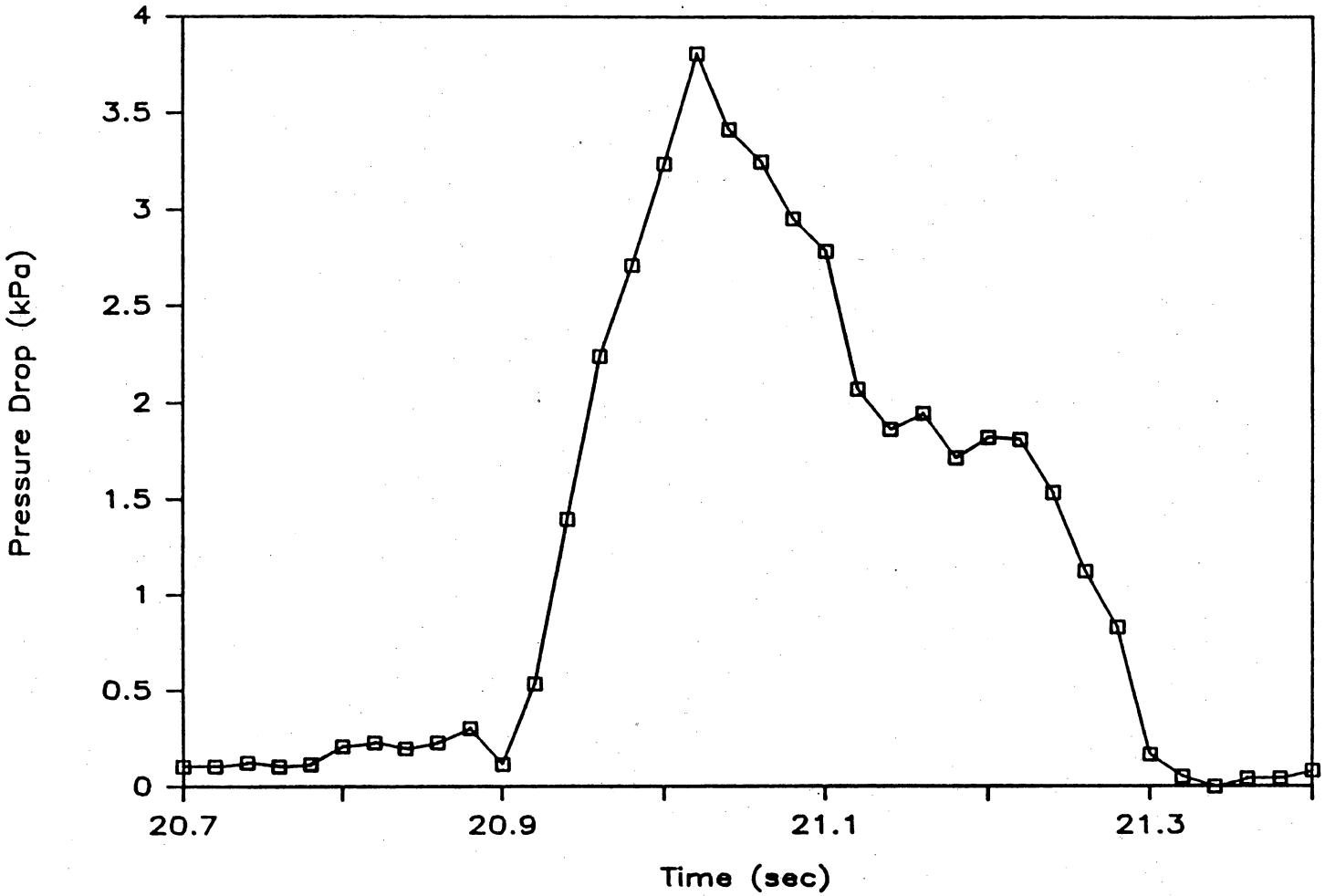

Figure D.85 Pressure Profile: Run 8, Plug #14

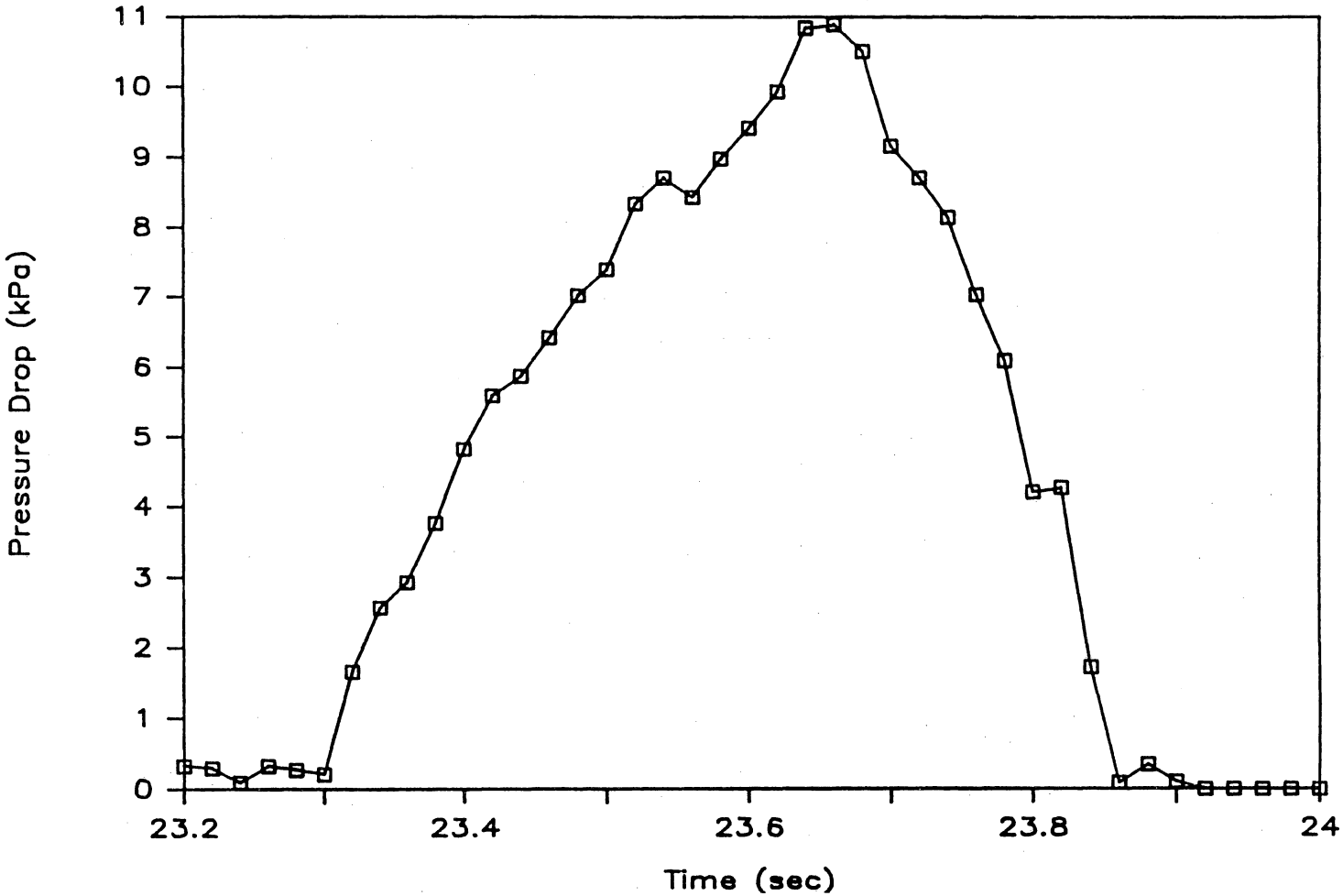

Figure D.86 Pressure Profile: Run 8, Plug #15

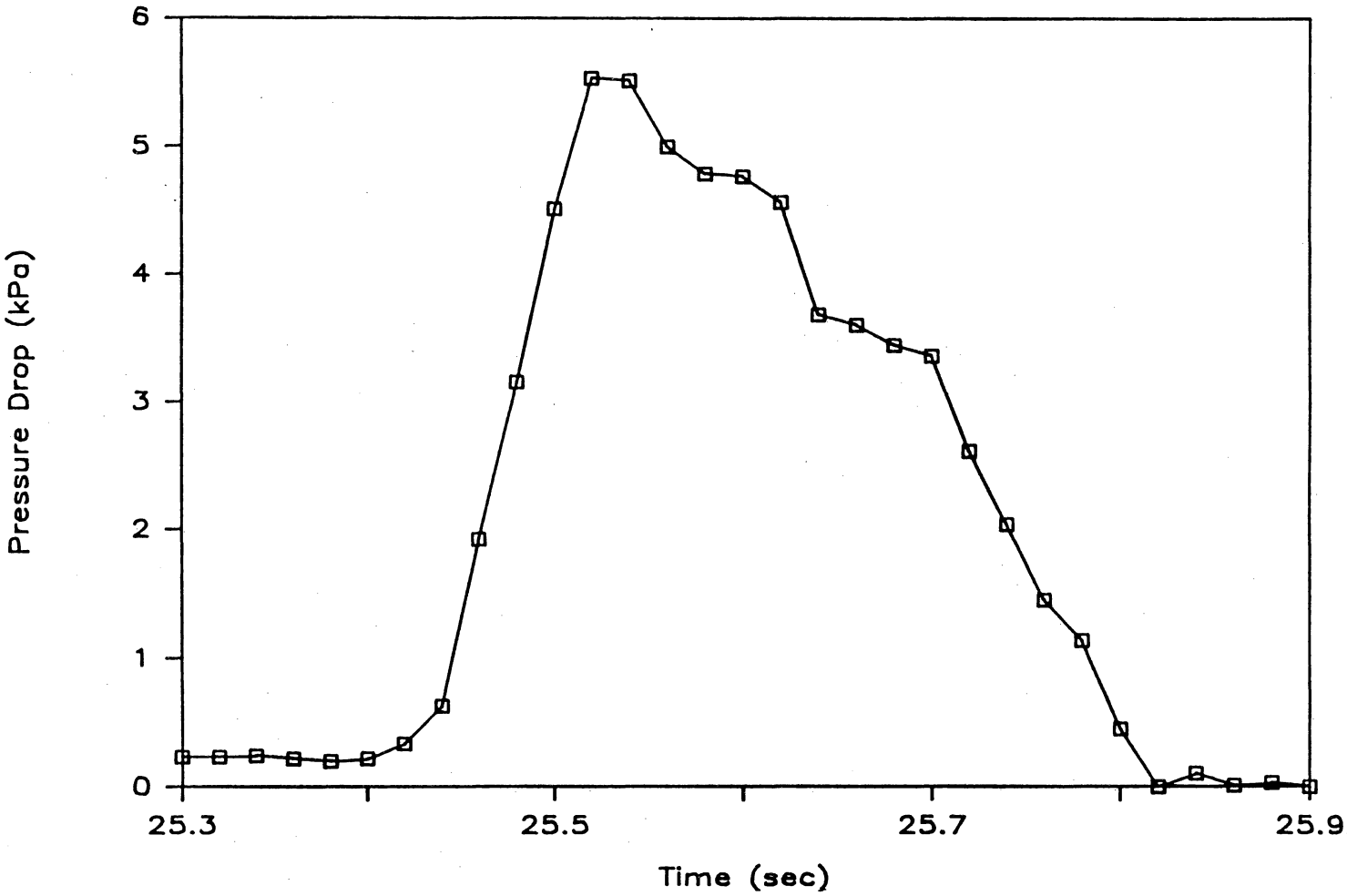

Figure D.87 Pressure Profile: Run 8, Plug #16

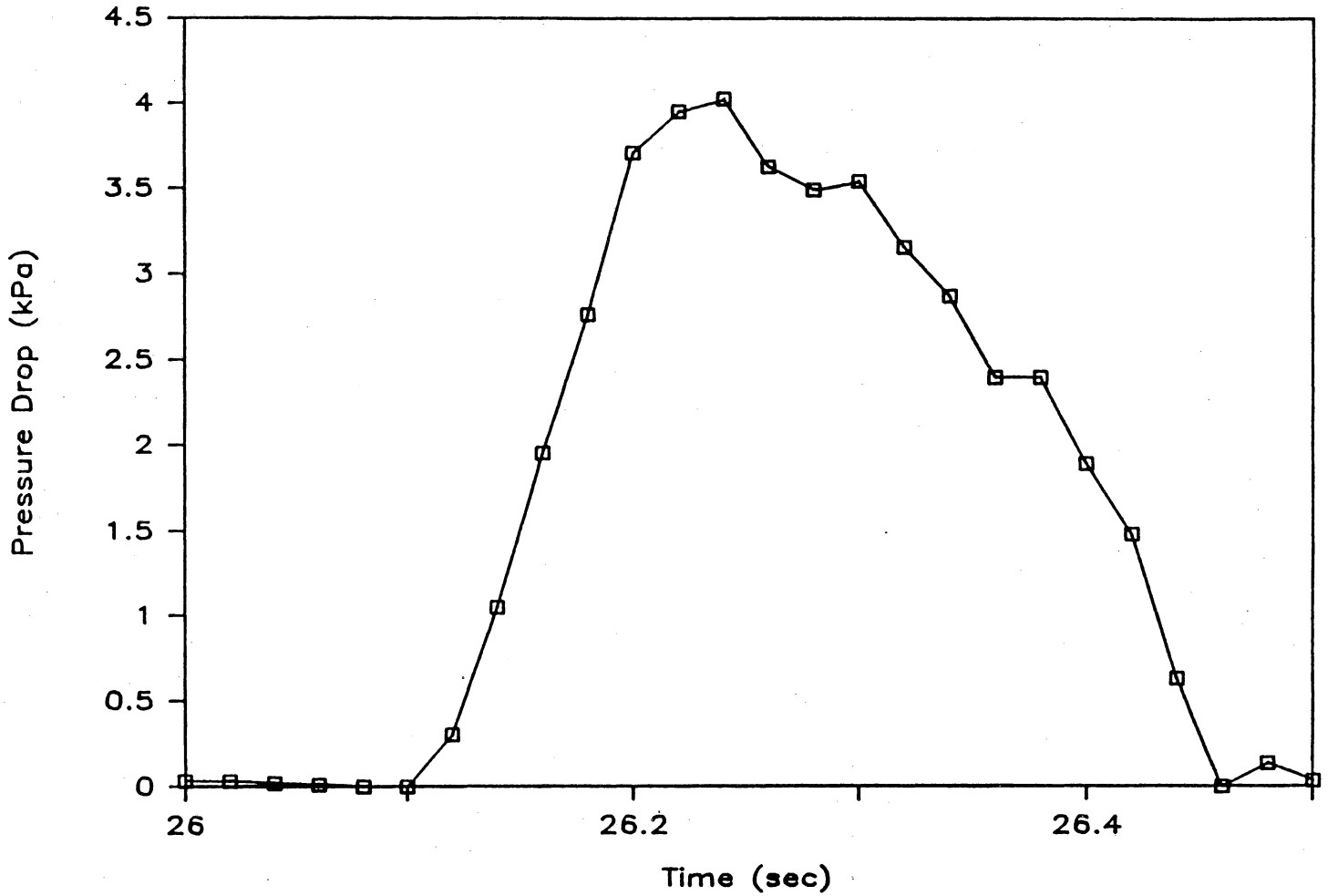

Figure D.88 Pressure Profile: Run 8, Plug #17

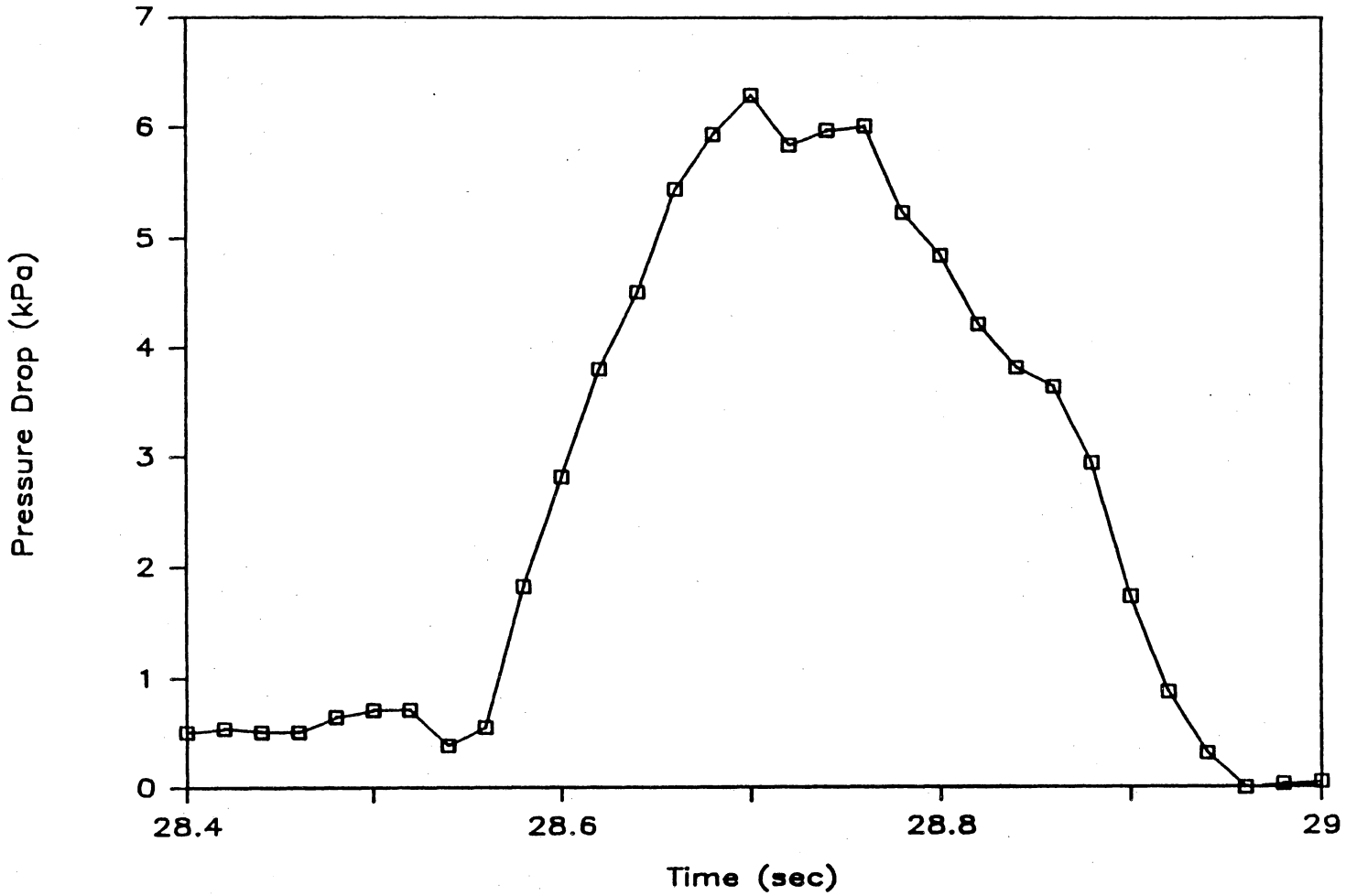

Figure D.89 Pressure Profile: Run 8, Plug #18

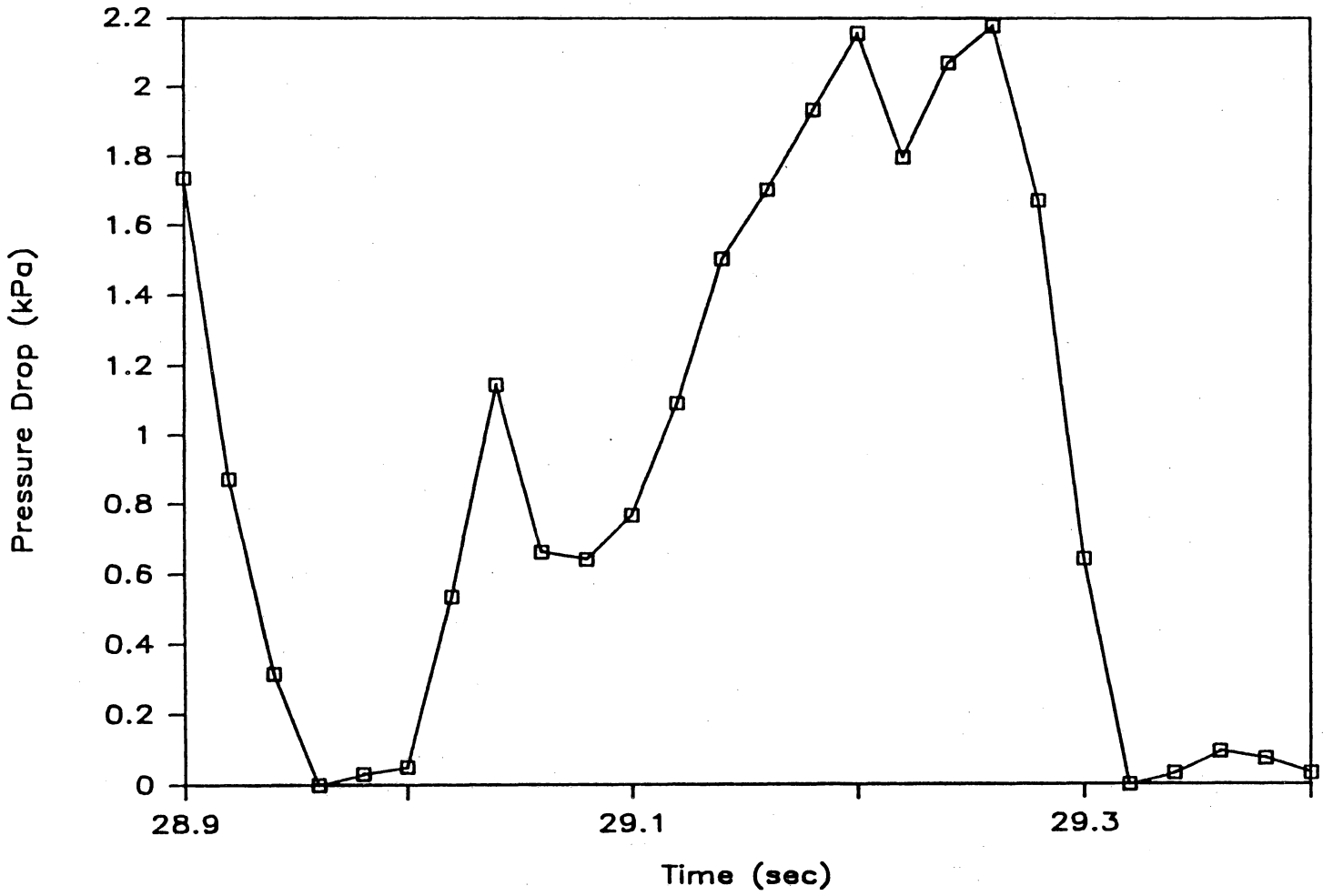

Figure D.90 Pressure Profile: Run 8, Plug #19

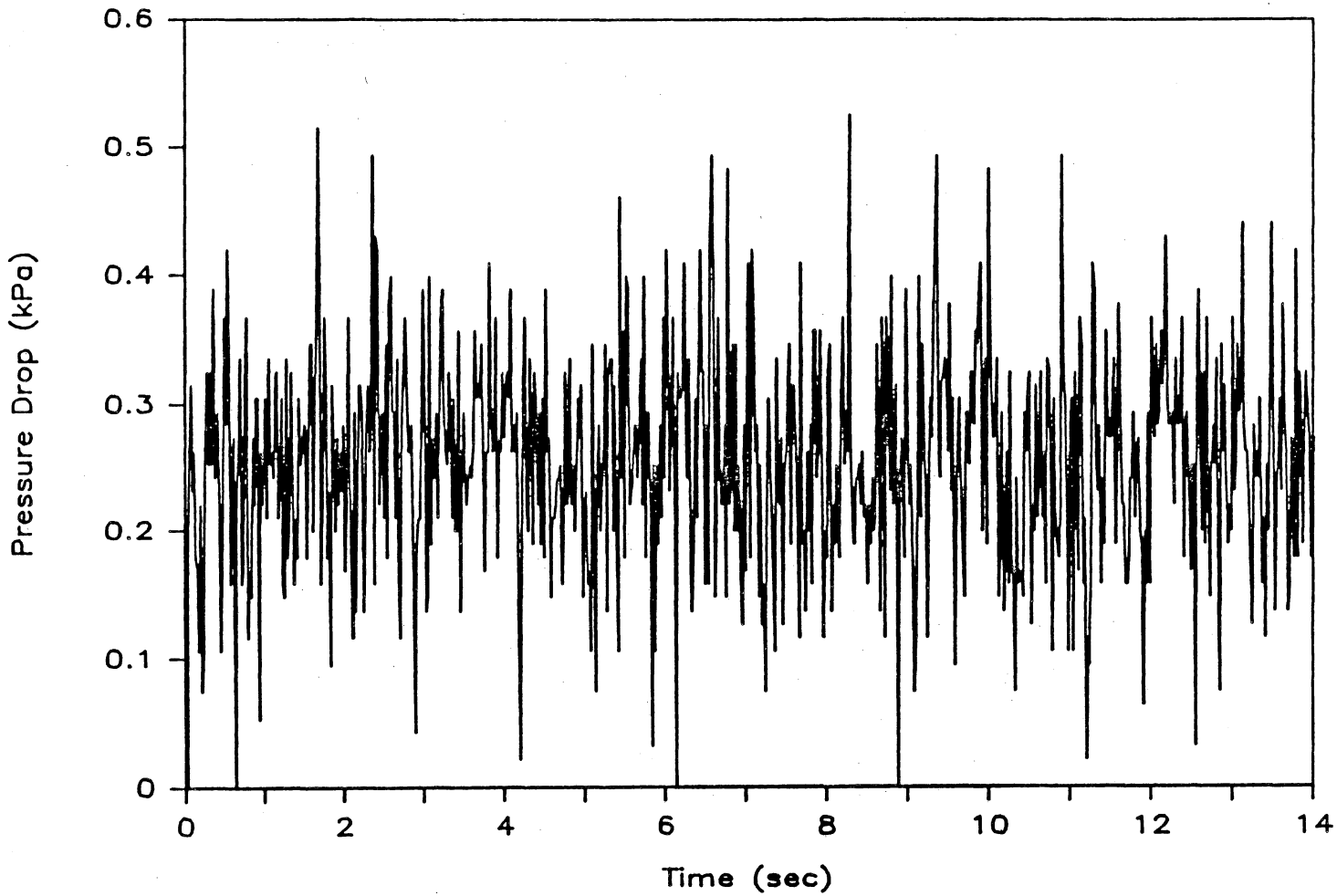

Figure D.91 Overall Pressure Profile: Run 9

The vita has been removed from the scanned document